DICOPPER AND DIRHODIUM PHOSPHORUSBIPYRIDYL LIGAND-BRIDGED COMPLEXES : ELECTROCATALYSTS FOR CARBON DIOXIDE REDUCTION

by

SADESH HARICHAND SOOKRAJ B.Sc(HONS), (NATAL)

A thesis submitted in partial fulfilment of the requirements for the degree of Doctor of Philosophy in the Faculty of Science, University of Natal, Pietermaritzburg
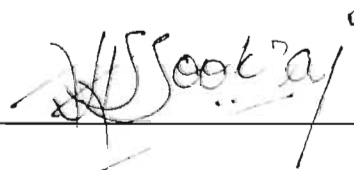
Department of Chemistry

University of Natal

Pietermaritzburg

December 1994

DECLARATION

I hereby certify that this research is the result of my own investigation which has not already been accepted for any degree and is not being submitted in candidature for any other degree.
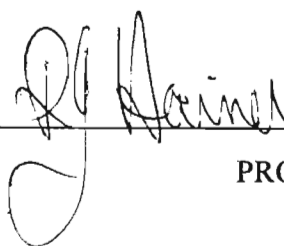
Signed _____

S. H. SOOKRAJ
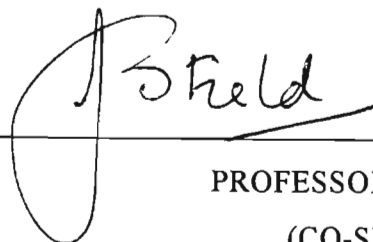
I hereby certify that this statement is correct.

Signed _____

PROFESSOR R. J. HAINES
(SUPERVISOR)

Signed _____

PROFESSOR J. S. FIELD
(CO-SUPERVISOR)

Department of Chemistry
University of Natal
Pietermaritzburg
December 1994

CONTENTS

ACKNOWLEDGEMENTS

SUMMARY

Chapter One reviews the electrochemistry of metal polypyridine complexes. The proposed mechanisms for the electrocatalytic reduction of carbon dioxide by these complexes are discussed. Some of the electron transfer processes are complex, while others involve simple one electron transfers.

Chapter Two deals with the synthesis and characterisation of 6-diphenylphosphino-2,2'-bipyridine (Ph_2Pbipy). This novel tridentate ligand has the ability to bridge across metal atoms or to coordinate in a pendant manner through the phosphorus atom.

Chapter Three deals with the synthesis and characterisation of a range of Ph_2Pbipy ligand - bridged dicopper (I) compounds. A key compound is $[Cu_2(\mu\text{-}Ph_2Pbipy)_2(MeCN)_2](PF_6)_2$ (5). The dication possesses labile acetonitrile ligands which have been substituted by a variety of neutral and anionic ligands. Compounds prepared this way include $[Cu_2(\mu\text{-}Ph_2Pbipy)_2(PhCN)_2](PF_6)_2$ (6), $[Cu_2(\mu\text{-}Ph_2Pbipy)_2(H_2O)_2](PF_6)_2$ (7), $[Cu_2(\mu\text{-}Ph_2Pbipy)_2(py)_2](PF_6)_2$ (8), $[Cu_2(\mu\text{-}Ph_2Pbipy)_2(4\text{-}Etpy)_2](PF_6)_2$ (12), $[Cu_2(\mu\text{-}Ph_2Pbipy)_2(\eta^2\text{-}bipy)](PF_6)_2$ (17), $[Cu_2(\mu\text{-}Ph_2Pbipy)_2(Ph_2PCH_2PPh_2)](PF_6)_2$ (22), $[Cu_2(\mu\text{-}Ph_2Pbipy)_2(\mu\text{-}I)](PF_6)$ (25), $[Cu_2(\mu\text{-}Ph_2Pbipy)_2(\mu\text{-}SEt)](PF_6)$ (28), $[Cu_2(\mu\text{-}Ph_2Pbipy)_2(\mu\text{-}O_2CH](PF_6)$ (31), and $[Cu_2(\mu\text{-}Ph_2Pbipy)_2(CN)_2]$ (35); X-ray crystal structure determinations have been completed for (5), (6), (7), (8), (12), (17), (25), (26) and (28). The solvento species, $[Cu_2(\mu\text{-}Ph_2Pbipy)_2(L)_2]^{2+}$ (L = MeCN, PhCN) has been shown to be an electrocatalyst for carbon dioxide reduction, the products of carbon dioxide reduction being carbon monoxide and carbonate ions. Electrocatalytic experiments were also carried out in the presence of water, the reduction products being carbon monoxide, methanol and methane; however, the dication $[Cu_2(\mu\text{-}Ph_2Pbipy)_2(L)_2]^{2+}$ breaks-up in the presence of water and copper metal deposits on the platinum electrode. It is thought that the deposited copper is actually responsible for the electrochemical reduction of carbon dioxide to methane and methanol. The electrochemistry of $[Cu_2(\mu\text{-}Ph_2Pbipy)_2(\mu\text{-}X)]^+$ (X = Cl, SEt, SCN) and $[Cu_2(\mu\text{-}Ph_2Pbipy)_2(\mu\text{-}Y)]^+$ (Y = O_2CH, O_2CPh, NO_3) have also been studied. The cations $[Cu_2(\mu\text{-}Ph_2Pbipy)_2(\mu\text{-}X)]^+$ or $[Cu_2(\mu\text{-}$

Ph$_2$Pbipy)$_2$(μ-Y)]$^+$ lose the bridging anionic ligand on electrochemical reduction to ultimately afford the neutral solvento species [Cu$_2$(μ-Ph$_2$Pbipy)$_2$(MeCN)$_2$]. The electrochemistry of [Cu$_2$(μ-Ph$_2$Pbipy)$_2$(CN)$_2$] under a carbon dioxide atmosphere indicates that it also functions as electrocatalyst for carbon dioxide reduction.

Chapter Four deals with the synthesis and characterisation of a range of platinum, palladium and rhodium complexes of the 6-diphenylphosphino-2,2'-bipyridyl ligand. The crystal structure of Rh(Ph$_2$Pbipy)$_2$(CO)Cl was determined and the compound used as a metal containing ligand in reactions with rhodium (I) precursors. In this way new Ph$_2$Pbipy ligand-bridged trirhodium compounds have been prepared viz. [Rh$_3$(μ-Ph$_2$Pbipy)$_2$(CO)$_3$(Cl)$_3$] and [Rh$_3$(μ-Ph$_2$Pbipy)$_2$(CO)$_5$(Cl)]X$_2$ (X = BF$_4$, PF$_6$ or SbF$_6$). A tricationic species [Rh$_3$(μ-Ph$_2$Pbipy)$_2$(CO)$_5$(MeCN)$_2$]X$_3$ (X = BF$_4$, PF$_6$ or SbF$_6$) has been prepared by the reaction of Ph$_2$Pbipy and [Rh(CO)$_2$(MeCN)$_2$]$^+$. These trirhodium cations function as electrocatalysts for carbon dioxide reduction but fragment on the time scale of the bulk electrolysis experiment.

ABBREVIATIONS

ampy	2-aminopyridine
2-am-4-metpy	2-amino-4-methylpyridine
bipy	2,2'-bipyridine
CO	carbon monoxide
CO_2	carbon dioxide
CO_3^{2-}	carbonate
COD	1,5-cyclooctadiene
CV	cyclic voltammogram
DABCO	1,4-diazabicyclo-[2,2,2]-octane
dmbipy	dimethyl-2,2'-bipyridine
DMF	N,N' - dimethylformamide
dppe	bis(diphenylphosphino)ethane
dppm	bis(diphenylphosphino)methane
Etpy	ethylpyridine
Et_4NCl	tetraethyl ammonium chloride
$\{^1H\}$	proton noise decoupled
LiCl	lithium chloride
merpy	mercaptopyridine
mg	milligram
ml	millilitre
mmol	millimol
mV	millivolt
MeOH	methanol
MeCN	acetonitrile
NHE	normal hydrogen electrode
nmr	nuclear magnetic resonance
PEt_3	triethylphosphine
$P(OMe)_3$	trimethylphosphite

PPh_3	triphenylphosphine
Ph_2Ppy	2-diphenylphosphinopyridine
Ph_2Pbipy	6-diphenylphosphino-2,2'-bipyridine
phen	1,10-phenanthroline
py	pyridine
RDE	rotating disc electrode
SCE	saturated calomel electrode
SSCE	saturated sodium chloride electrode
TBAH	tetrabutylammonium hexafluorophosphate
TBAP	tetrabutylammonium perchlorate
TPP	tetraphenylporphyrin
terpy	terpyridine
tht	tetrahydrothiophene
2-vpy	2-vinylpyridine
4-vpy	4-vinylpyridine
V	volts

LIST OF FIGURES

LIST OF SCHEMES

LIST OF TABLES

LIST OF PUBLICATIONS/CONFERENCE PROCEEDINGS

1. J. S. Field, R. J. Haines, C. D. Landsberg, C. J. Parry, S. Reiser, S. H. Sookraj, *The design of electrocatalysts for CO₂ reduction, di-, tri- and tetranuclear derivatives of Ruthenium*, June 1991, National Conference of the South African Chemical Institute, Grahamstown.

2. J. S. Field, R. J. Haines, C. J. Parry, S. H. Sookraj, *Novel Ruthenium (0), (I) and (II) compounds of 6-diphenylphosphino-2,2'-bipyridine*, June 1992, Biennial Conference of the Inorganic Section of the South African Chemical Institute, Warmbaths.

3. J. S. Field, R. J. Haines, C. J. Parry, S. H. Sookraj, *Synthesis and reactions of the novel Cu(I) dimer [Cu₂(Ph₂Pbipy)₂(MeCN)₂]²⁺*, June 1992, Biennial Conference of the Inorganic Section of the South African Chemical Institute, Warmbaths.

4. J. S. Field, R. J. Haines, C. P. Kubiak, C. J. Parry, S. Reiser, S. H. Sookraj, R. E. Wittrig, *Development of homogeneous electrocatalysts based on copper for the reduction of CO₂*, July 1992, International Conference on the chemistry of the Cu and Zn triads, University of Edinburgh, Scotland.

5. J. S. Field, R. J. Haines, C. P. Kubiak, S. H. Sookraj, R. E. Wittrig, October 1992, Annual Conference of the catalysis Society of South Africa, Kruger National Park.

6. J. S. Field, R. J. Haines, C. J. Parry, S. H. Sookraj, *South African Journal of Chemistry*, 1993, **46**, 62.

7. J. S. Field, R. J. Haines, C. J. Parry, S. H. Sookraj, 1993, *Polyhedron*, **12**, 2425.

8. J. S. Field, R. J. Haines, C. P. Kubiak, C. J. Parry, S. H. Sookraj, R. E. Wittrig, *Dinuclear complexes bridged by phosphorus polypyridine ligands as electrocatalysts for the reduction of CO₂,*, September 1993, International Conference on CO₂ utilisation, Bari - Italy.

9. J .S. Field, R. J. Haines, S. H. Sookraj, *Novel dinuclear copper (I) complexes: electrocatalysts for CO₂ reduction*, January 1994, National Conference of the South African Chemical Institute, Halfway House.

CHAPTER ONE

ELECTROCATALYTIC REDUCTION OF CARBON DIOXIDE

AIM

The aim of this chapter is to review the literature on the development of metal polypyridyl complexes as homogeneous electrocatalysts for carbon dioxide reduction. As an introduction the thermodynamics of carbon dioxide reduction are briefly discussed. In addition, the types of metal complexes known to function as homogeneous electrocatalysts for carbon dioxide reduction are identified; one example of each type is described, except in the case of the polypyridyl complexes where a range of examples are discussed in greater detail.

1.1. THE REDUCTION OF CARBON DIOXIDE

The steadily increasing amount of carbon dioxide in the Earth's atmosphere is becoming an environmental hazard because carbon dioxide is one of the gases responsible for the enhancement of the Greenhouse Effect; this increased emission into the atmosphere of gases enhancing the Greenhouse Effect can produce a change in the average seasonal temperature of our planet.[1] Carbon dioxide is estimated to be responsible for the highest relative contribution to the global warming (*see Table 1.1*).[2]

The problem of limiting carbon dioxide emission is complex as this species is generated in most metabolic and combustion processes, all essential to man's energy needs and strictly related to the living standards. Thus, it is clearly evident that one of the major challenges facing researchers today is the recovery and utilization of carbon dioxide,[2] *i.e.* if carbon dioxide could be harnessed it could be used as a cheap and readily available C_1 feedstock for the chemical industry.

Table 1.1. Percentage Contribution to Global Warming

GAS	PERCENTAGE
Carbon dioxide	50
Methane	18
Dinitrogen oxide	10
Chlorofluorocarbons	13
Ozone	15
Others	5

Carbon dioxide is a thermodynamically stable molecule and it is thus very difficult to convert it to useful chemicals. *Scheme 1.1* provides a useful summary of the thermodynamics of carbon dioxide reduction to C_1 fragments in acidic and basic media.

An attractive approach to the reduction of carbon dioxide is by means of electrochemical techniques; the thermodynamic potential required for the reduction of carbon dioxide in acetonitrile is -2.10V *vs* SCE.[3,4] However in practice even more cathodic potentials are required because of the presence of large overvoltages at the electrode surface. This has resulted in the search for more suitable electrodes and for electrocatalysts which reduce the overvoltages required.

The use of indium electrodes,[5] electrodes modified with polymers containing Pd,[6] and carbon electrodes modified with cobalt phthalocyanine complexes[7] have all resulted in significant lowering of the overpotential for heterogeneous carbon dioxide reduction. Porphyrins and macrocyclic complexes,[8,9] metal clusters,[10] bipyridine and polypyridine complexes[11,12] and

square planar complexes[13] are examples of homogeneous catalysts that have significantly lowered the overpotential for carbon dioxide reduction.

Scheme 1.1. Thermodynamic potentials involved in CO_2 reduction (values in volts)[18]

$$CO_2 \xrightarrow{-0.20} CO_2H \xrightarrow{-0.01} H_2C=O \xrightarrow{0.19} CH_3OH \xrightarrow{0.58} CH_4$$

$$CO_2 \longrightarrow CO \xrightarrow{-0.1} CO_2H$$

$$[\ 1M\ OH^-\ ]$$

$$CO_3^{2-} \xrightarrow{-1.0} HCO_2^- \xrightarrow{-0.07} H_2C=O \xrightarrow{-0.6} CH_3OH \xrightarrow{-0.25} CH_4$$
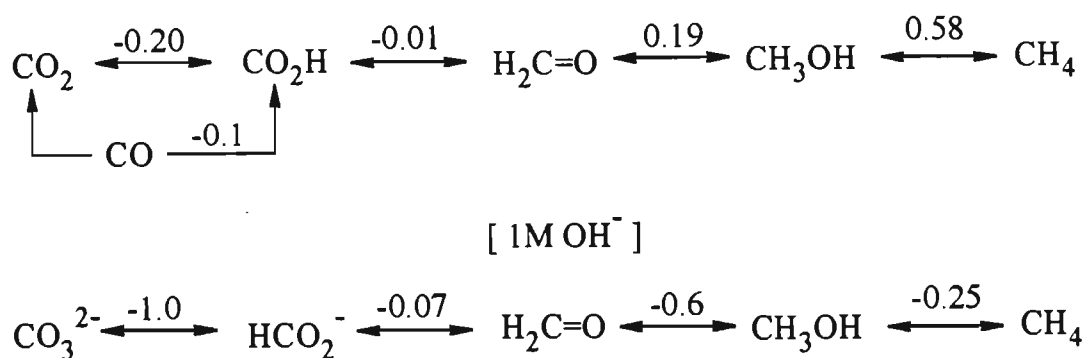
The nature of the reduction products depends crucially upon the reaction medium. In water, formic acid is the main product;[14,15]

$$2CO_2 + H_2O + 2e^- \rightarrow HCO_2^- + HCO_3^-$$

while oxalate and carbon monoxide are obtained together with formate in solvents of low proton availability such as dimethylformamide and dimethyl sulphoxide.[16,17]

$$2CO_2 + 2e^- \rightarrow C_2O_4^{2-}$$
$$2CO_2 + 2e^- \rightarrow CO + CO_3^{2-}$$
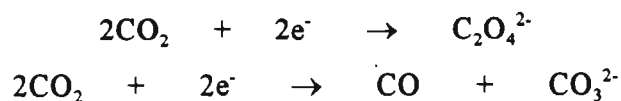
The addition of small amounts of water promotes the formation of formate as well as inducing further reduction to oxalate, and mainly to glycolate.[16,17]

The first step in the electrochemical reduction of carbon dioxide involves the formation of the highly reactive radical anion, CO_2^- , as illustrated in *Scheme 1.2*. The fate of the radical anion depends on the solvent, pH and electrode composition.[18] The mechanism illustrated in

Scheme 1.2 was proposed by Saveant and co-workers[3,19] and it postulates the dimerisation of two radical anions to form oxalate, the mechanisms for the formation of other reduction products also being illustrated in *Scheme 1.2*.

Carbon monoxide is formed when the radical anion combines with a carbon dioxide molecule to produce a bi-carbon species which undergoes a one electron reduction or reacts with another radical anion to form $C_2O_4^{2-}$ which has carbon-carbon coupling; this complex breaks up to form carbon monoxide and the carbonate anion by disproportionation. Formic acid is formed when the radical anion reacts with a molecule of water.

Scheme 1.2. Mechanism for formation of reduction products of CO_2 (from ref. 3)

$$CO_2 \quad + \quad 1e^- \quad \rightleftharpoons \quad CO_2^{\cdot -}$$

$$2CO_2^{\cdot -} \quad \longrightarrow \quad C_2O_4^{2-}$$

$$CO_2^{\cdot -} \quad + \quad H_2O \quad \longrightarrow \quad HCO_2^{\cdot} \;+\; OH^-$$

$$HCO_2^{\cdot} \quad + \quad 1e^- \quad \rightleftharpoons \quad HCO_2^-$$

and/or

$$HCO_2^{\cdot} \quad + \quad CO_2^{\cdot -} \quad \longrightarrow \quad HCO_2^- \;+\; CO_2$$

$$CO_2^{\cdot -} \quad + \quad CO_2 \quad \longrightarrow \quad O{=}C{-}O{-}C(O^-)(=O)$$

and/or

$$\longrightarrow \quad CO \;+\; CO_3^{2-}$$
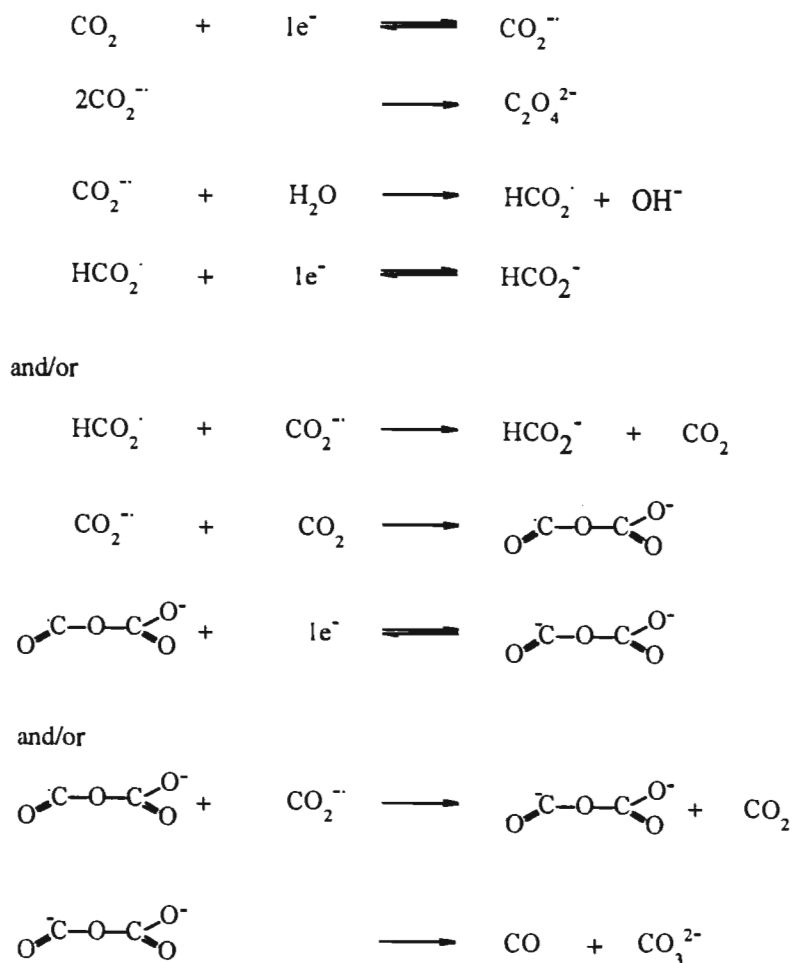
1.2. HOMOGENEOUS ELECTROCATALYTIC REDUCTION OF CARBON DIOXIDE BY METAL COMPLEXES

1.2.1. METAL MACROCYCLES AS ELECTROCATALYSTS

Although a large number of macrocyclic metal complexes have been synthesised, very little work has been done to address mechanistic questions. Pearce and Pletcher proposed one of the first mechanistic sequences from studies of cyclic voltammetry and bulk electrolysis for Co^{II} and Ni^{II} complexes.[20] The majority of the macrocyclic systems are square planar and contain neutral or negatively charged nitrogen or mixed nitrogen and oxygen donor atoms.

Iron ("0") porphyrins (generated by addition of three electrons to a iron (III) species) have recently been shown to catalyse the electrochemical reduction of carbon dioxide to carbon monoxide (*see Figure 1.1a*).[21] The cyclic voltammogram of TPPFe(III)Cl exhibits three reversible waves under an argon atmosphere. Under one atmosphere of carbon dioxide, the height of the third wave increases and becomes irreversible, indicating that the Fe("0") species actually functions as the elctrocatalyst.

It should be noted that in dimethylformamide with tetra-alkyl ammonium salts as supporting electrolyte, the porphyrin is destroyed by carboxylation and/or hydrogenation of the ring after a few catalytic cycles. However the addition of a hard electrophile such as Mg^{2+} in the form of nonhydrated $Mg(ClO_4)_2$ spectacularly enhances the catalytic wave (*see Figure 1.1b*) and the production of carbon monoxide.

The proposed mechanism illustrated in *Scheme 1.3*, initially involves the one electron reduction of the iron complex. This is followed by the introduction of one molecule of carbon dioxide into the iron co-ordination sphere. A second carbon dioxide molecule is added and it acts as a Lewis acid and promotes the cleavage of one C-O bond of the first carbon dioxide molecule thus leading to carbon monoxide formation. The way that the Mg^{2+} ions affect this process is dependent on temperature; at low temperatures the Mg^{2+} ions facilitate the

decomposition of the complex containing two molecules of carbon dioxide; while at room temperature the Mg^{2+} ions trigger the breaking of the bond at the level of the complex containing a single molecule of carbon dioxide in its co-ordination sphere. This system combines the action of an electron rich centre {iron ("0") porphyrins} where the reduction process starts and an electron deficient centre (Mg^{2+}) which assists the transformation of the bond system.
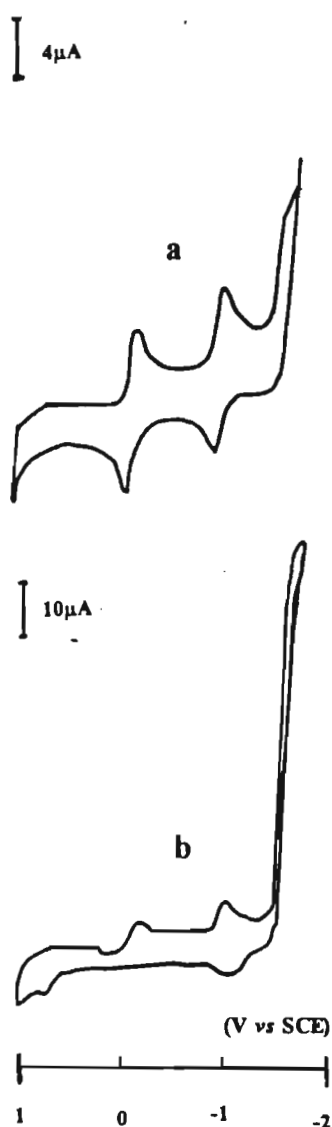
Figure 1.1. Cyclic voltammograms for TPPFeCl under a carbon dioxide atmosphere in; (a) the absence and (b) presence of Mg^{2+} ions

Scheme 1.3. Mechanism for carbon dioxide reduction using iron ("0") porphyrins and Mg^{2+} ions [21]
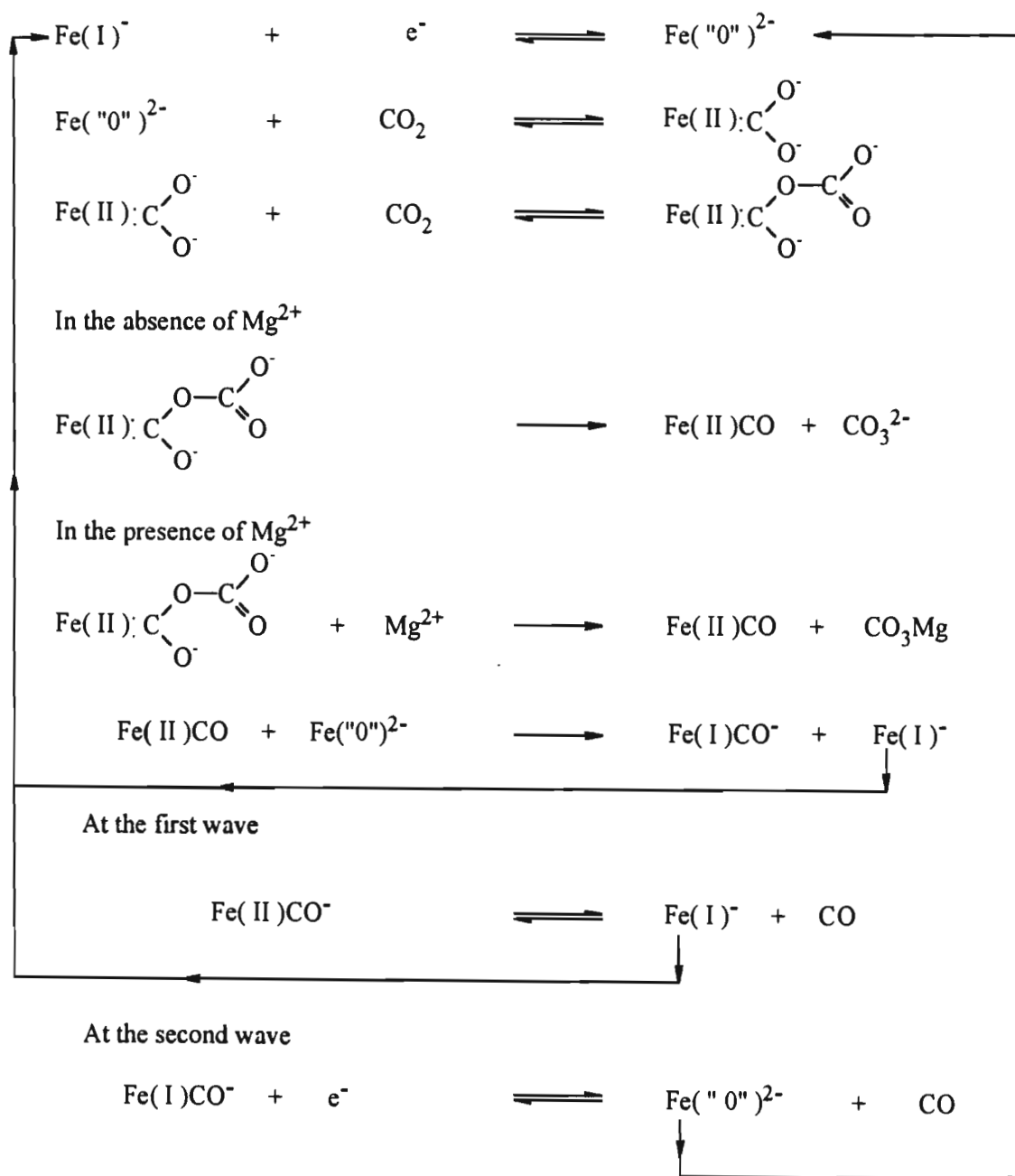
1.2.2. SQUARE PLANAR METAL COMPLEXES AS ELECTROCATALYSTS

Most metallo macrocycles and porphyrins exist as square planar complexes; however there exists an electronically and sterically distinct class of square planar complexes as represented by complexes such as $[M(triphos)L](BF_4)_2$ (for M = Ni, L is $P(OMe)_3$ and PEt_3; for M = Pd, L is MeCN, $P(OMe)_3$, PEt_3, $P(CH_2OH)_3$ and PPh_3; for M = Pt, L is PEt_3). On the basis of cyclic voltammetry and bulk electrolysis experiments, the Pd complexes are shown to catalyse the electrochemical reduction of carbon dioxide to carbon monoxide in acidic acetonitrile solutions as illustrated in *Scheme 1.4.*[22] It is interesting to note that the analogous nickel and platinum complexes do not catalyse the reduction of carbon dioxide.

DuBois and Miedaner proposed that the palladium complex undergoes a two electron reduction to form the Pd(0) complex; a proton from the acidic acetonitrile solution then displaces the ligand (L). A carbon dioxide molecule then inserts into the metal-hydride (Pd-H) bond; a second proton is then incorporated into the complex and this results in the formation of water and carbon monoxide while the starting complex is regenerated.

It has been shown that the rate depends on acid concentration with the maximum rate been achieved when $[HBF_4] = 2.9mM$; any increase in acid concentration then leads to a decrease in activity. The rate of reduction is also dependent on catalyst and carbon dioxide; the first order dependence of the rate on catalyst, carbon dioxide and acid at low concentrations strengthens the proposed mechanism where carbon dioxide insertion into the Pt-H bond is the rate determining step.

Scheme 1.4. Mechanism for CO$_2$ reduction by [Pd(triphos)L](BF$_4$)$_2$ [22]
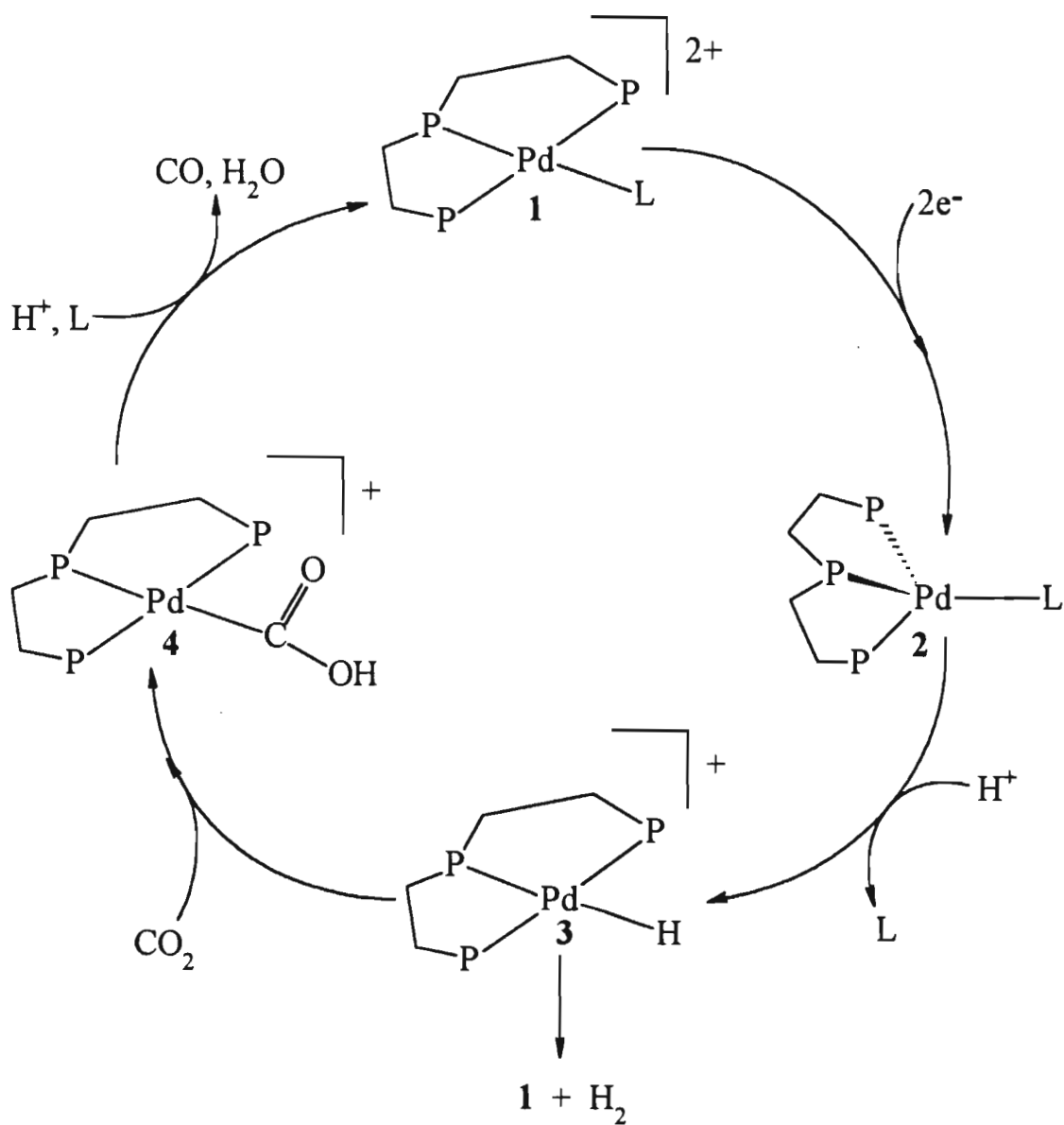
1.2.3. METAL CLUSTERS AS ELECTROCATALYSTS

Metal clusters have several advantages over monometallic systems. Firstly, they have a greater number of close lying frontier orbitals and therefore can undergo multi-electron processes more readily.[23] Secondly, clusters allow more modes of co-ordination of incoming substrates and thus differing degrees of activation. Thirdly, the metal-metal bonds of a cluster are readily cleaved rendering the atoms unsaturated and therefore very susceptible to attack by small molecules such as carbon monoxide, nitrogen, carbon dioxide and olefins.[23]

The orbitals responsible for reduction and oxidation in metal cluster complexes have been assigned.[24,25] The highest occupied molecular orbital (HOMO) is usually a σ-bonding molecular orbital of metal character and the lowest unoccupied molecular orbital (LUMO) is an anti-bonding molecular orbital of metal character. Consequently, a disadvantage of metal clusters is that they are susceptible to fragmentation.[26] However, this can be curtailed by means of a bidentate ligand ($Ph_2PCH_2PPh_2$, for example), or capping on the face of the cluster by donor ligands such as $HPPh_2$, or by hetero-atoms such as carbon, nitrogen, phosphorus or sulphur;[27] those clusters which undergo reversible one electron transfer processes usually contain such stabilising ligands or hetero-atoms. However, as both electrochemical reductions and oxidations tend to weaken the metal-metal interactions, many one electron processes are irreversible;[26] the less common two electron transfer process involving a reduction immediately following a structural re-arrangement.[27] Despite these drawbacks, there have been several cluster compounds synthesised which function as efficient electrocatalysts for the reduction of carbon dioxide.[28,29]

Kubiak and co-workers have reported a tri-nickel complex that functions as an electrocatalyst for carbon dioxide reduction.[30] The triangular nickel complex [Ni(μ_3-CNMe)(μ_3-I)(dppm)$_3$][PF$_6$] exhibits a reversible single electron reduction at $E_{1/2}$ = -1.09V *vs* Ag/AgCl; in the presence of carbon dioxide there is a significant current enhancement (*see Figure 1.2*). The reduction products correspond to the reductive disproportionation of carbon dioxide to carbon monoxide and carbonate anions, the proposed mechanism being illustrated in *Scheme 1.5*.

The reduction of carbon dioxide by the trinickel electrocatalyst occurs at a potential of -1.09V *vs* Ag/AgCl which is substantially lower than the overpotential required in the absence of electrocatalyst. It is proposed that initially an adduct of carbon dioxide with the reduced form of the trinickel cluster is formed. A second carbon dioxide molecule may then be inserted into the adduct in a "head-to-tail" fashion. A second electron is transferred from a second "activated" tri nickel complex; followed by asymmetric disproportionation of the head-to-tail dimer of carbon dioxide to carbon monoxide and carbonate ions.
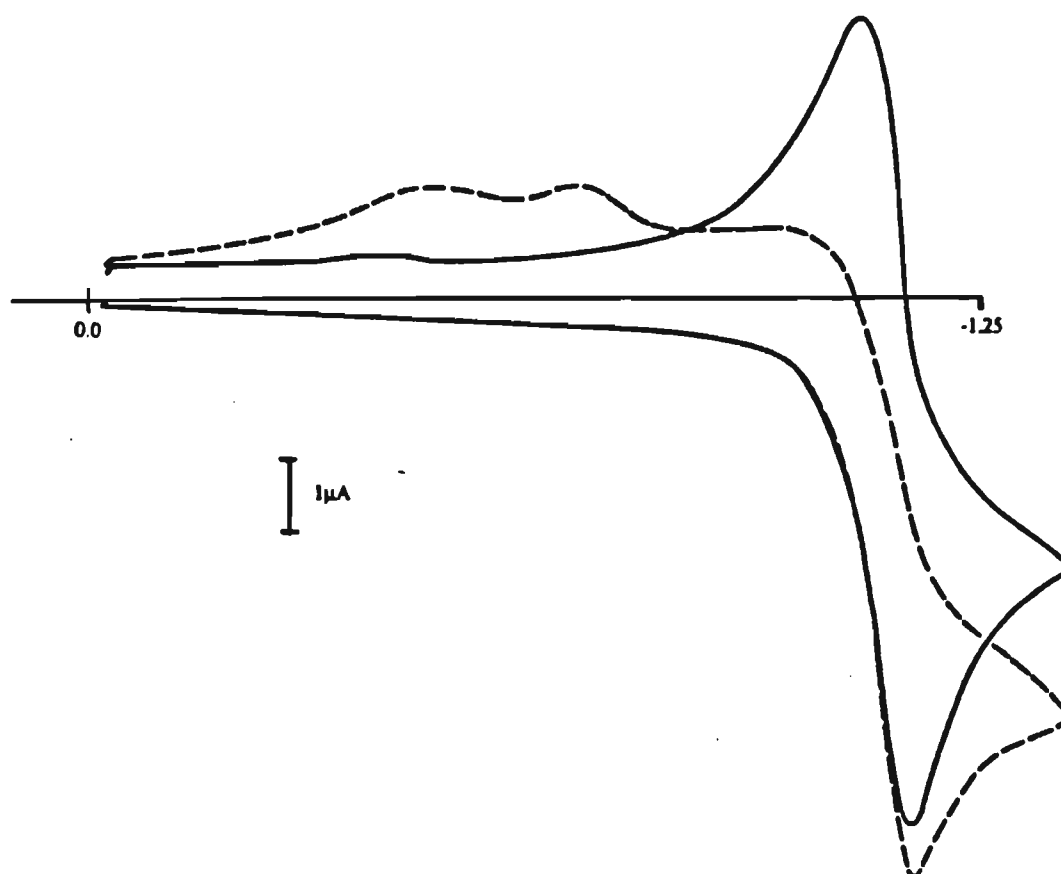
Figure 1.2. Cyclic voltammograms of [Ni(μ_3-CNMe)(μ_3-I)(dppm)$_3$][PF$_6$] under (-) nitrogen (---) under carbon dioxide

Scheme 1.5. Mechanism for CO_2 reduction by $[Ni(\mu_3\text{-}CNMe)(\mu_3\text{-}I)(dppm)_3]^{+}$ [30]
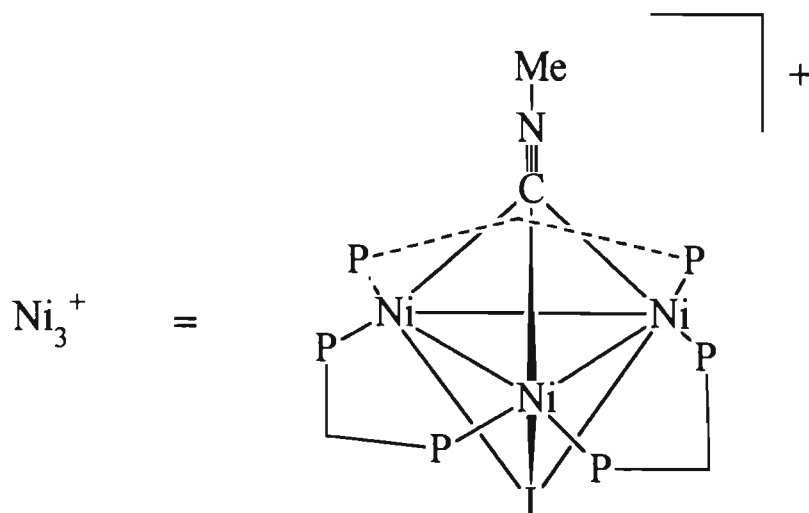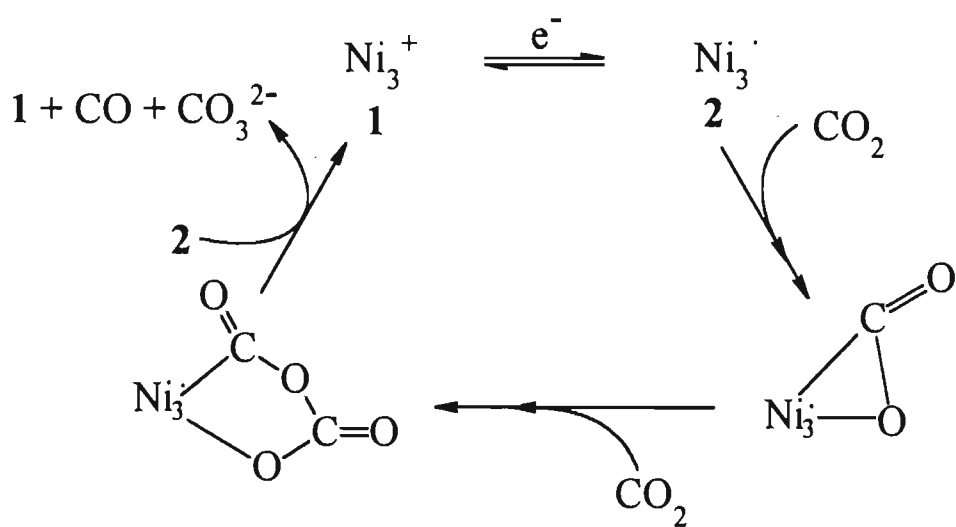
1.2.4. METAL POLYPYRIDYL COMPLEXES AS ELECTROCATALYSTS

The majority of the mechanistic data for carbon dioxide reduction has come from studies on complexes containing polypyridyl ligands. Polypyridine ligands are electron rich, π-unsaturated systems containing two or more nitrogen donor atoms. They are usually characterised by having low lying π^* orbitals and are thus useful in stabilising metals in low formal oxidation states. By utilising vacant π^* orbitals, polypyridine ligands can simultaneously act as " electron reservoirs " capable of storing electrons at potentials between -0.7V and -1.7V. Another appealing property of polypyridines like 2,2'-bipyridine and 1,10-phenanthroline is that they stabilise metals in a large number of oxidation states. Many complexes containing bipyridine, terpyridine and phenanthroline have proved to be effective electrocatalysts in the reduction of carbon dioxide.

$[Ru(bipy)_2(CO)_2][PF_6]_2$ was one of the earliest metal polypyridyl complexes that functioned as an electrocatalyst for carbon dioxide reduction in a water/dimethylformamide medium.[31] Formic acid and carbon monoxide as well as hydrogen are evolved in alkaline conditions while only carbon monoxide and hydrogen are evolved in acidic conditions. At pH6.0 carbon dioxide is reduced to carbon monoxide but there is a large amount of hydrogen that is also evolved; if the proton concentration is decreased by changing the solvent from water to water(pH6.0)/DMF (9:1, v/v) the amount of carbon monoxide produced increases while the amount of hydrogen evolved decreases. The reduction of carbon dioxide in water(pH9.5)/DMF (9:1, v/v) medium results in the formation of formic acid together with carbon monoxide and hydrogen. Due to the fact that formic acid is only produced in an alkaline medium, it is believed that $[Ru(bipy)_2(CO)(COOH)][PF_6]$ is involved as an intermediate.

Tanaka and co-workers carried out further studies on the $[Ru(bipy)_2(CO)_2][PF_6]_2$ and $[Ru(bipy)_2(CO)Cl][PF_6]$ systems.[32] A controlled potential electrolysis of a carbon dioxide saturated DMF solution containing n-Bu$_4$ClO$_4$ as supporting electrolyte and $[Ru(bipy)_2(CO)_2][PF_6]_2$ as catalyst resulted in the decomposition of $[Ru(bipy)_2(CO)_2][PF_6]_2$ with the formation of *ca.* 10% carbon monoxide. However, when the same experiment was

repeated with a water/DMF mixture(1:1, v/v) and with LiCl as supporting electrolyte; $[Ru(bipy)_2(CO)_2][PF_6]_2$ functioned efficiently as an electrocatalyst with carbon monoxide, hydrogen and formic acid as the main reduction products. This experiment indicated that water is necessary in order for $[Ru(bipy)_2(CO)_2][PF_6]_2$ to function efficiently as an electrocatalyst.

The cyclic voltammograms for $[Ru(bipy)_2(CO)_2][PF_6]_2$ show an irreversible two electron reduction at *ca.* -0.95V under an nitrogen atmosphere (*see Figure 1.3b*); while under a carbon dioxide atmosphere there is a significant increase in current at *ca.* -1.40V. The cyclic voltammograms for $[Ru(bipy)_2(CO)Cl]^+$ shows a reversible one electron reduction at -1.21V and an irreversible one electron reduction at *ca.* -1.41V (*see Figure 3a*) under a nitrogen atmosphere, there is a significant increase in the current at *ca.*-1.40V under a carbon dioxide atmosphere.

The following mechanism for the electrochemical reduction of carbon dioxide to carbon monoxide and formic acid by $[Ru(bipy)_2(CO)_2][PF_6]_2$ and $[Ru(bipy)_2(CO)Cl]^+$ has been proposed (*see Scheme 1.6*). $[Ru(bipy)_2(CO)_2][PF_6]_2$ undergoes a two electron reduction to form $[Ru(bipy)_2(CO)]$; this is accompanied by the loss of a molecule of carbon monoxide. $[Ru(bipy)_2(CO)Cl]^+$ undergoes a two electron reduction and loses a chloride ion to form $[Ru(bipy)_2(CO)]$.

$[Ru(bipy)_2(CO)]$ has one vacant site and a carbon dioxide molecule co-ordinates to the complex to form $[Ru(bipy)_2(CO)(COO)]$. This species is then protonated to form $[Ru(bipy)_2(CO)\{C(O)OH\}]^+$ which can either;

(i).   be protonated to form $[Ru(bipy)_2(CO)_2]^{2+}$; this is accompanied by the loss of a water molecule and $[Ru(bipy)_2(CO)_2]^{2+}$ can re-enter the catalytic cycle, or

(ii).   be protonated and undergo a two electron reduction to form $[Ru(bipy)_2(CO)]$; this is accompanied by the liberation of $HCOO^-$ and H^+ and $[Ru(bipy)_2(CO)]$ can re-enter the catalytic cycle.

[Ru(bipy)$_2$(CO)(COO)], [Ru(bipy)$_2$(CO){C(O)OH}]$^+$ and [Ru(bipy)$_2$(CO)$_2$]$^{2+}$ exist in equilibrium and there exists some evidence for the proposed mechanism. The x-ray crystal structure of [Ru(bipy)$_2$(CO)(COO)] has been determined (*see Figure 1.4*).[33] The x-ray crystal structure of [Ru(bipy)$_2$(CO){C(O)OCH$_3$}]$^+$ has also been determined, this complex serves as a model for [Ru(bipy)$_2$(CO){C(O)OH]$^+$ (*see Figure 1.5*).[34]

Scheme 1.6. Mechanism for carbon dioxide reduction by [Ru(bipy)$_2$(CO)$_2$]$^{2+}$ and [Ru(bipy)$_2$(CO)Cl]$^+$ [35]
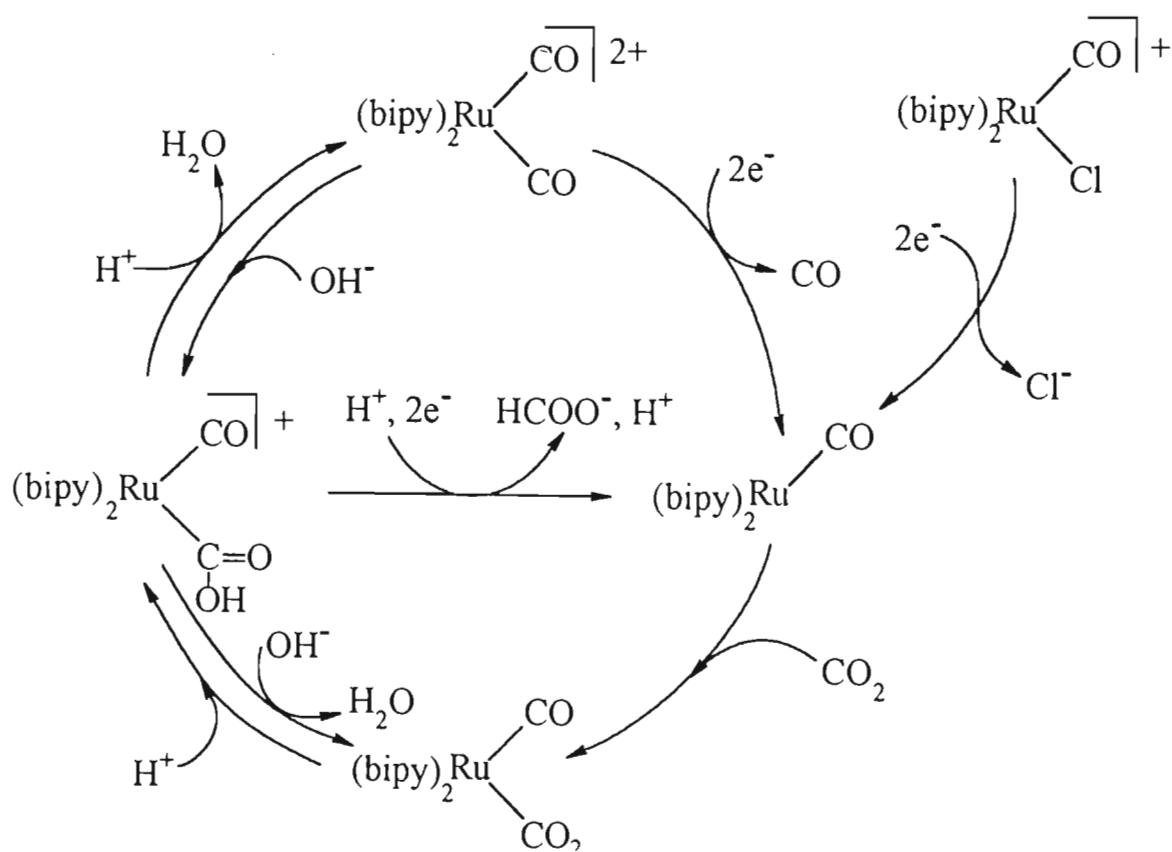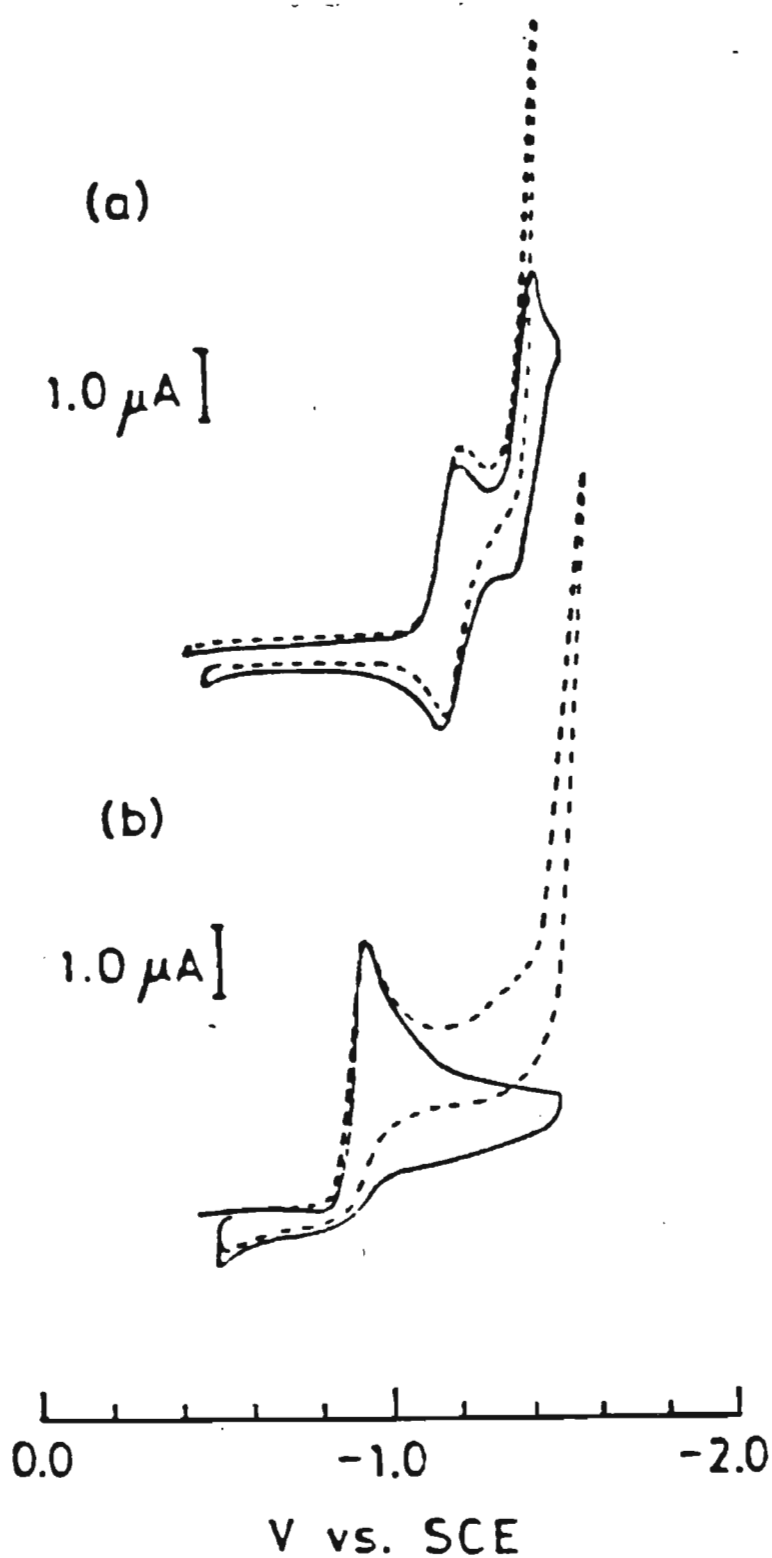
Figure 1.3. Cyclic voltammograms of [Ru(bipy)$_2$(CO)$_2$]$^{2+}$ and [Ru(bipy)$_2$(CO)Cl]$^+$ in H$_2$O/DMF under N$_2$ (-) and CO$_2$ (---) atmosphere
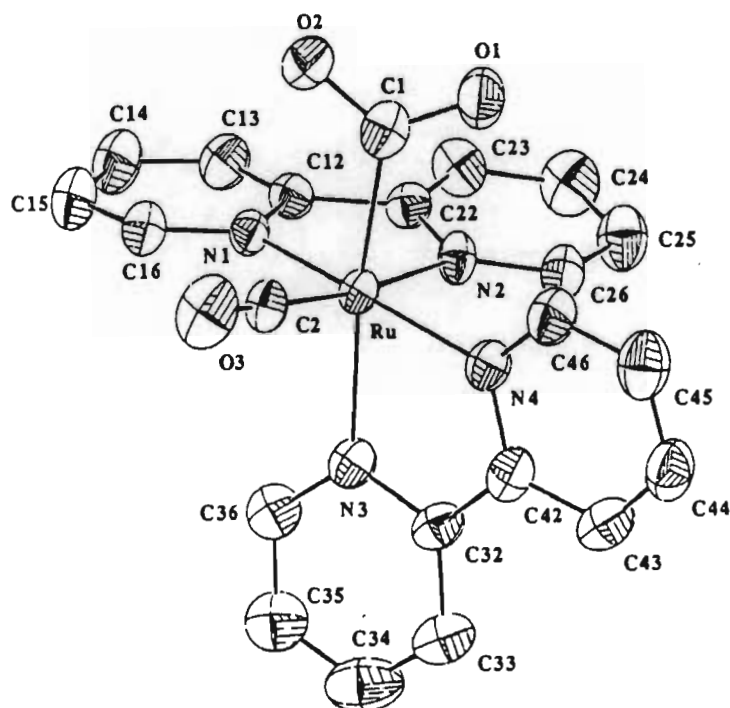
Figure 1.4. X-ray crystal structure of [Ru(bipy)$_2$(CO)(COO)]
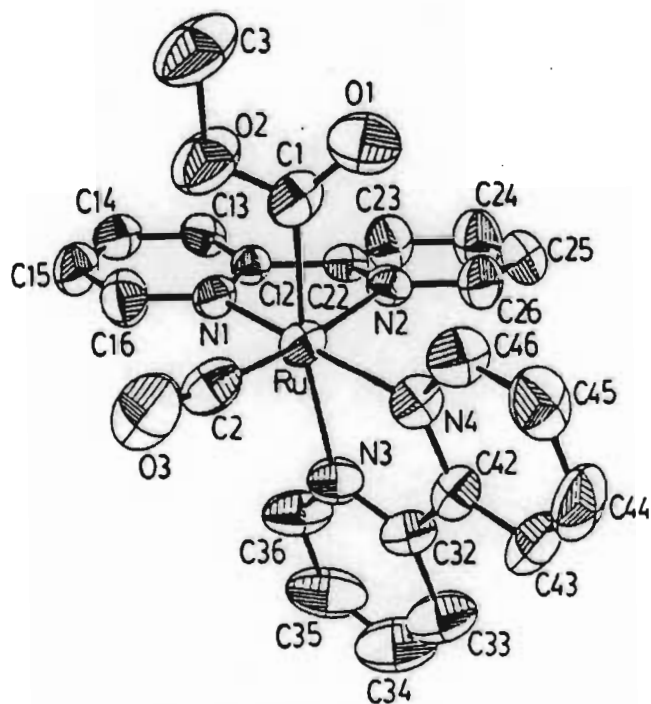
Figure 1.5. X-ray crystal structure of [Ru(bipy)$_2$(CO){C(O)OCH$_3$}]$^+$

Tanaka and co-workers pursued the electrochemical reduction of carbon dioxide by $[RuL^1(L^2)(CO)_2]^{2+}$ where L^1, L^2 = (bipy)$_2$, (bipy)(dmbipy), (dmbipy)$_2$ or (phen)$_2$ in acetonitrile/water (4:1, v/v), methanol or acetonitrile/methanol (4:1, v/v).[35] The cyclic voltammograms of $[Ru(bipy)_2(CO)_2]^{2+}$ in acetonitrile indicates a more negative shift in the potentials where the peaks occur; this also occurs for other $[RuL^1(L^2)(CO)_2]^{2+}$ complexes (*see Table 1.2*)

Table 1.2. Peak potentials for the irreversible reduction for $[RuL^1(L^2)(CO)_2]^{2+}$

L^1	L^2	E_p (V *vs* SCE)	SOLVENT
bipy	bipy	-0.95	dmf
		-1.03	MeCN
bipy	dmbipy	-1.05	dmf
		-1.13	MeCN
dmbipy	dmbipy	-1.05	dmf
		-1.13	MeCN
phen	phen	-1.07	MeCN

When the electrocatalytic studies of the ruthenium complexes were done using acetonitrile-water as the solvent system, it was found that carbon monoxide was the only reduction product (*see Table 1.3*).

Table 1.3. Amount of carbon monoxide formed during the electrochemical reduction of carbon dioxide catalysed by ruthenium complexes in MeCN-water(4:1, v/v)

Catalyst	Amount of product[a] : CO/μmol
$[Ru(bipy)_2(CO)_2]^{2+}$	209(67.2)
$[Ru(bipy)(dmbipy)(CO)_2]^{2+}$	223(71.8)
$[Ru(dmbipy)_2(CO)_2]^{2+}$	203(65.3)
$[Ru(phen)_2(CO)_2]^{2+}$	191(61.5)
$[Ru(phen)_2(CO)Cl]^+$	207(66.6)
$[Ru(bipy)(CO)_2Cl_2]$	273(87.8)
$[Ru(dmbipy)(CO)_2Cl_2]$	205(66.0)

a: Current efficiency (%) in parenthesis; 60C consumed

The electrocatalytic activity of the ruthenium complexes was also shown to exist when the experiments were conducted in carbon dioxide saturated methanol; however in methanol the reduction products are carbon monoxide and formic acid (*see Table 1.4*).

These experiments illustrated that the amounts of products are dependent on the electrocatalyst that is used for the reduction; carbon monoxide production increases while formic acid production decreases with increasing donor properties of the ligand; *i.e.* the amount of carbon monoxide generated increases in the order $[Ru(bipy)_2(CO)_2]^{2+}$ < $[Ru(bipy)(dmbipy)(CO)_2]^{2+}$ < $[Ru(dmbipy)_2(CO)_2]^{2+}$; the amount of carbon monoxide produced also increases in the order $[Ru(bipy)(CO)_2Cl_2]$ < $[Ru(dmbipy)(CO)_2Cl]$.

Table 1.4. Amount of product produced by the electrochemical reduction of carbon dioxide catalysed by ruthenium complexes in methanol.

Catalyst	Amount of product [a]: in μmol	
	CO	HCOO⁻
$[Ru(bipy)_2(CO)_2]^{2+}$	81(26.1)	154(49.5)
$[Ru(bipy)(dmbipy)(CO)_2]^{2+}$	106(34.2)	123(39.8)
$[Ru(dmbipy)_2(CO)_2]^{2+}$	139(44.7)	101(32.5)
$[Ru(phen)_2(CO)_2]^{2+}$ [b]	108(34.7)	76(24.5)
$[Ru(phen)_2(CO)Cl]^+$ [b]	123(39.6)	40(12.9)
$[Ru(bipy)(CO)_2Cl_2]$	85(27.3)	117(37.7)
$[Ru(dmbipy)(CO)_2Cl_2]$	122(39.2)	83(26.8)

a: current efficiency (%) in parenthesis, 60C consumed

b: in MeCN/MeOH (4:1, v/v) due to solubility of complexes

The [Re(bipy)(CO)₃Cl] complex was one of the first metal polypyridyl complexes that catalysed the reduction of carbon dioxide by both photochemical[36,37] and electrochemical[37,38] means. The reactivity of the [Re(bipy)(CO)₃Cl] was studied in a dimethylformamide solution containing either 0.1M Et₄NCl or Bu₄NClO₄ as supporting electrolyte. [Re(bipy)(CO)₃Cl] is a selective electrocatalyst for the reduction of carbon dioxide to carbon monoxide at a potential of -1.25V *vs* NHE.

The efficiency of the system shows a marked dependence on the amount of water present in solution (*see Figure 1.6*). The optimum efficiency of the system occurred when about 10% of water was present, higher amounts of water in solution leading to less efficiency and to a

decrease in catalytic activity; when no water was present the electro-generation of carbon monoxide was non-linear (*see Figure 1.6*).

Several bulk electrolysis experiments were conducted in an effort to determine which species was actually responsible for carbon dioxide reduction. When the electrolysis was conducted under a carbon dioxide atmosphere there was no accumulation of a reduced species in the cell; however after the cell was flushed with nitrogen, followed by two hours of electrolysis, an orange species accumulated in the solution and there was a dramatic decrease in electron consumption. When carbon dioxide was re-admitted into the system, the orange colour disappeared and the electrocatalytic reduction of carbon dioxide continued with the same efficiency as before (*see Figure 1.6, domain after point b*). From this piece of evidence it was concluded that the orange species was most probably the active precursor $[Re(bipy)(CO)_3Cl]^-$ and was responsible for the reduction of carbon dioxide. Similar results were obtained when the experiment was carried out in the presence of 10% of water; in the absence of carbon dioxide hydrogen was generated with a faradaic yield of 85%. In the presence of carbon dioxide the reduction of water was completely inhibited; this indicated that $[Re(bipy)(CO)_3Cl]^-$ was less reactive towards water than towards carbon dioxide. Under optimal conditions no formato-rhenium species, $[Re(bipy)(CO)_3HCOO]$, could be detected; thus implying that $[Re(bipy)(CO)_3Cl]$ is a highly specific electrocatalyst for the reduction of carbon dioxide to carbon monoxide.

When Et_4NCl or Bu_4NClO_4 were used as supporting electrolytes only carbon monoxide was detected as a product of the electrochemical reduction of carbon dioxide. When NH_4PF_6 was used as supporting electrolyte, no carbon monoxide was detected but almost quantitative amounts of hydrogen were formed, traces of the formato-rhenium complex were found and a green rhenium (0) dimer $[\{Re(bipy)(CO)_3\}_2]$ precipitated out of solution. From these studies it was proposed that in this system the nature of the supporting electrolyte or more importantly, whether it's anion was ligating (Cl^- or ClO_4^-) rather than PF_6^- played an important role in the observed electrocatalytic processes (*i.e.* carbon dioxide reduction, water reduction and dimer formation). It was concluded that when the vacant site was blocked by

excess ligating ligand, then the only process observed was the electrocatalytic reduction of carbon dioxide to carbon monoxide. When anion dissociation was promoted, the major processes where dimerisation and proton reduction, the latter being in fact formed by the presence of NH_4^+.
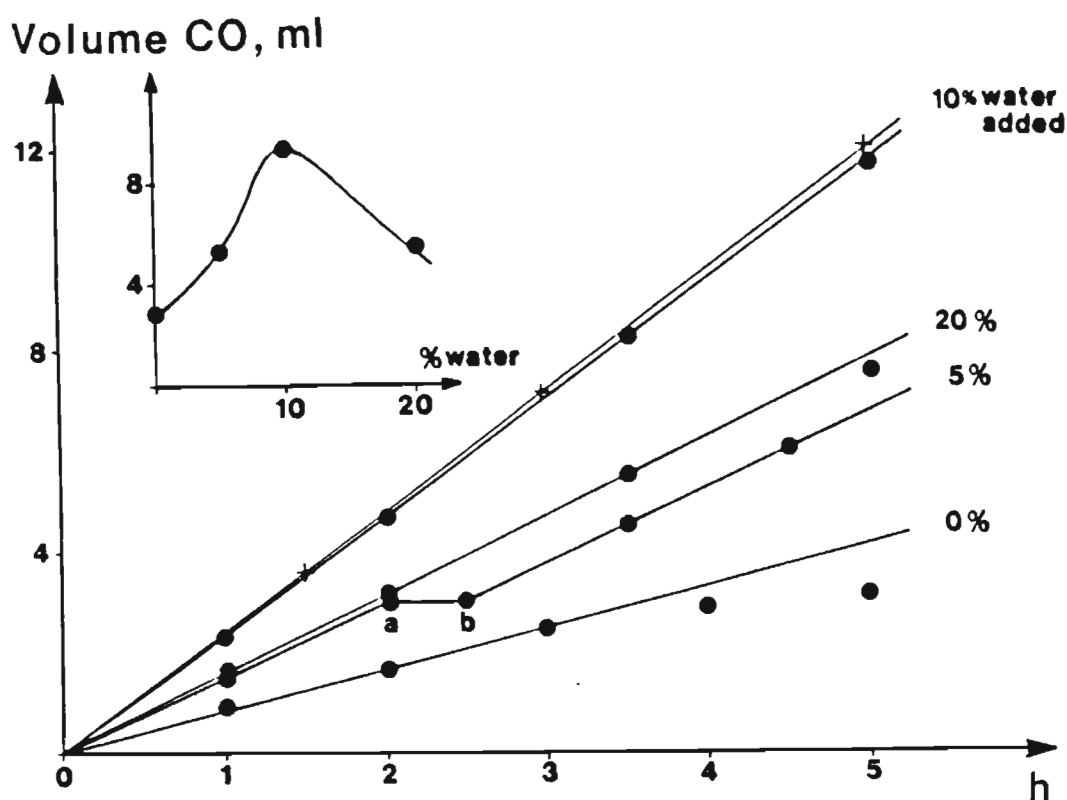
Figure 1.6. Graph of CO generated electrochemically as a function of water added and time

Hawecker and co-workers proposed that in the presence of excess ligating ligand (*see Scheme 1.7*) it can be assumed that the chloride ligand is always bonded to rhenium; *i.e.* there is always a Re-Cl bond present.[39,40] The first step involves a one electron reduction which is followed by the loss of a carbon monoxide molecule or a pyridine unit to give a sesqui bipyridine ligand (*i.e.* a bipyridine ligand in which only one nitrogen atom is coordinated), to give a seventeen electron rhenium complex that has a vacant site available for fixation of carbon dioxide. The reduction of carbon dioxide is initiated by formation of a

metallocarboxylic complex *via* nucleophilic attack of a formally zero valent rhenium centre on an electrophilic carbon centre of the carbon dioxide molecule. This is followed by the uptake of a proton and subsequent loss of a water molecule; another one electron reduction results in the regeneration of the starting material.

Scheme 1.7. Proposed mechanism for CO$_2$ reduction by [Re(bipy)(CO)$_3$Cl] [37]
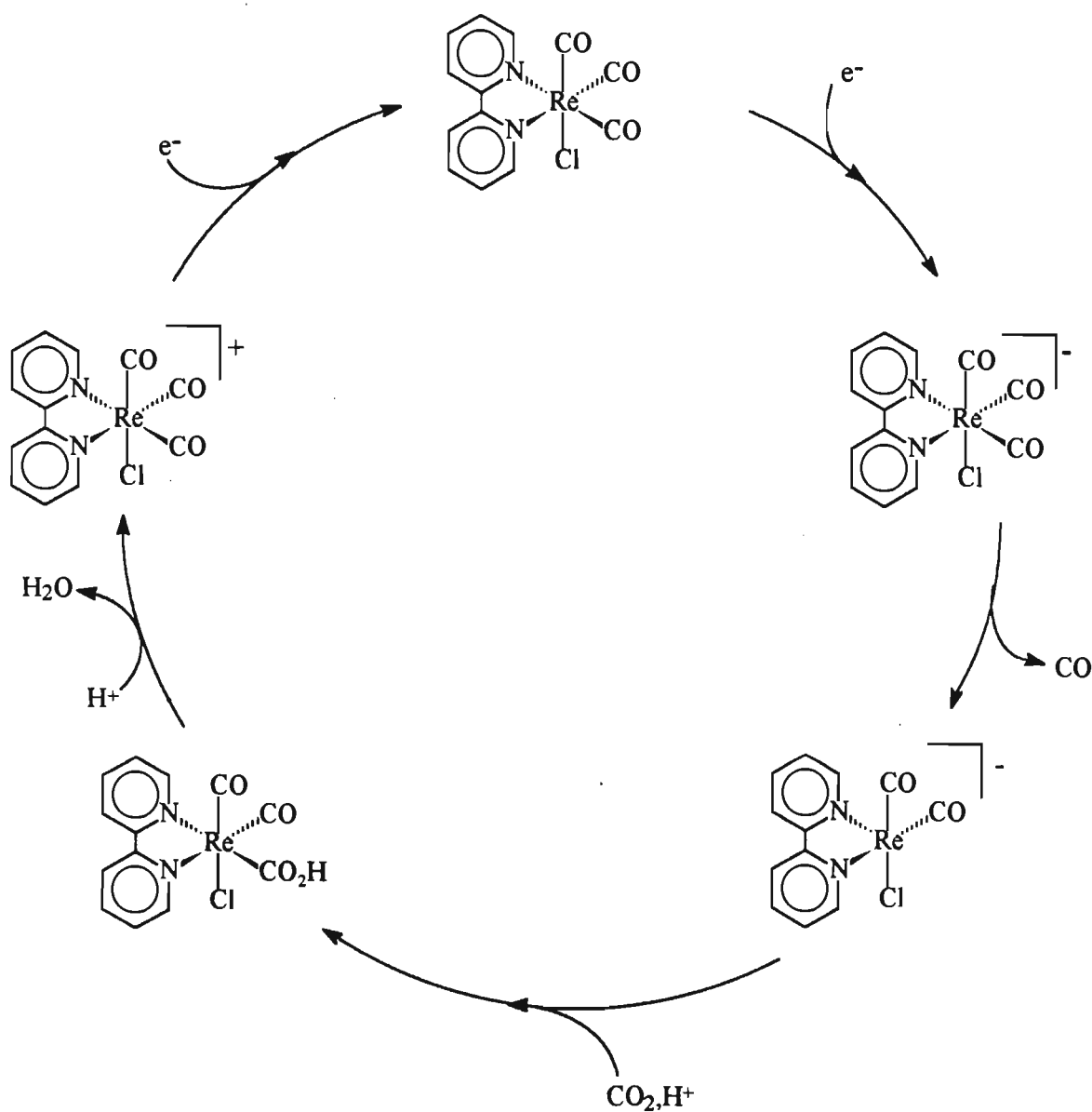
In the absence of excess chloride ions, it is proposed that the labilisation of a chloride ion from the rhenium complex results in the formation of a seventeen electron species which may pick up a second electron and a proton to give the hydrido complex [Re(bipy)(CO)$_3$H]. The carbon dioxide molecule then inserts into the Re-H bond which would then yield the formato complex. The formato group may then be displaced by a chloride ligand to regenerate the starting complex.

Sullivan and co-workers also investigated the electrocatalytic carbon dioxide reduction properties of the [Re(bipy)(CO)$_3$Cl] system but in acetonitrile with TBAH as supporting electrolyte.[18,41] From examination of the cyclic voltammogram the first reduction (*see Figure 1.7*) at E$_{\frac{1}{2}}$ = -1.35V *vs* SCE was assigned to be ligand localised while the second irreversible reduction at E$_{\frac{1}{2}}$ = -1.71V *vs* SCE is assigned to a metal based reduction.
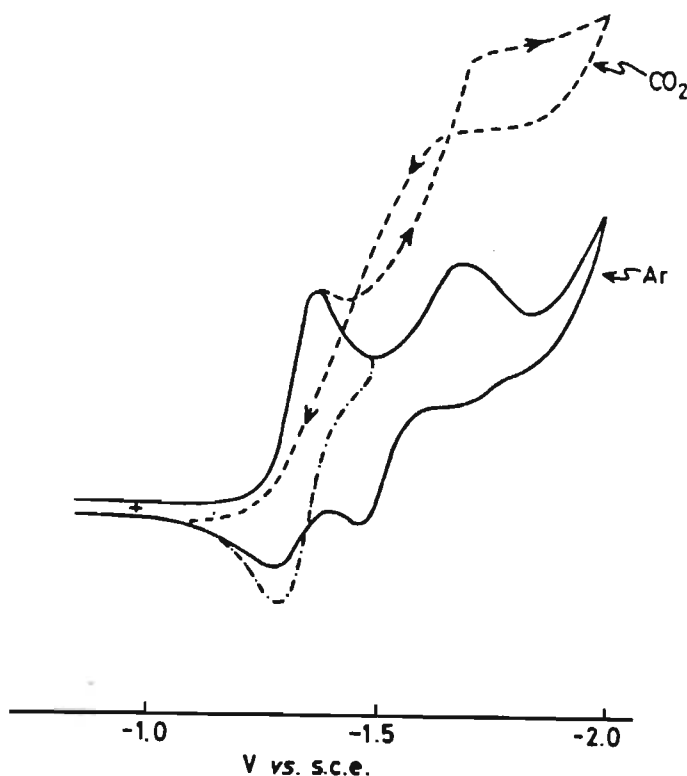
Figure 1.7. Cyclic voltammograms of [Re(bipy)(CO)$_3$Cl] in acetonitrile

Sullivan *et al* were not satisfied with the mechanism proposed by Hawecker *et al*[36,37] ; they felt that a mechanism that involved an intermediate with a sesqui-bipyridine ligand was not plausible because such an intermediate would rapidly lose the bipyridyl ligand and subsequently lose catalytic activity. They proposed that there are four competitive pathways involved in the production of carbon monoxide and formate with the rhenium system (*see Schemes 1.8 - 1.10*).

The first pathway (*see Scheme 1.8*) illustrates the proposed mechanism for carbon monoxide and carbonate ion formation. The first step involves a one electron reduction of $[Re(bipy)(CO)_3X]$; this in turn is followed by the slow labilisation of the halide anion to form the neutral intermediate $[Re(bipy)(CO)_3]$ which then reacts with a molecule of carbon dioxide to form $[Re(bipy)(CO)_3(CO_2)]$. This is then followed by a dimerisation reaction that is accompanied by the formation of a carbon monoxide molecule, the carbonato dimer then undergoing a one electron reduction to form $[Re(bipy)(CO)_3]$ and $[Re(bipy)(CO)_3(CO_3)]^-$; the anionic rhenium species then undergoes a further one electron reduction to yield the bicarbonate ion and $[Re(bipy)(CO)_3]$.

The second proposed pathway (*see Scheme 1.9*) involves the highly reactive intermediate $[Re(bipy)(CO)_3]^-$, which is generated by the one electron reduction of $[Re(bipy)(CO)_3X]^-$; this being accompanied by the liberation of the halide anion . A carbon dioxide molecule is then bonded to the rhenium complex; this is followed by a two electron reduction which is accompanied by the co-ordination of a second carbon dioxide molecule. An oxygen acceptor, A, is also involved in this step of the pathway; however the nature of the oxide ion acceptor is not known. This series of "successive" reactions in this step lead to the formation of carbon monoxide and the regeneration of $[Re(bipy)(CO)_3]^-$.

The third proposed mechanistic pathway leads to the production of formate (*see Scheme 1.10*). The first step involves the insertion of a carbon dioxide molecule into the Re-H bond in $[Re(bipy)(CO)_3H]$ and the formation of the formato complex $[Re(bipy)(CO)_3CO_2H]$; this is followed by a one electron reduction of the formato complex to form $[Re(bipy)(CO)_3CO_2H]^-$

Scheme 1.8. Proposed Pathway 1 for CO₂ reduction by [Re(bipy)(CO)₃X] [18]
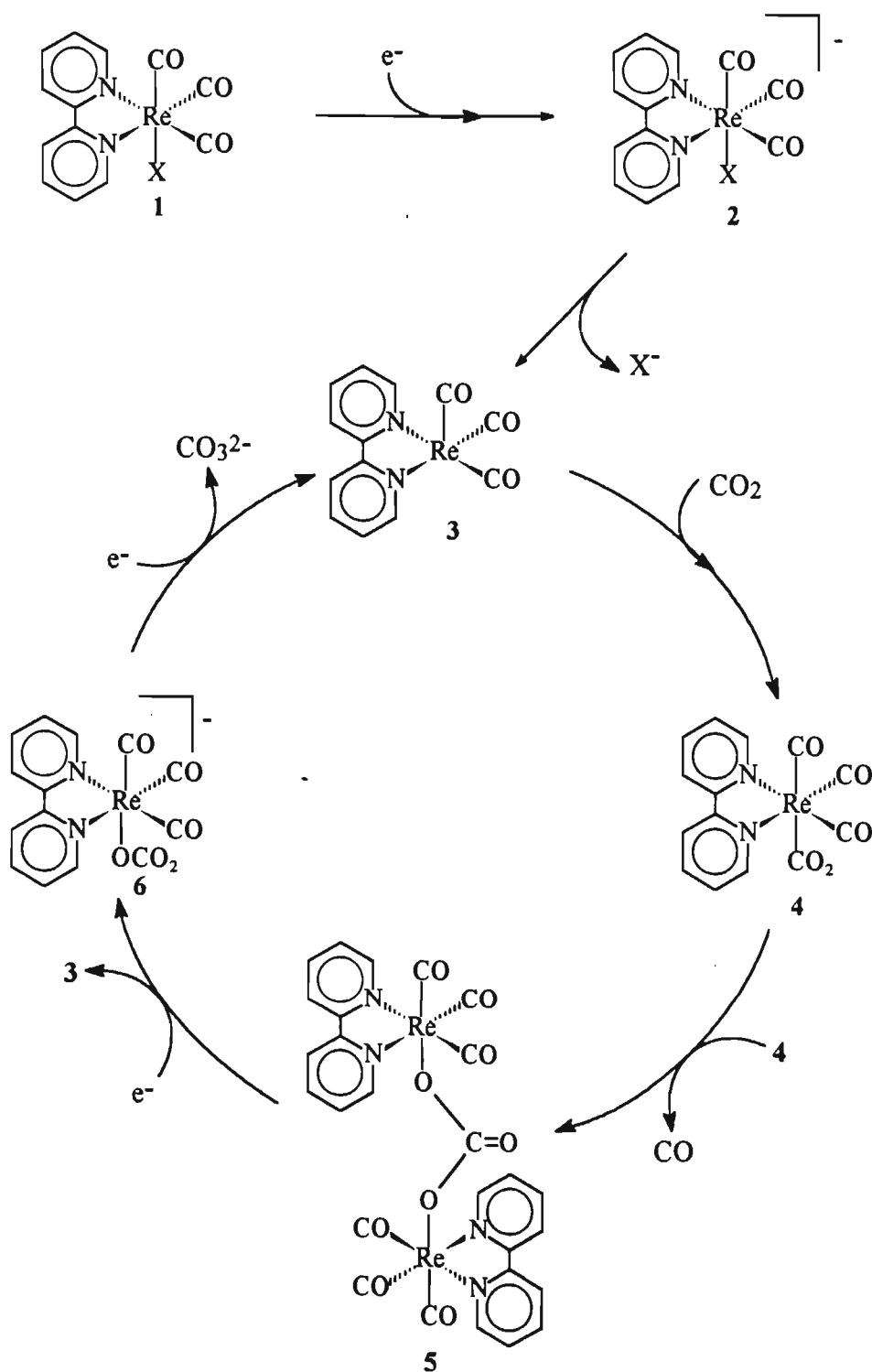
The formate group is then liberated from this complex by either one of the following routes:

(i). the slow dissociation of the formate to form $[Re(bipy)(CO)_3]$ and $HCOO^-$; or

(ii). a second one electron reduction occurs and this is followed by the rapid dissociation of formate and the generation of $[Re(bipy)(CO)_3]^-$.

The fourth pathway involves the direct interaction of $[Re(bipy)(CO)_3X]^-$ with carbon dioxide; however there is only limited evidence for this pathway at the present time.[42] It is believed that $[fac\text{-}Re(bipy)(CO)_3X]^-$ is only a catalyst precursor and that the rate limiting step is the further reduction of an intermediate complex.

Scheme 1.9. Proposed Pathway 2 for CO_2 reduction by $[Re(bipy)(CO)_3X]$ [18]
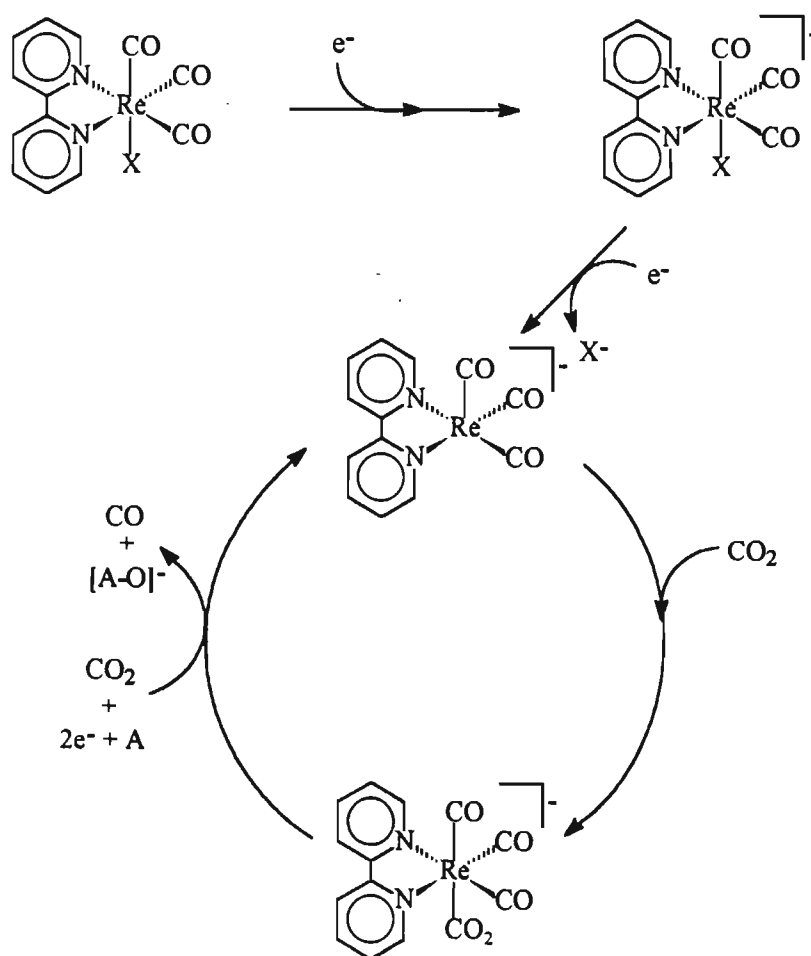
Scheme 1.10. Proposed Pathway 3 for CO$_2$ reduction by [Re(bipy)(CO)$_3$X] [18]
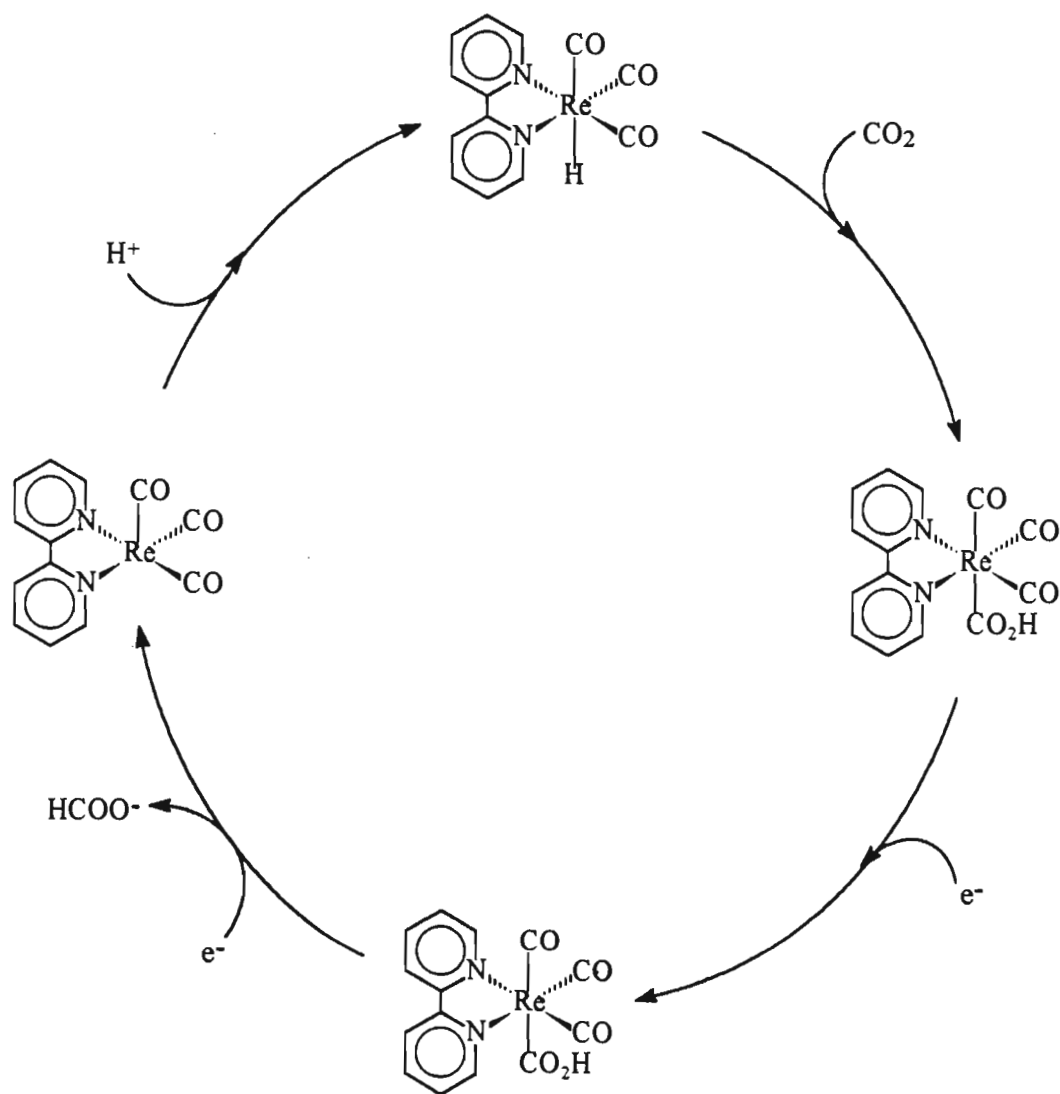
Christensen *et al* carried out an *in situ* infrared study of the electrochemical reduction of carbon dioxide catalysed by [Re(dmbipy)(CO)$_3$Cl] in an attempt to identify the intermediates in the catalytic cycle.[43] The infrared spectra indicate an absorption at 2150cm^{-1} due to gain of carbon monoxide; this is accompanied by a loss of carbon dioxide which can be observed as a decrease in the peak size at 2342cm^{-1}. There is a sharp band present at 1640cm^{-1} that is assigned to the carbonate ion; this band is not present when the experiment is conducted under a nitrogen atmosphere.

Infrared studies indicate that the intensity of both the carbon monoxide and carbonate ion band is far smaller than expected for the complete conversion of the carbon dioxide to carbon monoxide and the carbonate ion. This suggests that much of the carbon dioxide is held in the form of two complexes, A and B. The infrared spectra in the carbonyl region indicated that two species form on reduction in the presence of carbon dioxide. Complex A is formed initially with peaks at 2010, 1902 and 1878cm^{-1} while complex B is formed at more negative potentials with peaks at 1997 and 1860cm^{-1}.

The infrared spectra were used in an attempt to identify complexes A and B. By using ligand effect constants (ε) of -CO$_2$H and -CO$_2^-$; from the spectrum of *fac*-[Re(dmbipy)(CO)$_3$CO$_2$H] they obtained ε [CO$_2$H]^{cis} = 137 Nm^{-1} and ε [CO$_2$H]^{trans} = 65 Nm^{-1}. Using these values the υ(CO) frequencies for *fac*-[Re(dmbipy)(CO)$_3$CO$_2$H] were predicted to occur at 2014, 1914 and 1864cm^{-1}, which is in fair agreement with those observed for complex A; refining the fit predicts υ(CO) values of 2012, 1905 and 1876cm^{-1}.

There are two possibilities for complex B; one is that B is a further reduced species; using the ligand effect constants for (dmbipy$^-$), the υ(CO) frequencies for [Re(dmbipy$^-$)(CO)$_3$(CO$_2$H)] are predicted at 1992, 1867 and 1866cm^{-1} which are in good agreement with those observed. A second possibility for B is the deprotonated form of A; this would be expected to cause shifts between A and B of the same order of magnitude as those observed.

The following mechanism emerges from these initial observations in the absence of appreciable concentrations of proton donor (*see Scheme 1.11*). The first step involves the one electron reduction of [Re(dmbipy)(CO)$_3$Cl] which is followed by the loss of a chloride ion and the rapid co-ordination of carbon dioxide. [Re(dmbipy)(CO)$_3$(CO$_2$)] can either ;

(i).   undergo a one electron reduction and abstract a proton from water to form [Re(dmbipy)(CO)$_3$(CO$_2$H)] and hydroxide ions; the hydroxide ion reacts with a molecule of carbon dioxide to form a bicarbonate ion and a proton, or

(ii).   two equivalents of [Re(dmbipy)(CO)$_3$(CO$_2$)] can react with carbon dioxide and two equivalents of chloride ions; resulting in the formation of carbon monoxide and carbonate ions as well as the regeneration of the starting material [Re(dmbipy)(CO)$_3$Cl].

[Re(dmbipy)(CO)$_3$(CO$_2$H)] can also undergo two possible reactions;

(i).   a one electron reduction to form [Re(dmbipy)(CO)$_3$(CO$_2$H)]$^-$; which then reacts with a chloride ion and carbon dioxide to regenerate starting material [Re(dmbipy)(CO)$_3$Cl], carbonate ions and hydrogen gas.

(ii).   a one electron reduction to form [Re(dmbipy)(CO)$_3$(CO$_2$)]$^-$ and gaseous hydrogen. [Re(dmbipy)(CO)$_3$(CO$_2$)]$^-$ then reacts with a chloride ion and carbon dioxide to regenerate starting material ([Re(dmbipy)(CO)$_3$Cl]) and carbonate ions.

Christensen *et al* also proposed a mechanism for carbon dioxide reduction in the presence of 10%water (v/v) (*see Scheme 1.12*). The first step involves the one electron reduction of [Re(dmbipy)(CO)$_3$Cl] to generate [Re(dmbipy)(CO)$_3$Cl]$^-$ which loses the chloride anion and reacts rapidly with a molecule of carbon dioxide; this is followed by another one electron reduction that is accompanied by reaction with a proton to generate [Re(dmbipy)(CO)$_3$(CO$_2$H)] which then reacts with acetonitrile and a proton to form [Re(dmbipy)(CO)$_3$(CH$_3$CN)]$^+$ and carbon monoxide and water. [Re(dmbipy)(CO)$_3$(CH$_3$CN)]$^+$ undergoes a two electron reduction that is accompanied with the loss of an acetonitrile ligand to form [Re(dmbipy)(CO)$_3$]$^-$. [Re(dmbipy)(CO)$_3$]$^-$ can then react with carbon dioxide and a proton to form [Re(dmbipy)(CO)$_3$(CO$_2$H)] which can re-enter the catalytic cycle. The infra red spectrum

supports this mechanism because the peak due to the carbonate ion at $1650 cm^{-1}$ is no longer present.

Scheme 1.11. Mechanism for CO_2 reduction by $[Re(dmbipy)(CO)_3Cl]$ in the absence of appreciable concentrations of proton donor [43]
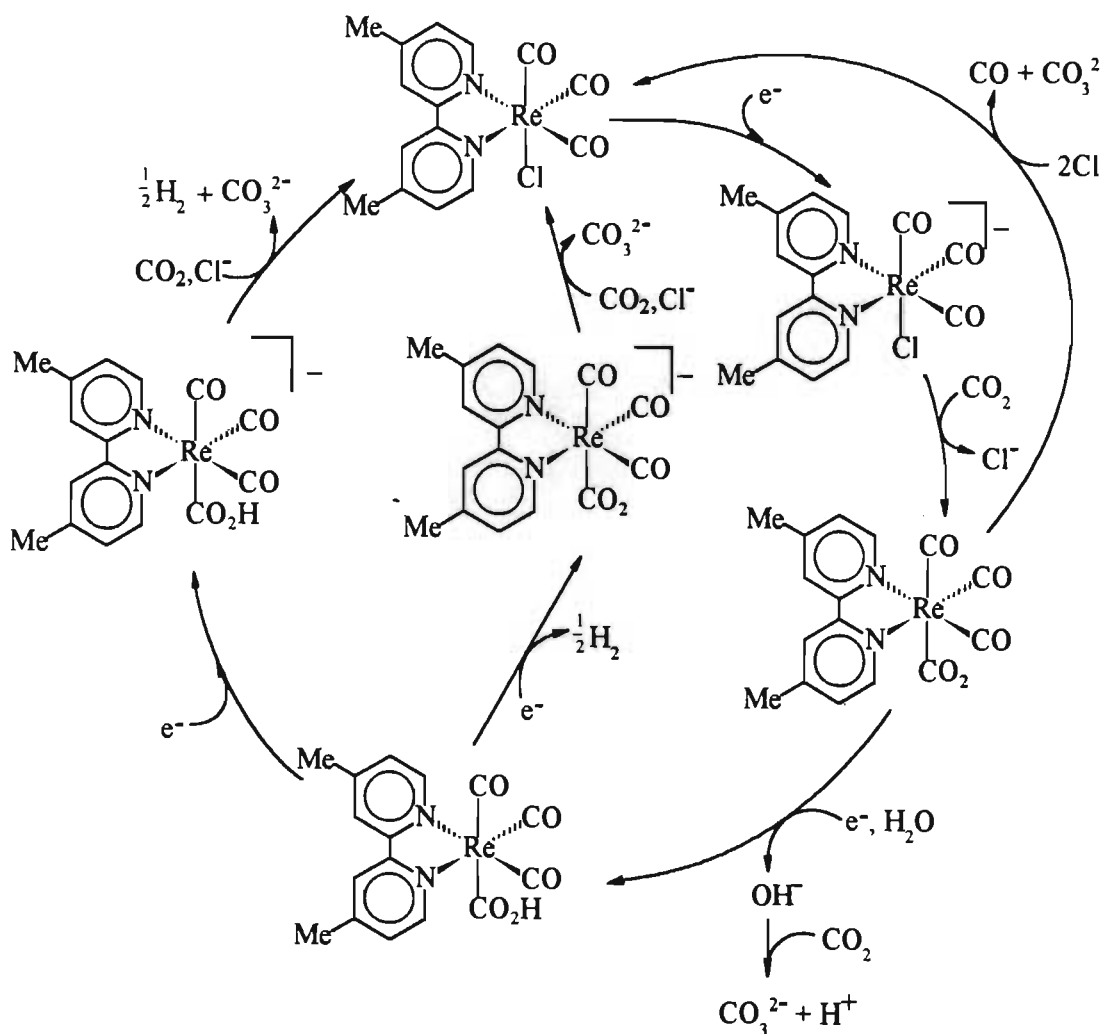
Scheme 1.12. Mechanism for CO$_2$ reduction by [Re(dmbipy)(CO)$_3$Cl] in the presence of water[43] .
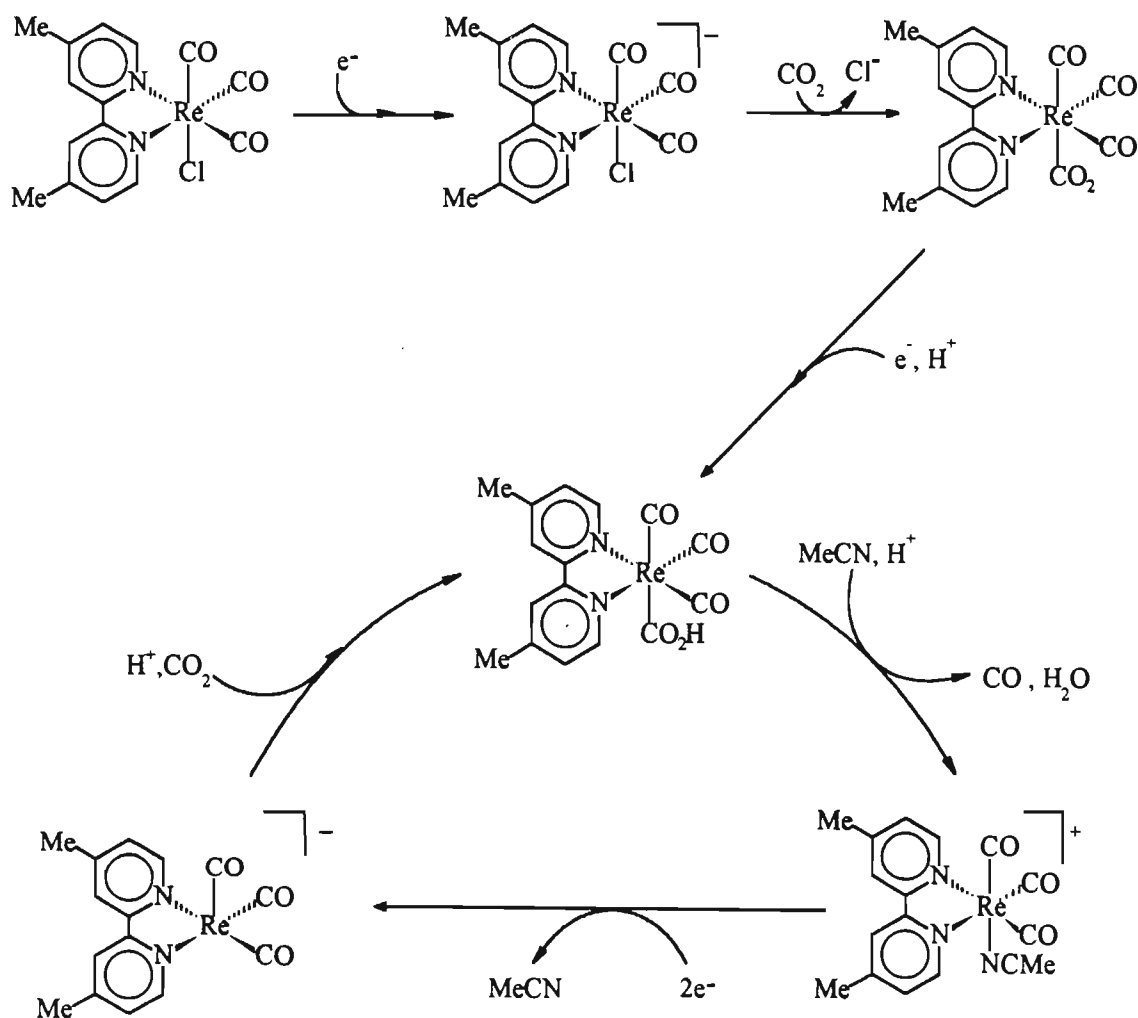
Sullivan *et al* reported that [Rh(bipy)$_2$X$_2$]$^+$ and [Ru(terpy)(dppe)Cl]$^+$ act as electrocatalysts for carbon dioxide reduction in acetonitrile.[44,45] The cyclic voltammogram of [Rh(bipy)$_2$X$_2$]$^+$ (*see Figure 1.8*) indicates that initially there is an irreversible two electron reduction which is followed by two stepwise one electron reductions to [Rh(bipy)$_2$] (*ca* -1.25V) and [Rh(bipy)$_2$]$^-$ (*ca* -1.55V) under a nitrogen atmosphere. When the experiment is repeated under a carbon dioxide atmosphere there is current enhancement at *ca* -1.55V.
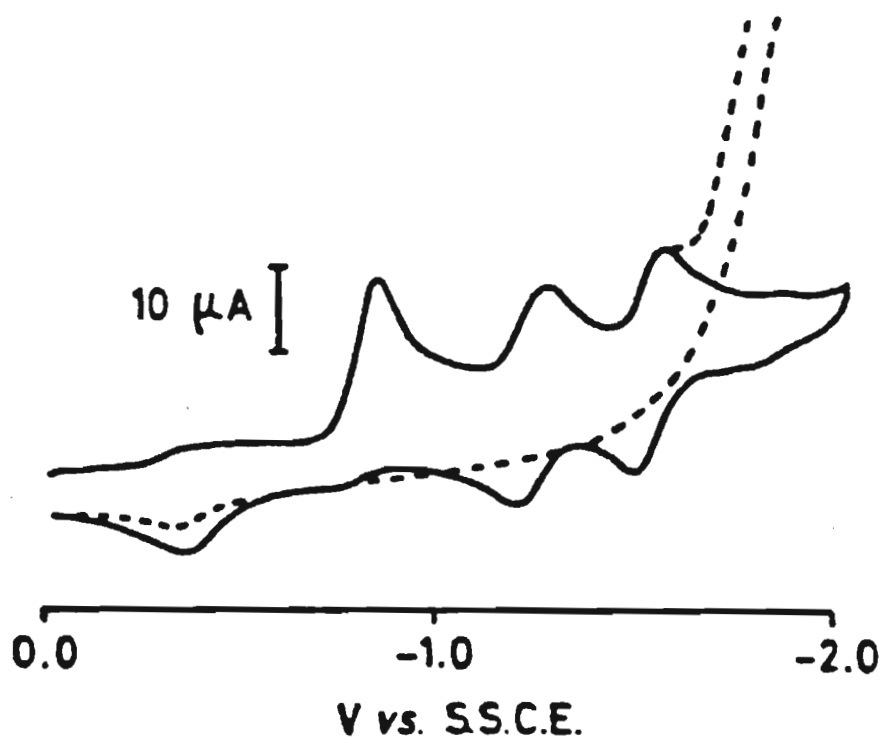
Figure 1.8. Cyclic voltammograms for [Rh(bipy)$_2$X$_2$]$^+$

Scheme 1.13 outlines the proposed mechanism; the first two electron reduction involves the formation of [Rh(bipy)$_2$] and the loss of the anionic ligands. [Rh(bipy)$_2$] then undergoes two one electron reductions to form [Rh(bipy)$_2$]$^-$ which then reacts with a carbon dioxide molecule to form [Rh(bipy)$_2$CO$_2$]$^-$. [Rh(bipy)$_2$CO$_2$]$^-$ then reacts with [N(*n*-Bu)$_4$]$^+$ (from the

supporting electrolyte) to form [Rh(bipy)₂CO₂H] which then undergoes a two electron reduction to form [Rh(bipy)₂] and HCOO⁻.

Scheme 1.13. Mechanism for CO_2 reduction by [Rh(bipy)₂X₂]⁺ [44]
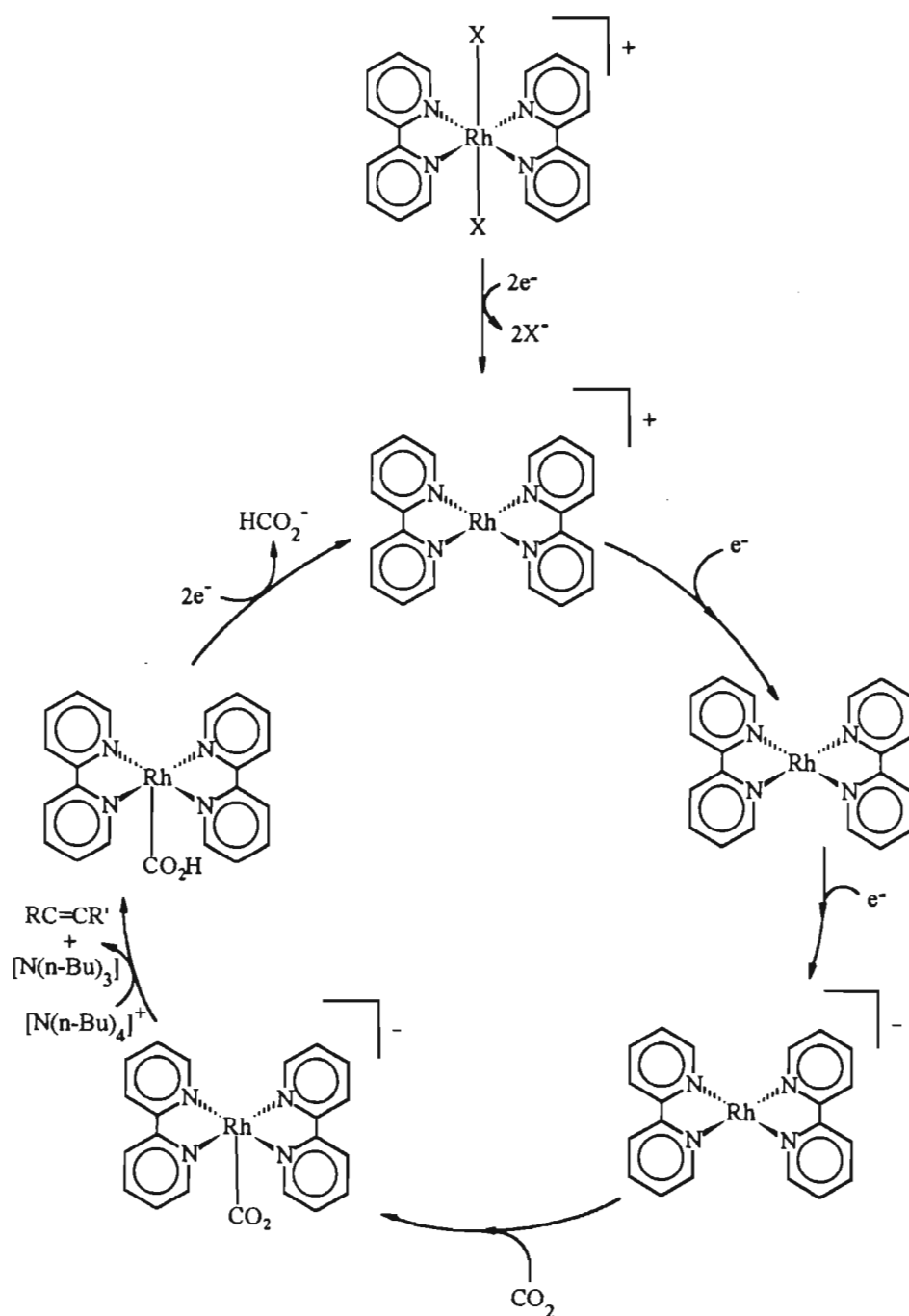
The cyclic voltammogram of [Ru(terpy)(dppe)Cl]$^+$ (*see Figure 1.9*) indicates a single irreversible two electron reduction at *ca* -1.4V under a nitrogen atmosphere; under a carbon dioxide atmosphere there is a small catalytic enhancement at the onset of the two electron reduction.[44] However at more negative potentials there is significant increase in catalytic activity.
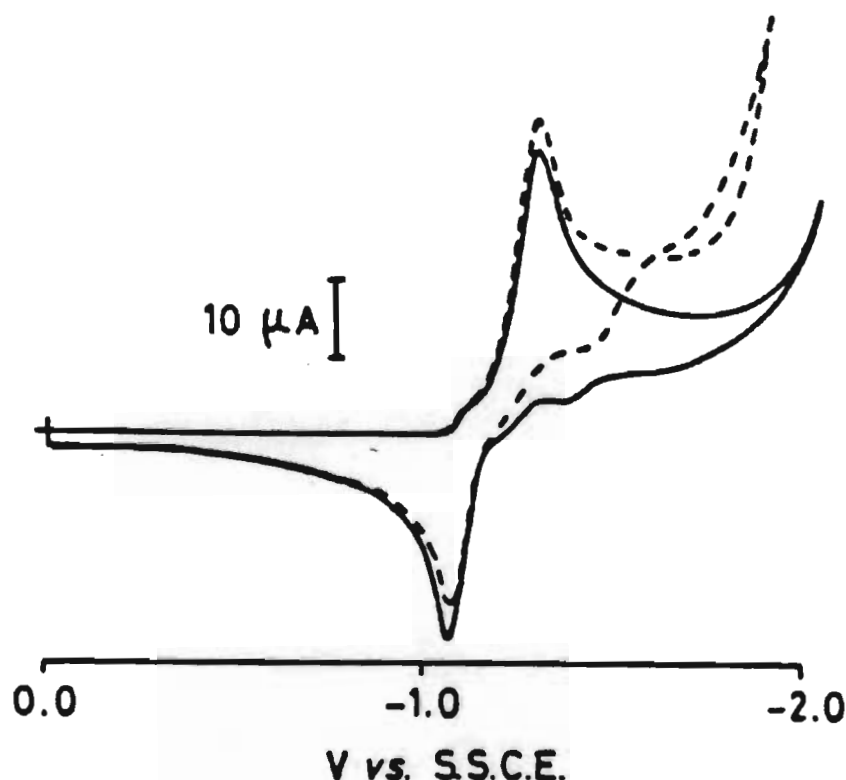
Figure 1.9. Cyclic voltammograms of [Ru(terpy)(dppe)Cl]$^+$

The following mechanism has been proposed (*see Scheme 1.14*); the first two electron reduction is accompanied by the loss of the chloride ion and results in the formation of [Ru(terpy)(dppe)]. A carbon dioxide molecule is then co-ordinated to form [Ru(terpy)(dppe)CO$_2$] which then reacts with [N(n-Bu)$_4$]$^+$ to form [Ru(terpy)(dppe)(CO$_2$H)]$^+$. This complex then loses a hydroxy group to form [Ru(terpy)(dppe)CO]$^{2+}$ which then undergoes a two electron reduction to form [Ru(terpy)(dppe)] ; this is accompanied by the loss of a carbon monoxide molecule. The hydroxy group reacts with a molecule of carbon dioxide to form HCO$_3^-$.

Scheme 1.14. Mechanism for CO₂ reduction by [Ru(terpy)(dppe)Cl]⁺ [44]
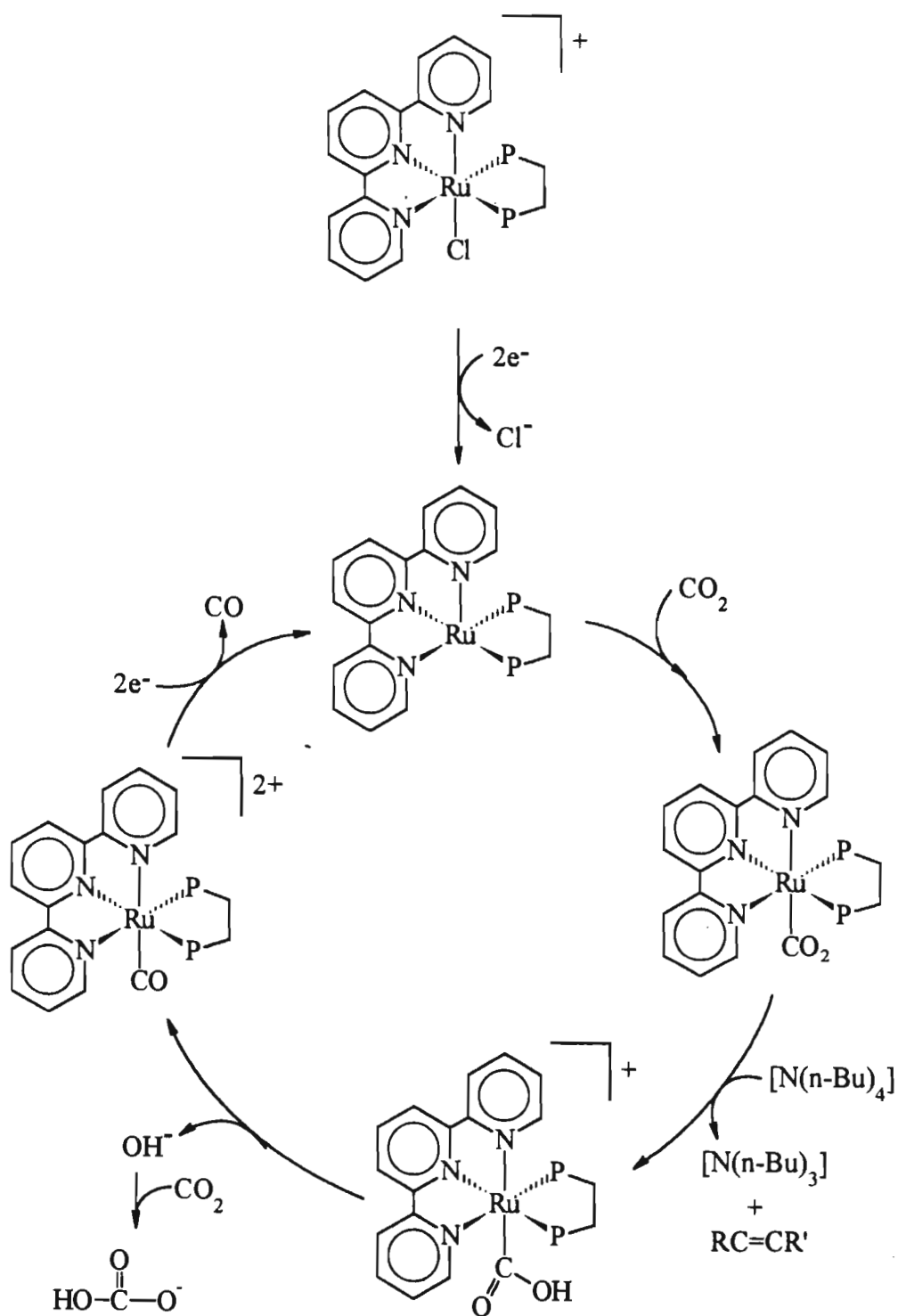
Brewer *et al* synthesised a range of novel rhodium and iridium compounds with various polypyridyl ligands; these compounds functioned as electrocatalysts for the electrochemical reduction of carbon dioxide.[46] The compounds have the general formula $[M(L)_2X_2]^+$ where M = Rh or Ir and L = 2,2'-bipyrimidine, 2,3-*bis*-(2-pyridyl)pyrazine, 2,3-*bis*-(2-pyridyl)-quinoxaline and 2,3-*bis*-(2-pyridyl)benzoquinoxaline. Bulk electrolysis experiments revealed that the reduction products are carbon monoxide and formic acid. The mechanism is similar to that proposed by Sullivan (*see Scheme 1.13*).[44,45]

The complex *cis*-[Os(bipy)$_2$(CO)H][PF$_6$] was synthesised by Sullivan and co-workers; they found that *cis*-[Os(bipy)$_2$(CO)H][PF$_6$] is an efficient electrocatalyst for the reduction of carbon dioxide in an acetonitrile/0.1M tetra-*n*-butyl ammonium hexafluorophosphate solution at a platinum working electrode.[18,47,48] Carbon monoxide is the dominant product of carbon dioxide reduction under anhydrous conditions but the addition of water results in up to 25% formate being formed.

The cyclic voltammograms of *cis*-[Os(bipy)$_2$(CO)H][PF$_6$] in argon deoxygenated acetonitrile solution that contains 0.1M TBAH as supporting electrolyte show two one electron bipyridine based reversible reductions at $E_{1/2}$ = -1.34V and $E_{1/2}$ = -1.60V (*vs* SSCE) (*see Figure 1.10*). When the same experiment was carried in a carbon dioxide saturated acetonitrile solution the current for the first peak remained unchanged while the current for the second peak was greatly enhanced, hence it could be concluded that the doubly reduced form *cis*-[Os(bipy)$_2$(CO)H]$^-$ is reactive towards carbon dioxide.

Sullivan *et al* proposed the following mechanism (*see Scheme 1.15*); the first step involves a one electron reduction of *cis*-[Os(bipy)$_2$(CO)H][PF$_6$] at *ca*. -1.35V to form the neutral complex *cis*-[Os(bipy)$_2$(CO)H]; a second one electron reduction results in the formation of the anionic species *cis*-[Os(bipy)$_2$(CO)H]$^-$. This doubly reduced species then reacts with a molecule of carbon dioxide to form an intermediate I$_a$. This intermediate can undergo either one of two reactions, depending on reaction conditions;

(i).   in dry acetonitrile I_a undergoes bimolecular self reaction and forms two neutral *cis*-[Os(bipy)$_2$(CO)H] complexes as well as carbon monoxide and carbonate ions; or

(ii).   in the presence of water a new pathway appears, the intermediate I_a reacts with water to form a second intermediate I_b; this intermediate can also react further *via* two pathways. The first involves I_b breaking up into the formate anion and the starting complex; while the second possibility involves the uptake of a molecule of carbon dioxide by I_b and this is followed by the dissociation of a molecule of carbon monoxide, HCO_3^- and starting complex.
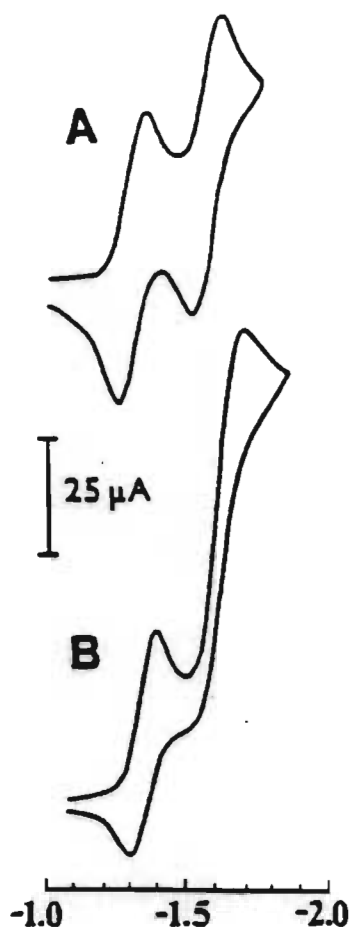
Figure 1.10. Cyclic voltammograms of *cis*-[Os(bipy)$_2$(CO)H][PF$_6$] under nitrogen (A) and carbon dioxide (B)

Scheme 1.15. Mechanism for CO$_2$ reduction by *cis*-[Os(bipy)$_2$(CO)H][PF$_6$] [48]

$$CO_2 + OH^- \xrightarrow{\text{fast}} HCO_3^-$$
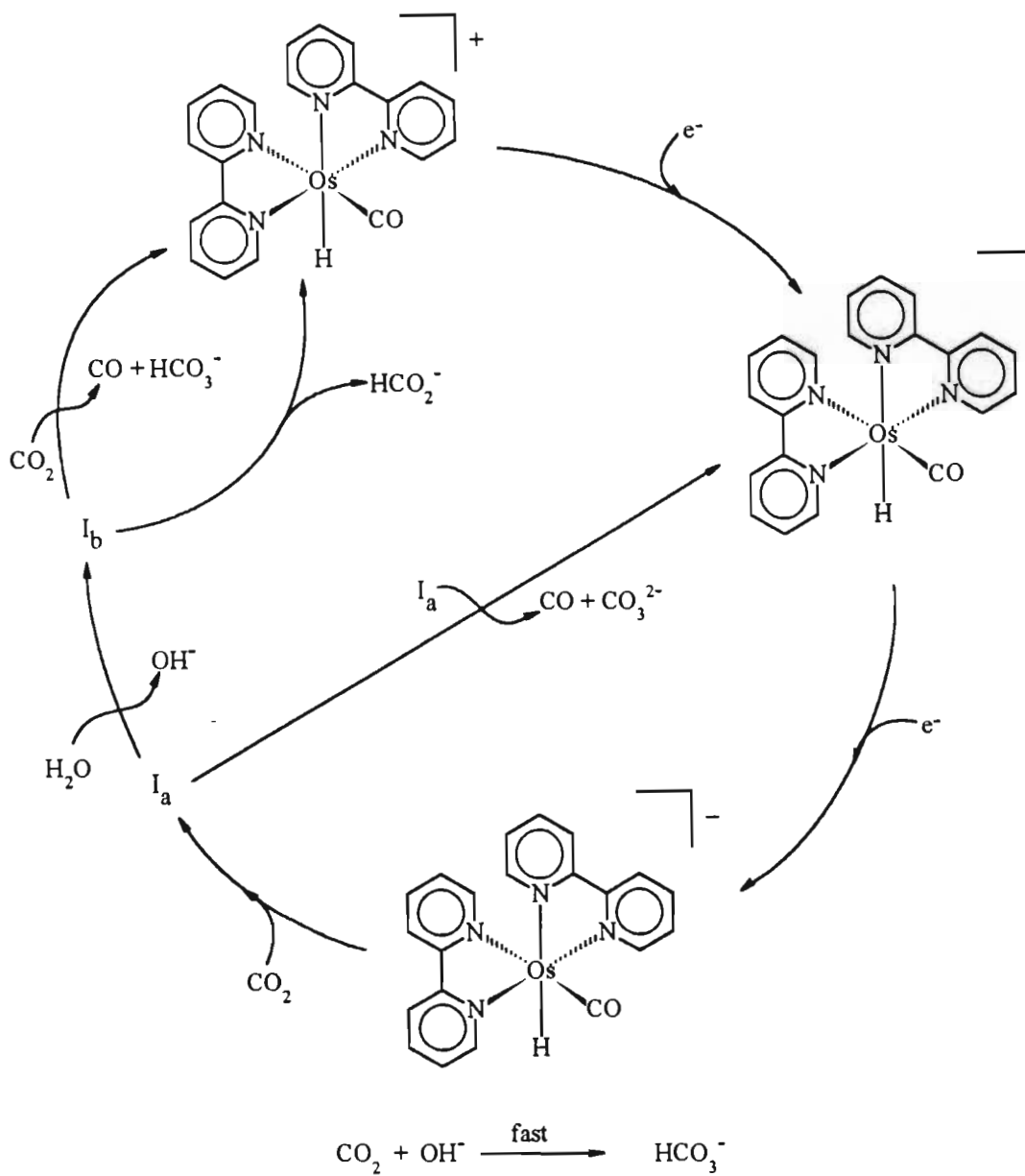
An alternate mechanism for the formation of HCO_3^- has been suggested; this involves the reaction of a hydroxide group (generated after the reaction between I_a and water) with a molecule of carbon dioxide to form HCO_3^-.

The following conclusions, based on the assumption that a competition exists between reaction of I_a with a second I_a and reaction of I_a with water, has been proposed; at high concentrations of water ([water] = 0.3M) or at low concentrations of complex the water dependent pathway increases in importance, the self reaction of I_a is no longer competitive and the rate determining step is assumed to be the reaction between *cis*-$[Os(bipy)_2(CO)H]^-$ and carbon dioxide. The following formulations for the intermediate I_a have been proposed;

(a).   an acyl intermediate, *cis*-$[Os(bipy)_2(CO)_2\{C(O)H\}]^-$, in which the addition of carbon dioxide induces acyl formation,

(b).   a higher co-ordinate carbon dioxide addition product, *cis*-$[Os(bipy)_2(CO_2)(CO)H]^-$,

(c).   a bipyridine ring opened intermediate, *cis*-$[Os(py-py)(bipy)(CO_2)(CO)H]^-$ where py-py is a sesqui co-ordinated bipyridine ligand, or

(d).   a carbon dioxide adduct of the bipyridine ligand.

From the appearance of carbon monoxide and HCO_3^- as products of the reaction involving I_b, a plausible explanation obtaining both products is to invoke protonation at either C of the co-ordinated carbon dioxide to give HCO_3^-, or at O to give carbon monoxide.

A deuterium labelled complex, *cis*-$[Os(bipy)_2(CO)D][PF_6]$, was used under conditions where the formate anion was a significant product, there was no proton incorporation into the osmium catalyst after 1.8 turnovers with respect to formate anion production. When *ca.* 0.7M D_2O was added to a *cis*-$[Os(bipy)_2(CO)H][PF_6]$ solution, upon electrolysis to 100°C passed, no decrease in the hydride stretch at 2005cm^{-1} was observed. Also when $^{13}CO_2$ was used as the source of carbon dioxide there was no incorporation into the carbonyl group of the catalyst after 5.5 turnovers of the catalyst with respect to carbon monoxide formation. These observations led Sullivan *et al* to propose an associative mechanism for the co-ordination of carbon dioxide rather than an insertion mechanism.

An interesting comparison was drawn between the mechanism for carbon dioxide reduction using *cis*-[Os(bipy)$_2$(CO)H][PF$_6$] as electrocatalyst and that proposed by Amatore and Saveant[3,19] for the uncatalysed reduction (*see Scheme 1.2*) of carbon dioxide in acetonitrile at a platinum electrode.

(i).   For the uncatalysed pathway, oxalate formation is the kinetically favoured pathway; but this pathway is suppressed in the osmium catalysed reaction. This occurs apparently as a consequence of carbon dioxide binding and subsequent bimolecular reaction of sterically demanding intermediates.

(ii).   For carbon monoxide production in the osmium catalysed reduction, dimerisation of I$_a$ replaces reaction between the radical carbon dioxide and free carbon dioxide in the uncatalysed reaction.

(iii). Formation of the formate anion is similar in both mechanisms; *i.e.* reaction of a proton with the radical carbon dioxide species or the reduced metal complex containing coordinated carbon dioxide; followed by a rapid electron transfer from an external reductant, *i.e.* the radical carbon dioxide in the uncatalysed process or reduced osmium in the catalysed process.

Sullivan and co-workers also showed that the complex *cis*-[Ru(bipy)$_2$(CO)H]$^+$ is an electrocatalyst for carbon dioxide reduction in acetonitrile.[49] The cyclic voltammograms of *cis*-[Ru(bipy)$_2$(CO)H]$^+$ (*see Figure 1.12*) in acetonitrile indicate that reversible redox processes occur at E$_{1/2}$ = -1.45V and -1.65V (*vs* SSCE) under a nitrogen atmosphere. When the solution is saturated with carbon dioxide there is a dramatic increase in peak current at both waves.

The following mechanism has been proposed (*see Scheme 1.16*); the first step involves a one electron reduction to form a neutral species; the addition of an electron enhances the electron density, this activates the Ru-H bond towards the insertion of carbon dioxide. The insertion of carbon dioxide into the Ru-H bond results in the formation of *cis*-[Ru(bipy)$_2$(CO)(CO$_2$H)] which then undergoes a bipyridine based one electron reduction to form *cis*-[Ru(bipy)$_2$(CO)(CO$_2$H)]$^-$; this reduction results in the loss of the formate ion which is

accompanied by the co-ordination of an acetonitrile ligand. *cis*-[Ru(bipy)$_2$(CO)(CH$_3$CN)]⁻ then reduces a molecule of water to regenerate *cis*-[Ru(bipy)$_2$(CO)H]⁺; this reduction is accompanied by the formation of a hydroxide ion and the loss of an acetonitrile ligand.
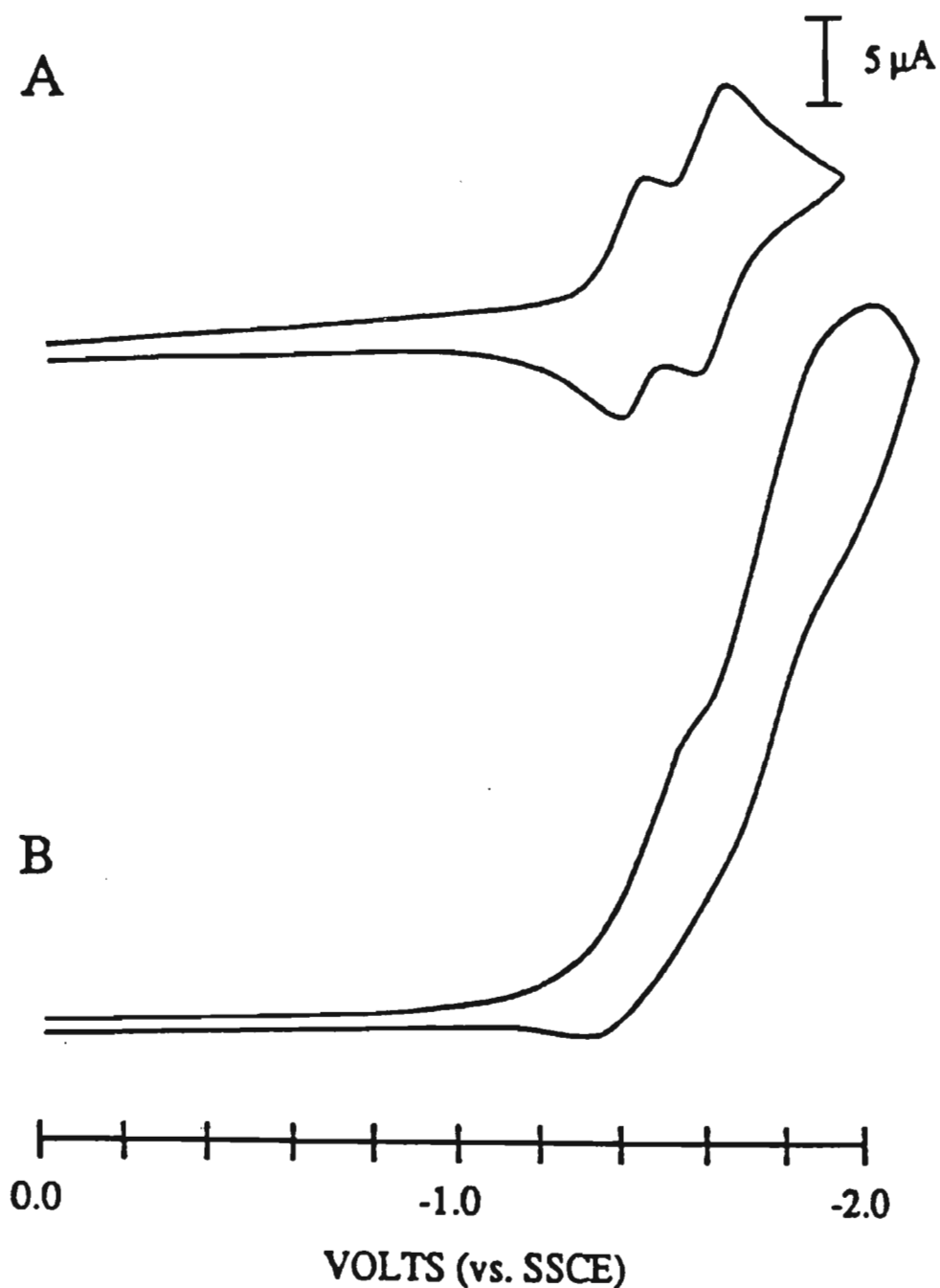
Figure 1.11. Cyclic voltammograms of *cis*-[Ru(bipy)$_2$(CO)H]⁺ under nitrogen (A) and carbon dioxide (B)

Scheme 1.16. Mechanism for CO₂ reduction by *cis*-[Ru(bipy)₂(CO)H]⁺ [49]
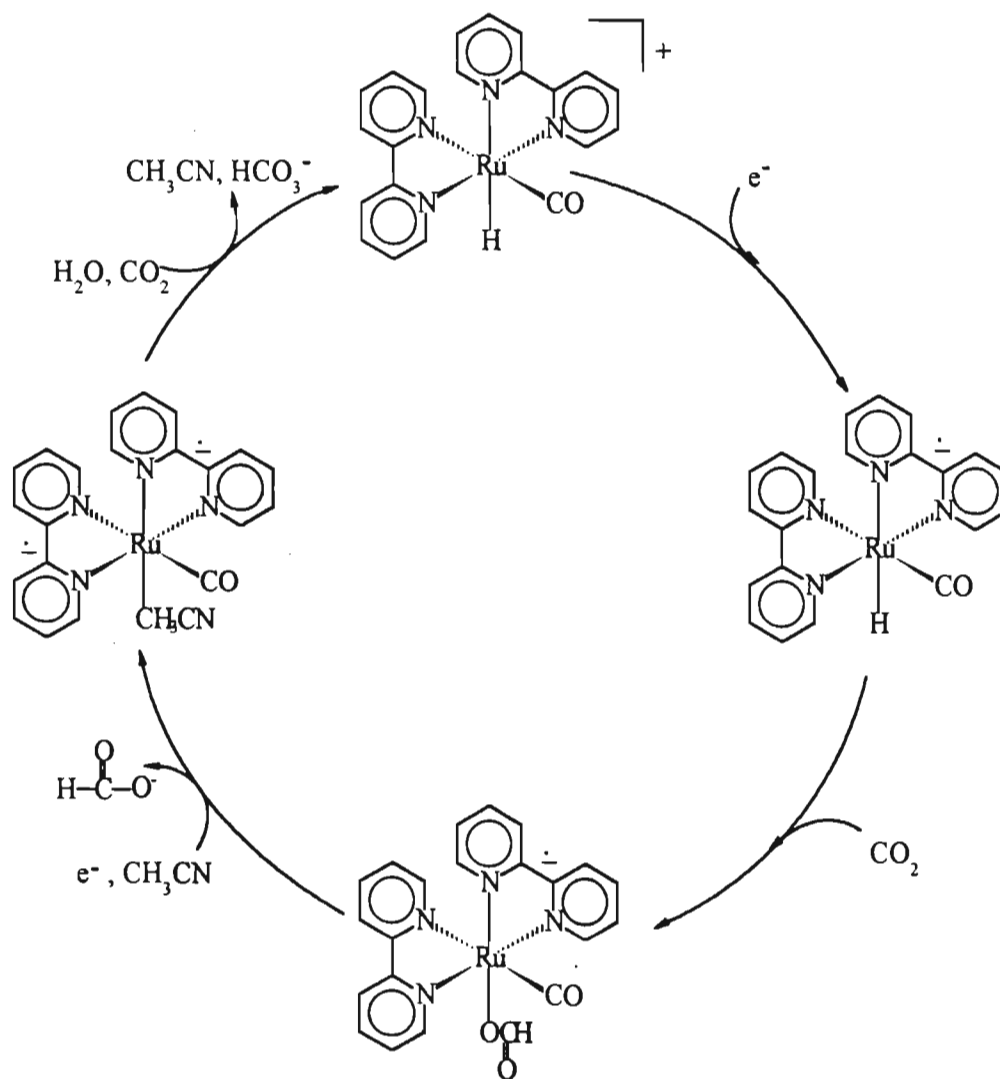
Carbon monoxide is formed as a co-product of the electrocatalytic reduction of carbon dioxide by *cis*-[Ru(bipy)$_2$(CO)H]$^+$. It has been proposed that *cis*-[Ru(bipy)$_2$(CO)H]$^+$ acts in a similar manner to *cis*-[Os(bipy)$_2$(CO)H]$^+$ (*see Scheme 1.15*); *i.e.* an associative attack of carbon dioxide on the doubly reduced formato or acetonitrile complexes. The bulk electrolysis was also conducted under $^{13}CO_2$ atmosphere; however there is no labelled carbonyl in the catalyst; the absence of a labelled carbonyl group is consistent with either proposed mechanism, *i.e.* either carbon dioxide insertion into the Ru-H bond or an associative attack.

1.3. CONCLUSION

In conclusion, it should be noted that the development of low overpotential electrocatalysts for carbon dioxide reduction will have profound effects on C_1 and/or C_2 chemistry; at the moment carbon dioxide has relatively little value as the end product of fossil fuel combustion, even though the environmental disadvantages associated with its continued emission into the atmosphere have been well documented. [50]

It is interesting to note that all of the transition metal polypyridine electrocatalysts that have been reviewed in this chapter are mononuclear polypyridine complexes which catalyse the electrochemical reduction of carbon dioxide to two electron products such as carbon monoxide, formate ions, carbonate ions, *etc*. It is our aim to try and drive the electrochemical reduction of carbon dioxide beyond these two electron products.

In order to achieve this we decided that dinuclear rather than mononuclear complexes are required to achieve this; we have synthesised the novel ligand, 6-diphenylphosphino-2,2'-bipyridine; which we believe will lead to the formation of dinuclear complexes that will catalyse the electrochemical reduction of carbon dioxide beyond these two electron products.

CHAPTER TWO

THE SYNTHESIS AND CHARACTERISATION OF THE NOVEL LIGAND : *6-DIPHENYLPHOSPHINO-2,2'-BIPYRIDINE*

AIM

The aim of the work described in this chapter was to synthesise and characterise the novel ligand, 6-diphenylphosphino-2,2'-bipyridine.

2.1. RESULTS AND DISCUSSION

The 6-diphenylphosphino-2,2'-bipyridyl (Ph$_2$Pbipy) ligand is synthesised *via* a four step procedure using 2,2'-bipyridine as the starting material (*see Scheme 2.1*), the methods used in the first three steps following established procedures.[51,52] The first step involves the methylation by methyl iodide of one of the nitrogen atoms of 2,2'-bipyridine to afford 2,2'-bipyridyinium monomethiodide. This step proceeds with good yields though a small amount of 2,2'-bipyridyinium dimethiodide is also formed. Fortunately the 2,2'-bipyridyinium dimethiodide is insoluble in methanol and precipitates out of solution as soon as it forms and is easily removed by filtration.[51] Suitable spectral and elemental analyses were obtained for 2,2'-bipyridyinium monomethiodide.

In the second step, a strongly alkaline solution of ferric salts is used to oxidise 2,2'-bipyridyinium monomethiodide to 1-methyl-2,2'-bipyridin-6-one in good yields.[52] Some caution is required when the 2,2'-bipyridyl monomethiodide is added to the alkaline solution of ferric salts in that the rate of addition should be such that the temperature of the solution does not exceed 10°C. If the temperature is not maintained below 10°C then there is a

decrease in the yield. Satisfactory spectral and elemental analyses were obtained for 1-methyl-2,2'-bipyridin-6-one.

Scheme 2.1. Synthesis of 6-diphenylphosphino-2,2'-bipyridine

2,2'-bipryidine

6-diphenylphosphino-2,2'-bipyridine
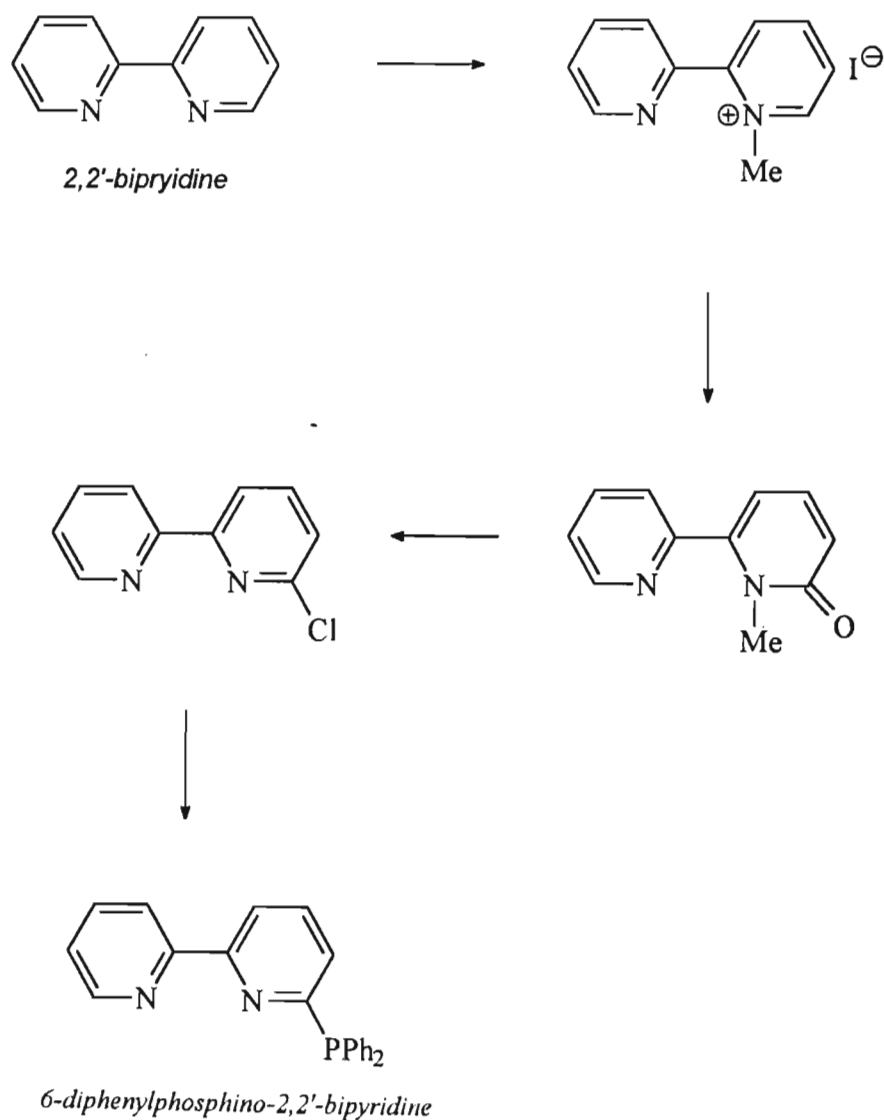
The third step of the procedure involves the chlorination of the keto group by phosphoryl chloride and phosphorus pentachloride; however this step proceeds with a low yield of *ca*.30%.[52] Several attempts to modify the method were attempted but there was no significant increase in the quantity of 6-chloro-2,2'-biyridine produced. Extreme caution should be taken when the ice is added to the solution once the reflux has been completed, the formation of HCl gas being the result of a highly exothermic reaction; if the ice is added too quickly the solution will boil over and a loss of product will result. Gas chromatography (of an acetone solution of the compound) indicates that only one product is obtained from this step; the mass spectrum displays a molecular ion peak at 190 confirming that the product is indeed 6-chloro-2,2'-bipyridine. Satisfactory spectral and elemental analyses were obtained for 6-chloro-2,2'-biyridine.

The fourth step of the reaction is new and involves the reaction between lithium diphenylphosphide and 6-chloro-2,2'-bipyridine. The first part of the reaction involves the preparation of lithium diphenylphosphide, from the reaction of freshly cut lithium metal with chlorodiphenylphosphine in ultra dry tetrahydrofuran.[53] The resultant red solution is filtered to remove excess lithium and lithium chloride and must be used within an hour of preparation for the best results. The 6-chloro-2,2'-bipyridine is dissolved in ultra dry tetrahydrofuran and added dropwise to the lithium diphenylphosphide solution at -78°C in an inert atmosphere. The 6-chloro-2,2'-bipyridyl ligand is added slowly so that the temperature does not rise above -70°C while the addition is carried out; if the temperature is allowed to get too high there will be a significant decrease in the amount of 6-diphenylphosphino-2,2'-biyridine produced.

Once the addition of 6-chloro-2,2'-bipyridyl is complete, the solution is allowed to warm up to room temperature and is stirred overnight. Hydrochloric acid is added to hydrolyse the free LiPPh$_2$, this step also results in the protonation of the phosphorous atom of the 6-diphenylphosphino-2,2'-bipyridyl ligand. The protonated form of the ligand is soluble in the aqueous layer of the solution, the two layers are separated and the organic impurities are removed in this manner. The aqueous layer is then basified with ammonia, resulting in the

removal of the proton from the ligand. The solution is then extracted with diethyl ether, the 6-diphenylphosphino-2,2'-ligand is soluble in the organic layer only and is thus easily removed from the aqueous layer.

The ligand obtained by extraction with diethyl ether is relatively pure, however some ligand in which the phosphorus has oxidised may have also formed. The oxidised ligand is also very soluble in diethyl ether. The solvent is removed under reduced pressure and the solid material is redissolved in chloroform. Methanol is added to the chloroform solution, this induces the crystallisation of the unoxidised form of the ligand from the solution because the oxidised form of the ligand is soluble in solution. The solvent is decanted and the pale yellow solid material is washed with cold methanol and dried *in vacuo*. Gas chromatography (of an acetone solution of the compound) indicates that only one product is obtained after recrystallisation from a chloroform-methanol solution. The molecular ion peak occurs at 340.3 confirming that the 6-diphenylphosphino-2,2,'-bipyridyl ligand has been formed.

The Ph$_2$Pbipy ligand is air sensitive, the phosphorus atom being readily oxidised to the corresponding phosphorus oxide; evidence for this is the appearance in the ^{31}P{^{1}H} nmr spectrum of a singlet at 19.98ppm, this value is characteristic of the oxidised phosphorus. Fortunately, the phosphine oxide is readily separated from Ph$_2$Pbipy by extraction into cold methanol. The ligand is stable up to temperatures of *ca* 130°C, but rapidly degrades on exposure to ultraviolet light.

Table 2.2 lists the characterisation data for the Ph$_2$Pbipy ligand. The ^{31}P{^{1}H} nmr spectrum consists of a sharp singlet at -3.71ppm, a chemical shift which clearly distinguishes the free ligand from the oxide (*vide supra*) and the coordinated ligand, both of which have a ^{31}P chemical shift downfield of that for the free ligand. The high field value is indicative of the high electron density on the phosphorus atom of the free ligand. As indicated in *Table 2.2*, the peaks in the ^{1}H nmr spectrum of the Ph$_2$Pbipy ligand can be assigned to individual protons

but complex coupling effects in the $^{13}C\{^{1}H\}$ nmr spectrum do not allow an equivalent assignment of the individual carbon atoms.

The remaining spectral data require little comment, except to note that the UV/vis spectrum of 2,2'-bipyridine and Ph$_2$Pbipy were recorded under the same conditions; two intense bands occur at 289 and 269nm are present in the UV/vis spectrum for 2,2'-bipyridine, the band at 269nm having a shoulder at 275nm; these bands correspond to π-π^* transitions. The UV/vis spectrum for Ph$_2$Pbipy (*see Figure 2.1*) has three bands at 289, 276 and 269nm corresponding to π-π^* transitions.

The very similar absorption spectra for 2,2'-bipyridine and 6-diphenylphosphino-2,2'-bipyridine suggest that the substitution of a hydrogen atom in the six position of 2,2'-bipyridine by a diphenylphosphido group does not influence the electronic structure of the bipyridyl moiety significantly.

The cyclic voltammograms of the Ph$_2$Pbipy ligand have been run in dichloromethane and acetonitrile; these show that the ligand is not reduced within the solvent limit.

The structure of Ph$_2$Pbipy has been solved[54] (*see Figure 2.2*). It is interesting to note that in the solid state the bipyridyl fragment of the ligand adopts a near planar *transoid* arrangement as found for 2,2'-bipyridine itself.[55] Although the free Ph$_2$Pbipy ligand has the expected *transoid* arrangement in the solid state there is the possibilty of free rotation around the interannular C-C bond. Indeed, the chelating bonding mode of 2,2'-bipyridine found in the vast majority of its complexes requires a *cisoid* arrangement about the interannular bond. In general, a near-planar configuration of the two pyridyl rings is observed in these complexes, the implication being that there is little difference in stability between the *transoid* and *cisoid* forms of the bipyridyl moiety.[55,56]
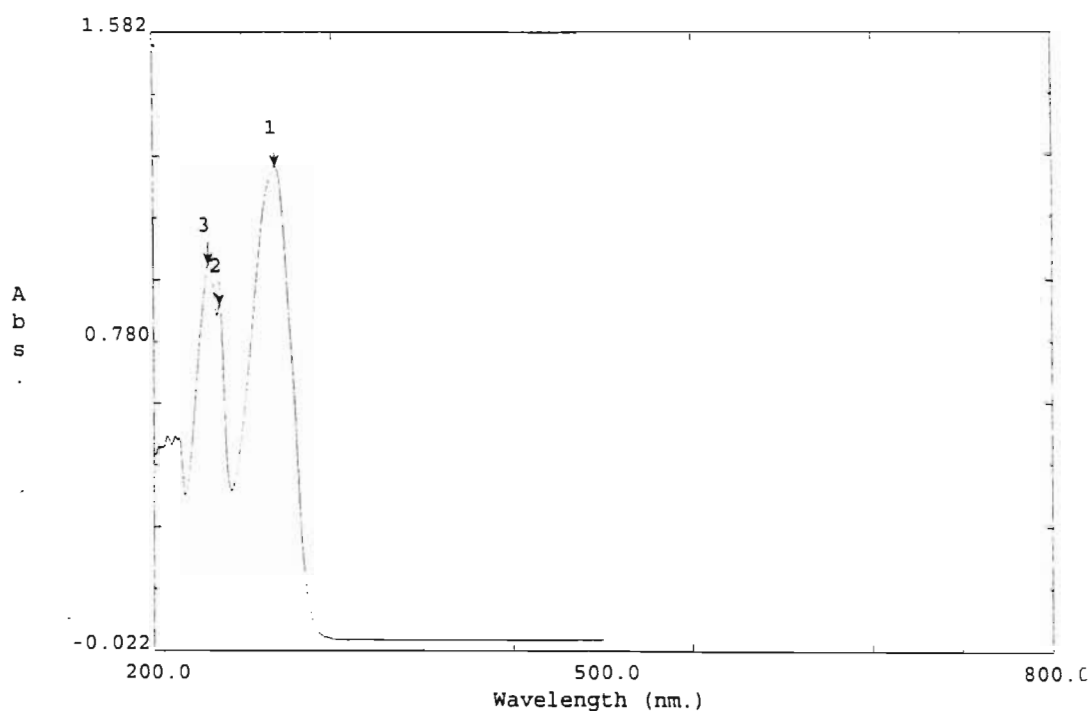
Figure 2.1. UV-Vis spectrum of 6-diphenylphosphino-2,2'-bipyridine
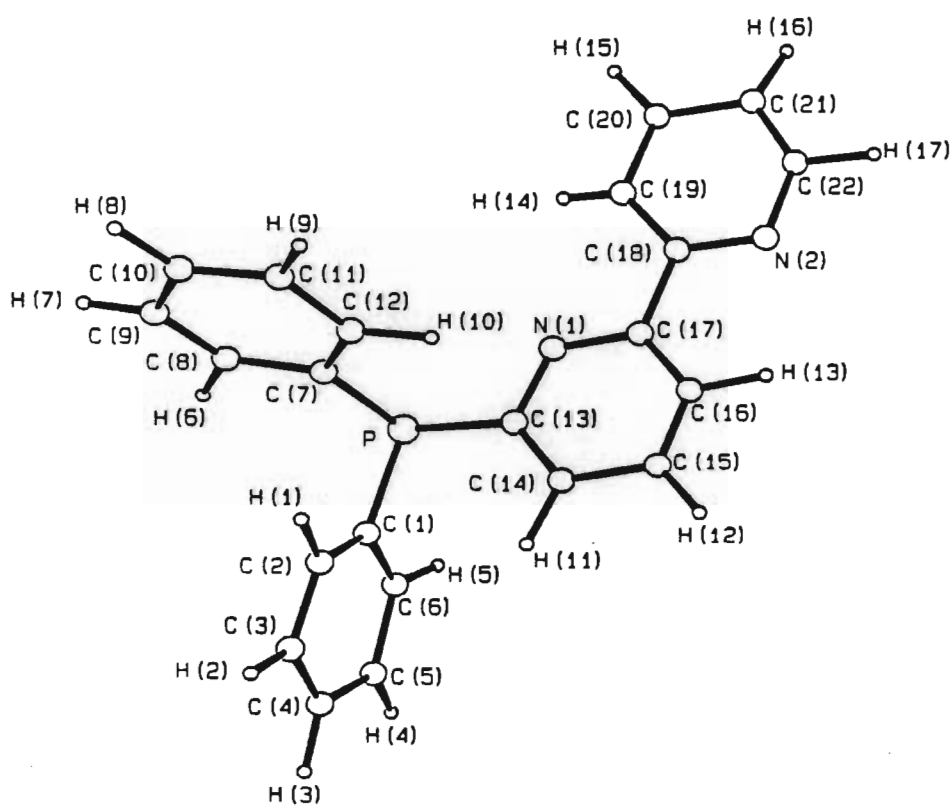
Figure 2.2. The molecular structure of 6-diphenylphosphino-2,2'-bipyridine

Ph₂Pbipy can be considered as either a 2,2'-bipyridyl substituted derivative of the ubiquitous triphenylphosphine or as a diphenylphosphido substituted derivative of the equally ubiquitous 2,2'-bipyridine. Alternatively, in terms of its coordination properties, Ph₂Pbipy can be considered to have "evolved" from a combination of some of the most widely used ligands in coordination chemistry (*see Scheme 2.2*), *viz.* PPh₃, 2,2'-bipyridine, pyridine, dppm and 2-diphenylphosphinopyridine.

Scheme 2.2. "Evolution" of 6-diphenylphosphino-2,2'-bipyridine
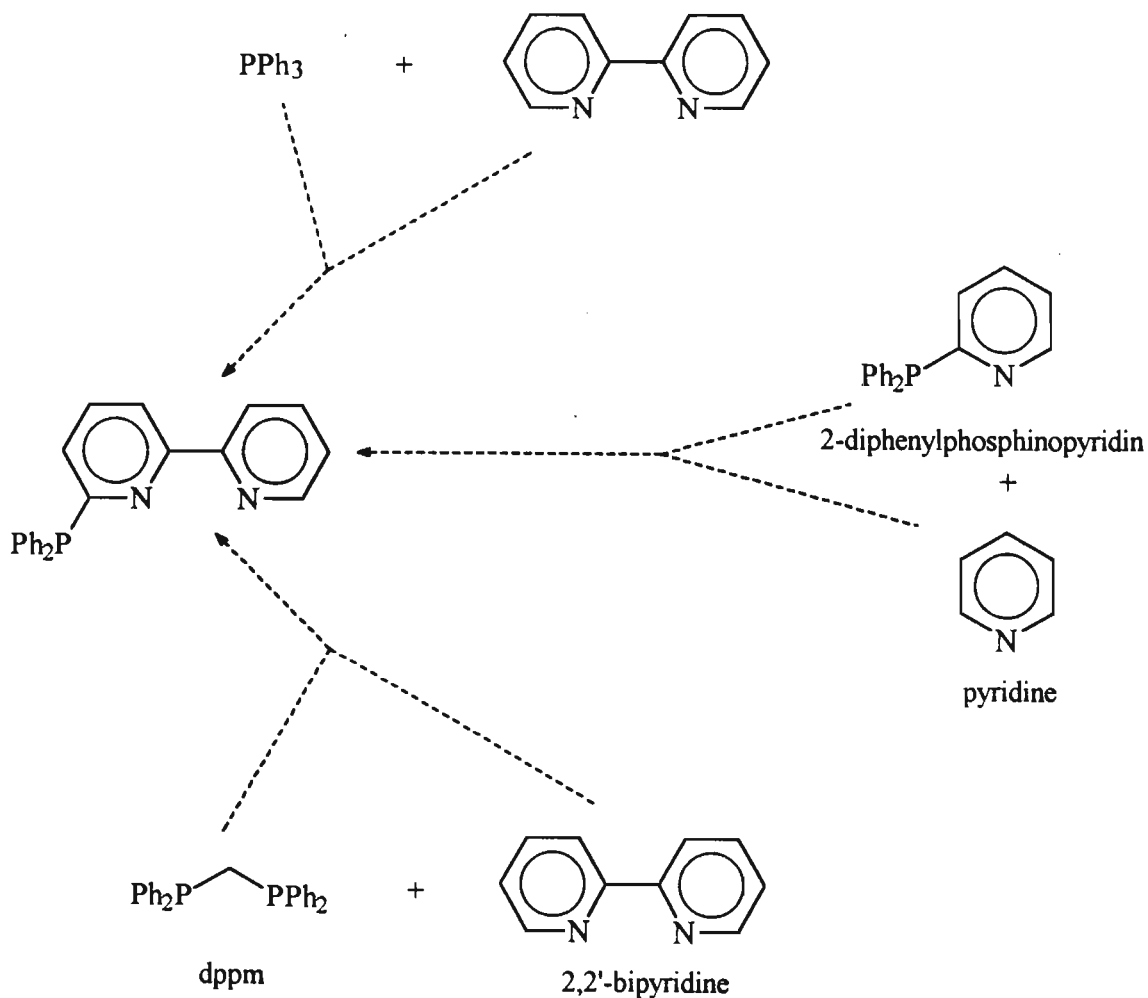
Ph$_2$Pbipy can adopt several possible modes of coordination (*see Scheme 2.3*). It has been established that Ph$_2$Pbipy can be regarded as a combination of several ligands (*see Scheme 2.2*), and therefore it can be argued that this "hybrid" ligand should be able to adopt the modes of coordination of the ligands it has evolved from.

It can coordinate as a monodenate ligand through the phosphorus atom as triphenylphosphine does. It is well known that 2,2,'-bipyridyl ligand coordinates to a metal atom in a chelating fashion[55] ; it can therefore be assumed that the bipyridyl fragment in the Ph$_2$Pbipy ligand will coordinate in a similar manner. 2-Diphenylphopshinopyridine and dppm are known to coordinate in a bridging manner[57,58]. The Ph$_2$Ppy portion of the ligand is thus capable of bridging across two metal atoms. There are several examples were the Ph$_2$Ppy chelates at one metal atom[59,60], and therefore it is possible that Ph$_2$Pbipy can also act as a tridentate chelating ligand.

Of the above possibilities the bridging mode of coordination appears most likely for Ph$_2$Pbipy. With this expectation in mind, a further aim of this study can be stated; to employ the Ph$_2$Pbipy ligand in the synthesis of metal complexes of copper and rhodium which are stabilised to fragmentation by the presence of the bridging ligand. As the work in the consequent chapters shows, this aim has largely been realised.

Scheme 2.3. Possible modes of coordination for Ph₂Pbipy

monodentate

bridging

chelating as a bidentate ligand

chelating as a tridentate ligand
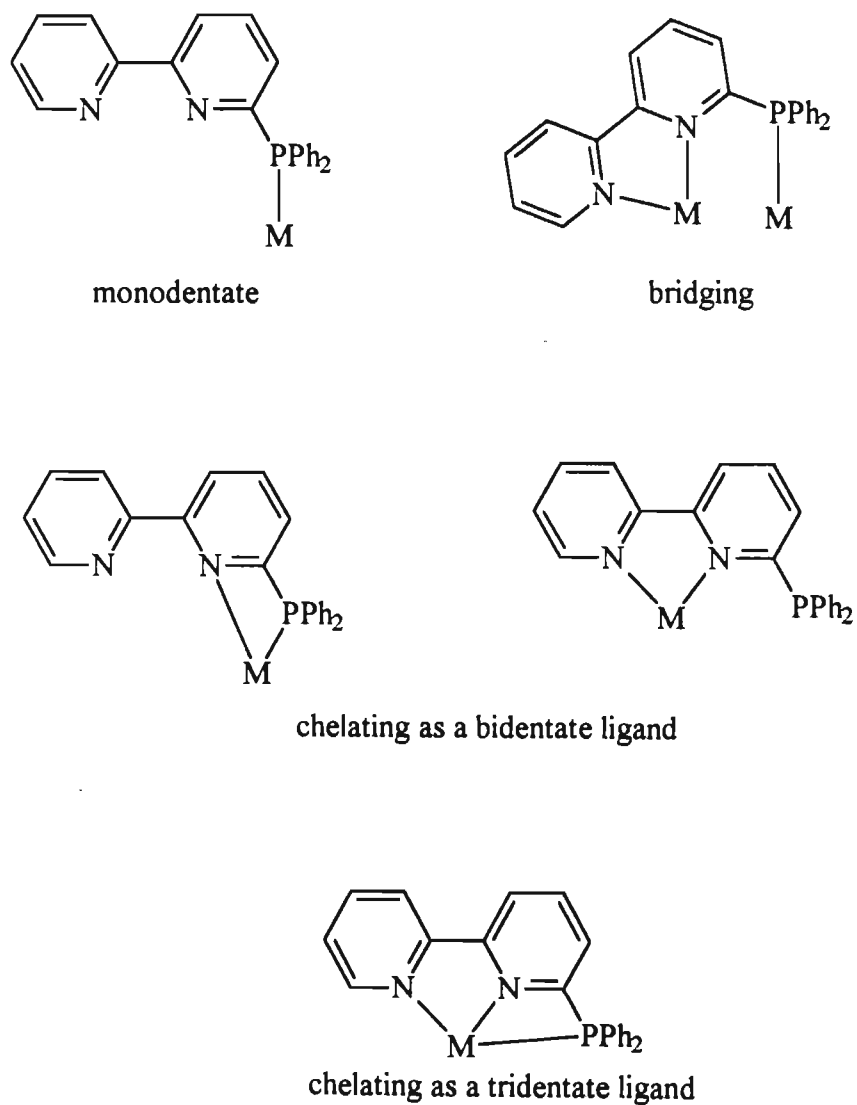
2.2. EXPERIMENTAL

2.2.1. *Synthesis of 2,2'-bipyridyinium-monomethiodide* (1)

A solution of 2,2'-bipyridine (*97g, 0.62mol*) and methyl iodide (*38.7ml, 0.62mol*) in methanol (*200ml*) was refluxed in a vacuum-sealed Schlenk tube (*500ml*) at 100°C for 15 hours.The solution was filtered to remove the yellow dimethiodide by-product and the filtrate evaporated to yield an orange/yellow residue. Unreacted 2,2'-bipyridine was extracted from this residue using petroleum ether (60-80°C) (*250ml*) as extractant. The residual monomethiodide was found to be sufficiently pure for the next step of the synthesis.

Yield: 84%

2.2.2. *Synthesis of 1-methyl-2,2'-bipyridin-6-one* (2)

Solid 2,2-bipyridyinium-monomethiodide (*156g, 0.52*mol) was added in small portions to a saturated aqueous solution (*800ml*) of $K_3[Fe(CN)_6]$ (*341g, 1.04mol*) and NaOH (*83g, 2,08mol*) and a rate such that the temperature of the solution did not exceed 10°C (ice-water bath). Following complete addition the reaction mixture was stirred at 10°C for 2 hours and subsequently at room temperature for a further 15 hours. The resulting black solution was extracted with ten 350ml aliquots of $CHCl_3$ and the aliquots combined and dried over magnesium sulphate for 3 hours. The solution was filtered and the filtrate evaporated to dryness. The residue was dried further in vacuo for at least 5 hours to afford the product sufficiently pure not to require crystallisation.

Yield: 88%

2.2.3. *Synthesis of 6-chloro-2,2'-bipyridine* (3)

A one litre round bottomed flask, fitted with a reflux condenser and a DMSO bubbler or a CaCl$_2$ drying tube, was charged with 1-methyl-2,2'-bipyridin-6-one (*86g, 0.46mol*), PCl$_5$ (*96g, 0.46mol*) and POCl$_3$ (*ca.200ml*). The mixture was refluxed at 130°C for 3 hours and then cooled to room temperature. Ice was added in small pieces down the condenser, producing a large quantity of HCl gas. Once evolution of gas had ceased, the resulting solution was basified with ammonia to a pH *ca.*10 and then allowed to stand at room temp for 24 hours. The black precipitate which separated was filtered, dried in air and extracted into boiling petroleum ether (60-80°C) (*500ml*). The yellow petroleum ether extract was decanted and filtered, and then treated with activated charcoal. After filtering and evaporation of the filtrate under reduced pressure, the pale yellow product was dried *in vacuo*.
Yield: 32%

2.2.4. *Synthesis of 6-diphenylphosphino-2,2'-bipyridine* (4)

A solution of ClPPh$_2$ (*27ml, 150mmol*) in THF (*90ml*) was added dropwise to a stirred suspension of freshly cut lithium (*2.1g, 300mmol*) in THF (*78ml*). On appearance of the characteristic red colour of LiPPh$_2$ stirring was continued for a further one hour. The red solution was then filtered to remove excess lithium and lithium chloride. The filtrate was cooled to -75°C and continuously stirred while a solution of 6-chloro-2,2'-bipyridine (*28.5g, 150mmol*) in THF (*84ml*) was added dropwise. The resulting black solution was stirred at room temperature for 15 hours. Hydrochloric acid was first added (*initially 100ml 3M HCl followed by 40ml concentrated HCl*) to hydrolyse any free LiPPh$_2$, the aqueous and organic layers were separated. Ammonia was added to the aqueous layer to bring the pH to *ca.* 10, this layer was the extracted with diethyl ether (*5 x 100ml*), the combined diethyl ether extracts were dried over magnesium sulphate, and the solvent removed under reduced pressure to afford the product as a light yellow residue. Recrystallisation from chloroform/methanol at -25°C gave a microcrystalline pale yellow solid.
Yield: 94%

Table 2.1. Elemental analyses obtained in the four step synthesis of Ph$_2$Pbipy

COMPLEX	CALCULATED(%)			FOUND(%)		
	C	H	N	C	H	N
2,2'-bipyridyinium monomethiodide	44.32	3.72	9.40	44.3	3.9	9.3
1-methyl-2,2'-bipyridin-6-one	70.95	5.41	15.04	70.7	5.5	14.9
6-chloro-2,2'-bipyridine	63.01	3.70	14.70	63.6	4.1	14.2
6-diphenylphosphino-2,2'-bipyridine	77.64	5.03	8.23	77.7	5.2	7.8

Table 2.2. Spectroscopic data for 6-diphenylphosphino-2,2'-bipyridine

^{31}P{^{1}H} n.m.r. *(ppm)*	-3.71
^{1}H n.m.r. *(ppm)*	8.62 (1H,dbrm,H$_6$), 8.31(2H,dbrm,H$_{4,4'}$), 7.65 (2H,tbrm,H$_{3',5}$) , 7.39 (10H,Ph), 7.19 (2H,m,H$_{3,5'}$)
^{13}C{^{1}H} n.m.r. *(ppm)*	120-150 (17C,d,aromatic CH's), 150-164 (5C,s,quat. C's)
Infrared *(cm^{-1})*	1421s,1431m,1472w,1477w,1550m,1565m,1572m,1583w
UV/vis *(nm)*	289 (π-π^*) 276 (π-π^*) 269 (π-π^*)
GC - MS	*m/z* 340.3

CHAPTER THREE

DINUCLEAR 6-DIPHENYLPHOSPHINO-2,2'-BIPRYIDINE LIGAND BRIDGED DERIVATIVES OF COPPER (I)

AIM

The transition metal polypyridine complexes which have been reported to catalyse the electrochemical reduction of carbon dioxide are all mononuclear. Two electron reduction products such as carbon monoxide, formate ions, *etc.* are always obtained. In an attempt to drive the electrochemical reduction of carbon dioxide beyond these two electron products it was decided that dinuclear rather than mononuclear polypyridyl complexes should be synthesised and tested for their electrocatalytic activity towards carbon dioxide. To this end, as described earlier, we have synthesised the novel ligand, 6-diphenylphosphino-2,2'-bipyridine (Ph$_2$Pbipy). Because of its potentially bridging capabilities this ligand should, on reaction with suitable precursors, lead to the formation of dinuclear complexes, that could catalyse the electrochemical reduction of carbon dioxide beyond the two electron stage. The specific aim of the work described in this chapter was to utilise the 6-diphenylphosphino-2,2'-bipyridine in the synthesis of ligand bridged dinuclear copper (I) complexes.

3.1. INTRODUCTION

There has been a dramatic increase in studies involving the chemistry of dicopper (I) complexes due to the increased attention to the role of copper complexes in influencing the reactivity of molecular oxygen, not only in biological systems but also in catalytic oxidation and dioxygen mediated processes.[61-66] The ligand dppm has been widely utilised as a bridging ligand to produce dinuclear complexes of a wide range of transition metals;[67] however this has not been the case for copper (I), which generally gives rise to a range of tri- and tetranuclear dppm bridged complexes rather than dinuclear species.[68-73] In fact, binuclear copper (I) complexes bridged by the dppm ligand have only been reported fairly recently in

the literature.[74-79] Some of these complexes will be discussed now in order to provide a background to the co-ordination behaviour of these dinuclear complexes. Lanfredi and co-workers have prepared a series of dppm bridged dicopper complexes, of which $[Cu_2(\mu\text{-}dppm)_2(\eta^1\text{-}O_2CPh)_2]$ and $[Cu_2(\mu\text{-}dppm)_2(\mu\text{-}O_2CPh)(\eta^1\text{-}O_2CPh)]$ are typical. In $[Cu_2(\mu\text{-}dppm)_2(\eta^1\text{-}O_2CPh)_2]$ both the copper atoms adopt near trigonal planar arrangement (*see Figure 3.1*) with a Cu-Cu separation of 3.359Å.[74,75]
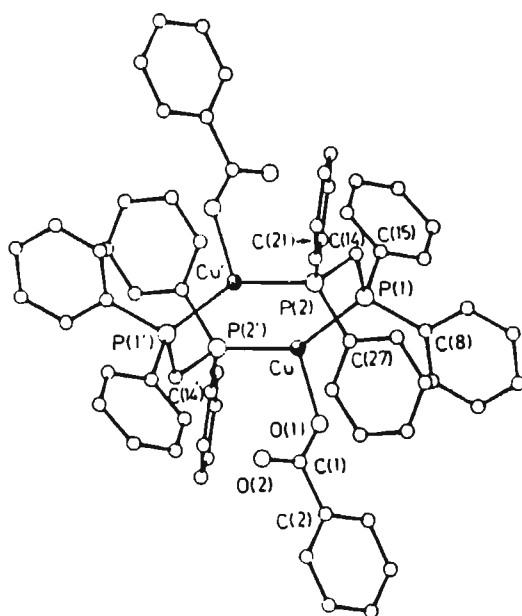
Figure 3.1. Molecular structure of $[Cu_2(\mu\text{-}dppm)_2(\eta\text{-}O_2CPh)_2]$
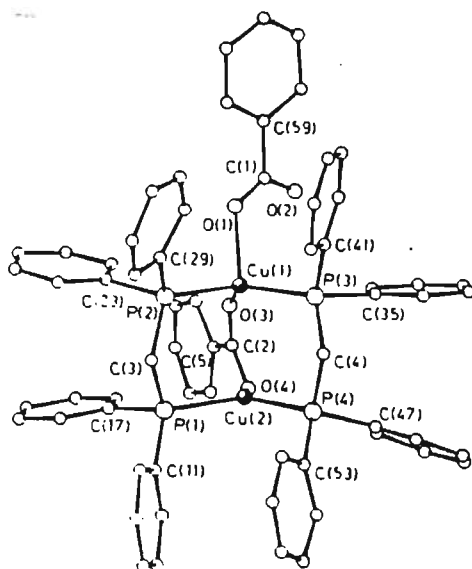
Figure 3.2. Molecular structure of $[Cu_2(\mu\text{-}dppm)_2(\mu\text{-}O_2CPh)(\eta\text{-}O_2CPh)]$

Interestingly, the Cu(1) atom in $[Cu_2(\mu\text{-dppm})_2(\mu\text{-}O_2CPh)(O_2CPh)]$ is pseudotetrahedrally coordinated while the Cu(2) atom is in a trigonal environment (*see Figure 3.2*). The presence of the bridging benzoate has had the effect of reducing the Cu(1)-Cu(2) distance to 2.9442Å.[74,75]

Gimeno and co-workers have synthesised $[Cu_2(\mu\text{-dppm})_2(MeCN)_4]^{2+}$ in which both copper atoms have a distorted tetrahedral coordination environment (*see Figure 3.3*); the Cu-Cu distance has been found to be 3.426Å.[78]
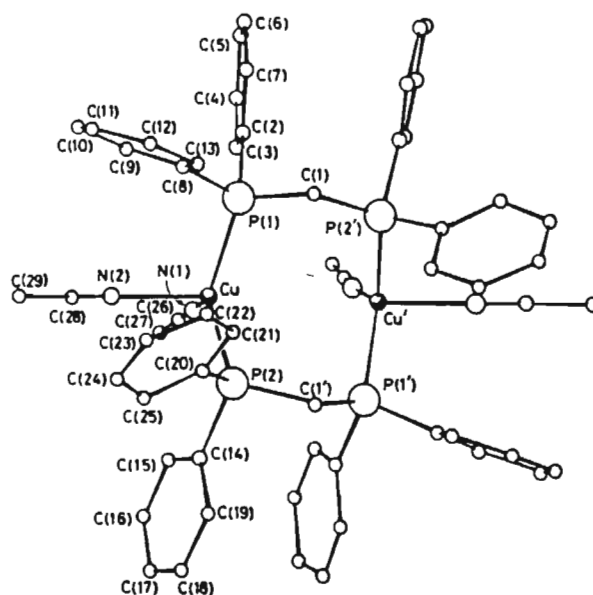
Figure 3.3. Molecular structure of $[Cu_2(\mu\text{-dppm})_2(MeCN)_4]^{2+}$

Gimeno and co-workers have also reported the only dinuclear copper (I) complexes containing bridging phophoruspyridyl ligands, having obtained a series of these complexes by reacting $[Cu(MeCN)_4]^+$ with the Ph$_2$Ppy ligand in different solvents and different molar ratios.[80] For example, $[Cu_2(\mu\text{-}Ph_2Ppy)_3(MeCN)]^{2+}$ was isolated from the reaction of $[Cu(MeCN)_4]^+$ and an excess of the Ph$_2$Ppy ligand; in this complex the Cu(1) atom is in a trigonal environment while the Cu(2) atom adopts a distorted tetrahedral configuration (*see Figure 3.4*). The presence of the three bridging Ph$_2$Ppy ligands has the effect of reducing the Cu-Cu distance to 2.721Å.
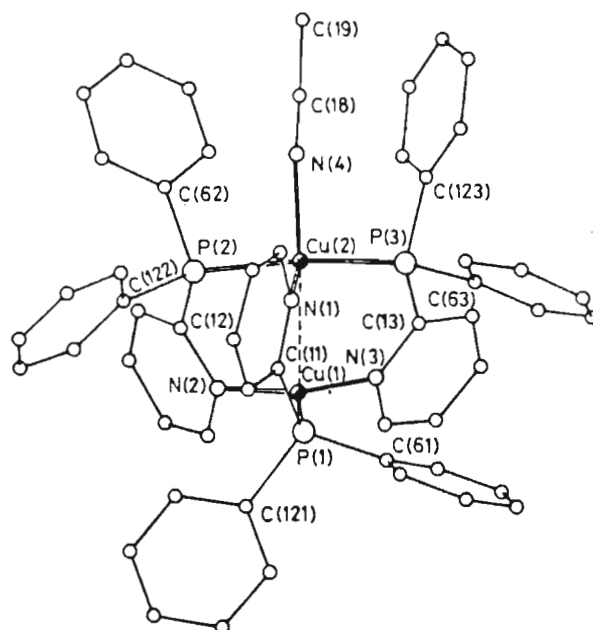
Figure 3.4. Molecular structure of [Cu$_2$(μ-Ph$_2$Ppy)$_3$(MeCN)$_2$]$^{2+}$

Investigations have been carried out in our laboratory on the reactivity of the Cu(1) precursor, [Cu(MeCN)$_4$]$^+$ with the ligands Ph$_2$Pquin and PhP(py)$_2$.[81,82] The reaction involving PhP(py)$_2$ has been shown to afford [Cu$_2${μ-PhP(py)$_2$}$_2$(MeCN)$_2$]$^{2+}$ in which each copper atom has a distorted tetrahedral arrangement and the Cu-Cu distance is 3.458(2)Å (*see Figure 3.5*). The reaction between [Cu(MeCN)$_4$]$^+$ and Ph$_2$Pquin results in the formation of [Cu$_2$(μ-PhP$_2$quin)$_2$(MeCN)$_2$]$^{2+}$ in which each copper atom is trigonally coordinated and the Cu-Cu distance is 2.585(1)Å (*see Figure 3.6*).

It can concluded from the examples discussed here that the copper atoms in dicopper (I) complexes that contain phosphorus or phosphorus polypyridyl bridging ligands will in all likelihood adopt one of the following stereochemistries;

i). both copper atoms have a tetrahedral coordination environment or,

ii). both copper atoms have a trigonal coordination environment or,

iii). one copper atom has a trigonal environment while the other copper atom has a tetrahedral environment.
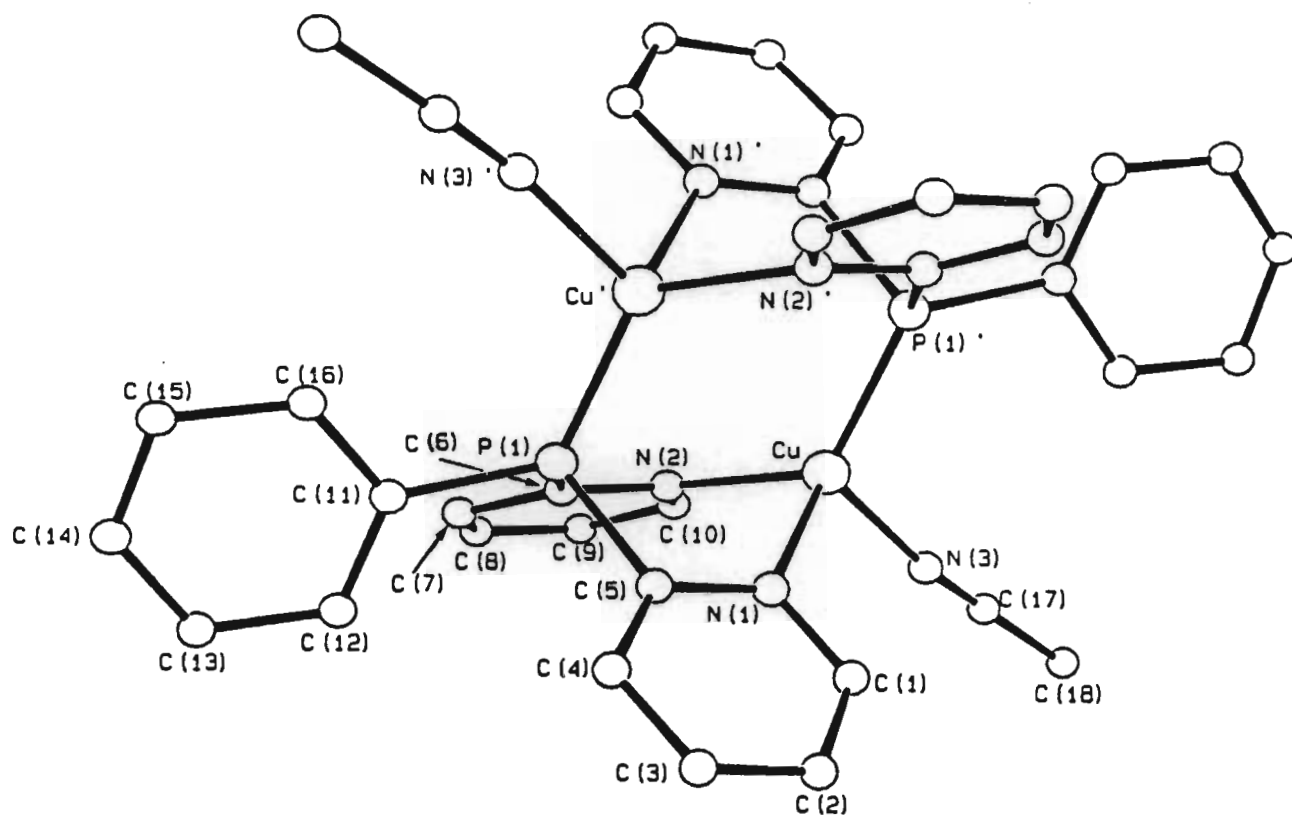
Figure 3.5. Molecular structure of $[Cu_2\{\mu\text{-}PhP(py)_2\}_3(MeCN)_2]^{2+}$
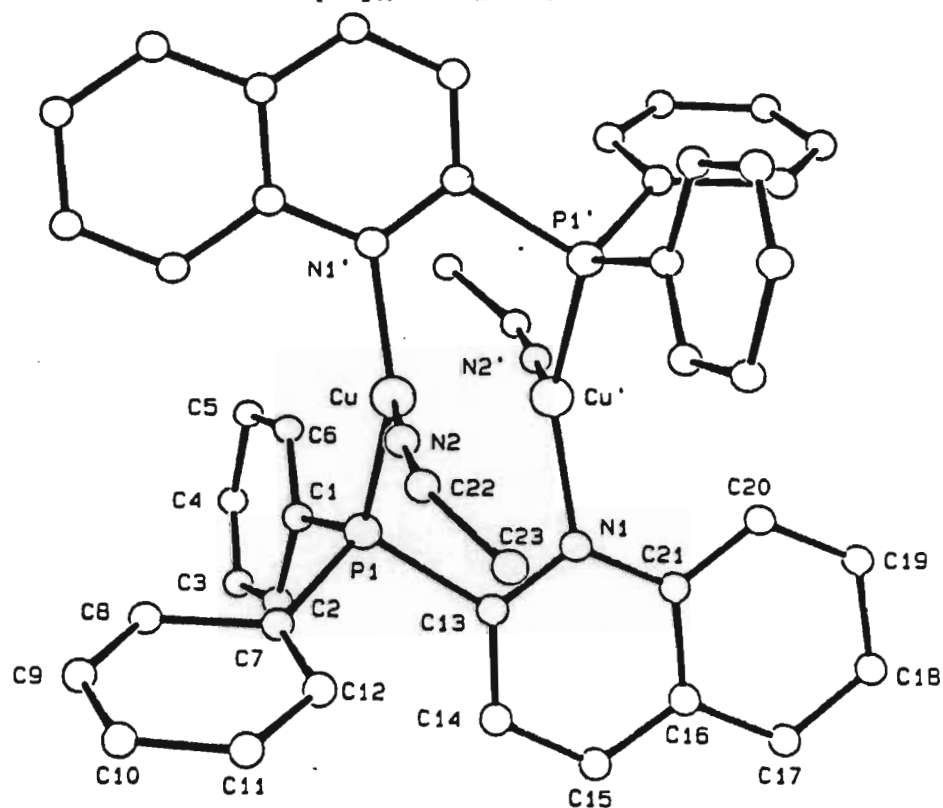
Figure 3.6. Molecular structure of $[Cu_2(\mu\text{-}PhP_2quin)_2(MeCN)_2]^{2+}$

3.2. RESULTS AND DISCUSSION

3.2.1. Introduction

The $^{31}P\{^1H\}$ nmr spectra obtained for all of the Ph_2Pbipy ligand bridged dicopper (I) complexes reported in this chapter exhibit featureless broad bands. It is assumed that the broadness arises from quadrupole relaxation[83] and in this context previously reported dicopper (I) complexes containing bridging dppm (*eg.* $[Cu_2(\mu\text{-dppm})_2(MeCN)_4]^{2+}$) and Ph_2Ppy (*eg.* $[Cu_2(\mu\text{-}Ph_2Ppy)_3(MeCN)]^{2+}$) ligands exhibit broad resonances in their $^{31}P\{^1H\}$ nmr spectra.[74-83] As a consequence $^{31}P\{^1H\}$ nmr spectroscopy proved to be a relatively insensitive technique for the characterisation of the dicopper (I) phosphorus bipyridyl ligand bridged complexes reported here.

3.2.2. Treatment of $[Cu(MeCN)_4]^+$ with Ph_2Pbipy : Synthesis, characterisation and crystal structure of $[Cu_2(Ph_2Pbipy)_2(MeCN)_2](PF_6)_2$ (5)

Reaction of $[Cu(MeCN)_4](PF_6)$[84] with an equimolar amount of Ph_2Pbipy in acetonitrile at room temperature was found to afford a product characterised as $[Cu_2(\mu\text{-}Ph_2Pbipy)_2(MeCN)_2](PF_6)_2$ (5), and isolated as an air stable yellow crystalline solid (*see Scheme 3.1*). The yield of this product was shown to vary with reaction time and the solvent used, the maximum yield being obtained when the reaction is allowed to proceed over 24 hours and when the solvent used is acetonitrile; any reduction in the length of time or change in solvent *eg.* to dichloromethane or acetone, results in a significant decrease in yield.

The ^1H nmr spectrum of this species in CD_2Cl_2 at room temperature exhibits resonances between 6.9 and 8.8ppm associated with the aromatic rings of the ligand, together with a sharp singlet at 2.00ppm; assigned to the methyl group of the acetonitrile; intergration of these peaks esatblished that two acetonitrile ligands are coordinated in the complex (*see Table 3.8*). The solid state infrared spectrum (KBr disk) exhibits absorptions characteristic of the Ph_2Pbipy ligand and the counterion PF_6^-, while the solution spectrum (CH_2Cl_2) exhibits a

clearly visible peak at $2304cm^{-1}$ assigned to the C-N stretching mode of the acetonitrile ligand (*see Table 3.7*). The $^{31}P\{^1H\}$ nmr spectrum in CD_2Cl_2 contains a broad signal centred at 4.9ppm; variable temperature $^{31}P\{^1H\}$ nmr spectral studies did not result in improved resolution (*see section 3.2.1*).

With the object of determining the exact mode of coordination of the Ph_2Pbipy ligand in $[Cu_2(\mu\text{-}Ph_2Pbipy)_2(MeCN)_2](PF_6)_2$, single crystals suitable for X-ray crystallography were grown by the slow diffusion of diethyl ether into a dichloromethane solution of the compound. The crystal structure of the complex consists of well separated $[Cu_2(\mu\text{-}Ph_2Pbipy)_2(MeCN)_2]^{2+}$ cations and PF_6^- anions, there being no intermolecular contacts significantly less than the sum of the van der Waals radii for the atoms concerned. The structure of the cation is depicted in *Figure 3.7* along with the atom numbering scheme. A full listing of interatomic distances and angles is given after *section 3.5* at the end of this chapter.

The cation possesses a crystallographically imposed centre of symmetry midway between the copper atoms. The copper atoms are bridged by two Ph_2Pbipy ligands in the "head-to-tail" configuration, each ligand coordinating to one copper atom through a phosphorus donor atom and to the other through a chelating bipyridyl fragment. Each copper atom has its coordination completed by an acetonitrile group, the geometry thus attained being irregular tetrahedral. The irregular geometry is caused as a result of the small angle of $79.9(1)°$ subtended by the bipyridyl fragment at the copper atom; other angles are closer to the idealised value of $109.5°$ but range up to $114.0(2)°$ as found for the N(2)-Cu-P(1') angle.

An interesting feature of this complex is that the coordinated acetonitrile ligand is not linear as evidenced by a N(3)-C(23)-C(24) angle of only $149(2)°$. The Cu-Cu' distance of $3.941(2)$Å is consistent with non bonding interaction between the copper atoms. These and other molecular parameters are discussed further in *section 3.2.14* in relation to those observed for other Ph_2Pbipy ligand bridged dicopper (I) complexes.
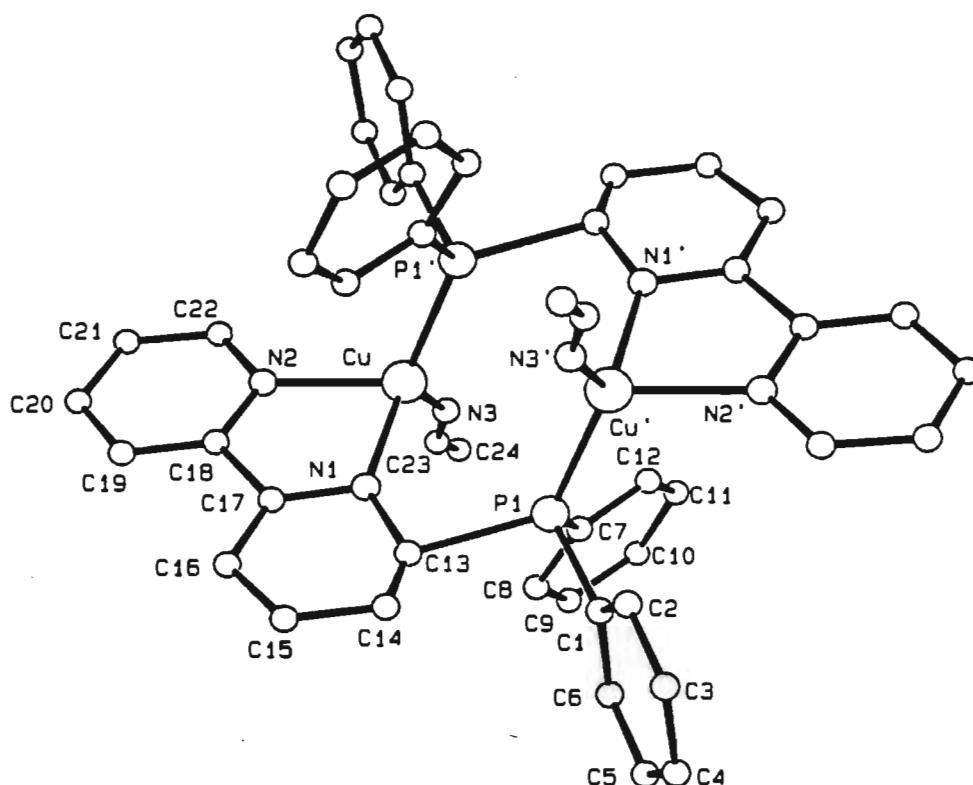
Figure 3.7. Molecular structure of [Cu₂(μ-Ph₂Pbipy)₂(MeCN)₂](PF₆)₂

3.2.3. Synthesis, characterisation and crystal structure of [Cu₂(Ph₂Pbipy)₂(PhCN)₂](PF₆)₂ (6)

With the object of synthesising species analogous to complex (5) in which other solvent molecules were co-ordianted, the reactions of [Cu(PhCN)₄](PF₆) with Ph₂Pbipy were also investigated. Reaction of these compounds in benzonitrile at room temperature was found to afford a product, isolated in high yield, the microanalysis of which was consistent with the formulation [Cu₂(μ-Ph₂Pbipy)₂(PhCN)₂](PF₆)₂ (6), which is obtained as air stable bright yellow crystals (*see Scheme 3.1*). Significantly this complex could also be obtained by dissolving the dicopper complex (5) in benzonitrile and precipitating with diethyl ether.

Scheme 3.1. Synthesis of $[Cu_2(\mu\text{-}Ph_2Pbipy)_2(MeCN)_2]^{2+}$, $[Cu_2(\mu\text{-}Ph_2Pbipy)_2(PhCN)_2]^{2+}$ **and** $[Cu_2(\mu\text{-}Ph_2Pbipy)_2(H_2O)_2]^{2+}$
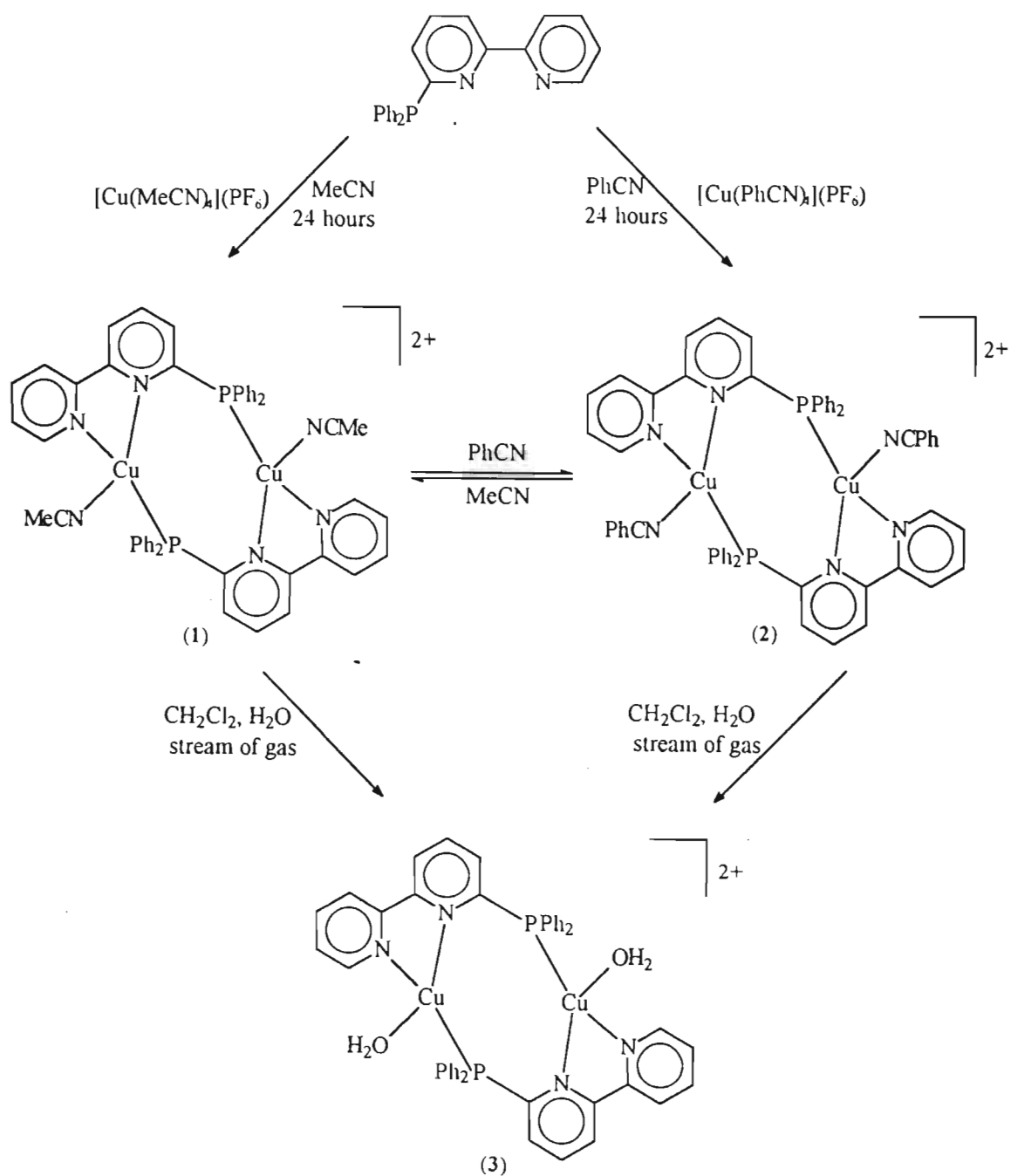
The ^{1}H nmr spectrum of the product, measured in CD_2Cl_2 at room temperature exhibits resonances between 6.9 and 8.8ppm readily assigned to the aromatic rings of the coordinated Ph_2Pbipy ligands. The sharp single methyl resonance at 2.00ppm observed in the ^{1}H nmr spectrum of the acetonitrile derivative (5) is no longer present (*see Table 3.8*). The solid state infrared spectrum (KBr disk) exhibits absorptions characteristic of the Ph_2Pbipy ligand and the anionic PF_6^- group, while the solution spectrum (measured in CH_2Cl_2) contains a peak at 2409cm^{-1} attributed to the C-N stretching vibration of the benzonitrile ligand (*see Table 3.7*). The $^{31}P\{^1H\}$ nmr spectrum, measured in CD_2Cl_2 contains a broad signal centred at 4.9ppm (*see section 3.2.1*).

Single crystals suitable for X-ray crystallography were grown by the slow diffusion of diethyl ether into a benzonitrile solution of $[Cu_2(\mu\text{-}Ph_2Pbipy)_2(PhCN)_2](PF_6)_2$. The crystal structure of (6) consists of well separated $[Cu_2(\mu\text{-}Ph_2Pbipy)_2(PhCN)_2]^{2+}$ cations and PF_6^- anions, there being no intermolecular contacts significantly less than the sum of the van der Waals radii for the atoms concerned. The structure of the cation is depicted in *Figure 3.8* along with the atom numbering scheme. A full listing of interatomic distances and angles is given after *section 3.5* at the end of this chapter.

Figure 3.8. **Molecular structure of** $[Cu_2(\mu\text{-}Ph_2Pbipy)_2(PhCN)_2](PF_6)_2$

The cation possesses a crystallographically imposed centre of symmetry midway between the copper atoms. As described before, the copper atoms are bridged by two Ph$_2$Pbipy ligands in the "head-to-tail" configuration, each ligand coordinating to one copper atom through a phosphorus donor atom and to the other through a chelating bipyridyl fragment. Each copper atom has its coordination completed by a benzonitrile group, the geometry thus attained being irregular tetrahedral. The irregular geometry is caused at least in part by the small angle of 79.9(1)° subtended by the bipyridyl fragment at the copper atom; other angles are closer to the idealised value of 109.5° and range up to 120.9(2)° for the N(3)-Cu-P(1) angle.

The coordinated benzonitrile ligand is linear as might be expected as evidenced by a N(3)-C(23)-C(24) angle of only 178.8(8)°. The Cu-Cu' distance of 3.795(2)Å is shorter than that obtained for complex (5) but is still too long to support direct copper-copper interaction. These and other molecular parameters are discussed further in *section 3.2.14* in relation to other closely related compounds whose crystal structures are reported in this thesis.

3.2.4. Synthesis, characterisation and crystal structure of [Cu$_2$(Ph$_2$Pbipy)$_2$(H$_2$O)$_2$](PF$_6$)$_2$ (7)

With the object of synthesising an aqua complex analogous to (5) that may be water soluble; attempts were made to replace the acetonitrile ligands in (5) with water molecules. However, when a suspension of the dicopper species (5) in water was stirred for 24 hours no replacement of the acetonitriles occurred. However, treatment of a dichloromethane solution of (5) with a small amount of water and a flow of gas (Ar, N$_2$, H$_2$, *etc*) resulted in the formation of [Cu$_2$(μ-Ph$_2$Pbipy)$_2$(H$_2$O)$_2$](PF$_6$)$_2$ (7) (*see Scheme 3.1*). The compound was isolated as orange crystals after the addition of diethyl ether to the dichloromethane water solution. It should be noted that if no gas is bubbled through the solution then no reaction occurs. This leads one to believe that the stream of gas may be involved in shifting the equilbrium of the reaction towards the formation of the aqua complex (7).

The ^{1}H nmr spectrum of the product, measured in CD$_2$Cl$_2$ at room temperature exhibits resonances between 7.3 and 8.6ppm readily assigned to the aromatic rings of the Ph$_2$Pbipy

ligand, a broad peak that lies between 4.5 and 4.8ppm is assigned to the hydrogen atoms on the coordinated water molecule (*see Table 3.8*). The solid state infrared spectrum (KBr disk) exhibits absorptions characteristic of the Ph_2Pbipy ligand and the anionic PF_6^- group. The $^{31}P\{^1H\}$ nmr spectrum, measured in CD_2Cl_2 exhibits a broad signal (*see section 3.2.1*).

Single crystals suitable for X-ray crystallography were grown by the slow diffusion of diethyl ether into a dichloromethane water solution of $[Cu_2(\mu-Ph_2Pbipy)_2(H_2O)_2](PF_6)_2$. The crystal structure of the complex consists of well separated $[Cu_2(\mu-Ph_2Pbipy)_2(H_2O)_2]^{2+}$ cations and PF_6^- anions, there being no intermolecular contacts significantly less than the sum of the van der Waals radii for the atoms concerned. The structure of the cation is depicted in *Figure 3.9* along with the atom numbering scheme. A full listing of interatomic distances and angles are given after *section 3.5* at the end of this chapter.

The cation possesses a crystallographically imposed centre of symmetry midway between the copper atoms. The two Ph_2Pbipy ligands bridge the copper atoms in a "head-to-tail" configuration, each ligand coordinating to one copper atom through a phosphorus donor atom and to the other through a chelating bipyridyl fragment. Each copper atom has its coordination completed by a water molecule, the geometry thus attained being irregular tetrahedral. The irregular geometry is probably caused as a result of the small angle of 79.9(1)° subtended by the bipyridyl fragment at the copper atom; other angles are closer to the idealised value of 109.5° and range up to 125.4(2)° for the P(1')-Cu-N(1) angle.

The Cu-Cu' distance of 3.084(4)Å is much shorter than that obtained for complex (5) but is still too long to support direct copper-copper interaction. The Cu-O distance is 2.209(4)Å and is normal. These and other molecular parameters are discussed further in *section 3.2.14* in relation to those observed for other Ph_2Pbipy ligand bridged dicopper (I) complexes. The dicopper aqua ligand complex (7) can also be prepared in a similar manner from the benzonitrile species (6).

Figure 3.9. Molecular structure of [Cu₂(μ-Ph₂Pbipy)₂(H₂O)₂](PF₆)₂
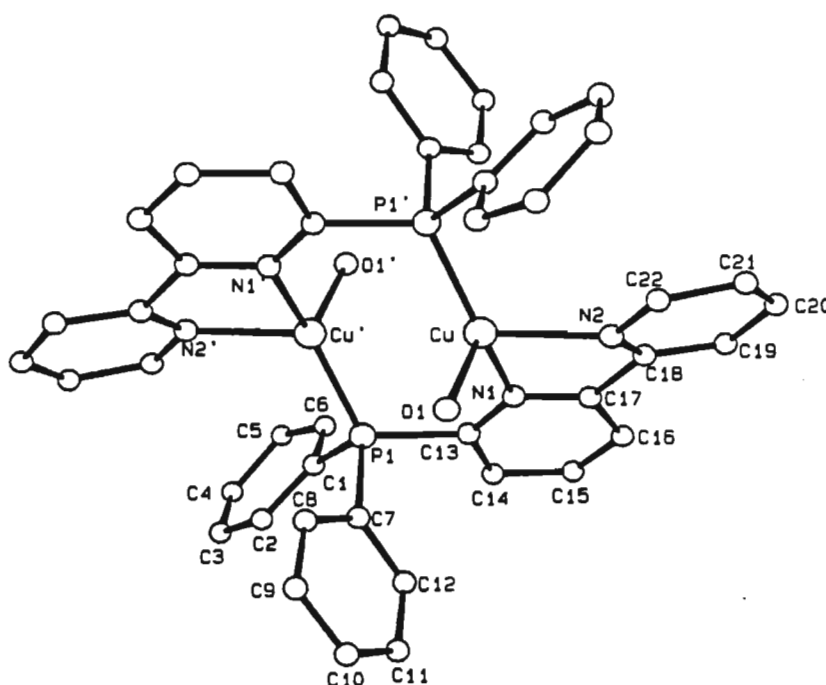
Figure 3.9. Molecular structure of [Cu$_2$(μ-Ph$_2$Pbipy)$_2$(H$_2$O)$_2$](PF$_6$)$_2$

It was anticipated that the acetonitrile ligands that were coordinated to the copper atoms in complex (5) were labile and a study of their substitution by other neutral and anionic ligands was initiated.

3.2.5. Substitution reactions of Cu₂(Ph₂Pbipy)₂(MeCN)₂](PF₆)₂ (5) with pyridines : Crystal structures of [Cu₂(Ph₂Pbipy)₂(py)₂](PF₆)₂ (8) and [Cu₂(Ph₂Pbipy)₂(4-Etpy)₂](PF₆)₂ (12)

The dicopper complex [Cu$_2$(μ-Ph$_2$Pbipy)$_2$(MeCN)$_2$](PF$_6$)$_2$ (5) has been reacted in dichloromethane with two mole equivalents of pyridine and a range of substituted pyridines (*see Scheme 3.2*). In all cases the acetonitrile ligands are easily displaced as evidenced by the disappearance of the resonance at 2.00ppm in the ^{1}H nmr spectra due to the methyl protons of the acetonitrile ligands. Compounds have been isolated as microcrystalline material and were found to afford products characterised as [Cu$_2$(Ph$_2$Pbipy)$_2$(L)$_2$](PF$_6$)$_2$ where L = py(**8**),

ampy(**9**), 2-vpy(**10**), 4-vpy(**11**), 4-Etpy(**12**), am-4-metpy(**13**) and merpy(**14**). Microanalytical analyses are given in *Table 3.6.*

Single crystals suitable for X-ray crystallography were grown by the slow diffusion of diethyl ether into a dichloromethane pyridine solution of $[Cu_2(\mu-Ph_2Pbipy)_2(py)_2](PF_6)_2$ The crystal structure of (**8**) consists of well separated $[Cu_2(\mu-Ph_2Pbipy)_2(py)_2]^{2+}$ cations and PF_6^- anions, there being no intermolecular contacts significantly less than the sum of the van der Waals radii for the atoms concerned. The structure of the cation is depicted in *Figure 3.10* along with the atom numbering scheme. A full listing of interatomic distances and angles are given after *section 3.5* at the end of this chapter.
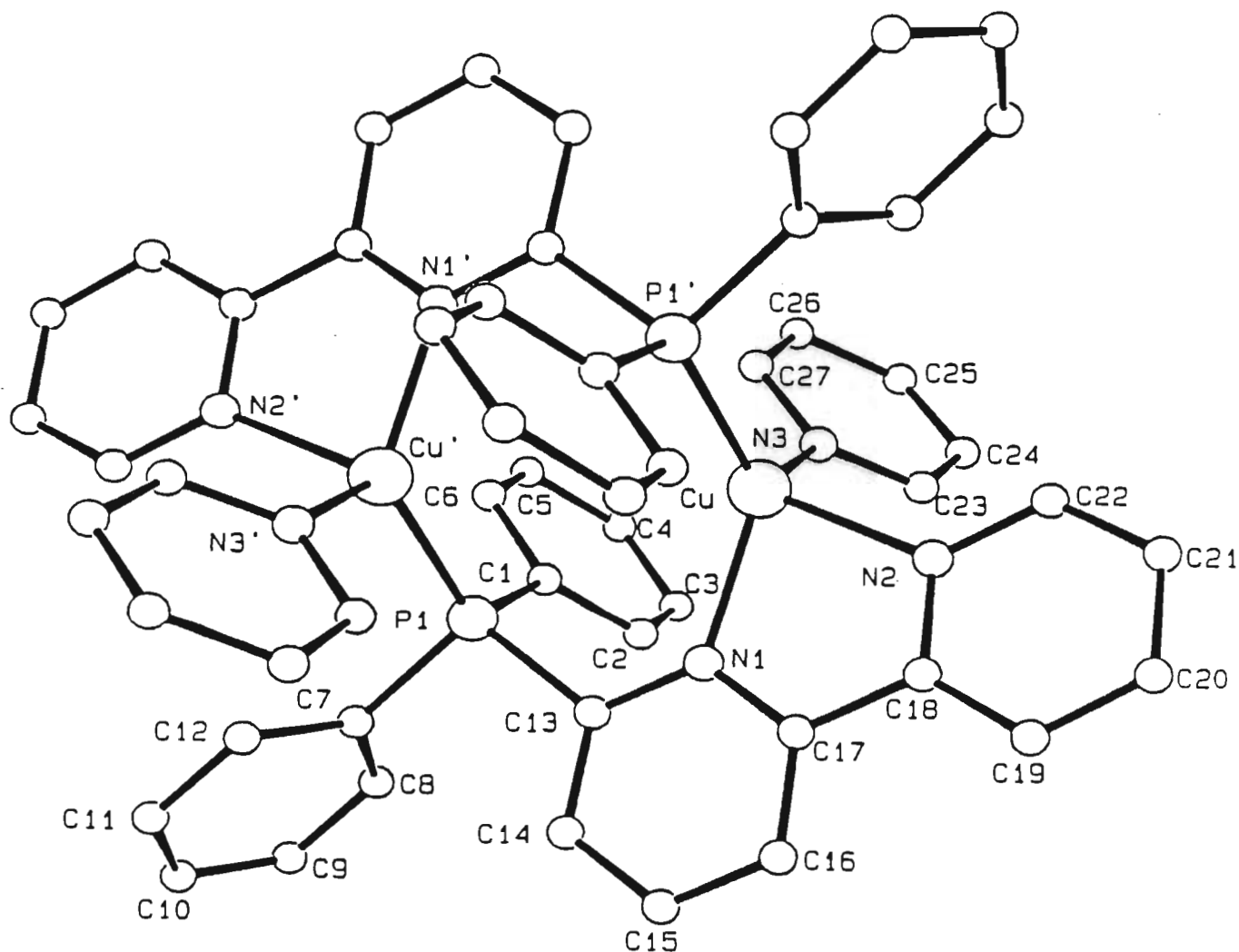
Figure 3.10. Molecular structure of $[Cu_2(\mu-Ph_2Pbipy)_2(py)_2](PF_6)_2$

Scheme 3.2. Substitution reactions [Cu$_2$(μ-Ph$_2$Pbipy)$_2$(MeCN)$_2$]$^{2+}$ with pyridines
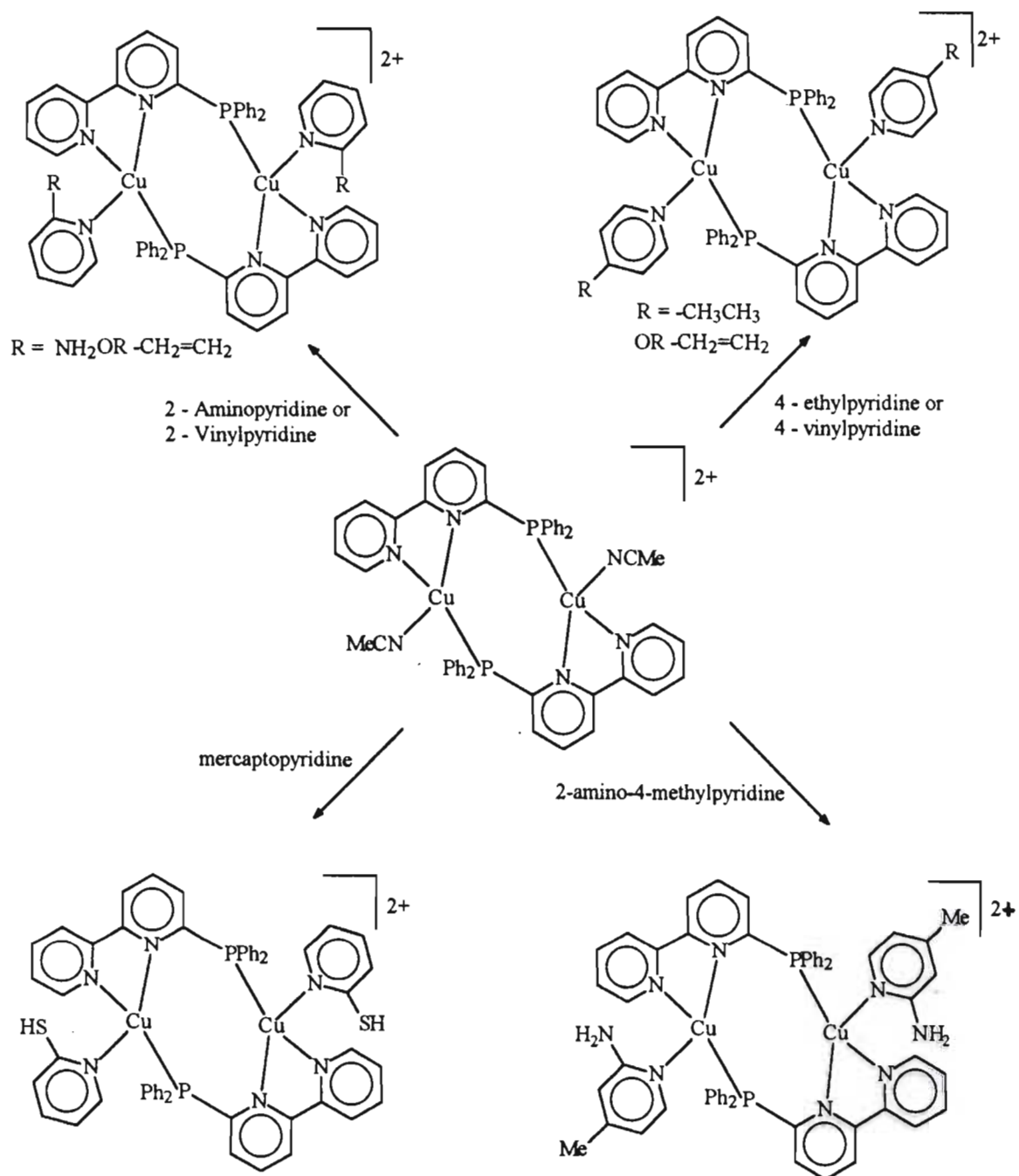
The cation possesses a crystallographically imposed centre of symmetry midway between the copper atoms. As described before, the copper atoms are bridged by two Ph_2Pbipy ligands in the "head-to-tail" configuration, each ligand coordinating to one copper atom through a phosphorus donor atom and to the other through a chelating bipyridyl fragment. Each copper atom has its coordination completed by a pyridyl ligand, the geometry thus attained being irregular tetrahedral. The irregular geometry is caused at least in part by the small angle of $79.6(1)°$ subtended by the bipyridyl fragment at the copper atom; other angles are closer to the idealised value of $109.5°$ and range up to $117.1(1)°$ for the N(1)-Cu-N(3) angle. The Cu-Cu' distance of $3.865(2)Å$ is shorter than that obtained for complex (5) but is still too long to support direct copper-copper interaction. These and other molecular parameters are discussed further in *section 3.2.14* in relation to those observed for other Ph_2Pbipy ligand bridged dicopper (I) complexes.

The solid state infrared spectra (KBr disk) of the dicopper complexes (8), (9), (10), (11), (12), (13) and (14) formed from the reaction of (5) with pyridyl or substituted pyridyl ligands display the characteristic Ph_2Pbipy ligand peaks as well as the PF_6^- anion peak (*see Table 3.7*). The $^{31}P\{^1H\}$ nmr spectra of these dicopper complexes exhibit broad featureless resonances (*see section 3.2.1*).

The ^1H nmr spectra of the dicopper complexes (8), (9), (10), (11), (12), (13) and (14) containing pyridyl or substituted pyridyl ligands exhibit resonances that lie between 7.6 and 8.5ppm associated with aromatic rings of the Ph_2Pbipy and the pyridyl and substituted pyridyl ligands (*see Table 3.8*). In many instances the substituent on the pyridyl ligand gives a proton nmr signal that occurs in a different region. Thus in $[Cu_2(\mu-Ph_2Pbipy)_2(ampy)_2](PF_6)_2$ (9) a broad signal due to the amino group occurs between 4.6 and 4.9ppm, while in $[Cu_2(\mu-Ph_2Pbipy)_2(2-vpy)_2](PF_6)_2$ (10) and $[Cu_2(\mu-Ph_2Pbipy)_2(4-vpy)_2](PF_6)_2$ (11) the doublet of doublets due to the vinylic protons occurs between 5.5 and 5.9ppm. In $[Cu_2(\mu-Ph_2Pbipy)_2(Etpy)_2](PF_6)_2$ (12) the ethyl group from the 4-ethyl pyridyl ligand gives rise to the characteristic pattern of a triplet and a quartet while in $[Cu_2(\mu-Ph_2Pbipy)_2(am-4-metpy)_2](PF_6)_2$

(13) the methyl group gives rise to a peak at 1.5ppm and the amino group gives rise to a broad signal between 4.5 and 4.7ppm.

In an attempt to establish that the substituted pyridyl ligands coordinate in a similar manner to the pyridyl ligand, single crystals suitable for X-ray crystallography were grown by the slow diffusion of diethyl ether into a dichloromethane solution of (12). The crystal structure of (12) consists of well separated $[Cu_2(\mu\text{-}Ph_2Pbipy)_2(4\text{-}Etpy)_2]^{2+}$ cations and PF_6^- anions, there being no intermolecular contacts significantly less than the sum of the van der Waals radii for the atoms concerned. The structure of the cation is depicted in *Figure 3.11* along with the atom numbering scheme. A full listing of interatomic distances and angles are given after *section 3.5* at the end of this chapter.

The cation possesses a crystallographically imposed centre of symmetry midway between the copper atoms. The two Ph_2Pbipy ligands bridge the copper atoms in a "head-to-tail" configuration, each ligand coordinating to one copper atom through a phosphorus donor atom and to the other through a chelating bipyridyl fragment. Each copper atom has it's coordination completed by the 4-ethyl pyridyl ligand, the geometry thus attained being irregular tetrahedral. The irregular geometry is caused at least in part by the small angle of 79.9(3)° subtended by the bipyridyl fragment at the copper atom; other angles are closer to the idealised value of 109.5° and range up to 115.6(2)° for the N(3)-Cu-P(1) angle. These and other molecular parameters are discussed further in *section 3.2.14* in relation to those observed for other Ph_2Pbipy ligand bridged dicopper (I) complexes.
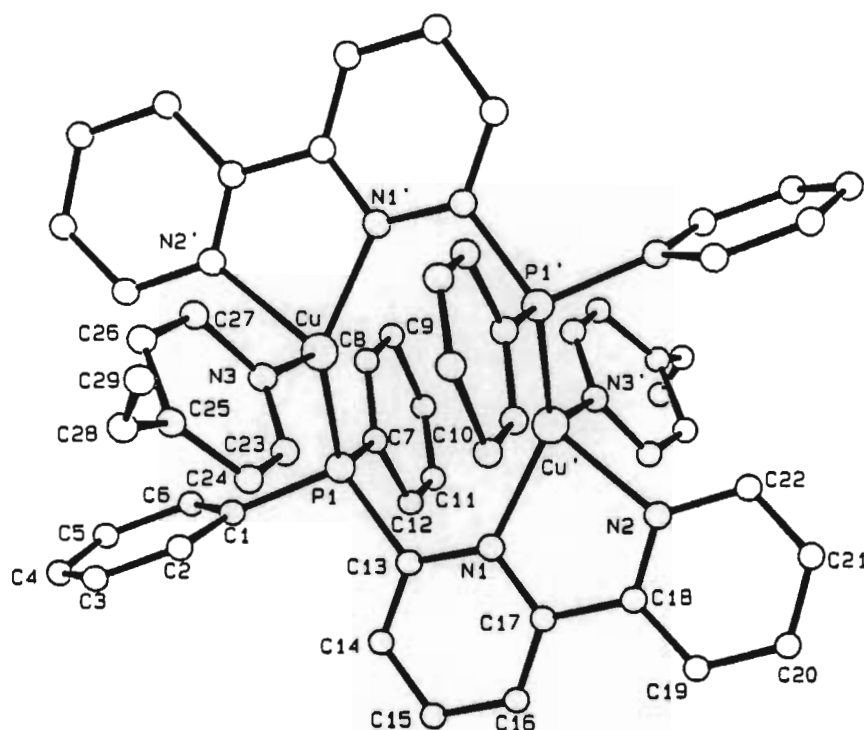
Figure 3.11. Molecular structure of [Cu$_2$(μ-Ph$_2$Pbipy)$_2$(4-Etpy)$_2$](PF$_6$)$_2$

3.2.6. Substitution reactions of [Cu$_2$(Ph$_2$Pbipy)$_2$(MeCN)$_2$](PF$_6$)$_2$ (5) with bridging polypyridines

The dicopper complex [Cu$_2$(μ-Ph$_2$Pbipy)$_2$(MeCN)$_2$](PF$_6$)$_2$ **(5)** has been reacted in dichloromethane with an equimolar amount of 4,4' - bipyridine and *trans*-1,2-*bis*(4-pyridyl)ethylene (*see Scheme 3.3*). A yellow precipitate formed as the dicopper dimer was added to the bipyridine. When the order of addition was reversed the precipitate still formed. The complexes synthesised are insoluble in all common organic solvents and therefore, no solution infrared, ^{1}H nmr, ^{13}C nmr or ^{31}P{^{1}H} nmr spectra could be obtained. Solid state infra red (KBr disk) spectra indicate that the Ph$_2$Pbipy ligand as well as the anionic PF$_6^-$ group are present (*see Table 3.4*).

Due to the fact that the complexes synthesised were so insoluble we proposed that most probably exist as polymers with the formulation {[Cu$_2$(μ-Ph$_2$Pbipy)$_2$(L)](PF$_6$)$_2$}$_n$ where L = 4,4'-bipyridine **(15)** or *trans*-1,2-*bis*(4-pyridyl)ethylene **(16)**. Microanalytical analyses fit very well with the proposed formulation for the compounds (*see Table 3.3*). It is interesting to note

that an analogous disilver complex, $\{[Ag_2(Ph_2Pbipy)_2(4,4'\text{-bipy})](PF_6)_2\}_n$ which has been characterised by x-ray crystallography is soluble in dichloromethane, acetonitrile and methanol.[85]

Scheme 3.3. Substitution reactions of (5) with bridging bipyridines
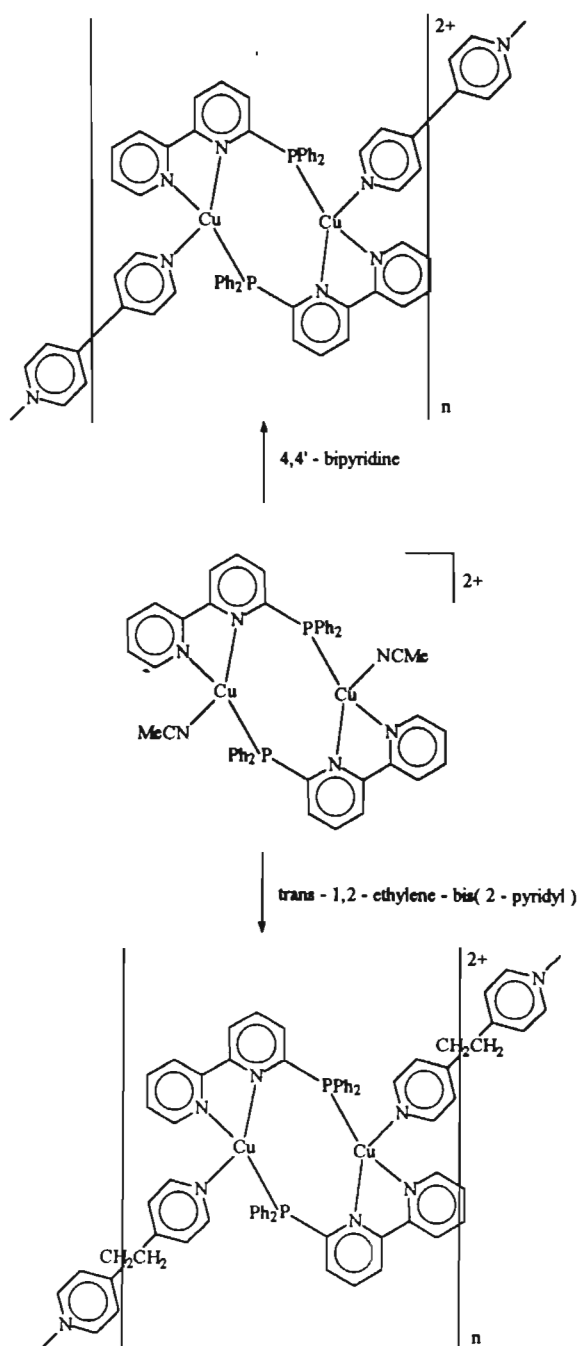
3.2.7. Substitution reactions of [Cu$_2$(Ph$_2$Pbipy)$_2$(MeCN)$_2$](PF$_6$)$_2$ (5) with chelating bipyridines: Crystal structure of [Cu$_2$(μ-Ph$_2$Pbipy)$_2$(η-2,2'-bipy)](PF$_6$)$_2$ (17)

Treatment of an acetonitrile solution of [Cu$_2$(μ-Ph$_2$Pbipy)$_2$(MeCN)$_2$](PF$_6$)$_2$ (5) with an equimolar amount of chelating bipyridine at room temperature affords air stable red crystalline solids characterised as [Cu$_2$(μ-Ph$_2$Pbipy)$_2$(η^2-L)](PF$_6$)$_2$ where L = 2,2'-bipyridine (17), 1,10-phenanthroline (18) or 2,3-*bis*(2-pyridyl)pyrazine (19) (*see Scheme 3.4*). The dicopper complex (17) was also prepared by treating an acetone solution of [Cu(MeCN)$_4$]$^+$ with one equivalent of 2,2'-bipyridine under a nitrogen atmosphere, this was followed by the addition of Ph$_2$Pbipy ligand and the precipitation of the product by the addition of hexane. The microanalytical analyses and the spectral data of complexes (17), (18) and (19) are given in *Tables 3.6, 3.7* and *3.8*.

In order to establish the molecular structure of these complexes, single crystals of (17) were grown at low temperature by the slow diffusion of hexane into an acetone solution of (17). The crystal structure of (17) consists of well separated [Cu$_2$(μ-Ph$_2$Pbipy)$_2$(η-2,2'-bipy)]$^{2+}$ cations and PF$_6^-$ anions, there being no intermolecular contacts significantly less than the sum of the van der Waals radii for the atoms concerned. The structure of the cation is depicted in *Figure 3.12* along with the atom numbering scheme. A full listing of interatomic distances and angles are given after *section 3.5* at the end of this chapter.

The copper atoms are bridged by two Ph$_2$Pbipy ligands, however the ligand coordinates in a different manner in this molecule to that in the other dicopper complexes described thus far. In complex (17) the Ph$_2$Pbipy ligand is coordinated in a "head-to-head" manner, *i.e* the phosphorus atoms of the ligands are bonded to the same copper atom. The bipyridyl fragments of each ligand chelate around the second copper atom, *i.e.* Cu(2). The coordination at the first copper atom is completed by a chelating 2,2'-bipyridyl ligand. Cu(1) has an irregular tetrahedral geometry that is caused at least in part by the small angle of 79.3(6)° subtended by the 2,2'-bipyridyl ligand at the copper atom. The presence of two chelating fragments on

Cu(2) also leads to the copper atom having an irregular tetrahedral geometry, the N(1)-Cu(2)-N(2) bond angle being 81.9(9)° while the N(3)-Cu(2)-N(4) bond angle is 79.2(9)°.

The Cu-Cu' distance of 3.683(2)Å is too long to support direct copper-copper interaction. These and other molecular parameters are discussed further in *section 3.2.14* in relation to those observed for other Ph₂Pbipy ligand bridged dicopper (I) complexes.

Figure 3.12. Molecular structure of [Cu₂(μ-Ph₂Pbipy)₂(η-2,2'-bipy)](PF₆)₂
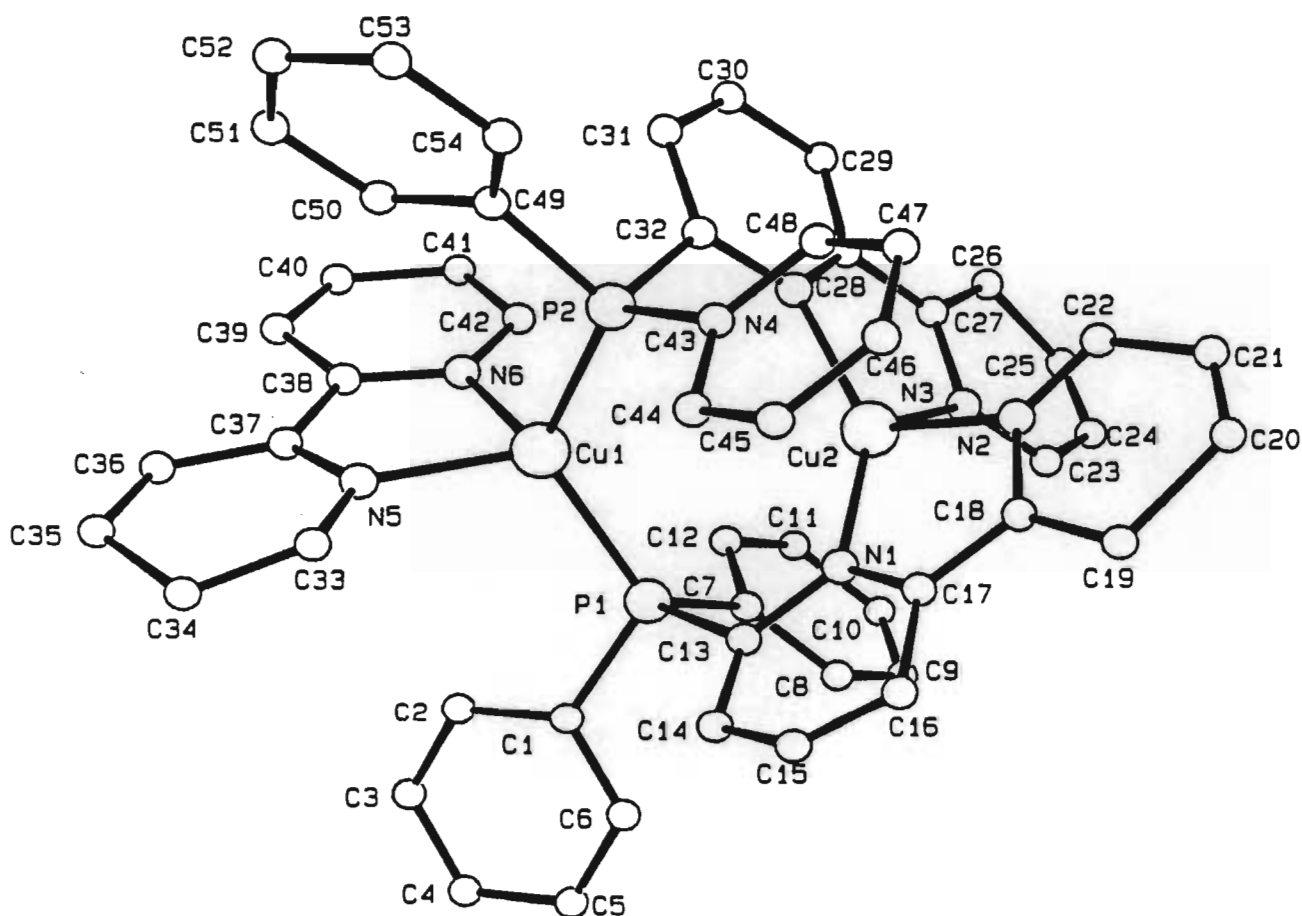
Scheme 3.4. Substitution reactions of (5) with chelating bipyridines
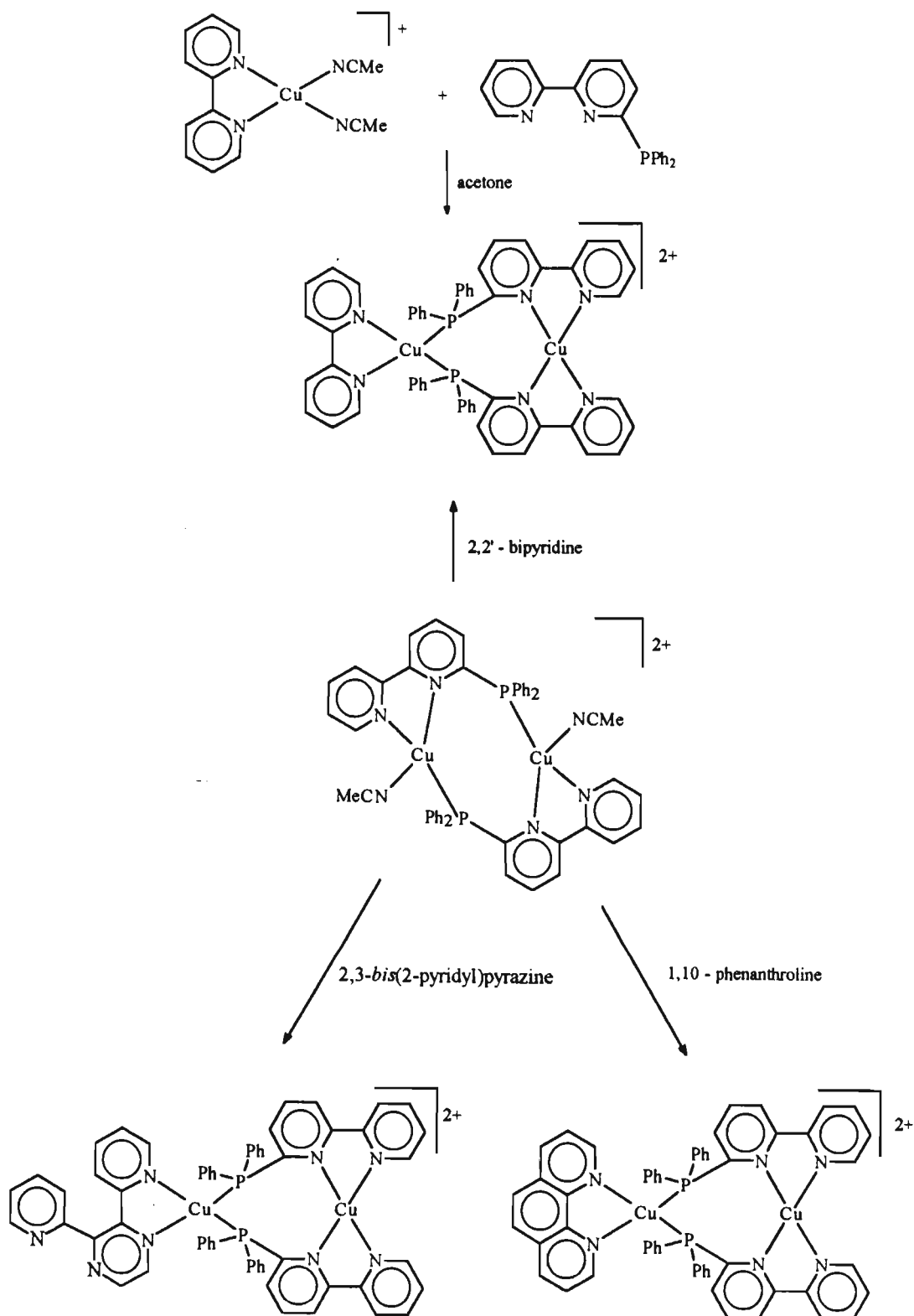
3.2.8. Substitution reactions of $[Cu_2(Ph_2Pbipy)_2(MeCN)_2](PF_6)_2$ (5) with heterocycles

The dicopper complex $[Cu_2(\mu\text{-}Ph_2Pbipy)_2(MeCN)_2](PF_6)_2$ (5) has been reacted in dichloromethane with two mole equivalents of nitrogen containing heterocycles (*see Scheme 3.5*). In all cases the acetonitrile ligands are easily displaced as evidenced by the disappearance of the resonance at 2.00ppm in the ^1H nmr spectra due to the methyl protons of the acetonitrile ligands. Compounds have been isolated as microcrystalline material and the microanalysis is consistent with the formulation $[Cu_2(\mu\text{-}Ph_2Pbipy)_2(L)_2](PF_6)_2$ where L = azaindole(20) or pyrazzole(21).

The reactions were initially attempted by reacting (5) with an equimolar amount of the heterocycle in an attempt to synthesise more "head-to-head" complexes similar to $[Cu_2(\mu\text{-}Ph_2Pbipy)_2(\eta\text{-}2,2'\text{-}bipy)](PF_6)_2$ (17), unfortunately this did not occur. The heterocycles coordinated in a manner similar to the pyridines and substituted pyridines (*see Scheme 3.2*). By adding a twice molar amount of the heterocycle we found that the yields were substantially increased. The infrared spectra (KBr disk) of the dicopper complexes (20) and (21) have the characteristic Ph_2Pbipy ligand peaks as well as the PF_6^- anion peak (*see Table 3.7*). The $^{31}P\{^1H\}$ nmr spectra of the dicopper complexes consists of a broad featureless band centred around 4.5ppm (*see section 3.2.1*).

The ^1H nmr spectra the dicopper complexes (20) and (21) have resonances that lie between 7.2 and 8.5ppm which are readily assigned to the aromatic rings of the co-ordinated Ph_2Pbipy and polypyridyl ligands. In $[Cu_2(\mu\text{-}Ph_2Pbipy)_2(azaindole)_2](PF_6)_2$ (20) a broad resonance due to the proton attached to the one nitrogen occurs between 1.8 and 1.9ppm, while in $[Cu_2(\mu\text{-}Ph_2Pbipy)_2(pyrazole)_2](PF_6)_2$ (21) the broad resonance due to the proton attached to the one nitrogen occurs between 1.6 and 2.1ppm (*see Table 3.8*).

Scheme 3.5. Substitution reactions of (5) with other heterocyclic ligands
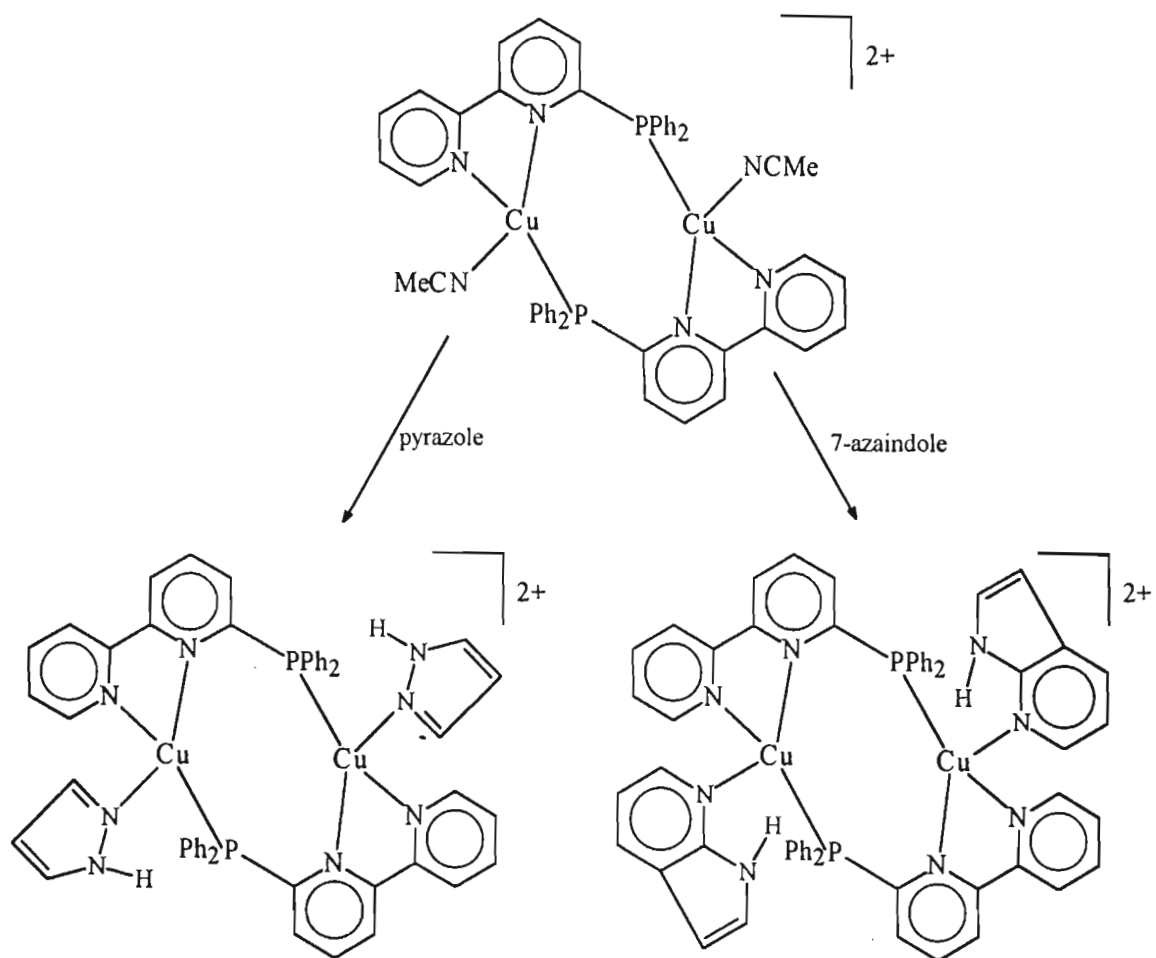
3.2.9. Substitution reactions of [Cu₂(Ph₂Pbipy)₂(MeCN)₂](PF₆)₂ (5) with diphosphorus ligands

Treatment of a dichloromethane solution of $[Cu_2(\mu\text{-}Ph_2Pbipy)_2(MeCN)_2](PF_6)_2$ (5) with one equivalent of a diphosphorus ligand was found to afford a product characterised as $[Cu_2(\mu\text{-}Ph_2Pbipy)_2(L)](PF_6)_2$ where L = dppm (22), dppe (23) or dppp (24) (*see Scheme 3.6*). The dicopper complexes (22), (23) and (24) are isolated as yellow-orange crystalline solids by the addition of diethyl ether to the respective dichloromethane solutions. Satisfactory microanalytical analyses for carbon, hydrogen, nitrogen and phosphorus were obtained (*see Table 3.6*)

The ^1H nmr spectra of these complexes exhibit resonances between 6.9 and 8.8ppm which are readily assigned to the aromatic rings of the co-ordinated Ph₂Pbipy and bidentate diphosphorus ligands; the absence of the signal at 1.86ppm which was due the methyl protons in (5) indicates that the acetonitrile ligands have been successfully replaced. The aliphatic protons (from the diphosphorus ligands) resonances appear in the nmr spectra between 3.2 and 3.5ppm for (22), 3.3 and 3.5ppm for (23) and 3.3 and 3.7ppm for (24); in fact these resonances confirm that the diphosphorus ligands are present (*see Table 3.5*). The $^{31}P\{^1H\}$ nmr spectra for the dicopper complexes containing the diphosphorus ligands unfortunately also exhibit broad bands which do not allow separate resonances for the different phosphorus atoms to be discerned. The characteristic Ph₂Pbipy, diphosphorus ligand and anionic PF_6^- peaks appear in the solid state infrared spectra (*see Table 3.4*).

The diphosphorus ligands could adopt either one of two modes of coordination; firstly, they could bridge across the two copper atoms which would result in the Ph₂Pbipy ligand adopting a "head-to-tail" coordination. In the second option, the diphosphorus ligands could chelate at one copper atom (as 2,2'-bipy does in complex (17)) and therefore the Ph₂Pbipy ligand would coordinate in a "head-to-head" manner but, due to the poor resolution of the $^{31}P\{^1H\}$ nmr spectra we cannot accurately predict which way these diphosphorus ligands coordinate. Despite several attempts to try and replace the acetonitrile ligand from the dicopper complex

(5) with PPh₃, no success was achieved, the ¹H nmr, ³¹P{¹H} nmr and infrared spectra recorded of the mixture being identical to that of the parent complex (5).

Scheme 3.6 Substitution reactions of (5) with diphosphorus ligands

Y = -CH₂-, -CH₂CH₂-, -CH₂CH₂CH₂-
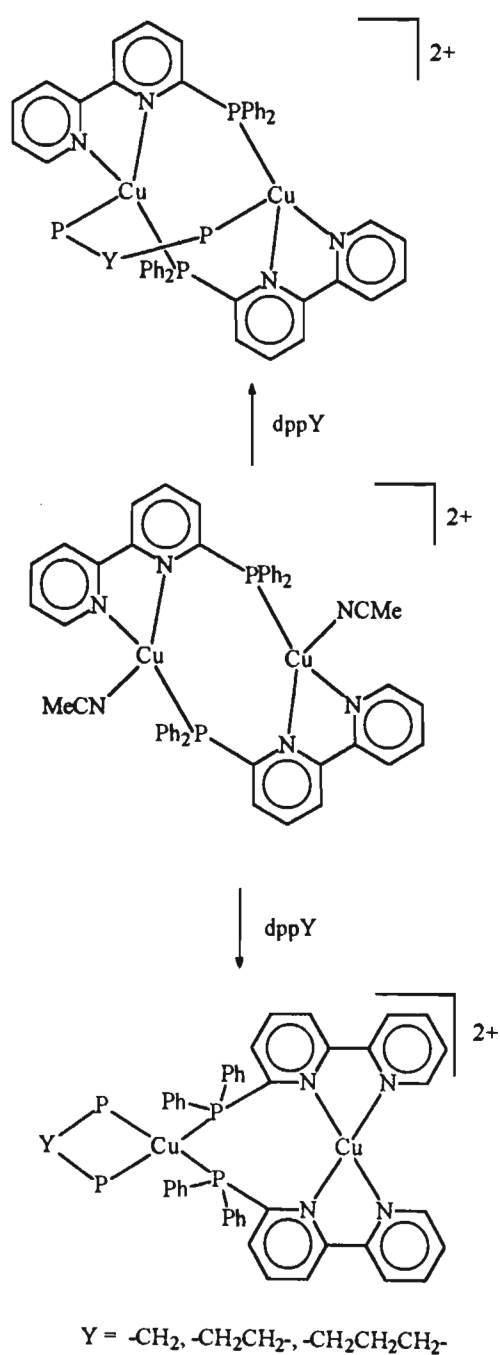
3.2.10. Substitution reactions of [Cu$_2$(Ph$_2$Pbipy)$_2$(MeCN)$_2$](PF$_6$)$_2$ (5) with halide ligands : Crystal structures of [Cu$_2$(μ-Ph$_2$Pbipy)$_2$(μ-I)](PF$_6$) (25) and [Cu$_2$(μ-Ph$_2$Pbipy)$_2$(μ-Br)](PF$_6$) (26)

Treatment of a dichloromethane solution [Cu$_2$(μ-Ph$_2$Pbipy)$_2$(MeCN)$_2$](PF$_6$)$_2$ (5) with one equivalent of the appropriate tetrabutylammonium halide salt was found to afford a product characterised as [Cu$_2$(μ-Ph$_2$Pbipy)$_2$(μ-L)](PF$_6$) where L = I (25), Br (26) or Cl (27) (*see Scheme 3.7*). The dicopper complexes (25), (26) and (27) are isolated as orange-yellow crystalline solids by the addition of diethyl ether to the respective dichloromethane solutions.

These dicopper complexes can also be synthesised by the addition of a dichloromethane solution of (5) to a suspension of the potassium halide salt or by addition of the potassium halide salt to a dichloromethane solution of (5). The yields obtained when the dicopper complexes (25), (26) and (27) are prepared by this method are slightly higher than when the tetrabutylammonium salts are used. The spectral data for these complexes are listed in *Tables 3.7* and *3.8*. Satisfactory microanalytical analyses were obtained for all complexes produced, halogen analyses also being obtained for these halogen bridged dicopper (I) complexes.

Several attempts were made to try and generate neutral dicopper complexes by addition of an excess of the appropriate halide ion to a refluxing solution of (25), (26) and (27) in dichloromethane. The dicopper parent complex (5) was reacted with an excess of halide salts and even refluxed in an excess of the different halide salts. However there was no evidence of the coordination of a second halide ion and the formation of a neutral species.

In order to determine the exact mode of coordination of the Ph$_2$Pbipy and the halide ligands in these complexes, single crystals of the iodo bridged species suitable for X-ray crystallography were grown by the slow evaporation of a dichloromethane solution of (25). The crystal structure of [Cu$_2$(μ-Ph$_2$Pbipy)$_2$(μ-I)](PF$_6$) consists of well separated [Cu$_2$(μ-Ph$_2$Pbipy)$_2$(μ-I)]$^+$ cations and a PF$_6^-$ anions, there being no intermolecular contacts significantly less than the sum of the van der Waals radii for the atoms concerned. The structure of the cation is depicted in *Figure 3.13* along with the atom numbering scheme. A

full listing of interatomic distances and angles is given after *section 3.5* at the end of this chapter.

Scheme 3.7. Substitution reactions of (5) with halide ligands
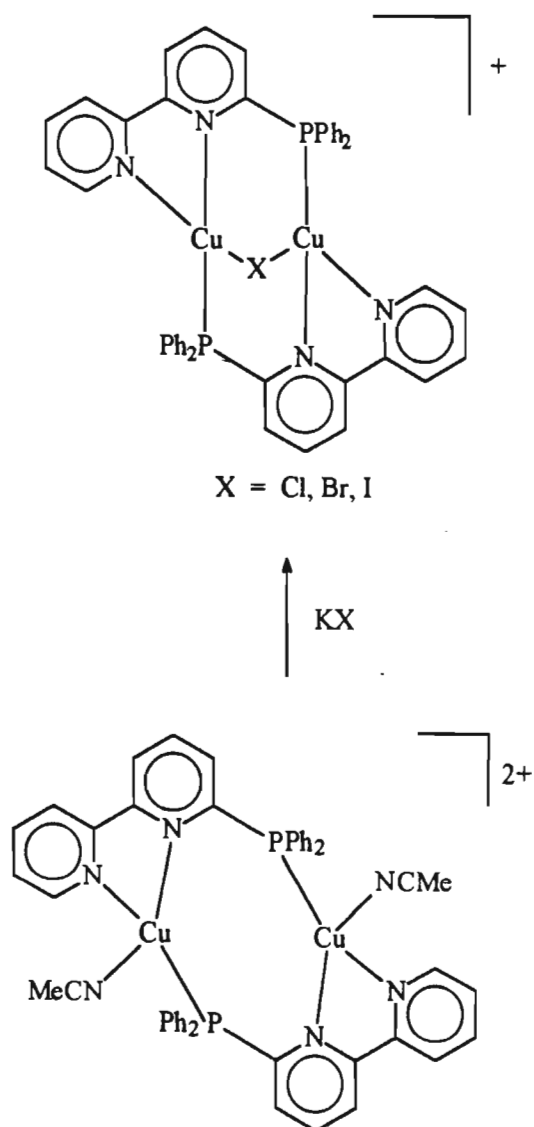
X = Cl, Br, I

KX

The cation possesses a crystallographically imposed two fold axis which passes through the bridging iodide atom. The copper atoms are bridged by two Ph_2Pbipy ligands in the "head-to-tail" configuration, each ligand coordinating to one copper atom through a phosphorus donor atom and to the other through a chelating bipyridyl fragment. The iodide ligand also bridges across the two copper atoms resulting in the geometry at each copper being irregular tetrahedral. The irregular geometry is caused at least in part by the small angle of $79.2(2)°$ subtended by the bipyridyl fragment at the copper atom; other angles are closer to the idealised value of $109.5°$ and range up to $127.8(2)°$ for the P(1')-Cu-N(1) angle. An interesting feature of this complex is that the presence of another bridging ligand results in a significant decrease in the Cu-Cu distance; thus Cu-Cu' distance of $2.770(1)Å$ is much smaller than the Cu-Cu distance of $3.941(2)Å$ in the parent dicopper complex (5). These and other molecular parameters are discussed further in *section 3.2.14* in relation to those observed for other Ph_2Pbipy ligand bridged dicopper (I) complexes.
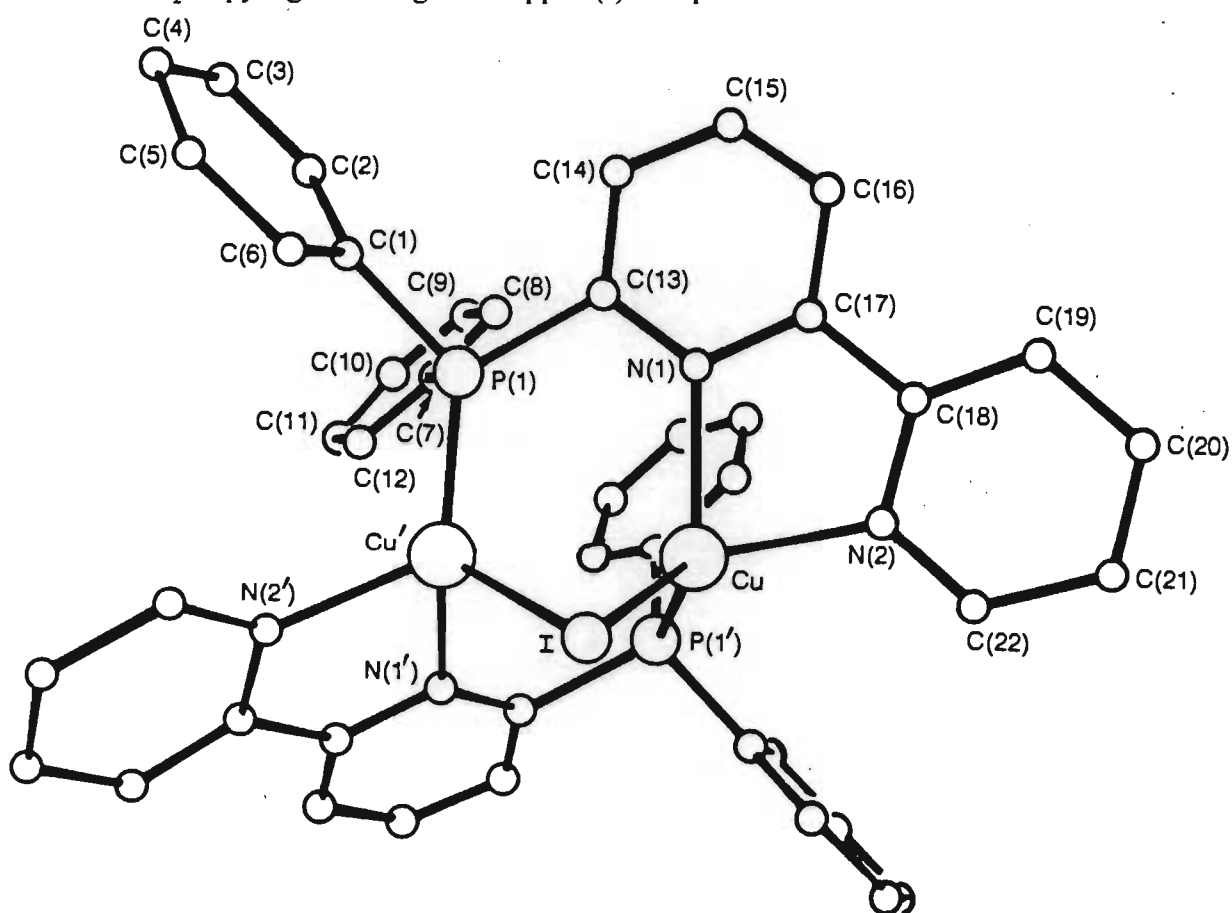
Figure 3.13. Molecular structure of $[Cu_2(\mu\text{-}Ph_2Pbipy)_2(\mu\text{-}I)](PF_6)$

In an attempt to show that the other halides also bridge across the copper atoms, single crystals of $[Cu_2(\mu\text{-}Ph_2Pbipy)_2(\mu\text{-}Br)](PF_6)$ (26) were grown by the slow diffusion of diethyl ether into a dichloromethane solution of (26). The crystal structure of (26) consists of well separated $[Cu_2(\mu\text{-}Ph_2Pbipy)_2(\mu\text{-}Br)]^+$ cations and PF_6^- anions, there being no intermolecular contacts significantly less than the sum of the van der Waals radii for the atoms concerned. The structure of the cation is depicted in *Figure 3.14* along with the atom numbering scheme. A full listing of interatomic distances and angles is given after *section 3.5* at the end of this chapter.
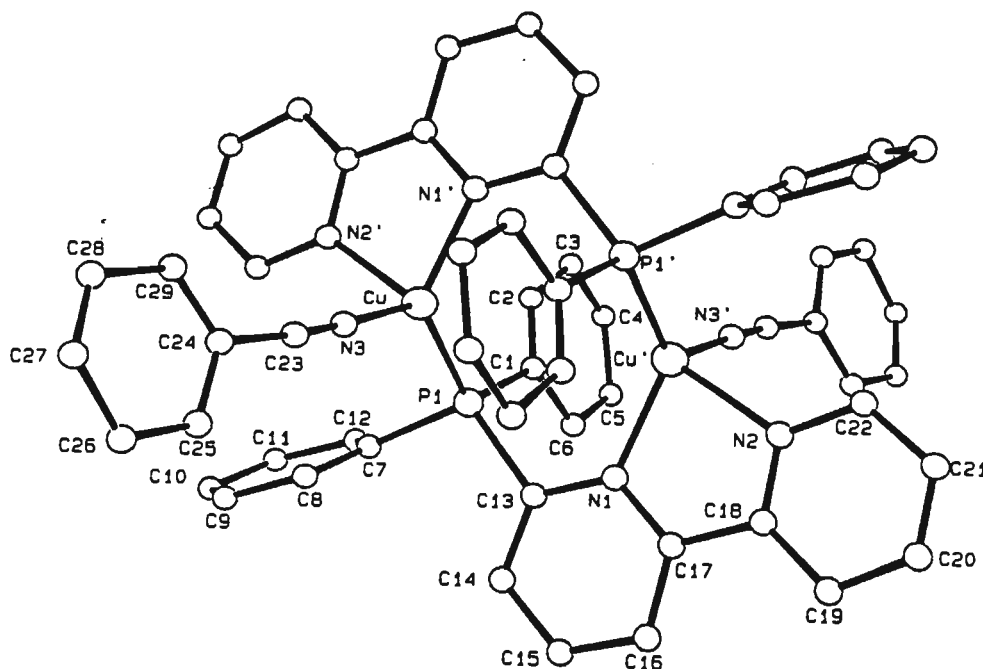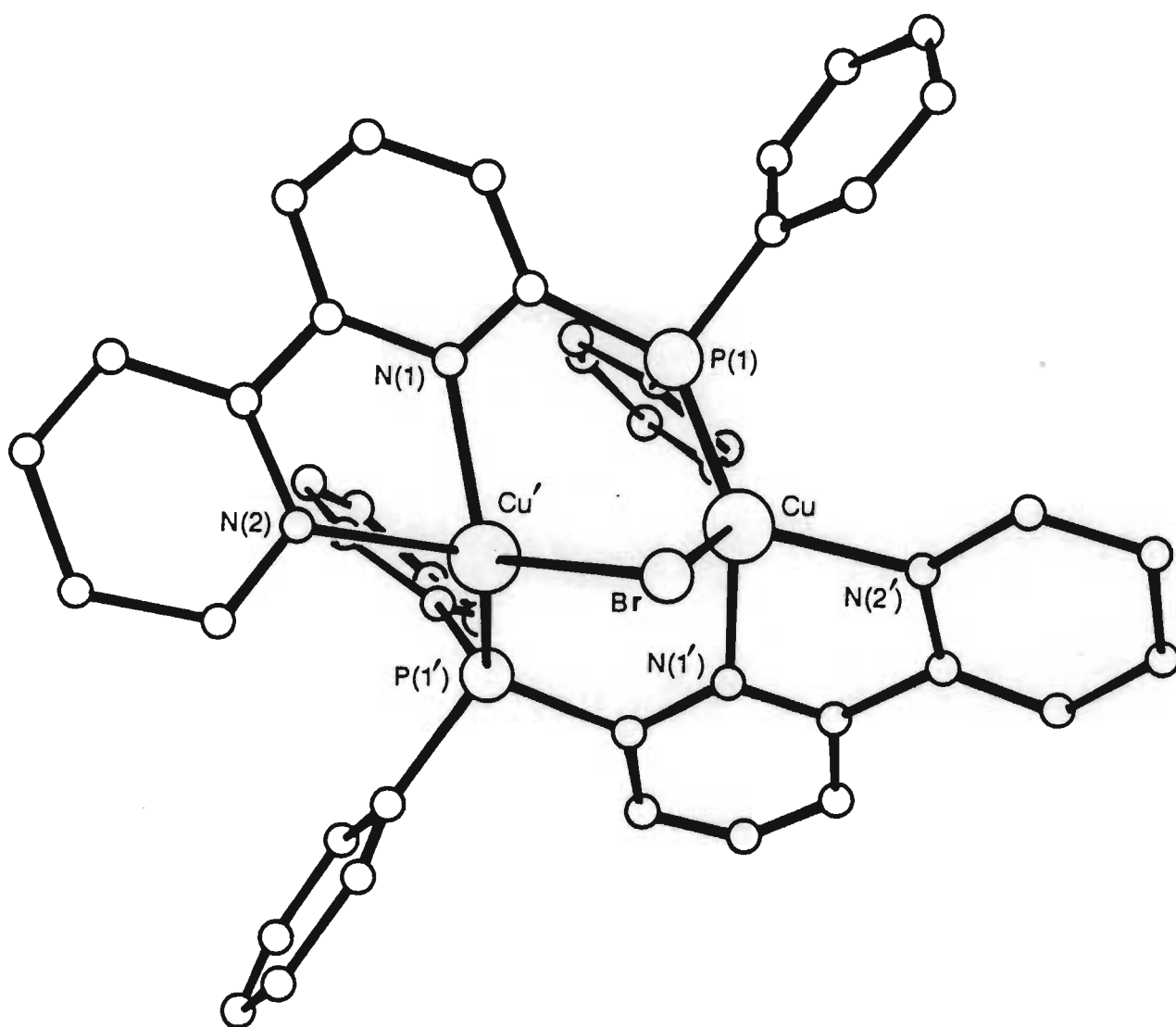

Figure 3.14. Molecular structure of $[Cu_2(\mu\text{-}Ph_2Pbipy)_2(\mu\text{-}Br)](PF_6)$

The cation possesses a crystallographically imposed two fold axis which passes through the bridging bromide atom. The copper atoms are bridged by two Ph$_2$Pbipy ligands in the "head-to-tail" configuration, each ligand coordinating to one copper atom through a phosphorus donor atom and to the other through a chelating bipyridyl fragment. The bromide ligand also bridges across the two copper atoms resulting in the geometry at each copper being irregular tetrahedral. The irregular geometry is probably caused as a result of the small angle of 78.8(6)° subtended by the bipyridyl fragment at the copper atom; other angles are closer to the idealised value of 109.5° and range up to 127.0(4)° for the P(1')-Cu-N(1) angle.

An interesting feature of this complex is that the presence of another bridging ligand results in a significant decrease in the Cu-Cu' distance, the Cu-Cu' distance of 2.762(4)Å is much shorter than the Cu-Cu' distance of 3.941(2)Å in the parent dicopper complex (5). These and other molecular parameters are discussed further in *section 3.2.14* in relation to those observed for other Ph$_2$Pbipy ligand bridged dicopper (I) complexes.

3.2.11. Substitution reactions of (5) with anionic sulphur donor ligands : Crystal structure of [Cu$_2$(μ-Ph$_2$Pbipy)$_2$(μ-SEt)](PF$_6$) (28)

Treatment of a suspension of the appropriate anionic sulphur donor ligand (sodium salt) with a dichloromethane solution of the dicopper complex (5) was found to afford products charcaterised as [Cu$_2$(μ-Ph$_2$Pbipy)$_2$(μ-L)](PF$_6$) where L = SEt (28), SCN (29) or S$_2$CN(Et)$_2$ (30) *(see scheme 3.8)*. The complexes can also be conveniently prepared by adding the appropriate sodium salt to a dichloromethane solution of (5). The complexes are obtained as orange-red crystalline solids and are air stable. Satisfactory microanalytical analyses were obtained for all complexes *(see Table 3.6)*

The ^{1}H nmr spectra of these complexes exhibits resonances between 6.9 and 8.8ppm which are readily assigned to the aromatic rings of the co-ordinated Ph$_2$Pbipy ligand; the absence of the signal at 2.00ppm which was due the methyl protons in (5) indicates that the acetonitrile ligands have been successfully replaced. The ^{1}H nmr spectra of (28) and (29)

exhibit the characteristic pattern of a triplet and a quartet assigned to the ethyl groups of the sulphur donor ligands (*see Table 3.8*).

Scheme 3.8. Substitution reactions of (1) with anionic sulphur donor ligands
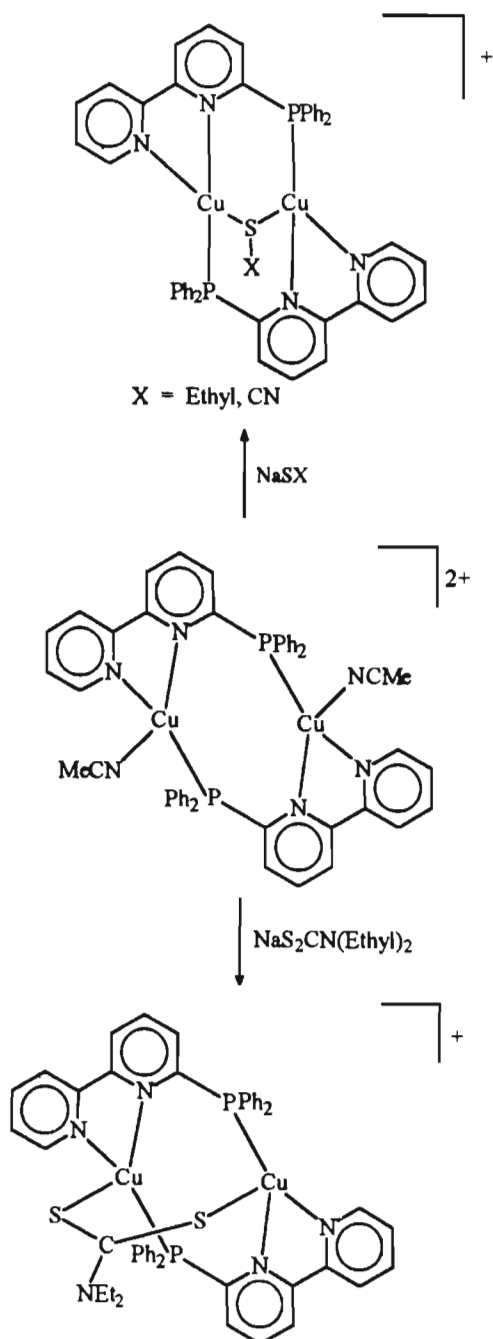
X = Ethyl, CN

NaSX

NaS₂CN(Ethyl)₂

The solid state infrared spectra of these complexes exhibit the typical Ph$_2$Pbipy peaks as well as a peak due to the carbon-nitrogen stretch of the SCN$^-$ ligand at 2100cm^{-1} for complex (29). The presence of the anionic PF$_6^-$ group also indicates that the dicopper complexes that are formed are cationic and not neutral. In complex (30) the two donor sulphur atoms of the dithiocarbamate presumably bridge the two copper atoms whereas in (28) and (29) a single sulphur atom bridges the two copper atoms.

In order to determine the exact mode of coordination of the Ph$_2$Pbipy ligand and the sulphur containing ligand in this complex, single crystals suitable for X-ray crystallography were grown by the slow evaporation of a dichloromethane solution of (28). The crystal structure of [Cu$_2$(μ-Ph$_2$Pbipy)$_2$(μ-SEt)](PF$_6$) (28) consists of well separated [Cu$_2$(μ-Ph$_2$Pbipy)$_2$(μ-SEt)]$^+$ cations and PF$_6^-$ anions, there being no intermolecular contacts significantly less than the sum of the van der Waals radii for the atoms concerned. The structure of the cation is depicted in *Figure 3.15* along with the atom numbering scheme. A full listing of interatomic distances and angles are given after *section 3.5* at the end of this chapter.

The copper atoms are bridged by two Ph$_2$Pbipy ligands in the "head-to-tail" configuration, each ligand coordinating to one copper atom through a phosphorus donor atom and to the other through a chelating bipyridyl fragment. The sulphur ligand also bridges across the two copper atoms resulting in the geometry at each copper being irregular tetrahedral. The irregular geometry is caused at least in part by the small angle of 79.2(2)° subtended by the bipyridyl fragment at the copper atom; other angles are closer to the idealised value of 109.5° and range up to 117.1(4)° for the P(1)-Cu(1)-S angle.

An interesting feature of this complex is that the presence of another bridging ligand results in a significant decrease in the Cu-Cu distance, the Cu(1)-Cu(2) distance of 2.697(6)Å is much smaller than the Cu-Cu' distance of 3.941(2)Å in the parent dicopper complex (5). These and other molecular parameters are discussed further in *section 3.2.14* in relation to those observed for other Ph$_2$Pbipy ligand bridged dicopper (I) complexes.
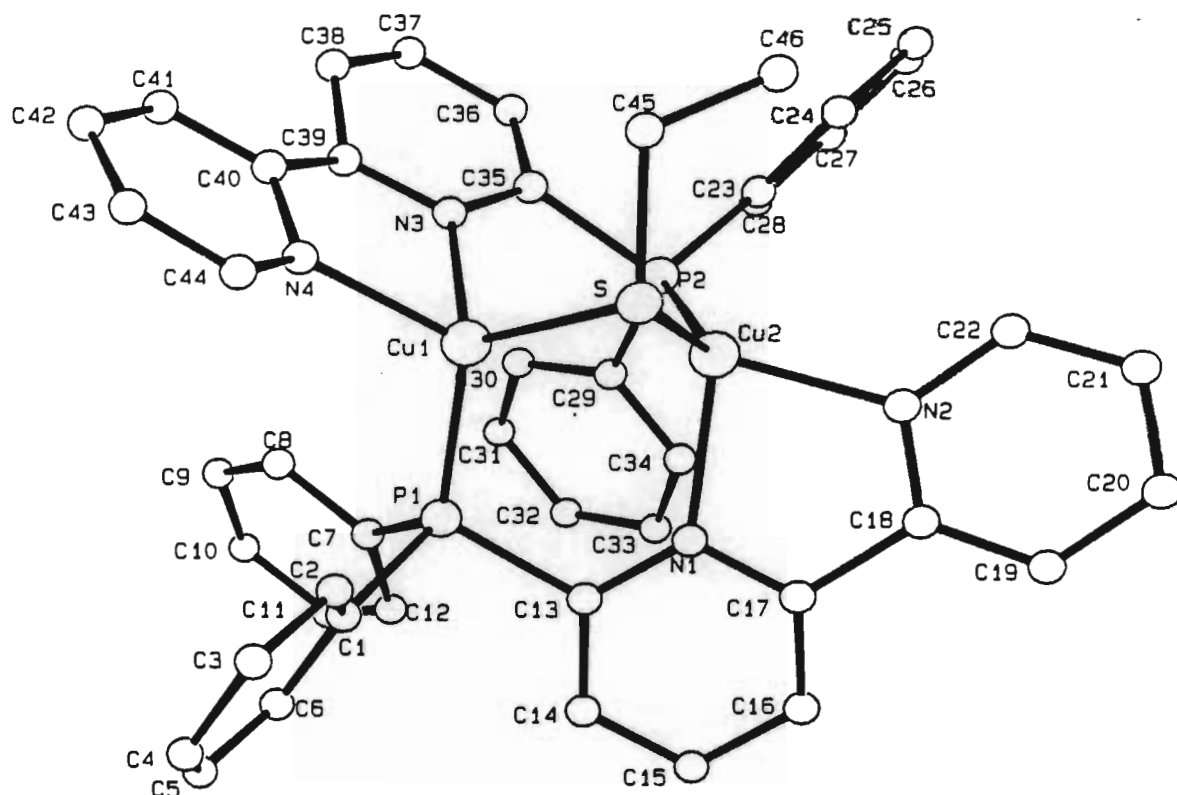
Figure 3.15. Molecular structure of [Cu₂(μ-Ph₂Pbipy)₂(μ-SEt)](PF₆)

3.2.12. Substitution reactions of (5) with anionic oxygen donor ligands

Treatment of a suspension of the appropriate anionic oxygen donor ligand (sodium salt) with a dichloromethane solution of the dicopper complex (5) was found to afford products characterised as [Cu₂(μ-Ph₂Pbipy)₂(μ-L)](PF₆) where L = O₂CH (31), O₂CCH₃ (32), O₂CPh (33) or O₃N (34) (*see Scheme 3.9*). The complexes can also be prepared by addition of the appropriate sodium salt to a dichloromethane solution of (5). The complexes are obtained as orange-red crystalline solids and are air stable. Satisfactory microanalytical analyses were obtained for all complexes (*see Table 3.6*).

The ¹H nmr spectra of these complexes exhibit resonances between 6.9 and 8.8ppm; the absence of the signal at 2.00ppm which was due the methyl protons in (5) indicates that the acetonitrile ligands have been successfully replaced. However, the formate ligand proton in

complex (31) gives rise to a single resonance at 1.46ppm and the methyl group of the acetate ligand in complex (32) resonates at 1.91ppm. (*see Table 3.8*).

The infrared spectra of these complexes exhibit the typical Ph_2Pbipy peaks as well as peaks due to the carbon-oxygen stretches for the carboxylato ligands in complexes (31), (32) and (33) as well as the nitrogen-oxygen stretches for the nitrato ligand in complex (34) (*see Table 3.4*). The presence of the anionic PF_6^- group in the infrared spectra at 837cm^{-1} also indicates that the dicopper complexes that are formed are cationic and not neutral. The carboxylate and nitrate groups bridge across the two copper atoms.

Several attempts were made to deprotonate the formate group that bridges across the copper atoms in complex (31), the deprotonating agents used being pyridine, hydroxide ions and DABCO. However, none of the deprotonating agents could abstract the proton.

3.2.13. Substitution reaction of (5) with cyanide

Treatment of a suspension of potassium cyanide with a dichloromethane solution of the dicopper complex (5) was found to afford a product, isolated in good yields, the microanalysis of which was consistent with the formulation $[Cu_2(\mu-Ph_2Pbipy)_2(CN)_2]$ (35) (*see Scheme 3.10*). The complex is obtained as an orange crystalline solid and is air stable.

The ^1H nmr spectrum in CD_2Cl_2 at room temperature exhibits resonances between 6.9 and 8.8ppm which are readily assigned to the aromatic rings of the co-ordinated Ph_2Pbipy ligand. The solid state infra red spectrum (KBr disk) exhibits peaks characteristic of the Ph_2Pbipy ligand, the appearance of the carbon-nitrogen stretches of the cyano ligand at 2170cm^{-1} indicating that the cyanide has coordinated. The disappearance of the peak due to the anionic PF_6^- group at 837cm^{-1} suggests that the complex formed is neutral; thus dicyano complex (35) is the first neutral complex that has been synthesised by substitution of the acetonitrile ligands in (5).

Scheme 3.9. Substitution reactions of (5) with anionic oxygen donor ligands
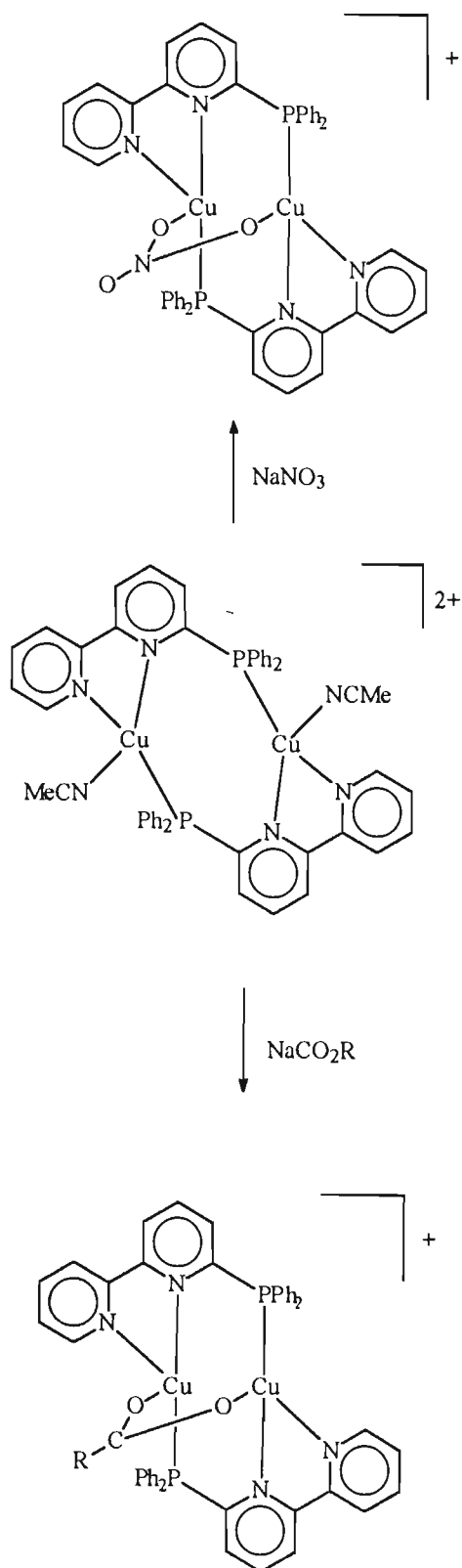
R = H, CH$_3$, Phenyl

Scheme 3.10. Substitution reaction of (5) with cyanide
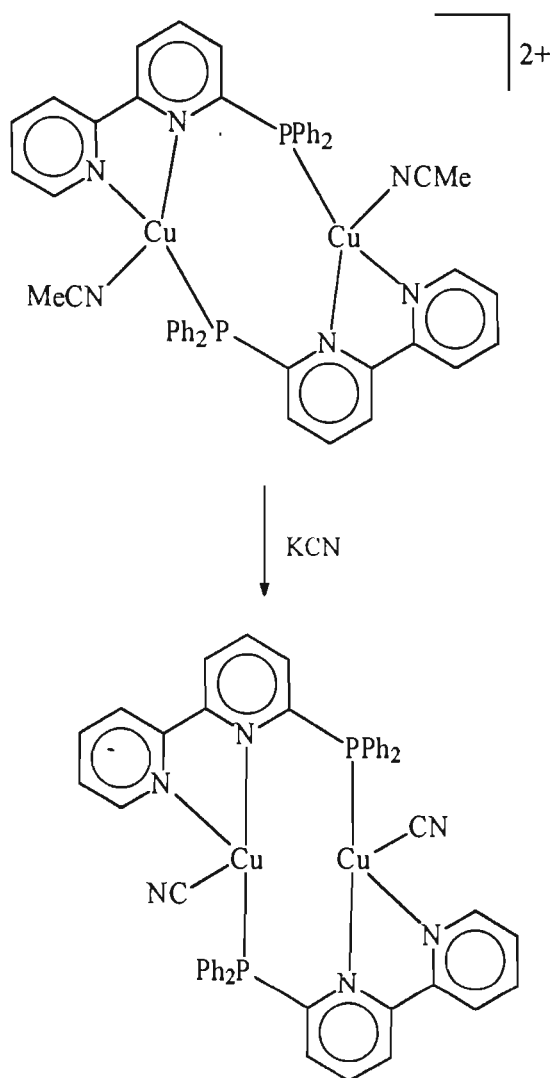
3.2.14. *Summary of crystallographic studies undertaken for dicopper complexes*

Tables 3.1 and *3.2* list the relevant structural parameters for the dicopper ligand bridged complexes whose structures have been established by X-ray crystallography.

Table 3.1. Important interatomic distances

COMPLEX	Cu-Cu (Å)	Cu-P (Å)	Cu-N^a (Å)	Cu-N^b (Å)	Cu- L (Å)
$[Cu_2(\mu-Ph_2Pbipy)_2(MeCN)_2]$ $(PF_6)_2$ **(5)**	3.940	2.191	2.068	2.103	2.076
$[Cu_2(\mu-Ph_2Pbipy)_2(PhCN)_2]$ $(PF_6)_2$ **(6)**	3.795	2.198	2.070	2.131	1.975
$[Cu_2(\mu-Ph_2Pbipy)_2(H_2O)_2]$ $(PF_6)_2$ **(7)**	3.084	2.169	2.043	2.120	2.209
$[Cu_2(\mu-Ph_2Pbipy)_2(py)_2]$ $(PF_6)_2$ **(8)**	3.865	2.205	2.077	2.110	2.052
$[Cu_2(\mu-Ph_2Pbipy)_2(4-Etpy)_2]$ $(PF_6)_2$ **(12)**	3.491	2.182	2.062	2.130	2.044
$[Cu_2(\mu-Ph_2Pbipy)_2(\eta-bipy)]$ $(PF_6)_2$ **(17)**	3.683	2.234 2.237	1.962 2.029	- -	2.031 2.145
$[Cu_2(\mu-Ph_2Pbipy)_2(\mu-I)]$ (PF_6) **(26)**	2.770	2.220	2.109	1.997	2.507
$[Cu_2(\mu-Ph_2Pbipy)_2(\mu-Br)]$ (PF_6) **(27)**	2.762	2.197	2.082	2.060	2.644
$[Cu_2(\mu-Ph_2Pbipy)_2(\mu-SEt)]$ (PF_6) **(29)**	2.697	2.207 2.221	2.107 2.159	2.159 2.041	2.314 2.289

a: This N belongs to the pyridine ring bonded directly to the P

b: This N belongs to the second pyridine ring of the bipyridyl fragment

The Cu-P and Cu-N interatomic distances fall within the expected ranges for these bonds.[76-80] It is evident that the Cu-Cu distances vary considerably as the non-Ph$_2$Pbipy ligands are changed. Thus a long Cu-Cu distance of 3.940Å is found in **(5)** the parent complex, while a

short value of 2.697Å is observed for the sulphur bridged complex, (**29**). The shortest Cu-Cu distances occur in complexes that have an additional bridging ligand, *i.e.* in addition to the bridging Ph_2Pbipy ligand. It appears that the third bridging ligand draws the two copper atoms together. The only exception to this trend is the $[Cu_2(\mu\text{-}Ph_2Pbipy)_2(H_2O)_2]^{2+}$ cation for which the Cu-Cu distance of 3.084Å is relatively short, despite the absence of a third bridging ligand. We have no explanation for this except to note that the Cu-O distance of 2.209Å is considerably longer than the equivalent Cu-L distances in (**5**), (**6**), (**7**), (**8**), (**12**) and (**17**). An interesting feature of the complexes containing a bridging ligand is that as the Cu-(X)-Cu (where X = I, Br or S) angle increases (Cu-I-Cu' = 63.2°, Cu-Br-Cu' = 66.8° and Cu(1)-S-Cu(2) = 71.7°) the copper-copper distance decreases. It is also worth noting that the C13-P interatomic bond distance in the coordinated ligand is not significantly changed from that of the free ligand, the distance is approximately 1.840Å in the coordinated ligands and 1.840Å in the free ligand.

It is noteworthy that the $Cu\text{-}P\text{-}C_{py}$ and the $Cu\text{-}N\text{-}C_{PPh_2}$ angles are 120° or greater in complexes were the copper-copper distances are large (*see Table 3.2*). This seems to indicate that the bridging unit of the Ph_2Pbipy ligand is "splayed out" in the sense that the M-P and M-N vectors are not parallel and in this way the large Cu-Cu' distances can be accommodated. A notable exception is the "head-to-head" dicopper complex (**17**) where the $Cu\text{-}P\text{-}C_{py}$ bond angles are much lower than 120°; this is probably due to steric crowding.

The P-Cu-Cu-N torsion angles are large and vary from 18° in $[Cu_2(\mu\text{-}Ph_2Pbipy)_2(\mu\text{-}SEt)](PF_6)$ (**25**) to 57° in $[Cu_2(\mu\text{-}Ph_2Pbipy)_2(\eta\text{-}bipy)](PF_6)_2$ (**17**). There is no direct correlation between these torsion angles and the Cu-Cu distance; for instance the $[Cu_2(\mu\text{-}Ph_2Pbipy)_2(MeCN)_2]^{2+}$ as the largest Cu-Cu distance of 3.940° but not the largest torsion angle (27°). What is evident, however, is that in complexes that contain another bridging ligand (*eg.* μ-I, μ-Br, μ-SEt) the torsion angles are decreased (*see Table 3.2*). The third bridging ligand appears to restrict the twisting of the Ph_2Pbipy ligand about the Cu-Cu bond.

Table 3.2. Important interatomic angles

COMPLEX	Cu-P-C$_{py}$ (°)	Cu-N^a-C$_{(PPh2)}$ (°)	P-C-N^a (°)	P-Cu-Cu-N^a (°)	DIHED. ANG.^{b} (°)
5	120.8	127.3	117.3	27	20
6	123.1	126.7	114.5	40	8
7	121.2	125.5	116.4	31	15
8	118.5	129.1	116.6	41	6
12	121.2	125.5	116.4	35	6
17	109.3	129.8	111.6	57	12
	102.4	125.8	115.0	46	6
26	118.2	127.1	111.6	20	12
27	116.1	127.9	114.4	20	13
29	113.8	127.7	115.1	18	13
	112.4	125.8	114.9	23	12

a: This N belongs to the pyridine ring bonded directly to the P

b: Dihedral angle between the pyridine rings of bipyridyl fragment

The dihedral angle between the pyridine rings of the bipyridyl fragment in [Cu$_2$(μ-Ph$_2$Pbipy)$_2$(MeCN)$_2$]$^{2+}$ is quite large at 20°; indicating that the bipyridyl fragment is no longer planar but has rather twisted around the interannular bond. Interestingly, there appears to be an inverse relationship between this dihedral angle and the P-Cu-Cu-N torsion angle for a particular Ph$_2$Pbipy ligand (*see Table 3.2*). Thus in the bromo-, iodo- and SEt-bridged complexes the P-Cu-Cu-N torsion angles are (as noted above) quite small yet the dihedral angles between the pyridine rings are relatively large. This does seem to indicate that the ligand can either twist around the interannular bond in the bipyridyl portion or about the Cu-

Cu vector in order to accommodate the stereochemical demands at each copper atom. The dihedral angle also serves to indicate the degree of delocalisation of the π electrons in the bipyridyl portion of the ligand, the greater the angle the less the extent of delocalisation.

3.3. ELECTROCHEMICAL STUDIES

As previously discussed one of the main aims of the work described in this chapter was to synthesise Ph_2Pbipy ligand-bridged dicopper (I) complexes which function as homogeneous catalysts for the electrochemical reduction of carbon dioxide. A selection of the dicopper species synthesised have been tested as electrocatalysts for the reduction of carbon dioxide, the results obtained by means of rotating disc electrode (RDE) and cyclic voltammetric (CV) techniques being reported here. *(See Appendix 2 for the essential theory pertaining to rotating disc electrode and cyclic voltammetry)*.

The focus of the electrochemical work is on the reductive electrochemistry of the systems studied because of our interest in these compounds as electrocatalysts for the reduction of carbon dioxide. Certain of the compounds whose synthesis and characterisation are described in this chapter gave cyclic voltammograms which did not allow a reasonably simple interpretation and/or were not reduced within the solvent limit (normally -2.25V for acetonitrile); their electrochemistry is not described here. Those dicopper Ph_2Pbipy ligand-bridged compounds for which the electrochemistry is reported are classified according to structural type.

3.3.1. Electrochemical studies on [Cu$_2$(μ-Ph$_2$Pbipy)$_2$(L)$_2$](PF$_6$)$_2$ [L = MeCN (5), PhCN (6), py (8) or vpy (10)]

The cyclic voltammogram of $[Cu_2(Ph_2Pbipy)_2(PhCN)_2](PF_6)_2$ (6) recorded in benzonitrile (0.1M TBAP) at room temperature under an argon atmosphere exhibits two one electron reduction waves at $E_{1/2}$ = -1.27 and $E_{1/2}$ = -1.50V *vs* Ag/AgCl *(see Figure 3.16)*. Both reductions appear to be chemically and electrochemically reversible, as evidenced by i_{pa}/i_{pc} values of 1.0 and peak to peak separations close to 59mV *(see Table 3.3)*. No new peaks appear and no peaks disappear during repetitive scans indicating that the cation $[Cu_2(Ph_2Pbipy)_2(PhCN)_2]^{2+}$ remains intact during the cycling process. The cyclic

voltammograms of the dicopper complexes (5), (8) an'd (10) all have the same form as that obtained for (6); a full list of potentials is given in *Table 3.3*. It is apparent from *Table 3.3* that potential shifts ($E_{1/2}$) become more cathodic as the terminal ligand becomes a stronger donor, *eg.* the $E_{1/2}$ values for complex (5) [L = MeCN] are more cathodic than the $E_{1/2}$ values for complex (6) [L = PhCN]; this is not unexpected because MeCN is a stronger donor than PhCN.

Under a carbon dioxide atmosphere at room temperature the initial reduction wave in the cyclic voltammogram of $[Cu_2(Ph_2Pbipy)_2(PhCN)_2](PF_6)_2$ at $E_{1/2}$ = -1.27V *vs* Ag/AgCl remained unaffected, however there was a significant current enhancement just beyond the second reduction wave (*see Figure 3.16*). This enhancement of the cathodic current indicated that (6) or more precisely the dication $[Cu_2(Ph_2Pbipy)_2(PhCN)_2]^{2+}$, behaves as an electrocatalyst for the reduction of carbon dioxide. The return anodic waves almost totally disappear indicating that the reduced form of $[Cu_2(Ph_2Pbipy)_2(PhCN)_2]^{2+}$, *viz.* $[Cu_2(Ph_2Pbipy)_2(PhCN)_2]^0$ is involved in complexation to the carbon dioxide molecule. It should be noted that the original features of the cyclic voltammogram are restored by purging the solution with argon for a few minutes. The cyclic voltammograms of the dicopper complexes (5), (8) and (10) all have the same form as that obtained for (6) under a carbon dioxide atmosphere.

In order to determine the products of the electrochemical reduction of carbon dioxide, bulk electrolysis experiments for (6) were performed at room temperature in acetonitrile (0.1M TBAP) at -1.65V *vs* Ag/AgCl over 20 hours; the concentration of the complex was 10^{-3} M. Gas chromatography of the head space indicates that carbon monoxide is formed as a product of the electrochemical reduction of carbon dioxide. A blank bulk electrolysis experiment was performed, *i.e.* the bulk electrolysis solution was prepared as described previously but no $[Cu_2(Ph_2Pbipy)_2(PhCN)_2](PF_6)_2$ was added. Gas chromatography showed that no carbon monoxide had formed, thus indicating that $[Cu_2(Ph_2Pbipy)_2(PhCN)_2]^{2+}$ was indeed catalysing the electrochemical reduction of carbon dioxide to carbon monoxide. $[Cu_2(Ph_2Pbipy)_2(PhCN)_2](PF_6)_2$ has proven to be an effective electrocatalyst for the reduction

of carbon dioxide in benzonitrile, the complex does not break up after prolonged bulk electrolysis experiments. The same is true for (5), (8) and (10).

The heterogeneous electron transfer kinetics for the two discrete reductions of the electrocatalyst (6) were studied by using rotating disk voltammetry. The rotating disc electrode voltammograms were recorded in acetonitrile (0.1M TBAP) at room temperature under argon (*see Figure 3.17*), and Koutecky-Levich plots were constructed for both the first and second electron transfers; these Koutecky-Levich plots indicated the both electron transfers are fully reversible since the plots of i_l^{-1} *vs* $\omega^{-\frac{1}{2}}$ passed through the origin (*see Figures 3.18 and 3.19*). As a result it was not possible to obtain a value for the rate constant k, by this technique. The results obtained from the Koutecky-Levich plots reinforce the observations made from the cyclic voltammetric experiment, *i.e.* both one electron transfers are reversible. Similar results were obtained for complexes (5) and (8) (*see Table 3.3*). In the case of the vinylpyridine complex $[Cu_2(Ph_2Pbipy)_2(MeCN)_2](PF_6)_2$ (10) however, it was possible to extract a value of k from the Koutecky-Levich plot for the first reduction since a plot of i_l^{-1} *vs* $\omega^{-\frac{1}{2}}$ has an intercept (*see Figure 3.20*). This was found to be 4.49mol.s^{-1} from a plot of log k *vs* $E_{\frac{1}{2}}$ (*see Figure 3.21*). The electron transfer for the second reduction is too rapid to allow the calculation of a rate constant by this technique. The vinylpyridine complex is of particular relevance to this study since it is this complex which could be used to polymerise the electrocatalyst on the electrode surface.
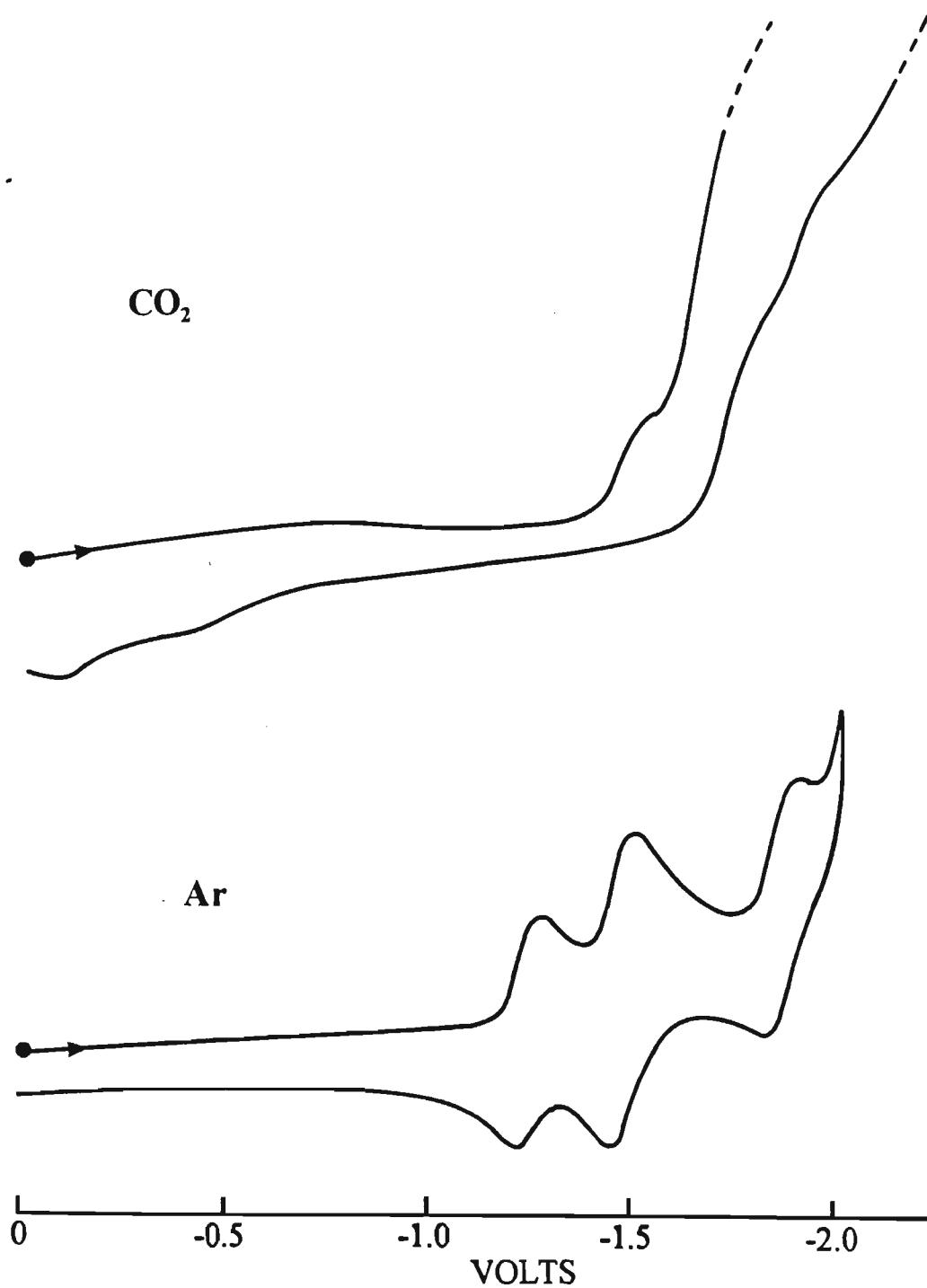
Figure 3.16. Cyclic voltammograms of $[Cu_2(Ph_2Pbipy)_2(PhCN)_2](PF_6)_2$ (6) measured in benzonitrile ($10^{-3}M$ solution, 0.1M TBAP) at Pt. Scan rate $200mV.s^{-1}$; T = $25°C$
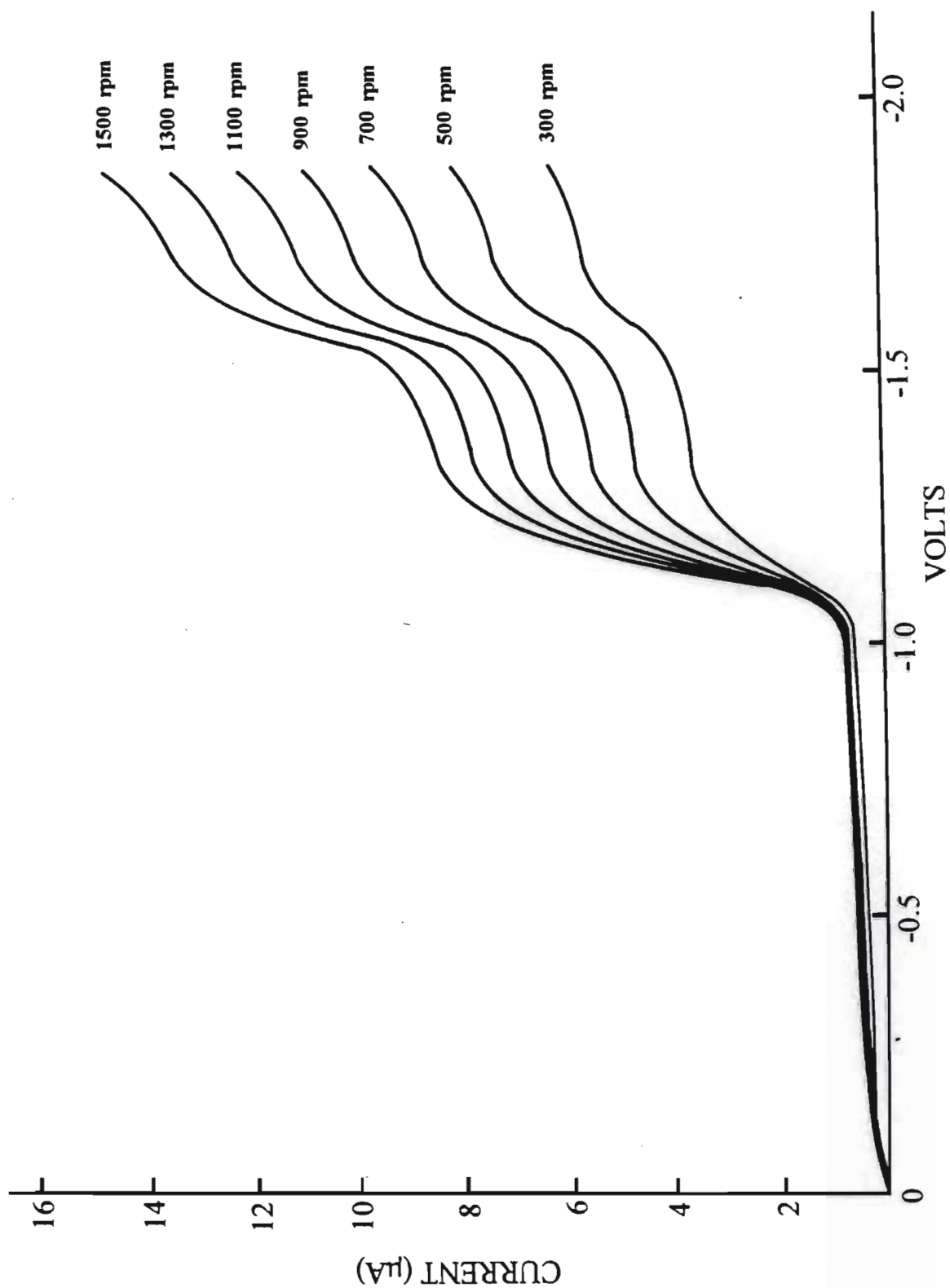
**Figure 3.17. Rotating disc electrode voltammogram of [Cu$_2$(Ph$_2$Pbipy)$_2$(PhCN)$_2$](PF$_6$)$_2$ (6)
measured in benzonitrile (10^{-3}M solution, 0.1M TBAP) at Pt. Scan rate 10mVs^{-1}; T = 25°C**
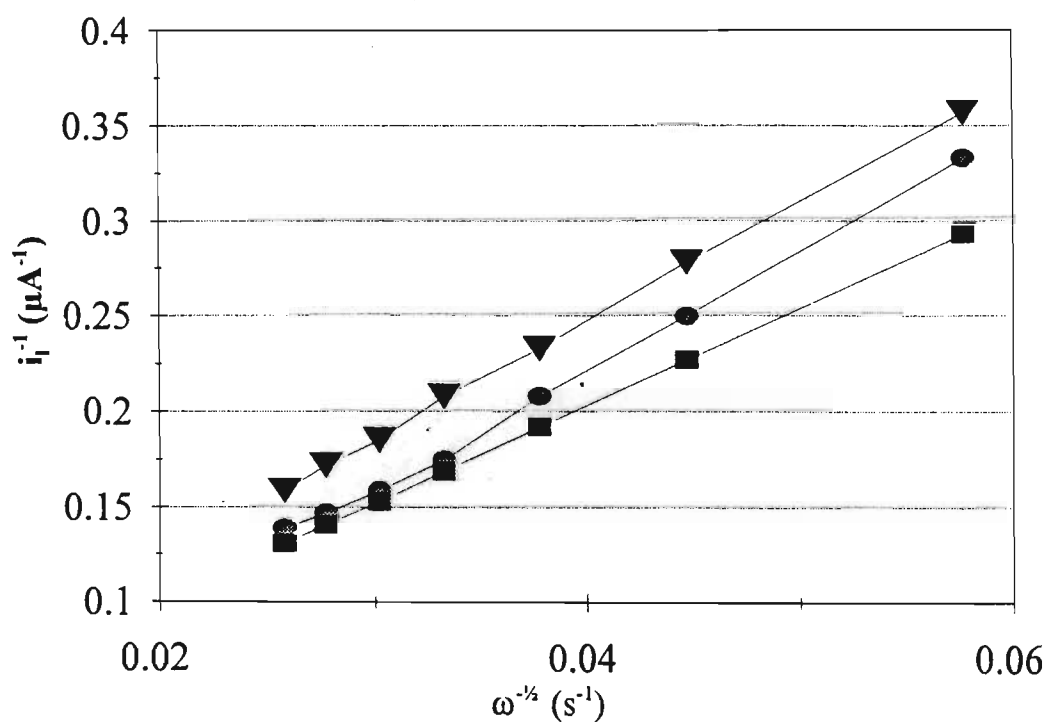
Figure 3.18. Levich plot for first electron transfer of $[Cu_2(Ph_2Pbipy)_2(PhCN)_2](PF_6)_2$ (6)
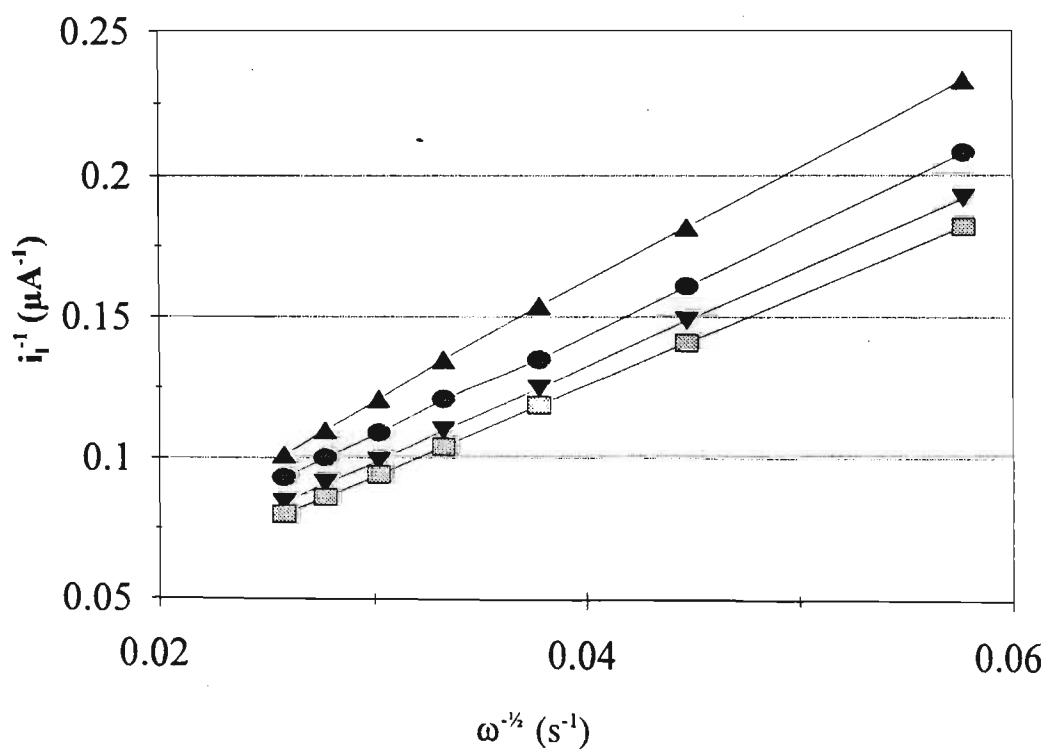
Figure 3.19. Levich plot for second electron transfer of $[Cu_2(Ph_2Pbipy)_2(PhCN)_2](PF_6)_2$ (6)
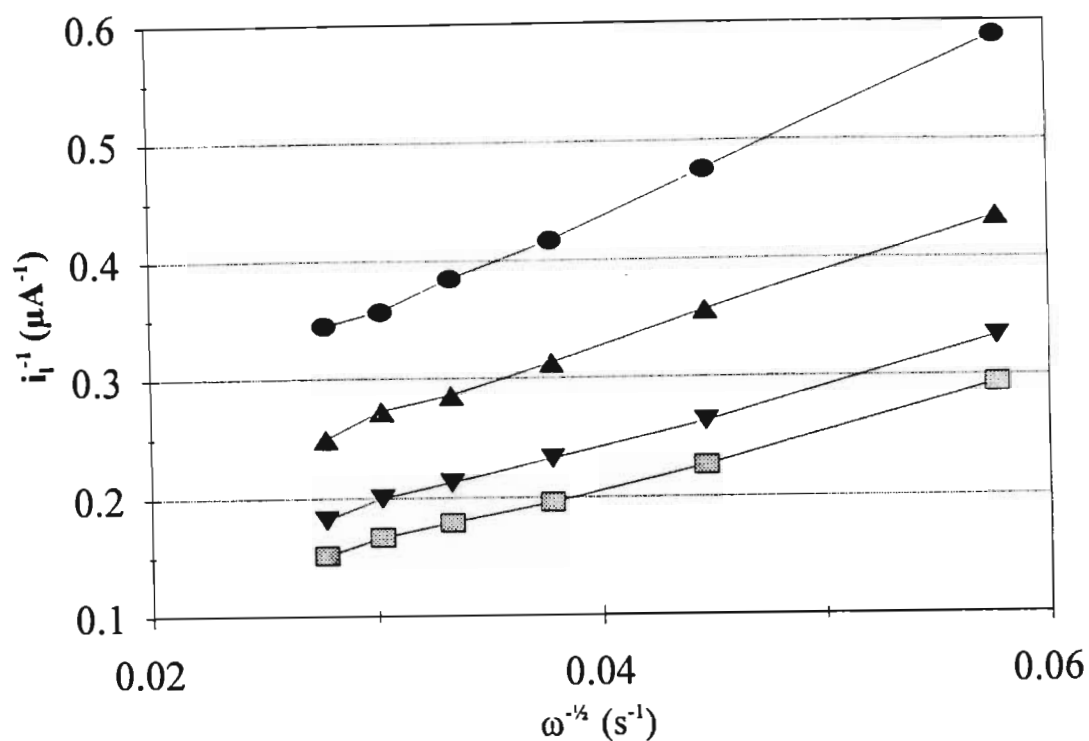
Figure 3.20. Levich plot for first electron transfer of [Cu₂(Ph₂Pbipy)₂(2-vpy)₂](PF₆)₂ (10)
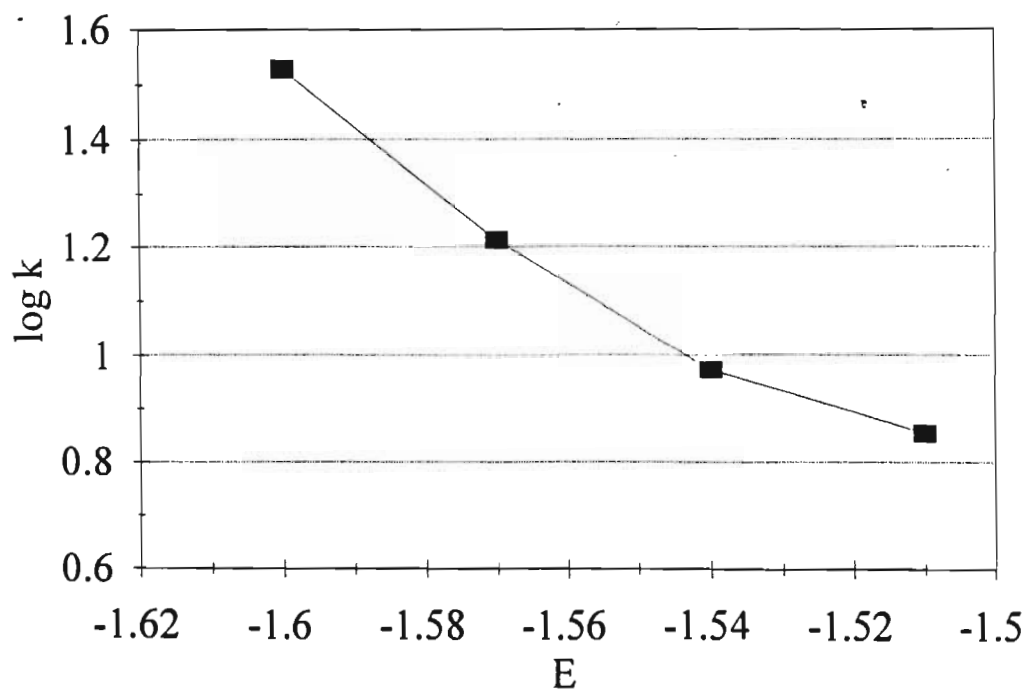
Figure 3.21. Plot of log k *vs* E for first electron transfer of [Cu₂(Ph₂Pbipy)₂(2-vpy)₂](PF₆)₂ (10)

In an attempt to drive the electrochemical reduction of carbon dioxide beyond two electron reduction products, such as carbon monoxide, 200µl of water was added to the bulk electrolysis solution of (6) and the experiment was repeated. Gas chromatographic analysis of the headspace gases obtained after 20 hours indicated the presence of the carbon monoxide peak as well as a new peak in the chromatogram; the retention time of the new peak corresponded to that of methane. A flame ionising detector was then used to detect if the gas was combustible; however two peaks appeared in the chromatogram when the flame ionising detector was used, the retention times of these peaks corresponding to those of methane and methanol. The methanol peak was several orders of magnitude smaller than the methane peak. GC-MS was also employed to confirm the identity of the methane, the mass spectrum of the methane component having a molecular ion peak of mass 15 corresponding to a CH_3 fragment.

Increasing the amount of water added to the bulk electrolysis solution (up to a maximum of 500µl) lead to a steady increase in the size of the peak due to methane and a corresponding decrease in the size of the carbon monoxide peak. However, upon close examination of the platinum working electrode it was discovered that copper metal had deposited onto the electrode during the bulk electrolysis, thus indicating that $[Cu_2(Ph_2Pbipy)_2(PhCN)_2]^{2+}$ had broken up. It has recently been reported[89] that copper electrodes do function as electrocatalysts for the reduction of carbon dioxide to methane and methanol and therefore the discovery of the copper on the working electrode convinced us that it is actually the deposited copper that causes that electrochemical reduction of carbon dioxide to methane and methanol. It seems that the addition of water to the bulk electrolysis solution somehow leads to the dicopper complex breaking up but when no water is added the dication remains intact and still functions as an electrocatalyst. Similar results were obtained with the dicopper complexes (5), (8) and (10).

Kubiak *et al* have carried out a comprehensive study on the electrocatalytic activity of the acetonitrile complex $[Cu_2(Ph_2Pbipy)_2(MeCN)_2](PF_6)_2$ (5) and have proposed a mechanism for

its catalysis of the electrochemical reduction of carbon dioxide to carbon monoxide and carbonate ions.[88] The reduction products were identified by gas chromatography and infrared spectroscopy. *Scheme 3.11* illustrates the proposed mechanism. It is thought that the initial step involves the addition of one electron to the dication to form $[Cu_2(Ph_2Pbipy)_2(MeCN)_2]^+$ and that this is followed by the addition of a second electron to afford the neutral species $[Cu_2(Ph_2Pbipy)_2(MeCN)_2]$. The acetonitrile molecules in the latter are replaced by carbon dioxide molecules which dimerise in a "head-to-tail" fashion, ultimately leading to the disproportionation of carbon dioxide *i.e.* $2CO_2 + 2e^- = CO + CO_3^{2-}$. A similar mechanism for catalysis of the electrochemical reduction of the benzonitrile species (**6**) presumably operates.

Scheme 3.11. Proposed mechanism for carbon dioxide reduction by (5)[88]
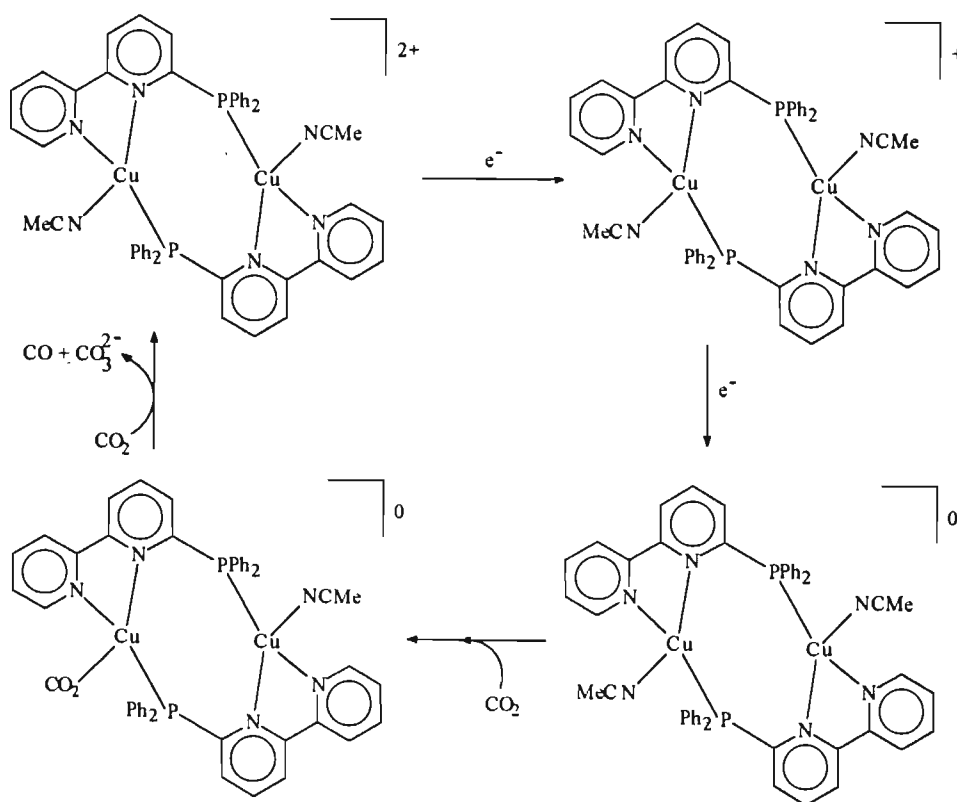
3.3.2. *Electrochemical studies on* $[Cu_2(\mu$-$Ph_2Pbipy)_2(\mu$-$L)](PF_6)$ *[L = Cl* (27)*, SEt* (28) *or SCN* (29)*]*

The cyclic voltammogram of $[Cu_2(\mu$-$Ph_2Pbipy)_2(\mu$-$Cl)](PF_6)$ (27) recorded in acetonitrile (0.1M TBAP) at room temperature under an argon atmosphere exhibits three reduction waves at E_{pc} = -1.73V, $E_{\frac{1}{2}}$ = -1.98V and $E_{\frac{1}{2}}$ = -2.11V *vs* Ag/AgCl; the first reduction wave is clearly considerably larger than the second two waves (*see Figure 3.22*). Kubiak *et al* have shown the both the first and second electron transfers in the acetonitrile complex $[Cu_2(\mu$-$Ph_2Pbipy)_2(MeCN)_2](PF_6)_2$ (5) are one electron transfers; a comparison of the limiting currents (i_l) obtained from the RDE voltammograms for the first reduction wave in (27) and the first two reduction waves in (5) shows that i_l for (27) is almost twice those obtained for (5). This indicates that the first reduction wave in (27) probably involves two electrons. This two electron reduction appears to be chemically irreversible, i_{pa}/i_{pc} < 1.0 (*see Table 3.4*). The two electron transfer reduction is postulated to be the result of an ECE mechanism for which the chemical step involves the loss of the bridging chloride ion and attack by the solvent molecules to afford $[Cu_2(Ph_2Pbipy)_2(MeCN)_2]^+$; the latter will be reduced immediately to the neutral species at the potential of E_{pc} = -1.73V (*see Table 3.4*). It can be assumed that the subsequent electron transfers involve the neutral $[Cu_2(\mu$-$Ph_2Pbipy)_2(MeCN)_2]$ species; indeed a peak at $E_{\frac{1}{2}}$ = -1.96V has been observed in the cyclic voltammogram of the acetonitrile species (5). However, a fourth peak at $E_{\frac{1}{2}}$ = -2.11V was not observed in the cyclic voltammogram of (5) because of the onset of the large solvent peak. The cyclic voltammograms and rotating disc electrode voltammograms of the dicopper complexes (28) and (29) have the same form as that obtained for (27); and thus their interpretation follows that for (27); a full list of potentials is given in *Table 3.4*.

Under a carbon dioxide atmosphere at room temperature, there was a significant current enhancement just beyond the initial reduction wave at E_{pc} = -1.73V. This enhancement of the cathodic current might indicate at first glance that $[Cu_2(\mu$-$Ph_2Pbipy)_2(\mu$-$Cl)]^+$ behaves as an electrocatalyst for the reduction of carbon dioxide. However, as discussed above, the species

present at the electrode surface at the potential where current enhancement occurs, is almost certainly the well established electrocatalyst, the neutral acetonitrile complex $[Cu_2(\mu$-$Ph_2Pbipy)_2(MeCN)]$. This species is presumably responsible for the electrocatalysis of carbon dioxide reduction. The original features of the cyclic voltammogram are restored by purging the solution with argon for a few minutes. Gas chromatographic analysis of the headspace gases obtained after 20 hours of a bulk electrolysis indicated the presence of the carbon monoxide. The same is true for **(28)** and **(29)**.
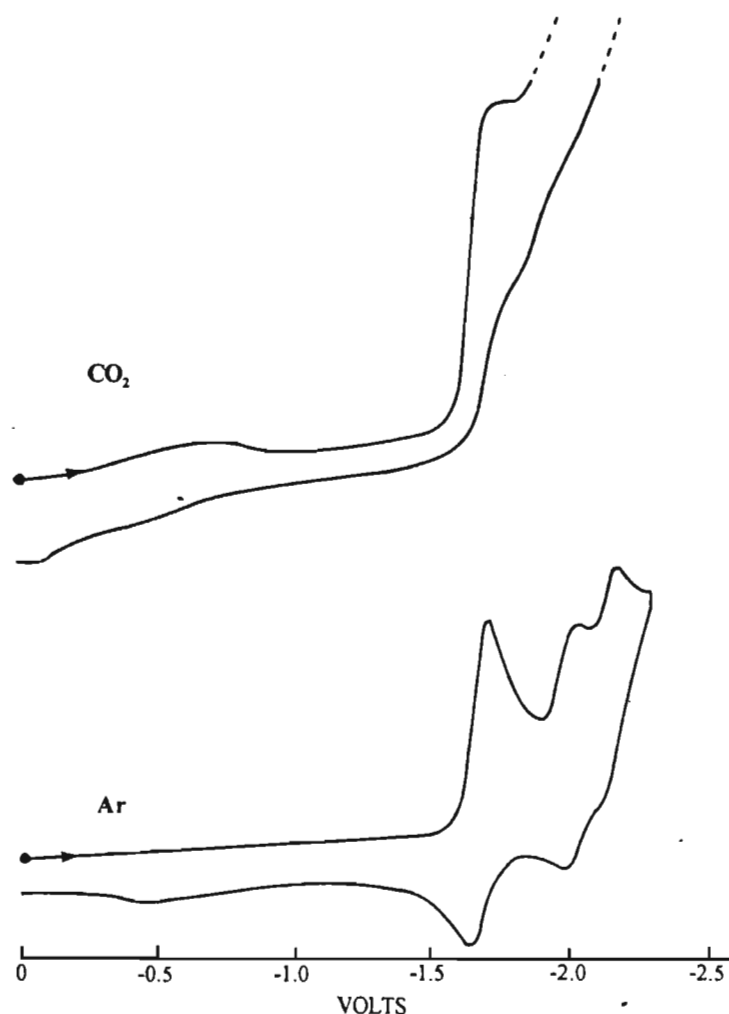
Figure 3.22. Cyclic voltammograms of $[Cu_2(\mu$-$Ph_2Pbipy)_2(\mu$-$Cl)](PF_6)$ **(27)** measured in acetonitrile (10^{-3}M solution, 0.1M TBAP) at Pt. Scan rate 200mV.s^{-1}; T = 25°C

3.3.3. Electrochemical studies on $[Cu_2(\mu\text{-}Ph_2Pbipy)_2(\mu\text{-}L)](PF_6)$ $[L = O_2CH$ (31),O_2CPh (33), NO_3 (29) or S_2CNEt (34)]

The cyclic voltammogram of $[Cu_2(\mu\text{-}Ph_2Pbipy)_2(\mu\text{-}O_2CPh)](PF_6)$ (33) recorded in acetonitrile (0.1M TBAP) at room temperature under an argon atmosphere exhibits three reduction waves at $E_{pc} = -1.72V$, $E_{\frac{1}{2}} = -2.02V$ and $E_{\frac{1}{2}} = -2.17V$ *vs* Ag/AgCl; the first reduction wave is clearly considerably larger than that for the second two waves (*see Figure 3.23*). A comparison of the limiting currents (i_l) obtained from the RDE voltammograms for the first reduction wave in $[Cu_2(\mu\text{-}Ph_2Pbipy)_2(\mu\text{-}O_2CPh)](PF_6)$ and the first two reduction waves in (5) shows that i_l for (33) is twice that obtained for (5). This indicates that the first reduction wave in (33) probably involves two electrons, this two electron reduction appears to be chemical irreversible, $i_{pa}/i_{pc} < 1.0$ (*see Table 3.5*). The two electron transfer reduction is postulated to be the result of an ECE mechanism for which the chemical step involves the loss of the bridging benzoate ion and attack by the solvent molecules to afford $[Cu_2(Ph_2Pbipy)_2(MeCN)_2]^+$; the latter will be reduced immediately to the neutral species at the potential of $E_{pc} = -1.72V$ (*see Table 3.5*). It can be assumed that the subsequent electron transfers involve the neutral $[Cu_2(\mu\text{-}Ph_2Pbipy)_2(MeCN)_2]$ species; indeed a peak is observed at $E_{\frac{1}{2}} = -1.96V$ in the cyclic voltammogram of the acetonitrile species (5). However, a fourth peak was not observed in the cyclic voltammogram of (5) because of the onset of the large solvent peak. The cyclic voltammograms and rotating disc electrode voltammograms of the dicopper complexes (31) and (34) have the same form as that obtained for (33); a full list of potentials is given in *Table 3.5*. It has been observed that as one replaces the neutral ligands with anionic ligands, the potential at which carbon dioxide is reduced becomes more cathodic. It is possible that the reason for this more cathodic potential is because the anionic bridging ligand has to be labilised before the complex can function as an electrocatalyst.

Under a carbon dioxide atmosphere at room temperature, there was a significant current enhancement just beyond the initial reduction wave at $E_{pc} = -1.72V$. This enhancement of the

cathodic current might indicate at first glance that $[Cu_2(\mu\text{-}Ph_2Pbipy)_2(\mu\text{-}O_2CPh)]^+$ behaves as an electrocatalyst for the reduction of carbon dioxide. However, as discussed above, the species present at the electrode surface at the potential at which current enhancement occurs, is almost certainly the well established acetonitrile complex $[Cu_2(\mu\text{-}Ph_2Pbipy)_2(MeCN)_2]$; this species is presumably responsible for the electrochemical reduction of carbon dioxide. The original features of the cyclic voltammogram are restored by purging the solution with argon for a few minutes. Gas chromatographic analysis of the headspace gases obtained after 20 hours of a bulk electrolysis experiment indicated the presence of the carbon monoxide. The same is true for (31) and (34).
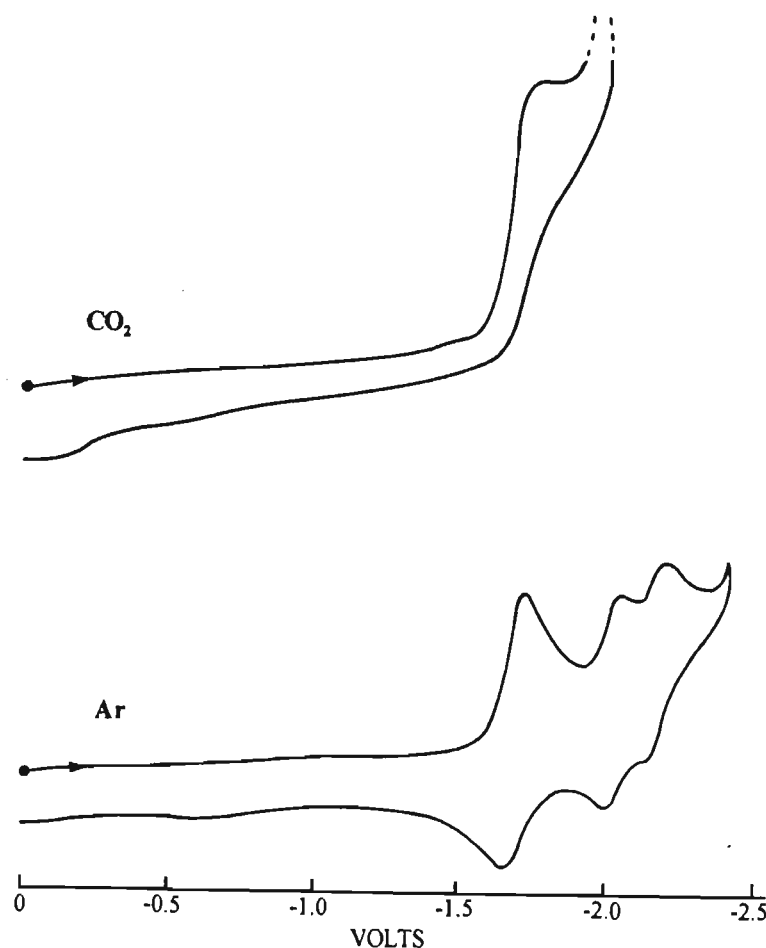
Figure 3.23. Cyclic voltammograms for $[Cu_2(Ph_2Pbipy)_2(O_2CPh)](PF_6)$ (33) measured in acetonitrile (10^{-3}M solution, 0.1M TBAP) at Pt. Scan rate 200mV.s^{-1}; T = 25°C

3.3.4. Electrochemical studies on [Cu₂(Ph₂Pbipy)₂(CN)₂] (35)

The cyclic voltammogram of $[Cu_2(\mu-Ph_2Pbipy)_2(CN)_2]$ (35) recorded in acetonitrile (0.1M TBAP) at room temperature under argon atmosphere exhibits two one electron reductions at $E_{1/2}$ = -1.65 and $E_{1/2}$ = -1.84V *vs* Ag/AgCl (*see Figure 3.24*). These one electron transfers appear to be chemically and electrochemically reversible, i_{pa}/i_{pc} = 1.0 and $\Delta Epp \approx 59mV$ for both the first and second electron transfers. No new peaks appear and no peaks disappear during a repetitive scan indicating that the complex remains intact during the cycling process.

Under a carbon dioxide atmosphere at room temperature, the initial reduction wave at $E_{1/2}$ = -1.65V *vs* Ag/AgCl remained unaffected; however there was a significant current enhancement just beyond the second reduction wave (*see Figure 3.24*). This enhancement of the cathodic current indicated that $[Cu_2(Ph_2Pbipy)_2(CN)_2]$ (35) behaves as an electrocatalyst for the reduction of carbon dioxide. It should be noted that the original features of the cyclic voltammogram are restored by purging the solution with argon for a few minutes. Gas chromatographic analysis of the headspace gases obtained after 20 hours of a bulk electrolysis experiment indicated the presence of the carbon monoxide. It should be noted that the potential at which carbon dioxide is reduced is more cathodic (by *ca* 0.25V) than in the acetonitrile complex (5). Presumably the reason for this more cathodic potential is because the complex is neutral and hence more difficult to reduce. On the basis of the available data it appears as if the mechanism for the electrochemical reduction of carbon dioxide by (35) involves the addition of an electron to the neutral complex (35) to form an anionic dicopper species followed by the addition of the second electron to form a dianionic copper species. It is believed that this dianionic species actually functions as the active electrocatalyst for the electrochemical reduction of carbon dioxide. However, further electrochemical studies are needed before a more accurate description of the mechanism can be proposed.
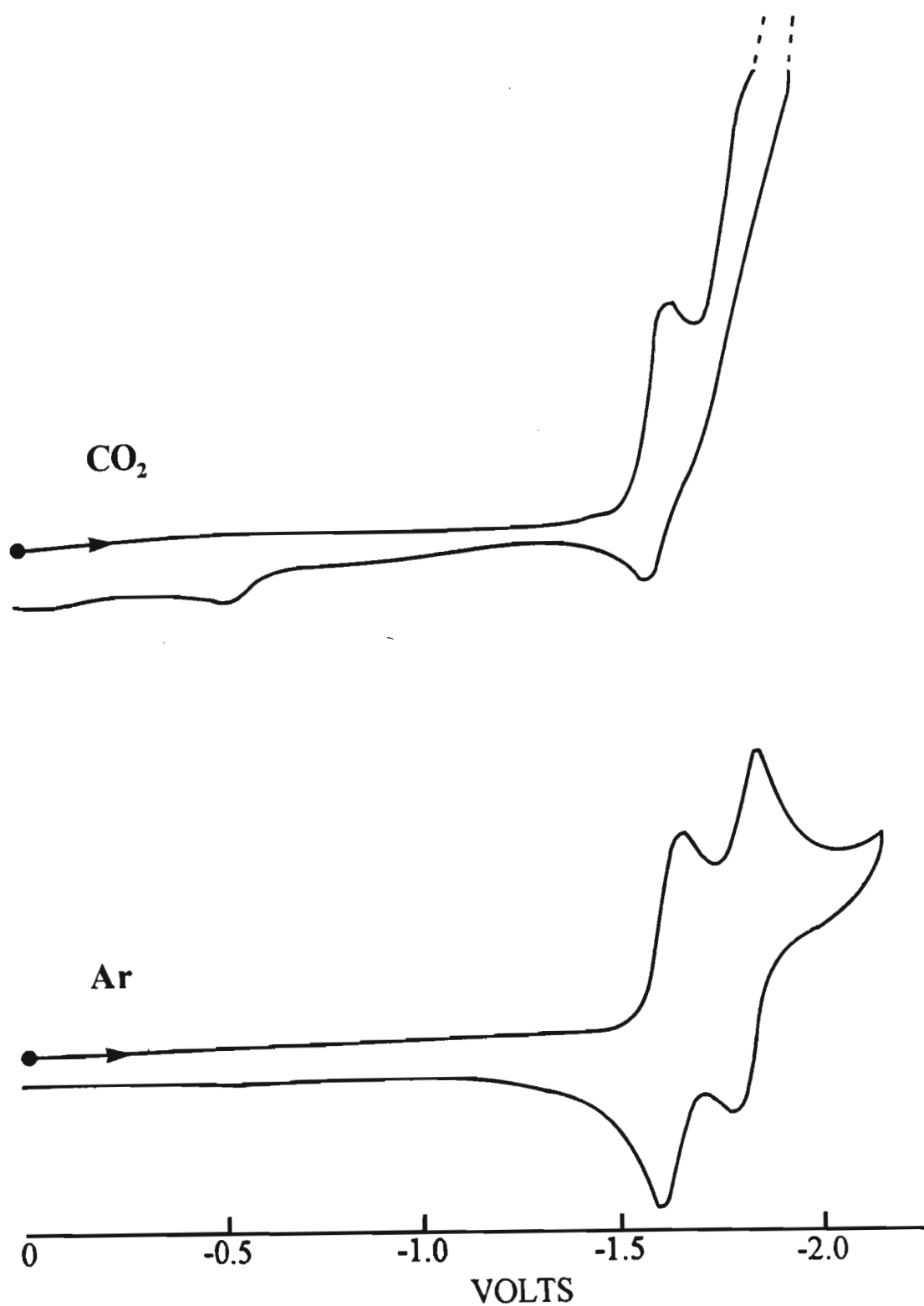
Figure 3.24. Cyclic voltammograms for [Cu$_2$(μ-Ph$_2$Pbipy)$_2$(CN)$_2$] (35) measured in acetonitrile (10^{-3}M solution, 0.1M TBAP) at Pt. Scan rate 200mV.s^{-1}; T = 25°C

3.3.5. Conclusion

Comparing the electrochemical results obtained on these dicopper complexes and those obtained for other dinuclear complexes synthesised by colleagues in our laboratories reveals some interesting facts. The analogous silver dimer, $[Ag_2(Ph_2Pbipy)_2(MeCN)_2]^{2+}$, has been synthesised and electrochemical experiments carried out (*see Figure 4.38*).[84] The cyclic voltammograms for the disilver complex indicates that the complex does not function as an electrocatalyst but rather breaks up and metallic silver deposits onto the electrode. A closer examination of the complex reveals that the silver-phosphorus and silver-nitrogen bond lengths are longer than the copper-phosphorus and copper-nitrogen bond lengths; this implies that ligand is most probably not as strongly bonded to the silver atom as it is to the copper atom. Therefore, it is essential that the ligand be strongly bonded to the metal atom if the complex is to function as an electrocatalyst for carbon dioxide reduction.
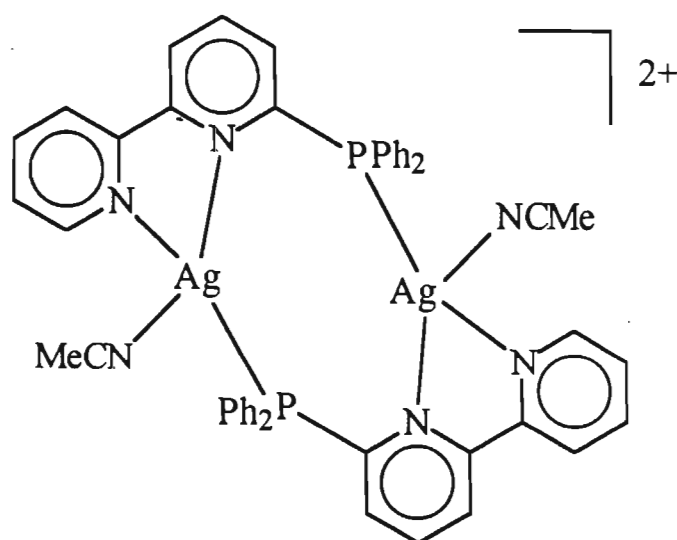
Figure 3.25. Structure of $[Ag_2(Ph_2Pbipy)_2(MeCN)_2]^{2+}$

The dicopper complexes $[Cu_2(Ph_2Pquin)_2(MeCN)_2]^{2+}$ and $[Cu_2\{PhP(py)_2\}(MeCN)_2]^{2+}$ have also been synthesised (*see Figures 3.3 and 3.4*).[81,82] The cyclic voltammogram experiments on these complexes indicate that they do not function as electrocatalysts but break up and deposit metallic copper on the electrode surface. The only difference between these dicopper complexes and $[Cu_2(\mu\text{-}Ph_2Pbipy)_2(MeCN)_2]^{2+}$ is the absence of a chelating 2,2'-bipyridine portion on the bridging ligand. It appears that the bipyridyl fragment is a necessary component of the phosphorus pyridyl bridging ligand. Presumably the role of the bipyridyl ligand is two fold;

(i).   to provide low lying π^* orbitals for acceptance of electrons from the electrode surface, and;

(ii).   through chelation at the second copper atom to stabilise the complex to fragmentation on electrochemical reduction.

Table 3.3. Electrochemical data for $[Cu_2(\mu\text{-}Ph_2Pbipy)_2(L)_2]^{2+}$ {L = MeCN (5), PhCN (6), py (8) or vpy (10)

Complex	First Electron Reduction					Second Electron Reduction				
	E_{pc} (V)	E_{pa} (V)	$E_{1/2}$ (V)	ΔE_{pp} (mV)	i_{pa}/i_{pc}	E_{pc} (V)	E_{pa} (V)	$E_{1/2}$ (V)	ΔE_{pp} (mV)	i_{pa}/i_{pc}
5	-1.41	-1.35	-1.38	62	1.0	-1.61	-1.55	-1.58	66	1.0
6	-1.30	-1.20	-127	64	1.0	-1.53	-1.46	-1.50	66	1.0
8	-1.54	-1.49	-1.52	58	1.0	-1.71	-1.65	-1.68	61	1.0
10	-1.53	-1.46	-1.49	72	1.0	-1.70	-1.64	-1.67	57	1.0

Table 3.4. Electrochemical data for [Cu$_2$(μ-Ph$_2$Pbipy)$_2$(μ-L)]$^+$ {L = Cl (27), SEt (28) or SCN (29)

Complex	First reduction				Second red.			Third red.		
	E_{pc} (V)	E_{pa} (V)	ΔE_{pp} (mV)	i_{pa}/i_{pc}	E_{pc} (V)	E_{pa} (V)	$E_{\frac{1}{2}}$ (V)	E_{pc} (V)	E_{pa} (V)	$E_{\frac{1}{2}}$ (V)
27	-1.73	-1.65	87	0.62	-2.00	-1.96	-1.98	-2.13	-2.09	-2.11
28	-1.74	-1.66	81	0.61	-2.04	-1.99	-2.02	-2.12	-2.07	-2.10
29	-1.74	-1.65	84	0.64	-2.02	-1.97	-2.00	-2.14	-2.10	-2.12

Table 3.5. Electrochemical data for [Cu$_2$(μ-Ph$_2$Pbipy)$_2$(μ-L)]$^+$ {L = O$_2$CH (31), O$_2$CPh (33) or O$_3$N (34)

Complex	First reduction				Second red.			Third red.		
	E_{pc} (V)	E_{pa} (V)	ΔE_{pp} (mV)	i_{pa}/i_{pc}	E_{pc} (V)	E_{pa} (V)	$E_{\frac{1}{2}}$ (V)	E_{pc} (V)	E_{pa} (V)	$E_{\frac{1}{2}}$ (V)
31	-1.69	-1.61	75	0.65	-2.04	-1.98	-2.02	-2.15	-2.10	-2.13
33	-1.72	-1.64	80	0.66	-2.04	-2.00	-2.02	-2.20	-2.14	-2.17
34	-1.72	-1.64	82	0.64	-2.05	-2.02	-2.04	-2.19	-2.15	-2.17

3.4. EXPERIMENTAL

Synthesis of [Cu$_2$(μ-Ph$_2$Pbipy)$_2$(MeCN)$_2$](PF$_6$)$_2$ (5)

An acetonitrile *(5ml)* solution of [Cu(MeCN)$_4$](PF$_6$) *(37.3mg, 0.1mmol)* was added to an acetonitrile *(5ml)* suspension of Ph$_2$Pbipy *(34.1mg, 0.1mmol)* ; the resultant solution was stirred for 24 hours. Diethyl ether *(10ml)* was added to precipitate the product out. The yellow powder obtained after filtration was recrystallised from acetonitrile/diethyl ether to afford yellow crystalline material.

Yield: 75%

Synthesis of [Cu$_2$(μ-Ph$_2$Pbipy)$_2$(PhCN)$_2$](PF$_6$)$_2$ (6)

[Cu$_2$(μ-Ph$_2$Pbipy)$_2$(MeCN)$_2$](PF$_6$)$_2$ *(59mg, 0.05mmol)* was dissolved in distilled benzonitrile *(10ml)* and the solution was stirred for 12 hours. Diethyl ether *(10ml)* was added carefully and the solution was allowed to stand overnight at 0°C; bright yellow crystalline material was collected by decanting the benzonitrile/diethyl ether solution; the crystals were washed with diethyl ether.

Yield: 85%

Synthesis of [Cu$_2$(μ-Ph$_2$Pbipy)$_2$(H$_2$O)$_2$](PF$_6$)$_2$ (7)

A dichloromethane/water *(15ml/0.5ml)* mixture containing [Cu$_2$(μ-Ph$_2$Pbipy)$_2$(MeCN)$_2$](PF$_6$)$_2$ *(118mg, 0.1mmol)* was refluxed for one hour with either carbon dioxide or hydrogen gas being bubbled through the solution. Diethyl ether *(10ml)* was added and the mixture was allowed to stand overnight at 0°C. The red crystalline material was obtained by decanting the mother liquor; the crystals were then washed with diethyl ether and dried *in vacuo*.

Yield: 57%

Synthesis of [Cu$_2$(μ-Ph$_2$Pbipy)$_2$(L)$_2$](PF$_6$)$_2$ where L = py (8), 2-ampy (9), 2-vpy (10), 4-vpy (11), etpy (12), 2-am-4-metpy (13) and merpy (14)

A dichloromethane *(5ml)* solution of pyridine or substituted pyridine *(0.2mmol)* was added to a dichloromethane solution of [Cu$_2$(μ-Ph$_2$Pbipy)$_2$(MeCN)$_2$](PF$_6$)$_2$ *(118mg, 0.1mmol)* and the mixture was stirred for 5 hours. Diethyl ether *(10ml)* was added and the mixture was allowed to stand overnight at 0°C. The yellow crystalline material was obtained by decanting the mother liquor; the crystals were then washed with diethyl ether.

Yield: **(8)** 70%, **(9)** 60%, **(10)** 58%, **(11)** 69%, **(12)** 70%, **(13)** 59% and **(14)** 77%

Synthesis of {[Cu(μ-Ph$_2$Pbipy)(4,4'-bipy)](PF$_6$)}$_{2n}$ (15)

A dichloromethane *(5ml)* solution of 4,4'- bipyridine *(15.4mg, 0.1mmol)* was added to a dichloromethane solution of [Cu$_2$(μ-Ph$_2$Pbipy)$_2$(MeCN)$_2$](PF$_6$)$_2$ *(118mg, 0.1mmol)* and the mixture stirred, a yellow precipitate formed almost immediately. The solid was washed with diethyl ether and dried under reduced pressure.

Yield: 77%

Synthesis of {[Cu(μ-Ph$_2$Pbipy)(trans -1,2 - bis{4 -pyridyl}ethylene)](PF$_6$)}$_{2n}$ (16)

A dichloromethane *(5ml)* solution of trans-1,2-*bis*(4-pyridyl)-ethylene *(19mg, 0.1mmol)* was added to a dichloromethane solution of [Cu$_2$(μ-Ph$_2$Pbipy)$_2$(MeCN)$_2$](PF$_6$)$_2$ *(118mg, 0.1mmol)* and the mixture was stirred for 5 hours. Diethyl ether *(10ml)* was added and the mixture allowed to stand overnight at 0°C. The yellow crystalline material was obtained by decanting the mother liquor; the crystals were then washed with diethyl ether and dried under reduced pressure.

Yield: 77%

Synthesis of [Cu$_2$(μ-Ph$_2$Pbipy)$_2$(η - 2,2' - bipy)](PF$_6$)$_2$ (17)
Method A:

To an acetone *(15ml)* solution of [Cu(MeCN)$_4$](PF$_6$) *(37.3mg, 0.1mmol)* was added solid 2,2' - bipyridine *(15.4mg, 0.1mmol)* and the resulting solution stirred for 45 minutes; the

Synthesis of [Cu₂(μ-Ph₂Pbipy)₂(L)](PF₆)₂ where L = azaindole (20) and pyrazole (21)

A dichloromethane *(5ml)* solution of the appropriate heterocycle *(0.1mmol)* was added to a dichloromethane solution of [Cu₂(μ-Ph₂Pbipy)₂(MeCN)₂](PF₆)₂ *(118mg , 0.1mmol)* and the mixture was stirred for 5 hours. Diethyl ether *(10ml)* was added and the mixture was allowed to stand overnight at 0°C. The crystalline material was obtained by decanting the mother liquor; the crystals were then washed with diethyl ether and dried *in vacuo.*

Yield: **(21)** 77%, **(22)** 67%

Synthesis of [Cu₂(μ-Ph₂Pbipy)₂(L)](PF₆)₂ where L = dppm (22), dppe (23) and dppp (24)

A dichloromethane *(5ml)* solution of the appropriate diphosphorus ligand *(0.1mmol)* was added to a dichloromethane solution of [Cu₂(μ-Ph₂Pbipy)₂(MeCN)₂](PF₆)₂ *(118mg , 0.1mmol)* and the mixture was stirred for 3 hours. Diethyl ether *(12ml)* was added and the mixture was allowed to stand overnight at 0°C. The yellow crystalline material was obtained by decanting the mother liquor; the crystals were then washed with diethyl ether.

Yield: **(22)** 89%, **(23)** 77% and **(24)** 73%

Synthesis of [Cu₂(μ-Ph₂Pbipy)₂(μ-L)](PF₆) where L = I (25), Br (26) and Cl (27)

Solid KX where X = I, Br or Cl, *(0.1mmol)* was added to a dichloromethane *(15ml)* solution of [Cu₂(μ-Ph₂Pbipy)₂(MeCN)₂](PF₆)₂ *(118mg , 0.1mmol)* and the mixture was stirred for 3 hours. Diethyl ether *(12ml)* was added and the mixture was allowed to stand overnight at 0°C. The red crystalline material was obtained by decanting the mother liquor; the crystals were then washed with diethyl ether and dried.

Yield: **(25)** 71%, **(26)** 77% and **(27)** 75%

Synthesis of [Cu₂(μ-Ph₂Pbipy)₂(μ - L)](PF₆) where L = SEt (28), SCN (29) and S₂CNEt (30)

Solid NaX where X = SEt, SCN or S₂CNEt, *(0.1mmol)* was added to a dichloromethane *(15ml)* solution of [Cu₂(μ-Ph₂Pbipy)₂(MeCN)₂](PF₆)₂ *(118mg , 0.1mmol)* and the mixture was stirred for 3 hours. Diethyl ether *(12ml)* was added and the mixture was allowed to stand

overnight at 0°C. The red crystalline material was obtained by decanting the mother liquor; the crystals were then washed with diethyl ether and dried.

Yield: **(28)** 45%, **(29)** 65% and **(30)** 78%

Synthesis of $[Cu_2(\mu\text{-}Ph_2Pbipy)_2(\mu\text{-}L)](PF_6)$ where L = O_2CH **(31)**, O_2CCH_3 **(32)**, O_2CPh **(33)** *and NO_3* **(34)**

Solid NaX where X = O_2CH, O_2CCH_3,, O_2CPh and NO_3 *(0.1mmol)* was added to a dichloromethane *(15ml)* solution of $[Cu_2(\mu\text{-}Ph_2Pbipy)_2(MeCN)_2](PF_6)_2$ *(118mg, 0.1mmol)* and the mixture was stirred for 3 hours. Diethyl ether *(12ml)* was added and the mixture was allowed to stand overnight at 0°C. The red crystalline material was obtained by decanting the mother liquor; the crystals were then washed with diethyl ether and dried.

Yield: **(31)** 78%, **(32)** 79%, **(33)** 80% and **(34)**71%

Synthesis of $[Cu_2(\mu\text{-}Ph_2Pbipy)_2(CN)_2]$ **(35)**

Solid potassium cyanide *(6.5 mg, 0.1mmol)* was added to a dichloromethane *(15ml)* solution of $\{[Cu(\mu\text{-}Ph_2Pbipy)(MeCN)](PF_6)\}_2$ *(118mg, 0.1mmol)* and the mixture was stirred for 3 hours. Diethyl ether *(12ml)* was added and the mixture was allowed to stand overnight at 0°C. The red crystalline material was obtained by decanting the mother liquor; the crystals were then washed with diethyl ether and dried.

Yield: 67%

3.5. EXPERIMENTAL PROCEDURES FOR ELECTROCHEMICAL INVESTIGATIONS

The electrochemical techniques employed were direct current rotating disc electrode (RDE), cyclic voltammetry and bulk electrolysis. The cell was purged with pure dry argon for 45 minutes before any experiments were performed. The RDE voltammetry was performed under an argon atmosphere. The initial cyclic voltammetry experiments were performed under and argon atmosphere, thereafter high purity carbon dioxide was bubbled through the solution for 15 minutes and the cyclic voltammery repeated. All experiments were performed at room temperature (298K). For bulk electrolysis the solution was purged for 45 minutes with argon and then for 15 minutes with high purity carbon dioxide. The bulk electrolysis experiments were carried out over twenty hours.

Tetrabutylammonium perchlorate (TBAP) was used as the supporting electrolyte in a $0.1M$ concentration, the sample concentration being $10^{-3}M$. TBAP was recrystallised from 9:1 ethanol/water mixture and dried *in vacuo* at 100°C.

All cyclic voltammetric and rotating disc electrode experiments employed a conventional three electrode cell, with a platinum spiral wire auxiliary electrode and a reference electrode comprising a AgCl coated spiral silver wire dipped into a 0.1M solution of TBAP in the relevant solvent and separated from the electrolyte solution by a fine frit. All potentials are quoted relative to our Ag/AgCl reference electrode, against which the [ferrocene]$^{+/0}$ couple has the following $E_{\frac{1}{2}}$ values:

$\qquad$ 0.44V in benzonitrile (ΔE_p = 75mV at 100mVs^{-1})

$\qquad$ 0.38V in acetonitrile (ΔE_p = 70mV at 100mVs^{-1})

Ferrocene was usually added to the solution under investigation at the end of each experiment as an internal standard to check on the stability of the reference electrode. In cases where this was not possible, *eg.* when the oxidation waves from the sample interfered with the [ferrocene]$^{+/0}$ couple, ferrocene was run immediately before, or after, the experiment under identical conditions.

The working electrode was a platinum disc electrode ($0.013cm^2$) of local construction (University of Natal, Faculty of Science Workshop). Its surface was freshly polished using 2-6μm diamond paste until no scratches were observed at tenfold magnification. Before being inserted into the solution, the electrode was rinsed with acetone and distilled water and dried in a warm air stream.

Table 3.6. Microanalytical data for dicopper complexes

COMPLEX	CALCULATED(%)			FOUND(%)		
	C	H	N	C	H	N
5	48.86	3.42	7.12	48.77	3.40	7.01
6	55.05	3:28	6.22	54.88	3.13	6.18
7	46.61	3.38	4.94	46.70	3.33	5.01
8	51.64	3.53	6.69	51.88	3.60	6.83
9	50.44	3.61	8.71	50.23	3.60	8.88
10	53.18	3.85	6.42	53.34	3.90	6.44
11	53.18	3.85	6.42	52.99	3.88	6.28
12	53.10	3.99	6.41	53.44	4.04	6.66
13	51.19	3.84	8.53	51.55	4.10	8.26
14	49.13	3.36	6.37	49.57	3.69	6.12
15	51.72	3.38	6.70	51.33	3.32	6.93
16	52.47	3.62	6.56	52.89	3.97	6.93
17	53.42	3.40	6.44	53.03	3.31	6.09
18	52.63	3.31	6.58	53.10	3.56	6.77
19	52.30	3.33	8.41	52.69	3.57	8.12
20	52.22	3.48	8.40	51.88	3.21	8.09
21	48.67	3.43	9.08	48.90	3.70	8.76

Table 3.6.   /continued

COMPLEX	CALCULATED(%)			FOUND(%)		
	C	H	N	C	H	N
22	55.92	3.81	3.78	56.45	4.09	3.66
23	56.19	3.91	3.74	56.54	4.23	4.01
24	56.47	4.00	3.71	55.90	4.23	3.90
25	48.95	3.17	5.19	48.60	3.34	5.45
26	51.18	3.32	5.43	50.93	3.45	5.55
27	53.48	3.47	5.67	53.23	3.67	5.81
28	54.49	3.88	5.53	54.23	3.91	5.67
29	53.47	3.39	6.93	53.66	3.79	6.65
30	53.45	4.03	6.36	53.39	3.87	6.11
31	54.17	3.54	5.62	53.89	3.76	5.79
32	54.60	3.69	5.54	54.35	3.44	5.37
33	57.04	3.66	5.22	57.34	3.78	5.34
34	52.08	3.38	6.90	51.87	3.67	6.65
35	54.99	3.41	8.36	54.78	3.65	8.12

Table 3.7. Infra red spectral data (KBr disk)

All the complexes contain the following peaks due to the Ph_2Pbipy ligand; 968(m), 1114(m), 1164(m), 1242(m), 1421(s), 1431(m), 1472(w), 1477(w), 1550(m), 1565(m), 1572(m), and 1583(w)cm^{-1}. In addition all the dicopper complexes (with the exception of complex (**32**)) have the PF_6^- peak at 837(s)cm^{-1}.

COMPLEX	PEAKS(cm^{-1})
$[Cu_2(\mu\text{-}Ph_2Pbipy)_2(MeCN)_2](PF_6)_2$	2304.4(s) (C-N)
$[Cu_2(\mu\text{-}Ph_2Pbipy)_2(PhCN)_2](PF_6)_2$	2409.4(s) (C-N)
$[Cu_2(\mu\text{-}Ph_2Pbipy)_2(\mu\text{-}SCN)](PF_6)$	2110.0(s) (C-N)
$[Cu_2(\mu\text{-}Ph_2Pbipy)_2(\mu\text{-}O_2CH)](PF_6)$	1577.1(s) (C-O)
$[Cu_2(\mu\text{-}Ph_2Pbipy)_2(\mu\text{-}O_2CCH_3)](PF_6)$	1561.2(s), 1595.0(m) (C-O)
$[Cu_2(\mu\text{-}Ph_2Pbipy)_2(\mu\text{-}O_2CPh)](PF_6)$	1556.4(s), 1593.1(m) (C-O)
$[Cu_2(\mu\text{-}Ph_2Pbipy)_2(\mu\text{-}NO_3)](PF_6)$	1620.1(s), 1637.4(m), 1780.8(m) (N-O)
$[Cu_2(\mu\text{-}Ph_2Pbipy)_2(CN)_2]$	2169.7(s) (C-N)

Table 3.8. ^{1}H nmr spectral data

All the complexes exhibit the characteristic resonances assigned to the aromatic protons of the phenyl and bipyridyl fragments between 6.9 and 8.8ppm.

COMPLEX	PEAKS(ppm)
$[Cu_2(\mu\text{-}Ph_2Pbipy)_2(MeCN)_2](PF_6)_2$	1.86 (3H, -CH$_3$)
$[Cu_2(\mu\text{-}Ph_2Pbipy)_2(ampy)_2](PF_6)_2$	4.6-4.9 (2H, br, -NH$_2$)
$[Cu_2(\mu\text{-}Ph_2Pbipy)_2(2\text{-vpy})_2](PF_6)_2$	5.5-5.9 (4H, -CH$_2$CH$_2$)
$[Cu_2(\mu\text{-}Ph_2Pbipy)_2(4\text{-vpy})_2](PF_6)_2$	5.5-5.9 (4H, -CH$_2$CH$_2$)
$[Cu_2(\mu\text{-}Ph_2Pbipy)_2(4\text{-Etpy})_2](PF_6)_2$	1.1 (3H, -CH$_3$), 3.4 (2H, -CH$_2$-)
$[Cu_2(\mu\text{-}Ph_2Pbipy)_2(am\text{-}4\text{-metpy})_2](PF_6)_2$	1.5 (3H, -CH$_3$), 4.5-4.7 (2H, br, -NH$_2$)
$[Cu_2(\mu\text{-}Ph_2Pbipy)_2(azaindole)_2](PF_6)_2$	1.8-1.9 (1H, br, -NH)
$[Cu_2(\mu\text{-}Ph_2Pbipy)_2(pyrazzole)_2](PF_6)_2$	1.6-1.9 (1H, br, -NH)
$[Cu_2(\mu\text{-}Ph_2Pbipy)_2(dppm)](PF_6)_2$	3.2-3.5 (2H, -CH$_2$-)
$[Cu_2(\mu\text{-}Ph_2Pbipy)_2(dppe)](PF_6)_2$	3.3-3.5 (4H, -CH$_2$CH$_2$-)
$[Cu_2(\mu\text{-}Ph_2Pbipy)_2(dppp)](PF_6)_2$	3.3-3.4 (6H, -CH$_2$CH$_2$CH$_2$-)
$[Cu_2(\mu\text{-}Ph_2Pbipy)_2(\mu\text{-SEt})](PF_6)$	1.1 (3H, -CH$_3$), 3.5 (2H, -CH$_2$-)
$[Cu_2(\mu\text{-}Ph_2Pbipy)_2(\mu\text{-}S_2CNEt_2)](PF_6)$	1.2 (6H, -CH$_3$), 3.3 (4H, -CH$_2$-)
$[Cu_2(\mu\text{-}Ph_2Pbipy)_2(\mu\text{-}O_2CH)](PF_6)$	1.5 (1H, -H)
$[Cu_2(\mu\text{-}Ph_2Pbipy)_2(\mu\text{-}O_2CCH_3)](PF_6)$	1.9 (3H, -CH$_3$)

Table 3.9. Crystal data for [Cu$_2$(μ-Ph$_2$Pbipy)$_2$(MeCN)$_2$](PF$_6$)$_2$

Formula	Cu$_2$C$_{48}$H$_{40}$N$_6$P$_4$F$_{12}$
Molecular mass	1179.85
Crystal system	monoclinic
Space group	P2$_1$ / c
a (Å)	11.6709
b (Å)	9.4240
c (Å)	22.8851
β (°)	93
V (Å^3)	2512
Z	2
D_c (g cm^{-3})	1.56
F (000)	1192
μ (cm^{-1})	11
Absorption corrections	Semi Empirical[87]
Measured intensities	3865
Unique intensities	3027
Unique intensities with [$F_o > 3\sigma$ (F_o)]	2386
$\Delta\rho_{max}$ (eÅ^{-3})	2.107
Maximum least squares shift to error ratio	0.306
Weighting scheme parameter g in $w = 1/[\sigma^2(F) + g\,(F^2)]$	0.0026
R = Σ (F_o - F_c) / ΣF_o	0.0821
R$_w$ = Σ_w ½ (F_o - F_c) / ΣF_w½F_o	0.0903
Scan Mode	ω - 2θ
ω scan angle	0.90 + 0.34tanθ
Horizontal Aperture Width (mm)	2.70 + 0.40tanθ
Scattering Range	3 $\leq \theta \leq$ 23
Number of parameters	205

Table 3.10. Fractional Coordinates (x10^4) and Isotropic Thermal Factors (Å^2 , x10^3) for [Cu$_2$(μ-Ph$_2$Pbipy)$_2$(MeCN)$_2$](PF$_6$)$_2$

	x/a	y/b	z/c	U$_{eq}$
Cu	3611(1)	232(1)	436(1)	33(1)
P (1)	5235(2)	1154(3)	788(1)	29(1)
N (1)	6536(6)	1827(8)	-125(3)	28(2)
N (2)	7383(6)	668(8)	-1077(3)	34(2)
N (3)	2404(7)	1637(9)	66(4)	37(2)
C (1)	4989(8)	2254(10)	1405(4)	37(2)*
C (2)	3913(9)	2930(12)	1410(5)	46(3)*
C (3)	3673(11)	3901(14)	1862(6)	68(4)*
C (4)	4523(12)	4132(15)	2335(7)	71(4)*
C (5)	5563(12)	3515(16)	2319(7)	76(4)*
C (6)	5805(10)	2544(13)	1862(5)	55(3)*
C (7)	6287(8)	-143(10)	1070(4)	37(2)*
C (8)	7426(9)	215(11)	1199(5)	47(3)*
C (9)	8170(11)	-793(15)	1483(6)	68(4)*
C (10)	7775(11)	-2175(15)	1595(6)	67(4)*
C (11)	6642(11)	-2534(14)	1426(6)	66(3)*
C (12)	5900(9)	-1489(11)	1172(5)	44(3)*
C (13)	6054(7)	2372(10)	345(4)	33(2)

Table 3.10. /continued

	x/a	y/b	z/c	$\underline{U}_{eq}$
C (14)	6083(9)	3829(10)	472(5)	47(3)
C (15)	6622(10)	4731(11)	93(5)	52(3)
C (16)	7143(10)	4178(11)	-385(5)	46(3)
C (17)	7068(7)	2715(10)	-482(4)	33(2)
C (18)	7570(7)	2056(10)	-1002(4)	35(2)
C (19)	8220(9)	2826(11)	-1375(5)	44(3)
C (20)	8689(9)	2150(14)	-1838(5)	56(3)
C (21)	8520(10)	697(13)	-1917(5)	53(3)
C (22)	7839(10)	11(12)	-1522(5)	51(3)
C (23)	1509(14)	1922(18)	-73(5)	85(5)
C (24)	671(11)	2994(15)	-262(7)	76(4)
P (2)	143(2)	6570(3)	8545(1)	49(1)
F (1)	1243(8)	6925(13)	8237(4)	129(3)
F (2)	9003(8)	6267(13)	-1163(5)	139(4)
F (3)	97(9)	8016(10)	-1163(5)	127(3)
F (4)	102(12)	5135(11)	-1765(7)	166(5)

Table 3.10. /continued

	x/a	y/b	z/c	$\underline{U}_{eq}$
F (5)	9451(11)	7120(20)	-1989(5)	186(6)
F (6)	10853(14)	6119(23)	-930(6)	231(7)

* isotropic temperature factor

$$\underline{U}_{eq} = \frac{1}{3} \sum_i \sum_j \underline{U}_{ij} \underline{a}^*_i \underline{a}^*_j (a_i . a_j)$$

Table 3.11. Anisotropic Thermal Factors ($\mathring{A}^2$, x10^3) for [Cu$_2$(μ-Ph$_2$Pbipy)$_2$(MeCN)$_2$](PF$_6$)$_2$

	U (11)	U (22)	U (33)	U (23)	U (13)	U (12)
Cu	32(1)	33(1)	34(1)	2(1)	4(1)	-7(1)
P (1)	31(1)	28(1)	30(1)	0(1)	5(1)	-4(1)
N (1)	26(4)	32(4)	25(4)	5(4)	2(3)	-8(3)
N (2)	33(4)	35(5)	36(5)	8(4)	7(4)	-3(4)
N (3)	30(4)	43(5)	37(5)	5(4)	-3(4)	3(4)
C (13)	29(5)	34(5)	36(6)	6(5)	-2(4)	-3(4)
C (14)	56(6)	23(5)	63(8)	-9(5)	19(6)	-9(5)
C (15)	71(8)	29(5)	57(7)	3(5)	17(6)	-13(5)
C (16)	57(7)	30(5)	52(7)	3(5)	9(6)	-7(5)
C (17)	32(5)	35(5)	32(6)	5(4)	-4(4)	-7(4)
C (18)	24(4)	43(6)	38(6)	10(5)	5(4)	3(4)
C (19)	44(6)	46(6)	44(6)	13(5)	12(5)	-5(5)
C (20)	45(6)	74(9)	49(7)	14(6)	15(6)	-8(6)
C (21)	57(7)	54(7)	50(7)	7(6)	5(6)	-1(6)
C (22)	56(6)	51(7)	51(7)	6(6)	26(6)	-2(5)
C (23)	102(12)	126(14)	28(7)	2(8)	4(7)	56(10)
C (24)	66(8)	70(9)	89(11)	16(8)	-6(8)	27(7)
P (2)	46(2)	44(2)	57(2)	3(1)	11(1)	-6(1)

Table 3.11. /continued

	U (11)	U (22)	U (33)	U (23)	U (13)	U (12)
F (1)	98(6)	195(11)	99(7)	-61(7)	57(6)	-78(7)
F (2)	103(7)	162(10)	160(10)	-67(8)	81(7)	-72(7)
F (3)	121(8)	102(7)	162(10)	-52(7)	38(7)	-29(6)
F (4)	182(12)	86(7)	246(16)	-82(9)	130(12)	-60(7)
F (5)	154(11)	313(21)	86(8)	15(11)	-28(7)	55(13)
F (6)	201(14)	363(25)	129(11)	113(14)	26(10)	158(16)

Table 3.12. Interatomic distances (Å) for [Cu$_2$(μ-Ph$_2$Pbipy)$_2$(MeCN)$_2$](PF$_6$)$_2$

Cu-P(1)	2.191(3)	Cu'-N(3)'	2.073(9)
Cu-Cu'	3.941(2)	Cu-N(1)	2.070(9)
Cu-N(2)	2.106(9)	P(1)-C(1)	1.790(10)
P(1)-C(7)	1.820(10)	P(1)-C(13)	1.840(9)
N(1)-C(13)	1.348(12)	N(1)-C(17)	1.348(13)
N(2)-C(18)	1.335(13)	N(2)-C(22)	1.333(14)
N(3)-C(23)	1.105(15)	C(1)-C(2)	1.408(14)
C(1)-C(6)	1.39(2)	C(2)-C(3)	1.42(2)
C(3)-C(4)	1.44(2)	C(4)-C(5)	1.35(2)
C(5)-C(6)	1.43(2)	C(7)-C(8)	1.384(15)
C(7)-C(12)	1.371(15)	C(8)-C(9)	1.42(2)
C(9)-C(10)	1.41(2)	C(10)-C(11)	1.39(2)
C(11)-C(12)	1.41(2)	C(13)-C(14)	1.403(14)
C(14)-C(15)	1.394(15)	C(15)-C(16)	1.39(2)
C(16)-C(17)	1.399(15)	C(17)-C(18)	1.495(14)
C(18)-C(19)	1.383(13)	C(19)-C(20)	1.38(2)
C(20)-C(21)	1.39(2)	C(21)-C(22)	1.40(2)
C(23)-C(24)	1.45(2)	P(2)-F(1)	1.541(8)
P(2)-F(2)	1.552(8)	P(2)-F(3)	1.520(10)

Table 3.12. /continued

P(2)-F(4)	1.527(10)	P(2)-F(5)	1.513(12)
P(2)-F(6)	1.476(13)		

Table 3.13. Interatomic angles (°) for [Cu₂(μ-Ph₂Pbipy)₂(MeCN)₂](PF₆)₂ ·

P(1)-Cu-N(3)	116.5(2)	P(1')-Cu'-N(1)	123.3(2)
P(1')-Cu'-N(2)	113.9(2)	N(1)-Cu'-N(2)	79.9(3)
N(1)-Cu'-N(3')	114.7(3)	N(2)-Cu'-N(3')	98.7(3)
Cu'-N(1)-C(13)	127.0(2)	Cu'-N(1)-C(17)	113.8(2)
Cu'-N(2)-C(18)	113.4(3)	Cu'-N(2)-C(22)	127.6(3)
Cu-P(1)-C(1)	109.9(3)	Cu-P(1)-C(7)	114.3(3)
C(1)-P(1)-C(7)	104.4(5)	Cu-P(1)-C(13)	120.8(3)
C(1)-P(1)-C(13)	100.9(5)	C(7)-P(1)-C(13)	104.5(4)
C(13)-N(1)-C(17)	118.6(8)	C(18)-N(2)-C(22)	118.9(8)
Cu-N(3)-C(23)	151.3(12)	P(1)-C(1)-C(2)	117.2(8)
P(1)-C(1)-C(6)	124.6(8)	C(2)-C(1)-C(6)	118.1(10)
C(1)-C(2)-C(3)	120.9(11)	C(2)-C(3)-C(4)	119.1(12)
C(3)-C(4)-C(5)	119.5(14)	C(4)-C(5)-C(6)	121.0(14)
C(1)-C(6)-C(5)	121.1(11)	P(1)-C(7)-C(8)	121.9(8)
P(1)-C(7)-C(12)	117.4(8)	C(8)-C(7)-C(12)	120.7(10)
C(7)-C(8)-C(9)	119.1(11)	C(8)-C(9)-C(10)	120.3(13)
C(9)-C(10)-C(11)	119.3(13)	C(10)-C(11)-C(12)	119.3(12)
C(7)-C(12)-C(11)	121.0(10)	P(1)-C(13)-N(1)	117.5(7)
P(1)-C(13)-C(14)	120.2(8)	N(1)-C(13)-C(14)	122.1(9)

Table 3.13. /continued

C(13)-C(14)-C(15)	118.3(10)	C(14)-C(15)-C(16)	120.0(10)
C(15)-C(16)-C(17)	118.1(10)	N(1)-C(17)-C(16)	122.8(9)
N(1)-C(17)-C(18)	116.4(8)	C(16)-C(17)-C(18)	120.8(9)
N(2)-C(18)-C(17)	116.1(8)	N(2)-C(18)-C(19)	121.8(9)
C(17)-C(18)-C(19)	122.1(9)	C(18)-C(19)-C(20)	119.5(10)
C(19)-C(20)-C(21)	119.6(10)	C(20)-C(21)-C(22)	116.8(11)
N(2)-C(22)-C(21)	123.4 (11)	N(3)-C(23)-C(24)	149(2)
F(1)-P(2)-F(2)	177.2(8)	F(1)-P(2)-F(3)	93.5(6)
F(2)-P(2)-F(3)	85.4(6)	F(1)-P(2)-F(4)	88.9(6)
F(2)-P(2)-F(4)	92.0(6)	F(3)-P(2)-F(4)	176.0(8)
F(1)-P(2)-F(5)	88.4(8)	F(2)-P(2)-F(5)	89.0(8)
F(3)-P(2)-F(5)	90.9(9)	F(4)-P(2)-F(5)	85.9(10)
F(1)-P(2)-F(6)	89.7(8)	F(2)-P(2)-F(6)	92.8(9)
F(3)-P(2)-F(6)	86.2(10)	F(4)-P(2)-F(6)	97.0(11)
F(5)-P(2)-F(6)	176.5(12)		

Table 3.14. Crystal data for [Cu$_2$(μ-Ph$_2$Pbipy)$_2$(PhCN)$_2$](PF$_6$)$_2$

Formula	Cu$_2$C$_{56}$H$_{44}$N$_6$P$_4$F$_{12}$
Molecular mass	1279.97
Crystal system	monoclinic
Space group	P2$_1$ / c
a (Å)	10.7065
b (Å)	14.8973
c (Å)	17.8663
β (°)	95
V (Å^3)	2836
Z	2
D_c (g cm^{-3})	1.5
F (000)	1188
μ (cm^{-1})	10
Absorption corrections	Semi Empirical[87]
Measured intensities	4270
Unique intensities	3427
Unique intensities with [$F_o > 3\sigma$ (F_o)]	2689
$\Delta\rho_{max}$ (eÅ^{-3})	0.546
Maximum least squares shift to error ratio	0.006
Weighting scheme parameter g in $w = 1/[\sigma^2(F) + g\,(F^2)]$	0.0067
R = Σ ($F_o - F_c$) / ΣF_o	0.0581
R$_w$ = Σ_w ½ ($F_o - F_c$) / ΣF_w½F_o	0.0676
Scan Mode	ω - 2θ
ω scan angle	0.44 + 0.34tanθ
Horizontal Aperture Width (mm)	2.70 + 0.40tanθ
Scattering Range	3 $\leq \theta \leq$ 23
Number of parameters	370

Table 3.15. Fractional Coordinates ($x10^4$) and Isotropic Thermal Factors (Å^2 , $x10^3$) for $[Cu_2(\mu\text{-}Ph_2Pbipy)_2(PhCN)_2](PF_6)_2$

	x/a	y/b	z/c	$\underline{U}_{eq}$
Cu	5217(1)	-960(1)	4327(1)	45(1)
P (1)	6244(1)	-983(1)	5453(1)	41(1)
N (1)	4841(4)	-131(3)	6392(3)	41(1)
N (2)	3544(5)	1405(4)	6461(3)	51(1)
N (3)	3799(6)	-1786(4)	4064(3)	60(2)
C (1)	7531(5)	-167(4)	5606(3)	42(1)
C (2)	7855(6)	280(5)	4969(4)	54(2)
C (3)	8858(7)	895(5)	5057(4)	66(2)
C (4)	9474(7)	1058(5)	5747(5)	67(2)
C (5)	9141(6)	609(6)	6367(4)	61(2)
C (6)	8144(6)	-5(5)	6310(4)	54(2)
C (7)	6996(6)	-2074(4)	5523(4)	50(2)
C (8)	6218(8)	-2839(5)	5421(5)	74(2)
C (9)	6748(12)	-3695(6)	5349(5)	95(3)
C (10)	8081(13)	-3768(7)	5398(6)	98(3)
C (11)	8825(9)	-3020(7)	5501(5)	83(3)
C (12)	8323(7)	-2153(5)	5584(4)	61(2)
C (13)	5465(6)	-891(4)	6324(4)	47(2)

Table 3.15. /continued

	x/a	y/b	z/c	$\underline{U}_{eq}$
C (14)	5493(8)	-1581(5)	6847(4)	66(2)
C (15)	4855(8)	-1444(6)	7491(5)	83(3)
C (16)	4216(8)	-667(6)	7561(5)	74(2)
C (17)	4189(6)	-8(5)	7002(4)	50(2)
C (18)	3428(6)	821(5)	7016(4)	49(2)
C (19)	2621(8)	974(6)	7576(5)	71(2)
C (20)	1917(9)	1758(7)	7537(5)	81(2)
C (21)	2021(8)	2359(7)	6971(6)	91(3)
C (22)	2882(7)	2170(6)	6423(4)	69(2)
C (23)	3021(7)	-2285(5)	3848(4)	54(2)
C (24)	2072(6)	-2915(4)	3570(4)	53(2)
C (25)	1561(7)	-3441(5)	4089(5)	68(2)
C (26)	612(8)	-4073(5)	3814(7)	84(3)
C (27)	283(9)	-4137(6)	3044(7)	82(3)
C (28)	809(9)	-3594(7)	2545(6)	89(3)
C (29)	1744(8)	-2966(6)	2801(5)	70(2)
P (2)	7283(3)	891(2)	8647(2)	88(1)
F (1)	8349(7)	570(4)	9271(3)	124(2)

Table 3.15. /continued

	x/a	y/b	z/c	$\underline{U}_{eq}$
F (2)	8429(10)	1024(5)	8131(5)	169(3)
F (3)	7208(8)	-106(5)	8359(6)	186(3)
F (4)	7484(9)	1867(5)	8906(4)	151(3)
F (5)	6364(10)	1221(7)	8001(6)	214(4)
F (6)	6316(10)	734(8)	9163(8)	241(5)

* isotropic temperature factor

$$\underline{U}_{eq} = \tfrac{1}{3} \sum_i \sum_j \underline{U}_{ij} \underline{a}^*_i \underline{a}^*_j (a_i . a_j)$$

Table 3.16. Anisotropic Thermal Factors ($Å^2$, x10^3) for [Cu$_2$(μ-Ph$_2$Pbipy)$_2$(PhCN)$_2$](PF$_6$)$_2$

	U (11)	U (22)	U (33)	U (23)	U (13)	U (12)
Cu	37(1)	48(1)	50(1)	2(1)	0(1)	-1(1)
P (1)	33(1)	41(1)	48(1)	4(1)	2(1)	0(1)
N (1)	34(3)	47(3)	41(3)	2(2)	1(2)	-2(2)
N (2)	40(3)	54(3)	58(4)	-5(3)	3(3)	7(3)
N (3)	49(3)	56(4)	74(4)	-4(3)	1(3)	-3(3)
C (1)	27(3)	46(4)	53(4)	-2(3)	1(3)	-2(3)
C (2)	43(4)	60(4)	60(4)	-3(4)	10(3)	-14(3)
C (3)	52(4)	80(6)	67(5)	-6(4)	13(4)	-23(4)
C (4)	49(4)	65(5)	88(6)	-3(4)	10(4)	-9(4)
C (5)	43(4)	72(5)	68(5)	-10(4)	-3(4)	-3(4)
C (6)	42(4)	53(4)	64(4)	-2(3)	-6(3)	-1(3)
C (7)	59(4)	44(4)	46(4)	1(3)	2(3)	5(3)
C (8)	97(6)	44(4)	78(5)	1(4)	2(5)	6(4)
C (9)	151(11)	51(5)	85(7)	11(5)	12(7)	18(6)
C (10)	147(11)	69(6)	80(6)	3(5)	28(7)	41(7)
C (11)	90(6)	87(7)	77(6)	19(5)	28(5)	44(6)
C (12)	54(4)	72(5)	60(4)	10(4)	14(3)	29(4)
C (13)	39(3)	53(4)	50(4)	5(3)	5(3)	-1(3)

Table 3.16. /continued

	U (11)	U (22)	U (33)	U (23)	U (13)	U (12)
C (14)	71(5)	64(5)	65(5)	25(4)	13(4)	15(4)
C (15)	72(6)	99(7)	85(6)	41(5)	38(5)	23(5)
C (16)	65(5)	90(6)	70(5)	25(5)	22(4)	3(5)
C (17)	43(4)	60(4)	49(4)	-4(3)	8(3)	-11(3)
C (18)	33(3)	62(5)	51(4)	-15(3)	2(3)	-5(3)
C (19)	65(5)	85(6)	63(5)	-29(4)	14(4)	-3(4)
C (20)	85(6)	92(7)	66(6)	-13(5)	15(5)	15(5)
C (21)	69(5)	108(8)	94(7)	-45(6)	-7(5)	24(5)
C (22)	69(5)	73(5)	63(5)	-22(4)	2(4)	19(4)
C (23)	48(4)	47(4)	65(4)	-7(4)	0(3)	3(4)
C (24)	41(4)	44(4)	73(5)	-8(3)	-2(3)	1(3)
C (25)	59(5)	59(5)	85(6)	16(4)	-1(4)	-10(4)
C (26)	66(5)	51(5)	132(9)	1(5)	1(6)	-8(4)
C (27)	67(6)	56(5)	122(9)	-18(5)	-7(6)	2(4)
C (28)	80(6)	89(7)	93(7)	-32(6)	-22(5)	11(6)
C (29)	66(5)	71(5)	69(5)	-6(4)	-5(4)	1(4)
P (2)	102(2)	82(2)	78(2)	2(1)	-1(1)	7(1)
F (1)	148(6)	120(5)	102(4)	7(4)	-6(4)	35(5)

Table 3.16. /continued

	U (11)	U (22)	U (33)	U (23)	U (13)	U (12)
F (2)	217(9)	164(8)	133(6)	30(5)	60(7)	31(6)
F (3)	179(8)	112(6)	255(10)	-56(6)	-46(7)	-20(5)
F (4)	220(8)	88(5)	142(6)	-14(4)	-2(6)	12(5)
F (5)	227(10)	175(8)	211(10)	17(7)	-136(8)	17(2)
F (6)	176(9)	219(10)	354(16)	109(10)	165(11)	40(7)

Table 3.17. Interatomic distances (Å) for [Cu₂(μ-Ph₂Pbipy)₂(PhCN)₂](PF₆)₂

Cu-P(1)	2.198(2)	Cu-N(3)	1.975(6)
Cu-Cu'	3.795(2)	Cu'-N(1)	2.070(6)
Cu'-N(2)	2.131(6)	P(1)-C(1)	1.838(6)
P(1)-C(7)	1.812(7)	P(1)-C(13)	1.839(7)
N(1)-C(13)	1.328(8)	N(1)-C(17)	1.362(8)
N(2)-C(18)	1.335(9)	N(2)-C(22)	1.340(9)
N(3)-C(23)	1.155(9)	C(1)-C(2)	1.391(9)
C(1)-C(6)	1.382(9)	C(2)-C(3)	1.408(10)
C(3)-C(4)	1.364(11)	C(4)-C(5)	1.369(12)
C(5)-C(6)	1.402(10)	C(7)-C(8)	1.414(10)
C(7)-C(12)	1.419(9)	C(8)-C(9)	1.407(12)
C(9)-C(10)	1.425(15)	C(10)-C(11)	1.371(14)
C(11)-C(12)	1.413(11)	C(13)-C(14)	1.387(10)
C(14)-C(15)	1.409(11)	C(15)-C(16)	1.357(12)
C(16)-C(17)	1.398(10)	C(17)-C(18)	1.480(10)
C(18)-C(19)	1.401(10)	C(19)-C(20)	1.388(12)
C(20)-C(21)	1.364(14)	C(21)-C(22)	1.435(12)
C(23)-C(24)	1.436(10)	C(24)-C(25)	1.369(10)
C(24)-C(29)	1.387(10)	C(25)-C(26)	1.436(12)

Table 3.17. /continued

C(26)-C(27)	1.390(15)	C(27)-C(28)	1.366(14)
C(28)-C(29)	1.414(12)	P(2)-F(1)	1.590(6)
P(2)-F(2)	1.615(9)	P(2)-F(3)	1.572(8)
P(2)-F(4)	1.535(7)	P(2)-F(5)	1.524(8)
P(2)-F(6)	1.469(9)		

Table 3.18. Interatomic angles (°) for [Cu$_2$(μ-Ph$_2$Pbipy)$_2$(PhCN)$_2$](PF$_6$)$_2$

P(1)-Cu-N(3)	120.9(2)	Cu-P(1)-C(1)	115.3(2)
Cu-P(1)-C(7)	104.8(2)	C(1)-P(1)-C(7)	105.1(3)
Cu-P(1)-C(13)	123.1(2)	C(1)-P(1)-C(13)	102.7(3)
C(7)-P(1)-C(13)	104.1(3)	C(13)-N(1)-C(17)	119.4(5)
C(18)-N(2)-C(22)	120.4(6)	Cu-N(3)-C(23)	173.5(6)
P(1)-C(1)-C(2)	116.0(5)	P(1)-C(1)-C(6)	122.3(5)
C(2)-C(1)-C(6)	121.8(6)	C(1)-C(2)-C(3)	117.9(6)
C(2)-C(3)-C(4)	120.9(7)	C(3)-C(4)-C(5)	120.2(7)
C(4)-C(5)-C(6)	121.1(7)	C(1)-C(6)-C(5)	118.1(7)
P(1)-C(7)-C(8)	117.5(5)	P(1)-C(7)-C(12)	121.0(5)
C(8)-C(7)-C(12)	121.1(7)	C(7)-C(8)-C(9)	120.3(9)
C(8)-C(9)-C(10)	118.3(10)	C(9)-C(10)-C(11)	120.7(9)
C(10)-C(11)-C(12)	122.4(9)	C(7)-C(12)-C(11)	117.1(8)
P(1)-C(13)-N(1)	114.5(5)	P(1)-C(13)-C(14)	122.2(5)
N(1)-C(13)-C(14)	123.3(6)	C(13)-C(14)-C(15)	117.5(7)
C(14)-C(15)-C(16)	119.2(7)	C(15)-C(16)-C(17)	120.6(7)
N(1)-C(17)-C(16)	120.0(7)	N(1)-C(17)-C(18)	116.8(6)
C(16)-C(17)-C(18)	123.2(6)	N(2)-C(18)-C(17)	116.1(6)
N(2)-C(18)-C(19)	122.1(7)	C(17)-C(18)-C(19)	121.7(7)

Table 3.18. /continued

C(18)-C(19)-C(20)	118.1(8)	C(19)-C(20)-C(21)	120.5(8)
C(20)-C(21)-C(22)	118.7(9)	N(2)-C(22)-C(21)	120.2(8)
N(3)-C(23)-C(24)	178.8(8)	C(23)-C(24)-C(25)	117.1(7)
C(23)-C(24)-C(29)	118.8(7)	C(25)-C(24)-C(29)	124.1(7)
C(24)-C(25)-C(26)	117.4(8)	C(25)-C(26)-C(27)	119.1(9)
C(26)-C(27)-C(28)	121.7(8)	C(27)-C(28)-C(29)	120.3(9)
C(24)-C(29)-C(28)	117.4(8)	F(1)-P(2)-F(2)	84.4(4)
F(1)-P(2)-F(3)	87.5(4)	F(2)-P(2)-F(3)	87.0(5)
F(1)-P(2)-F(4)	90.2(4)	F(2)-P(2)-F(4)	87.9(5)
F(3)-P(2)-F(4)	174.5(5)	F(1)-P(2)-F(5)	174.4(6)
F(2)-P(2)-F(5)	90.0(6)	F(3)-P(2)-F(5)	92.7(5)
F(4)-P(2)-F(5)	89.1(5)	F(1)-P(2)-F(6)	90.8(6)
F(2)-P(2)-F(6)	175.2(6)	F(3)-P(2)-F(6)	92.2(7)
F(4)-P(2)-F(5)	92.8(6)	F(5)-P(2)-F(6)	94.8(7)

Table 3.19. Crystal data for $[Cu_2(\mu\text{-}Ph_2Pbipy)_2(H_2O)_2](PF_6)_2$

Formula	$Cu_2C_{44}H_{38}N_4O_2P_4F_{12}$
Molecular mass	1133.78
Crystal system	monoclinic
Space group	$P2_1 / n$
a (Å)	11.2678
b (Å)	11.8015
c (Å)	18.5354
β (°)	90
V (Å³)	2465
Z	2
D_c (g cm⁻³)	1.5
F (000)	1144
μ (cm⁻¹)	11
Absorption corrections	Semi Empirical[87]
Measured intensities	3738
Unique intensities	2933
Unique intensities with $[F_o > 3\sigma (F_o)]$	1893
$\Delta\rho_{max}$ (eÅ⁻³)	1.113
Maximum least squares shift to error ratio	-0.12
Weighting scheme parameter g in $w = 1/[\sigma^2(F) + g(F^2)]$	0.029
$R = \Sigma (F_o - F_c) / \Sigma F_o$	0.1136
$R_w = \Sigma_w \frac{1}{2} (F_o - F_c) / \Sigma F_w \frac{1}{2} F_o$	0.1240
Scan Mode	$\omega - 2\theta$
ω scan angle	$0.92 + 0.34\tan\theta$
Horizontal Aperture Width (mm)	$2.70 + 0.40\tan\theta$
Scattering Range	$3 \leq \theta \leq 23$
Number of parameters	194

Table 3.20. Fractional Coordinates (x10⁴) and Isotropic Thermal Factors (Å², x10³) for [Cu₂(μ-Ph₂Pbipy)₂(H₂O)₂](PF₆)₂

	x/a	y/b	z/c	$\underline{U}_{eq}$
Cu	896(2)	981(2)	72(1)	42(1)
P (1)	-744(3)	1657(3)	509(2)	36(1)
O	1815(16)	250(11)	1016(8)	94(5)
N (1)	-1714(10)	-365(10)	829(6)	34(3)
N (2)	-2166(13)	-2263(10)	143(7)	50(3)
C (1)	-364(12)	2836(12)	1094(8)	37(4)*
C (2)	-580(15)	3973(14)	899(9)	48(4)*
C (3)	-154(17)	4825(17)	1315(10)	63(5)*
C (4)	510(18)	4618(19)	1933(11)	71(6)*
C (5)	761(16)	3488(16)	2146(10)	58(5)*
C (6)	222(14)	2632(14)	1736(8)	47(4)*
C (7)	-1875(13)	2231(13)	-101(8)	41(4)*
C (8)	-1601(14)	2486(14)	-786(9)	46(4)*
C (9)	-2421(18)	2928(18)	-1255(10)	67(5)*
C (10)	-3578(17)	3153(17)	-1013(11)	66(5)*
C (11)	-3891(19)	2913(19)	-274(12)	76(6)*
C (12)	-2994(16)	2493(15)	130(10)	54(4)*
C (13)	-1645(13)	686(13)	1086(8)	40(4)*

Table 3.20. /continued

	x/a	y/b	z/c	$\underline{U}_{eq}$
C (14)	-2188(16)	1032(15)	1687(9)	54(4)*
C (15)	-2925(15)	238(15)	2059(9)	55(5)*
C (16)	-3077(16)	-802(14)	1803(9)	53(4)*
C (17)	-2391(14)	-1100(14)	1153(8)	45(4)*
C (18)	-2540(14)	-2217(14)	820(8)	45(4)*
C (19)	-3106(17)	-3146(16)	1154(10)	64(5)*
C (20)	-3241(17)	-4168(15)	771(10)	60(5)*
C (21)	-2860(20)	-4191(18)	101(12)	74(6)*
C (22)	-2313(15)	-3267(15)	-226(9)	53(4)*
P (2)	5187(5)	6414(5)	7849(3)	80(2)
F (1A)	5598(17)	5720(27)	8527(11)	109(11))*
F (2A)	6515(9)	6440(22)	7562(13)	195(25)*
F (3A)	4776(18)	7110(27)	7171(11)	158(18)*
F (4A)	4987(21)	5398(16)	7471(16)	211(26)*
F (5A)	3858(8)	6389(21)	8135(12)	85(9)*
F (6A)	5386(21)	7431(15)	8227(16)	300(43)*
F (1B)	3854(8)	6792(18)	7921(10)	161(13)*
F (2B)	5360(17)	6575(20)	8684(4)	152(12)*

Table 3.20. /continued

	x/a	y/b	z/c	$\underline{U}_{eq}$
F (3B)	6520(8)	6036(19)	7776(11)	381(49)*
F (4B)	5523(18)	7551(8)	7734(11)	180(14)*
F (5B)	5013(17)	6253(20)	7013(3)	119(8)*
F (6B)	4850(17)	5278(7)	7963(11)	172(13)*

* isotropic temperature factor

$$\underline{U}_{eq} = \frac{1}{3} \sum_i \sum_j \underline{U}_{ij} \underline{a}^*_i \underline{a}^*_j (a_i.a_j)$$

Table 3.21. Anisotropic Thermal Factors ($\mathring{A}^2$, $\times 10^3$) for $[Cu_2(\mu\text{-}Ph_2Pbipy)_2(H_2O)_2](PF_6)_2$

	U (11)	U (22)	U (33)	U (23)	U (13)	U (12)
Cu	45(1)	31(1)	51(1)	-1(1)	14(1)	2(1)
P (1)	39(2)	32(2)	38(2)	-4(2)	8(2)	2(2)
O	136(14)	50(8)	91(10)	4(8)	-35(10)	10(9)
N(1)	42(7)	30(7)	31(6)	3(5)	16(5)	2(5)
N (2)	66(9)	31(7)	53(9)	6(6)	18(7)	2(7)
P (2)	84(4)	90(4)	66(3)	11(3)	-3(3)	-24(3)

Table 3.22. Interatomic distances (Å) for [Cu$_2$(μ-Ph$_2$Pbipy)$_2$(H$_2$O)$_2$](PF$_6$)$_2$

Cu-P(1)'	2.169(4)	Cu-O	2.209(14)
Cu-Cu'	3.084(4)	P(1)-C(1)	1.815(15)
Cu-N(1)	2.121(4)	Cu-N(2)	2.042(5)
P(1)-C(7)	1.833(15)	P(1)-C(13)	1.868(15)
N(1)-C(13)	1.33(2)	N(1)-C(17)	1.30(2)
N(2)-C(18)	1.33(2)	N(2)-C(22)	1.38(2)
C(1)-C(2)	1.41(2)	C(1)-C(6)	1.38(2)
C(2)-C(3)	1.36(2)	C(3)-C(4)	1.39(2)
C(4)-C(5)	1.42(2)	C(5)-C(6)	1.40(2)
C(7)-C(8)	1.34(2)	C(7)-C(12)	1.37(2)
C(8)-C(9)	1.37(2)	C(9)-C(10)	1.40(3)
C(10)-C(11)	1.44(3)	C(11)-C(12)	1.35(3)
C(13)-C(14)	1.34(2)	C(14)-C(15)	1.43(2)
C(15)-C(16)	1.33(2)	C(16)-C(17)	1.47(2)
C(17)-C(18)	1.47(2)	C(18)-C(19)	1.41(2)
C(19)-C(20)	1.41(3)	C(20)-C(21)	1.31(3)
C(21)-C(22)	1.39(3)	P(2)-F(1A)	1.570(1)
P(2)-F(2A)	1.589(1)	P(2)-F(3A)	1.570(1)
P(2)-F(4A)	1.408(1)	P(2)-F(5A)	1.589(1)

Table 3.22. /continued

P(2)-F(6A)	1.408(1)	P(2)-F(1B)	1.573(1)
P(2)-F(2B)	1.572(1)	P(2)-F(3B)	1.573(1)
P(2)-F(4B)	1.409(1)	P(2)-F(5B)	1.573(1)
P(2)-F(6B)	1.410(1)	F(1A)-F(2B)	1.09(3)
F(1A)-F(3B)	1.776(13)	F(1A)-F(6B)	1.44(2)
F(2A)-F(3B)	0.621(8)	F(2A)-F(4B)	1.75(2)
F(3A)-F(1B)	1.776(12)	F(3A)-F(4B)	1.44(2)
F(3A)-F(5B)	1.09(3)	F(4A)-F(5B)	1.32(3)
F(4A)-F(6B)	0.94(3)	F(5A)-F(1B)	0.620(8)
F(5A)-F(6B)	1.75(2)	F(6A)-F(2B)	1.32(3)
F(6A)-F(4B)	0.94(3)		

Table 3.23. Interatomic angles (°) for [Cu$_2$(μ-Ph$_2$Pbipy)$_2$(H$_2$O)$_2$](PF$_6$)$_2$

P(1)'-Cu-O	104.3(5)	Cu'-P(1)-C(1)	107.7(5)
Cu'-P(1)-C(7)	119.9(5)	C(1)-P(1)-C(7)	104.4(7)
Cu-N(1)-C(13)	126.7(4)	Cu-N(1)-C(17)	111.3(4)
Cu-N(2)-C(18)	111.3(2)	Cu-N(2)-C(22)	127.0(4)
Cu'-P(1)-C(13)	116.8(5)	C(1)-P(1)-C(13)	104.9(7)
C(7)-P(1)-C(13)	101.7(7)	C(13)-N(1)-C(17)	119.4(13)
C(18)-N(2)-C(22)	117.9(14)	P(1)-C(1)-C(2)	122.4(11)
P(1)-C(1)-C(6)	119.6(11)	C(2)-C(1)-C(6)	117.9(14)
C(1)-C(2)-C(3)	120(2)	C(2)-C(3)-C(4)	122(2)
C(3)-C(4)-C(5)	120(2)	C(4)-C(5)-C(6)	116(2)
C(1)-C(6)-C(5)	123(2)	P(1)-C(7)-C(8)	120.4(12)
P(1)-C(7)-C(12)	122.1(13)	C(8)-C(7)-C(12)	117(2)
C(7)-C(8)-C(9)	122(2)	C(8)-C(9)-C(10)	120(2)
C(9)-C(10)-C(11)	120(2)	C(10)-C(11)-C(12)	115(2)
C(7)-C(12)-C(11)	127(2)	P(1)-C(13)-N(1)	113.5(11)
P(1)-C(13)-C(14)	122.6(13)	N(1)-C(13)-C(14)	124(2)
C(13)-C(14)-C(15)	118(2)	C(14)-C(15)-C(16)	121(12)
C(15)-C(16)-C(17)	117(2)	N(1)-C(17)-C(16)	122(2)

Table 3.23. /continued

N(1)-C(17)-C(18)	118.2(14)	C(16)-C(17)-C(18)	119.9(14)
N(2)-C(18)-C(17)	113.5(14)	N(2)-C(18)-C(19)	122(2)
C(17)-C(18)-C(19)	123(2)	C(18)-C(19)-C(20)	120(2)
C(19)-C(20)-C(21)	117(2)	C(20)-C(21)-C(22)	123(2)
N(2)-C(22)-C(21)	121(2)	F(1A)-P(2)-F(2A)	90.0(1)
F(1A)-P(2)-F(3A)	180.0(0)	F(2A)-P(2)-F(3A)	90.0(1)
F(1A)-P(2)-F(4A)	90.0(1)	F(2A)-P(2)-F(4A)	90.0(0)
F(3A)-P(2)-F(4A)	90.0(1)	F(1A)-P(2)-F(5A)	90.0(0)
F(2A)-P(2)-F(5A)	179.9(0)	F(3A)-P(2)-F(5A)	90.0(0)
F(4A)-P(2)-F(5A)	90.0(1)	F(1A)-P(2)-F(6A)	90.0(1)
F(2A)-P(2)-F(6A)	90.0(1)	F(3A)-P(2)-F(6A)	90.0(1)
F(4A)-P(2)-F(6A)	180.0(0)	F(5A)-P(2)-F(6A)	90.0(1)
F(1A)-P(2)-F(1B)	111.2(6)	F(2A)-P(2)-F(1B)	157.4(3)
F(3A)-P(2)-F(1B)	68.8(6)	F(4A)-P(2)-F(1B)	97.6(13)
F(5A)-P(2)-F(1B)	22.6(3)	F(6A)-P(2)-F(1B)	82.4(13)
F(1A)-P(2)-F(2B)	40.4(10)	F(2A)-P(2)-F(2B)	102.2(12)
F(3A)-P(2)-F(2B)	139.6(10)	F(4A)-P(2)-F(2B)	127.8(11)
F(5A)-P(2)-F(2B)	77.8(12)	F(6A)-P(2)-F(2B)	52.2(11)
F(1B)-P(2)-F(2B)	90.0(1)	F(1A)-P(2)-F(3B)	68.8(6)

Table 3.23. /continued

F(2A)-P(2)-F(3B)	22.6(3)	F(3A)-P(2)-F(3B)	111.2(6)
F(4A)-P(2)-F(3B)	82.4(13)	F(5A)-P(2)-F(3B)	157.4(3)
F(6A)-P(2)-F(3B)	97.6(13)	F(1B)-P(2)-F(3B)	180.0(0)
F(2B)-P(2)-F(3B)	90.0(1)	F(1A)-P(2)-F(4B)	122.6(10)
F(2A)-P(2)-F(4B)	71.2(8)	F(3A)-P(2)-F(4B)	57.4(10)
F(4A)-P(2)-F(4B)	141.2(11)	F(5A)-P(2)-F(4B)	108.8(8)
F(6A)-P(2)-F(4B)	38.8(11)	F(1B)-P(2)-F(4B)	90.0(1)
F(2B)-P(2)-F(4B)	90.0(1)	F(3B)-P(2)-F(4B)	90.0(1)
F(1A)-P(2)-F(5B)	139.6(10)	F(2A)-P(2)-F(5B)	77.9(12)
F(3A)-P(2)-F(5B)	40.4(10)	F(4A)-P(2)-F(5B)	52.2(11)
F(5A)-P(2)-F(5B)	102.1(12)	F(6A)-P(2)-F(5B)	127.8(11)
F(1B)-P(2)-F(5B)	90.0(1)	F(2B)-P(2)-F(5B)	180.0(0)
F(3B)-P(2)-F(5B)	90.0(1)	F(4B)-P(2)-F(5B)	90.0(1)
F(1A)-P(2)-F(6B)	57.5(10)	F(2A)-P(2)-F(6B)	108.8(9)
F(3A)-P(2)-F(6B)	122.6(10)	F(4A)-P(2)-F(6B)	38.8(11)
F(5A)-P(2)-F(6B)	71.2(9)	F(6A)-P(2)-F(6B)	141.2(11)
F(1B)-P(2)-F(6B)	90.0(1)	F(2B)-P(2)-F(6B)	90.0(1)
F(3B)-P(2)-F(6B)	90.0(1)	F(4B)-P(2)-F(6B)	180.0(0)
F(5B)-P(2)-F(6B)	90.0(1)	P(2)-F(1A)-F(2B)	69.9(5)

Table 3.23. /continued

P(2)-F(1A)-F(3B)	55.7(3)	F(2B)-F(1A)-F(3B)	99.2(10)
P(2)-F(1A)-F(6B)	55.7(4)	F(2B)-F(1A)-F(6B)	112.9(7)
F(3B)-F(1A)-F(6B)	81.4(8)	P(2)-F(2A)-F(3B)	77.2(2)
P(2)-F(2A)-F(4B)	49.6(3)	F(3B)-F(2A)-F(4B)	118(2)
P(2)-F(3A)-F(1B)	55.7(3)	P(2)-F(3A)-F(4B)	55.7(4)
F(1B)-F(3A)-F(4B)	81.4(8)	P(2)-F(3A)-F(5B)	69.9(5)
F(1B)-F(3A)-F(5B)	99.1(10)	F(4B)-F(3A)-F(5B)	112.8(6)
P(2)-F(4A)-F(5B)	70.4(7)	P(2)-F(4A)-F(6B)	70.7(6)
F(5B)-F(4A)-F(6B)	138.3(11)	P(2)-F(5A)-F(1B)	77.2(1)
P(2)-F(5A)-F(6B)	49.6(4)	F(1B)-F(5A)-F(6B)	118(2)
P(2)-F(6A)-F(2B)	70.3(7)	P(2)-F(6A)-F(4B)	70.7(6)
F(2B)-F(6A)-F(4B)	138.2(11)	P(2)-F(1B)-F(3A)	55.5(3)
P(2)-F(1B)-F(5A)	80.2(2)	F(3A)-F(1B)-F(5A)	131(2)
P(2)-F(2B)-F(1A)	69.7(5)	P(2)-F(2B)-F(6A)	57.5(4)
F(1A)-F(2B)-F(6A)	122.3(11)	P(2)-F(3B)-F(1A)	55.5(3)
P(2)-F(3B)-F(2A)	80.1(1)	F(1A)-F(3B)-F(2A)	131(2)
P(2)-F(4B)-F(2A)	59.2(5)	P(2)-F(4B)-F(3A)	66.9(6)
F(2A)-F(4B)-F(3A)	88.3(10)	P(2)-F(4B)-F(6A)	70.5(5)
F(2A)-F(4B)-F(6A)	99.8(11)	F(3A)-F(4B)-F(6A)	123.8(11)

Table 3.23. /continued

P(2)-F(5B)-F(3A)	69.7(5)	P(2)-F(5B)-F(4A)	57.5(4)
F(3A)-F(5B)-F(4A)	122.2(11)	P(2)-F(6B)-F(1A)	66.9(6)
P(2)-F(6B)-F(4A)	70.4(5)	F(1A)-F(6B)-F(4A)	123.8(11)
P(2)-F(6B)-F(5A)	59.1(5)	F(1A)-F(6B)-F(5A)	88.3(10)
F(4A)-F(6B)-F(5A)	99.8(11)		

Table 3.24. Crystal data for $[Cu_2(\mu\text{-}Ph_2Pbipy)_2(py)_2](PF_6)_2$

Formula	$Cu_2C_{54}H_{44}N_6P_4F_{12}$
Molecular mass	1255.95
Crystal system	triclinic
Space group	$P(1)$
a (Å)	10.8062
b (Å)	11.4582
c (Å)	12.4049
α (°)	63
β (°)	85
γ (°)	83
V (Å^3)	1363
Z	1
D_c (g cm^{-3})	1.53
F (000)	960
μ (cm^{-1})	10.2
Absorption corrections	Semi Empirical[87]
Measured intensities	3994
Unique intensities	3619
Unique intensities with $[F_o > 3\sigma(F_o)]$	3335
$\Delta\rho_{max}$ (eÅ^{-3})	2.230
Maximum least squares shift to error ratio	-3.41
Weighting scheme parameter g in $w = 1/[\sigma^2(F) + g(F^2)]$	0.010
$R = \Sigma(F_o - F_c)/\Sigma F_o$	0.0694
$R_w = \Sigma w^{1/2}(F_o - F_c)/\Sigma Fw^{1/2}F_o$	0.0912
Scan Mode	$\omega - 2\theta$
ω scan angle	$0.78 + 0.34\tan\theta$
Horizontal Aperture Width (mm)	$2.70 + 0.40\tan\theta$
Scattering Range	$3 \leq \theta \leq 23$
Number of parameters	352

Table 3.25. Fractional Coordinates ($\times 10^4$) and Isotropic Thermal Factors (Å^2 , $\times 10^3$) For $[Cu_2(\mu\text{-}Ph_2Pbipy)_2(py)_2](PF_6)_2$

	x/a	y/b	z/c	$\underline{U}_{eq}$
Cu	427(1)	978(1)	821(1)	39(1)
P (1)	-1300(2)	1045(2)	-1442(2)	35(1)
P (2)	-6454(2)	3583(2)	2770(2)	64(1)
N (1)	-1473(5)	1461(5)	563(5)	36(1)
N (2)	-108(6)	1447(6)	2269(5)	50(1)
N (3)	1593(6)	2390(7)	-225(6)	53(2)
C (1)	-288(7)	2347(7)	-2322(7)	42(2)
C (2)	-467(7)	3568(7)	-2334(7)	49(2)
C (3)	280(9)	4518(8)	-3108(8)	61(2)
C (4)	1170(9)	4318(10)	-3857(8)	66(2)
C (5)	1372(9)	3060(11)	-3847(8)	77(3)
C (6)	623(8)	2084(8)	-3037(7)	57(2)
C (7)	-2548(6)	1393(7)	2488(6)	43(2)
C (8)	-2891(7)	2643(8)	-3357(7)	53(2)
C (9)	-3840(8)	2862(10)	-4094(8)	65(2)
C (10)	-4463(9)	1840(12)	-4013(8)	71(3)
C (11)	-4117(8)	566(10)	-3165(9)	72(2)
C (12)	-3173(7)	354(8)	-2388(8)	59(2)

Table 3.25. /continued

	x/a	y/b	z/c	$\underline{U}_{eq}$
C (13)	-2143(6)	1525(6)	-321(6)	37(1)
C (14)	-3431(7)	1848(9)	-379(8)	62(2)
C (15)	-4037(7)	2132(10)	526(8)	76(2)
C (16)	-3369(7)	2075(9)	1447(8)	60(2)
C (17)	-2091(7)	1728(7)	1446(6)	40(2)
C (18)	-1338(6)	1671(6)	2413(6)	40(2)
C (19)	-1857(7)	1873(8)	3370(7)	59(2)
C (20)	-1083(9)	1874(10)	4213(8)	71(2)
C (21)	181(9)	1678(9)	4053(8)	67(3)
C (22)	621(8)	1470(9)	3086(8)	66(2)
C (23)	1554(11)	3484(10)	-71(9)	93(3)
C (24)	2429(23)	4421(16)	-701(15)	156(7)
C (25)	3277(23)	4240(28)	-1451(19)	145(8)
C (26)	3350(11)	3085(21)	-1641(14)	118(5)
C (27)	2452(8)	2168(11)	-940(9)	69(3)
F (1)	-5044(4)	3204(6)	3134(5)	91(2)
F (2)	-6342(6)	2666(7)	2121(6)	115(2)
F (3)	-6838(7)	2340(8)	3957(5)	119(2)

Table 3.25. /continued

	x/a	y/b	z/c	$\underline{U}_{eq}$
F (4)	-7851(5)	3932(7)	2397(9)	145(3)
F (5)	-6587(9)	4367(10)	3528(10)	193(4)
F (6)	3925(10)	-5265(11)	1648(9)	179(4)

* isotropic temperature factor

$$\underline{U}_{eq} = \tfrac{1}{3}\, \Sigma_i \Sigma_j \underline{U}_{ij} \underline{a}^*_i \underline{a}^*_j (a_i . a_j)$$

Table 3.26. Anisotropic Thermal Factors ($\mathring{A}^2$, x10^3) for [Cu$_2$(μ-Ph$_2$Pbipy)$_2$(py)$_2$](PF$_6$)$_2$

	U (11)	U (22)	U (33)	U (23)	U (13)	U (12)
Cu	31(1)	42(1)	46(1)	-23(1)	4(1)	-1(1)
P (1)	29(1)	41(1)	37(1)	-21(1)	2(1)	0(1)
P (2)	40(1)	65(1)	85(2)	-45(1)	1(1)	1(1)
N (1)	28(3)	37(3)	43(3)	-24(3)	2(3)	-1(2)
N (2)	44(4)	53(4)	51(3)	-36(3)	-5(3)	-2(3)
N (3)	37(4)	66(5)	55(4)	-10(4)	-3(3)	-17(3)
C (1)	36(4)	48(5)	41(4)	-18(4)	5(3)	-6(3)
C (2)	52(4)	43(4)	53(4)	-20(4)	2(4)	-6(3)
C (3)	60(5)	52(5)	69(6)	-16(4)	-1(5)	-14(4)
C (4)	64(6)	72(6)	63(5)	-16(5)	3(5)	-26(5)
C (5)	67(6)	110(8)	56(6)	41(6)	24(5)	-33(6)
C (6)	49(5)	64(5)	59(5)	31(4)	12(4)	-12(4)
C (7)	32(4)	55(4)	41(4)	-26(4)	0(3)	0(3)
C (8)	45(4)	65(5)	47(5)	-24(4)	-8(4)	10(4)
C (9)	52(5)	89(7)	52(5)	-24(5)	-7(4)	7(5)
C (10)	50(5)	104(9)	56(6)	-36(6)	-11(4)	0(5)
C (11)	57(5)	86(7)	72(6)	-37(5)	-16(5)	-1(5)
C (12)	42(4)	60(5)	74(6)	-32(4)	-9(4)	-3(4)

Table 3.26. /continued

	U (11)	U (22)	U (33)	U (23)	U (13)	U (12)
C (13)	30(3)	42(4)	39(4)	-22(3)	5(3)	5(3)
C (14)	35(4)	92(7)	56(5)	-45(5)	0(4)	11(4)
C (15)	34(4)	124(8)	69(6)	59(6)	-3(4)	17(4)
C (16)	37(4)	79(6)	66(5)	-47(5)	3(4)	6(4)
C (17)	37(4)	43(4)	42(4)	-25(3)	6(3)	-1(3)
C (18)	38(4)	37(4)	46(4)	-26(3)	-8(3)	-2(3)
C (19)	54(5)	77(6)	47(4)	-39(4)	3(4)	1(4)
C (20)	71(6)	81(6)	63(5)	-50(5)	11(5)	-8(5)
C (21)	71(7)	71(6)	58(5)	-43(5)	-2(5)	-15(5)
C (22)	57(5)	78(6)	62(6)	-45(5)	2(4)	-10(4)
C (23)	139(9)	65(6)	71(7)	-14(5)	-17(6)	-46(6)
C (24)	243(25)	108(11)	106(12)	6(10)	-69(14)	-107(15)
C (25)	138(19)	189(22)	100(13)	32(17)	-50(13)	-114(19)
C (26)	49(6)	224(18)	80(11)	37(12)	-10(6)	-41(9)
C (27)	36(5)	112(8)	58(6)	2(6)	1(4)	-13(5)
F (1)	43(3)	140(5)	89(4)	-57(4)	-1(3)	8(3)
F (2)	83(4)	140(5)	121(5)	-101(5)	1(4)	9(4)
F (3)	130(5)	159(7)	71(4)	-42(4)	18(4)	-62(5)

Table 3.26. /continued

	U (11)	U (22)	U (33)	U (23)	U (13)	U (12)
F (4)	52(3)	130(6)	248(9)	-124(6)	-34(5)	-25(4)
F (5)	146(8)	182(8)	249(11)	-187(8)	1(7)	-3(6)
F (6)	172(9)	186(10)	167(9)	88(8)	-82(7)	-115(8)

Table 3.27. Interatomic distances (Å) for [Cu$_2$(μ-Ph$_2$Pbipy2)$_2$(py)$_2$](PF$_6$)$_2$

Cu-N(1)	2.077(1)	Cu-N(2)	2.110(2)
Cu'-P(1)	2.205(1)	Cu-N(3)	2.052(2)
P(1)-C(1)	1.826(2)	P(1)-C(7)	1.839(2)
P(1)-C(13)	1.845(2)	N(1)-C(13)	1.338(2)
N(1)-C(17)	1.363(2)	N(2)-C(18)	1.335(3)
N(2)-C(22)	1.349(2)	N(3)-C(23)	1.345(3)
N(3)-C(27)	1.307(3)	C(1)-C(2)	1.383(3)
C(1)-C(6)	1.363(3)	C(2)-C(3)	1.377(3)
C(3)-C(4)	1.347(4)	C(4)-C(5)	1.427(4)
C(5)-C(6)	1.408(3)	C(7)-C(8)	1.384(3)
C(7)-C(12)	1.391(3)	C(8)-C(9)	1.361(3)
C(9)-C(10)	1.380(4)	C(10)-C(11)	1.395(4)
C(11)-C(12)	1.392(3)	C(13)-C(14)	1.396(3)
C(14)-C(15)	1.392(3)	C(15)-C(16)	1.379(3)
C(16)-C(17)	1.391(3)	C(17)-C(18)	1.482(3)
C(18)-C(19)	1.368(3)	C(19)-C(20)	1.397(3)
C(20)-C(21)	1.368(4)	C(21)-C(22)	1.359(3)
C(23)-C(24)	1.420(5)	C(24)-C(25)	1.313(11)
C(25)-C(26)	1.437(10)	C(26)-C(27)	1.442(5)

Table 3.27. /continued

P(2)-F(1)	1.583(1)	P(2)-F(2)	1.573(2)
P(2)-F(3)	1.590(2)	P(2)-F(4)	1.571(2)
P(2)-F(5)	1.554(2)	P(2)-F(6)	1.494(2)

Table 3.28. Interatomic angles (°) for [Cu₂(μ-Ph₂Pbipy)₂(py)₂](PF₆)₂

N(1)-Cu-N(2)	79.6(1)	N(1)-Cu-N(3)	117.1(1)
N(2)-Cu-N(3)	102.8(1)	Cu'-P(1)-C(13)	118.5(3)
C(1)-P(1)-C(7)	102.2(1)	C(1)-P(1)-C(13)	105.5(1)
C(7)-P(1)-C(13)	100.5(1)	Cu-N(1)-C(13)	129.1(1)
Cu-N(1)-C(17)	113.1(1)	C(13)-N(1)-C(17)	117.7(2)
Cu-N(2)-C(18)	114.1(1)	Cu-N(2)-C(22)	128.4(1)
C(18)-N(2)-C(22)	117.4(2)	Cu-N(3)-C(23)	119.2(2)
Cu-N(3)-C(27)	120.2(2)	C(23)-N(3)-C(27)	120.2(2)
P(1)-C(1)-C(2)	122.8(2)	P(1)-C(1)-C(6)	116.3(2)
C(2)-C(1)-C(6)	120.8(2)	C(1)-C(2)-C(3)	118.2(2)
C(2)-C(3)-C(4)	123.3(2)	C(3)-C(4)-C(5)	119.1(2)
C(4)-C(5)-C(6)	117.4(2)	C(1)-C(6)-C(5)	121.1(2)
P(1)-C(7)-C(8)	122.6(2)	P(1)-C(7)-C(12)	118.2(2)
C(8)-C(7)-C(12)	119.2(2)	C(7)-C(8)-C(9)	120.7(2)
C(8)-C(9)-C(10)	120.9(2)	C(9)-C(10)-C(11)	119.7(2)
C(10)-C(11)-C(12)	119.2(2)	C(7)-C(12)-C(11)	120.4(2)
P(1)-C(13)-N(1)	116.6(1)	P(1)-C(13)-C(14)	119.9(2)
N(1)-C(13)-C(14)	123.3(2)	C(13)-C(14)-C(15)	117.8(2)
C(14)-C(15)-C(16)	120.0(2)	C(15)-C(16)-C(17)	118.6(2)

Table 3.28. /continued

N(1)-C(17)-C(16)	122.5(2)	N(1)-C(17)-C(18)	117.3(2)
C(16)-C(17)-C(18)	120.1(2)	N(2)-C(18)-C(17)	115.4(2)
N(2)-C(18)-C(19)	121.9(2)	C(17)-C(18)-C(19)	122.7(2)
C(18)-C(19)-C(20)	119.5(2)	C(19)-C(20)-C(21)	118.8(2)
C(20)-C(21)-C(22)	118.0(2)	N(2)-C(22)-C(21)	124.3(2)
N(3)-C(23)-C(24)	120.4(4)	C(23)-C(24)-C(25)	120.6(6)
C(24)-C(25)-C(26)	120.8(5)	C(25)-C(26)-C(27)	115.0(5)
N(3)-C(27)-C(26)	122.9(4)	F(1)-P(2)-F(2)	91.9(1)
F(1)-P(2)-F(3)	89.4(1)	F(2)-P(2)-F(3)	86.4(1)
F(1)-P(2)-F(4)	178.6(1)	F(2)-P(2)-F(4)	86.7(1)
F(3)-P(2)-F(4)	90.3(1)	F(1)-P(2)-F(5)	87.4(1)
F(2)-P(2)-F(5)	174.4(2)	F(3)-P(2)-F(5)	88.0(2)
F(4)-P(2)-F(5)	94.0(1)	F(1)-P(2)-F(6)	89.9(1)
F(2)-P(2)-F(6)	92.8(2)	F(3)-P(2)-F(6)	178.9(2)
F(4)-P(2)-F(6)	90.4(1)	F(5)-P(2)-F(6)	92.8(2)

Table 3.29. Crystal data for [Cu$_2$(μ-Ph$_2$Pbipy)$_2$(4-etpy)$_2$](PF$_6$)$_2$

Formula	Cu$_2$C$_{58}$H$_{44}$N$_6$P$_4$F$_{12}$
Molecular mass	1396.99
Crystal system	monoclinic
Space group	P2$_1$ / n
a (Å)	13.8814
b (Å)	11.9978
c (Å)	21.3390
β (°)	105
V (Å^3)	3432
Z	2
D_c (g cm^{-3})	1.3
F (000)	1320
μ (cm^{-1})	8
Absorption corrections	Semi Empirical[87]
Measured intensities	5189
Unique intensities	4193
Unique intensities with [$F_o > 3\sigma$ (F_o)]	3252
$\Delta\rho_{max}$ (eÅ^{-3})	1.412
Maximum least squares shift to error ratio	0.811
Weighting scheme parameter g in $w = 1/[\sigma^2(F) + g\,(F^2)]$	0.025
R = Σ (F_o - F_c) / Σ F_o	0.1070
R$_w$ = Σ_w ½ (F_o - F_c) / Σ F_w½F_o	0.1156
Scan Mode	ω - 2θ
ω scan angle	0.90 + 0.34tanθ
Horizontal Aperture Width (mm)	2.70 + 0.40tanθ
Scattering Range	3 $\leq$ θ $\leq$ 23
Number of parameters	249

Table 3.30. Fractional Coordinates ($\times 10^4$) and Isotropic Thermal Factors ($\mathring{A}^2$, $\times 10^3$) For $[Cu_2(\mu\text{-}Ph_2Pbipy)_2(4\text{-}Etpy)_2](PF_6)_2.CH_2Cl_2$

	x/a	y/b	z/c	$\underline{U}_{eq}$
Cu	4510(1)	1010(1)	10419(1)	51(1)
P (1)	4456(2)	1561(2)	9436(1)	45(1)
N (1)	4394(5)	-419(6)	8805(3)	41(1)
N (2)	5229(6)	-2419(6)	8953(4)	57(2)
N (3)	3190(6)	455(7)	10560(4)	59(2)*
C (1)	3562(6)	2712(7)	9248(4)	46(2)*
C (2)	3820(7)	3782(9)	9156(5)	58(2)*
C (3)	3137(8)	4654(10)	9060(6)	74(3)*
C (4)	2144(9)	4415(11)	9066(6)	79(3)*
C (5)	1874(10)	3357(12)	9149(7)	87(4)*
C (6)	2583(8)	2489(10)	9235(6)	72(3)*
C (7)	5581(6)	2183(8)	9284(4)	46(2)*
C (8)	5735(7)	2284(10)	8666(5)	66(8)*
C (9)	6567(9)	2823(11)	8576(6)	78(3)*
C (10)	7254(9)	3249(10)	9124(6)	77(3)*
C (11)	7113(9)	3160(11)	9732(6)	80(3)*
C (12)	6289(8)	2616(9)	9819(5)	64(3)*
C (13)	4013(6)	646(7)	8745(4)	45(2)*

Table 3.30. /continued

	x/a	y/b	z/c	$\underline{U}_{eq}$
C (14)	3376(7)	988(8)	8171(5)	56(2)*
C (15)	3111(8)	282(10)	7659(5)	69(3)*
C (16)	3483(8)	-818(9)	7709(5)	66(3)*
C (17)	4119(7)	-1126(8)	8303(4)	50(2)*
C (18)	4556(6)	-2248(8)	8409(4)	51(2)*
C (19)	4322(9)	-3078(10)	7933(6)	77(3)*
C (20)	4766(10)	-4158(12)	8040(7)	89(4)*
C (21)	5490(9)	-4288(11)	8617(6)	81(3)*
C (22)	5718(8)	-3425(10)	9069(5)	69(3)*
C (23)	2590(8)	-210(9)	10158(5)	66(3)*
C (24)	1702(10)	-625(12)	10278(7)	90(4)*
C (25)	1422(9)	-263(12)	10796(7)	85(4)*
C (26)	2026(12)	374(15)	11201(9)	116(5)*
C (27)	2971(10)	686(13)	11092(8)	99(4)*
C (28)	404(13)	-690(17)	10912(10)	122(5)*
C (29)	560(19)	-1416(23)	11429(14)	182(10)*
P (2)	3873(3)	3021(3)	6707(2)	74(1)
F (1)	4291(9)	1817(7)	6972(6)	134(3)

Table 3.30. /continued

	x/a	y/b	z/c	$\underline{U}_{eq}$
F (2)	4152(8)	2817(10)	6048(5)	151(4)
F (3)	3639(8)	3268(8)	7376(4)	125(3)
F (4)	2799(9)	2615(13)	6456(8)	207(6)
F (5)	3482(10)	4196(9)	6461(6)	157(4)
F (6)	4941(8)	3527(11)	7002(7)	161(4)
Cl (1)	4039(13)	692(16)	12925(9)	129(6)
Cl (2)	2685(13)	-1073(16)	13072(9)	139(7)
C (30)	3899(13)	-512(16)	13375(9)	195(33)

* isotropic temperature factor

$$\underline{U}_{eq} = \tfrac{1}{3} \sum_i \sum_j \underline{U}_{ij} \underline{a}^{*}_{i} \underline{a}^{*}_{j} (a_i . a_j)$$

Table 3.31. Anisotropic Thermal Factors (Å^2, x10^3) for $[Cu_2(\mu\text{-}Ph_2Pbipy)_2(Etpy)_2](PF_6)_2.CH_2Cl_2$

	U (11)	U (22)	U (33)	U (23)	U (13)	U (12)
Cu	76(1)	34(1)	41(1)	3(1)	11(1)	3(1)
P (1)	62(1)	29(1)	42(1)	2(1)	8(1)	2(1)
N (1)	56(4)	30(4)	37(3)	0(3)	12(3)	-3(3)
N (2)	92(6)	20(4)	61(5)	0(3)	21(4)	5(4)
N (3)	77(5)	51(5)	54(5)	-3(4)	27(4)	2(4)
P (2)	95(2)	57(2)	69(2)	4(1)	18(2)	8(2)
F (1)	180(9)	76(5)	168(9)	34(6)	85(7)	36(6)
F (2)	185(10)	193(11)	86(6)	11(7)	55(6)	68(8)
F (3)	186(9)	109(7)	93(6)	29(5)	59(6)	55(6)
F (4)	128(8)	237(16)	240(18)	-118(14)	17(9)	-36(9)
F (5)	236(12)	108(7)	145(9)	65(7)	83(9)	90(8)
F (6)	123(8)	166(10)	170(11)	0(9)	-5(7)	-35(7)
Cl (1)	120(12)	162(17)	107(13)	-50(12)	35(10)	-17(12)
Cl (2)	93(11)	177(21)	161(18)	-17(15)	56(11)	7(10)
C (30)	55(34)	188(85)	327(104)	-84(80)	23(45)	49(45)

Table 3.32. Interatomic distances (Å) for [Cu$_2$(μ-Ph$_2$Pbipy)$_2$(4-Etpy)$_2$](PF$_6$)$_2$.CH$_2$Cl$_2$

Cu-P(1)	2.183(2)	Cu-N(3)	2.044(8)
Cu-Cu'	3.491(2)	Cu'-N(1)	2.062(5)
Cu'-N(2)	2.129(5)	P(1)-C(1)	1.830(9)
P(1)-C(7)	1.833(9)	P(1)-C(13)	1.813(9)
N(1)-C(13)	1.304(12)	N(2)-C(22)	1.376(13)
N(3)-C(23)	1.302(13)	N(3)-C(27)	1.280(2)
C(1)-C(2)	1.360(13)	C(1)-C(6)	1.380(13)
C(2)-C(3)	1.390(15)	C(3)-C(4)	1.41(2)
C(4)-C(5)	1.35(2)	C(5)-C(6)	1.41(2)
C(7)-C(8)	1.395(14)	C(7)-C(12)	1.399(12)
C(8)-C(9)	1.381(15)	C(9)-C(10)	1.40(2)
C(10)-C(11)	1.36(2)	C(11)-C(12)	1.370(15)
C(13)-C(14)	1.374(13)	C(14)-C(15)	1.358(15)
C(15)-C(16)	1.411(15)	C(16)-C(17)	1.392(15)
C(17)-C(18)	1.470(13)	C(18)-C(19)	1.399(15)
C(19)-C(20)	1.43(2)	C(20)-C(21)	1.38(2)
C(21)-C(22)	1.39(2)	C(23)-C(24)	1.41(2)
C(24)-C(25)	1.34(2)	C(25)-C(26)	1.29(2)
C(25)-C(28)	1.58(2)	C(26)-C(27)	1.44(2)

Table 3.32. /continued

C(28)-C(29)	1.38(3)	P(2)-F(1)	1.604(8)
P(2)-F(2)	1.571(9)	P(2)-F(3)	1.573(9)
P(2)-F(4)	1.526(11)	P(2)-F(5)	1.552(8)
P(2)-F(6)	1.575(10)	Cl(1)-C(30)	1.772(0)
Cl(2)-C(30)	1.773(0)		

Table 3.33. Interatomic angles (°) for [Cu₂(μ-Ph₂Pbipy)₂(4-Etpy)₂](PF₆)₂.CH₂Cl₂

P(1)-Cu-N(3)	115.6(2)	Cu-P(1)-C(1)	106.9(3)
Cu-P(1)-C(7)	118.3(3)	C(1)-P(1)-C(7)	102.4(4)
Cu-P(1)-C(13)	121.1(3)	C(1)-P(1)-C(13)	102.2(4)
C(7)-P(1)-C(13)	103.2(4)	C(13)-N(1)-C(17)	119.3(7)
C(18)-N(2)-C(22)	120.3(9)	Cu-N(3)-C(23)	123.2(7)
Cu'-N(1)-C(13)	125.5(4)	Cu'-N(1)-C(17)	115.0(3)
Cu'-N(2)-C(18)	113.7(3)	Cu'-N(2)-C(22)	126.0(4)
Cu-N(3)-C(27)	119.2(9)	C(23)-N(3)-C(27)	117.3(10)
P(1)-C(1)-C(2)	123.7(7)	P(1)-C(1)-C(6)	117.8(7)
C(2)-C(1)-C(6)	118.4(9)	C(1)-C(2)-C(3)	122.4(9)
C(2)-C(3)-C(4)	118.5(11)	C(3)-C(4)-C(5)	119.8(12)
C(4)-C(5)-C(6)	120.3(12)	C(1)-C(6)-C(5)	120.6(11)
P(1)-C(7)-C(8)	123.3(7)	P(1)-C(7)-C(12)	117.3(7)
C(8)-C(7)-C(12)	119.4(8)	C(7)-C(8)-C(9)	120.8(10)
C(8)-C(9)-C(10)	117.8(11)	C(9)-C(10)-C(11)	122.1(11)
C(10)-C(11)-C(12)	119.8(11)	C(7)-C(12)-C(11)	120.0(10)
P(1)-C(13)-N(1)	116.5(6)	P(1)-C(13)-C(14)	123.2(7)
N(1)-C(13)-C(14)	120.2(8)	C(13)-C(14)-C(15)	120.6(9)
C(14)-C(15)-C(16)	120.3(10)	C(15)-C(16)-C(17)	116.8(10)

Table 3.33. /continued

N(1)-C(17)-C(16)	122.7(9)	N(1)-C(17)-C(18)	115.8(8)
C(16)-C(17)-C(18)	121.4(9)	N(2)-C(18)-C(17)	116.9(8)
N(2)-C(18)-C(19)	120.8(9)	C(17)-C(18)-C(19)	122.1(9)
C(18)-C(19)-C(20)	121.4(11)	C(19)-C(20)-C(21)	115.4(13)
C(20)-C(21)-C(22)	121.0(12)	N(2)-C(22)-C(21)	120.9(10)
N(3)-C(23)-C(24)	122.4(11)	C(23)-C(24)-C(25)	119.3(13)
C(24)-C(25)-C(26)	118.0(14)	C(24)-C(25)-C(28)	119.2(14)
C(26)-C(25)-C(28)	123(2)	C(25)-C(26)-C(27)	121(2)
N(3)-C(27)-C(26)	121.5(14)	C(25)-C(28)-C(29)	112(2)
F(1)-P(2)-F(2)	91.4(5)	F(1)-P(2)-F(3)	89.5(5)
F(2)-P(2)-F(3)	177.0(7)	F(1)-P(2)-F(4)	93.8(8)
F(2)-P(2)-F(4)	94.7(8)	F(3)-P(2)-F(4)	88.1(7)
F(1)-P(2)-F(5)	179.0(7)	F(2)-P(2)-F(5)	89.1(6)
F(3)-P(2)-F(5)	90.0(5)	F(4)-P(2)-F(5)	87.0(8)
F(1)-P(2)-F(6)	89.4(7)	F(2)-P(2)-F(6)	89.5(7)
F(3)-P(2)-F(6)	87.7(7)	F(4)-P(2)-F(6)	174.6(7)
F(5)-P(2)-F(6)	89.7(7)	Cl(1)-C(30)-Cl(2)	109.8(0)

Table 3.34. Crystal data for $[Cu_2(\mu\text{-}Ph_2Pbipy)_2(\eta\text{-}bipy)](PF_6)_2$

Formula	$Cu_2C_{54}H_{42}N_6P_4F_{12}$
Molecular mass	1253.94
Crystal system	monoclinic
Space group	C2
a (Å)	22.2116
b (Å)	19.3331
c (Å)	13.7165
β (°)	100
V (Å³)	5800
Z	4
D_c (g cm^{-3})	1.4
F (000)	2380
μ (cm^{-1})	9
Absorption corrections	Semi Empirical[87]
Measured intensities	4358
Unique intensities	3888
Unique intensities with $[F_o > 3\sigma (F_o)]$	2948
$\Delta\rho_{max}$ (eÅ^{-3})	1.130
Maximum least squares shift to error ratio	0.161
Weighting scheme parameter g in $w = 1/[\sigma^2(F) + g (F^2)]$	0.018
$R = \Sigma (F_o - F_c) / \Sigma F_o$	0.1075
$R_w = \Sigma_w \frac{1}{2} (F_o - F_c) / \Sigma F_w \frac{1}{2} F_o$	0.1146
Scan Mode	$\omega - 2\theta$
ω scan angle	$0.60 + 0.34\tan\theta$
Horizontal Aperture Width (mm)	$2.70 + 0.40\tan\theta$
Scattering Range	$3 \le \theta \le 23$
Number of parameters	313

Table 3.35. Fractional Coordinates (x10^4) and Isotropic Thermal Factors (Å^2 , x10^3) for [Cu$_2$(μ-Ph$_2$Pbipy)$_2$(η-bipy)](PF$_6$)$_2$

	x/a	y/b	z/c	U$_{eq}$
Cu(1)	2738(1)	-2562(1)	5228(2)	43(1)
Cu(2)	2256(1)	-2765(2)	2535(2)	56(1)
P (1)	1812(2)	-2164(3)	4570(4)	46(1)
P (2)	3198(2)	-3392(3)	4491(4)	43(1)
N (1)	1535(8)	-3068(9)	3069(12)	49(4)*
N (2)	1941(10)	-3521(12)	1470(16)	72(6)*
N (3)	2358(12)	-1956(15)	1524(19)	91(7)*
N (4)	3167(7)	-2583(10)	2889(11)	46(4)*
N(5)	2849(10)	-2694(12)	6717(15)	74(5)*
N (6)	3449(7)	-1825(8)	5720(11)	41(4)*
C (1)	1351(10)	-1869(11)	5418(16)	62(6)*
C (2)	1639(10)	-1556(11)	6294(16)	211(29)*
C (3)	1297(10)	-1168(11)	6859(16)	182(22)*
C (4)	668(10)	-1091(11)	6548(16)	145(16)*
C (5)	381(10)	-1404(11)	5673(16)	153(16)*
C (6)	723(10)	-1792(11)	5108(16)	136(14)*
C (7)	1712(8)	-1434(9)	3682(13)	64(6)*
C (8)	1166(8)	-1350(9)	3014(13)	109(11)*

Table 3.35. /continued

	x/a	y/b	z/c	$\underline{U}_{eq}$
C (9)	1099(8)	-796(9)	2351(13)	107(11)*
C (10)	1577(8)	-327(9)	2357(13)	116(11)*
C (11)	2122(8)	-412(9)	3025(13)	115(11)*
C (12)	2190(8)	-965(9)	3688(13)	74(7)*
C (13)	1345(9)	-2886(11)	3933(14)	46(4)*
C (14)	905(15)	-3177(18)	4332(25)	94(9)*
C (15)	616(17)	-3776(22)	3830(29)	109(11)*
C (16)	693(15)	-3940(19)	2952(25)	95(9)*
C (17)	1210(11)	-3603(13)	2568(18)	62(6)*
C (18)	1401(11)	-3801(13)	1682(18)	63(6)*
C (19)	1044(17)	-4281(22)	1073(29)	113(11)*
C (20)	1370(19)	-4455(23)	103(30)	117(12)*
C (21)	1843(16)	-4183(19)	-1(26)	98(9)*
C (22)	2170(13)	-3710(16)	728(22)	79(7)*
C (23)	1943(17)	-1666(21)	832(29)	105(10)*
C (24)	2110(19)	-1094(23)	231(31)	117(12)*
C (25)	2595(19)	-928(23)	300(28)	114(12)*
C (26)	3113(16)	-1337(21)	929(26)	101(10)*

Table 3.35. /continued

	x/a	y/b	z/c	$\underline{U}_{eq}$
C (27)	2967(12)	-1780(14)	1579(19)	68(6)*
C (28)	3387(9)	-2131(12)	2308(15)	51(5)*
C (29)	3995(12)	-1994(14)	2317(20)	72(7)*
C (30)	4391(14)	-2381(17)	3062(23)	93(9)*
C (31)	4189(12)	-2836(15)	3711(19)	73(7)*
C (32)	3559(9)	-2903(11)	3611(15)	47(5)*
C (33)	2512(17)	-3079(22)	7154(28)	106(11)*
C (34)	2481(40)	-3004(59)	8229(74)	253(35)*
C (35)	2783(41)	-2444(56)	8930(69)	246(34)*
C (36)	3330(20)	-2232(26)	8295(33)	131(14)*
C (37)	3265(14)	-2254(18)	7253(23)	87(8)*
C (38)	3609(9)	-1820(12)	6690(16)	51(5)*
C (39)	4101(12)	-1402(14)	7179(19)	68(6)*
C (40)	4384(12)	-1002(15)	6603(21)	73(7)*
C (41)	4223(10)	-1016(12)	5543(18)	58(5)*
C (42)	3737(9)	-1437(11)	5134(15)	47(5)*
C (43)	2811(7)	-4093(7)	3783(10)	49(5)*
C (44)	2340(7)	-4435(7)	4138(10)	66(6)*
C (45)	2056(7)	-5005(7)	3629(10)	89(8)*

Table 3.35. /continued

	x/a	y/b	z/c	$\underline{U}_{eq}$
C (46)	2244(7)	-5234(7)	2765(10)	110(10)*
C (47)	2715(7)	-4892(7)	2410(10)	98(9)*
C (48)	2999(7)	-4322(7)	2920(10)	57(5)*
C (49)	3816(8)	-3837(11)	5280(12)	54(5)*
C (50)	4107(8)	-3486(11)	6121(12)	91(9)*
C (51)	4531(8)	-3831(11)	6825(12)	96(9)*
C (52)	4664(8)	-4526(11)	6688(12)	136(14)*
C (53)	4373(8)	-4876(11)	5848(12)	223(31)*
C (54)	3949(8)	-4532(11)	5143(12)	206(27)*
P (3)	3897(3)	317(3)	3131(5)	60(2)*
F (1)	3718(11) .	-435(15)	3284(19)	140(8)*
F (2)	3270(10)	401(13)	2331(16)	125(7)*
F (3)	3548(12)	418(15)	4026(20)	149(8)*
F (4)	4476(9)	180(11)	3919(14)	108(6)*
F (5)	4317(12)	257(16)	2363(20)	149(9)*
F (6)	4015(12)	1151(17)	3122(21)	159(10)*
P (4)	5000	-1050(6)	0	73(3)
F (7)	4280(9)	-1038(11)	-357(14)	107(6)*
F (8)	4972(11)	-1637(13)	753(18)	129(7)*

Table 3.35. /continued

	x/a	y/b	z/c	$\underline{U}_{eq}$
F (9)	4969(14)	-514(18)	802(24)	167(10)*
P (5)	851(8)	405(11)	9348(13)	96(5)*
F (10)	1500(22)	399(27)	9779(34)	131(14)*
F (11)	934(27)	1111(38)	9077(46)	174(21)*
F (12)	984(26)	78(34)	8390(43)	160(19)*
F (13)	172(20)	391(24)	8975(32)	121(13)*
F (14)	762(25)	613(32)	10420(42)	155(19)*
F (15)	865(23)	-304(31)	9893(40)	148(17)*

Table 3.36. Anisotropic Thermal Factors ($\overset{\circ}{A}{}^{2}$, x10^{3}) for [Cu$_{2}$(μ-Ph$_{2}$Pbipy)$_{2}$(η-bipy)](PF$_{6}$)$_{2}$

	U (11)	U (22)	U (33)	U (23)	U (13)	U (12)
Cu(1)	49(1)	36(1)	44(1)	-6(1)	9(1)	-9(1)
Cu(2)	51(1)	60(2)	60(2)	6(1)	14(1)	-20(1)
P (1)	49(3)	37(3)	54(3)	-2(2)	16(2)	-4(2)
P (2)	42(3)	43(3)	46(3)	-3(2)	9(2)	-5(2)
P (3)	59(3)	57(4)	65(4)	13(3)	14(3)	5(3)
P (4)	56(5)	121(11)	43(6)	-16(18)	12(5)	-42(20)
P (5)	90(11)	109(13)	85(11)	-15(10)	6(9)	27(10)

Table 3.37. Interatomic distances (Å) for [Cu$_2$(μ-Ph$_2$Pbipy)$_2$(η-bipy)](PF$_6$)$_2$

Cu(1)-P(1)	2.234(6)	Cu(1)-P(2)	2.237(6)
Cu(1)-N(5)	2.03(2)	Cu(1)-N(6)	2.140(2)
Cu(2)-N(1)	1.96(2)	Cu(2)-N(2)	2.100(2)
Cu(2)-N(3)	2.13(2)	Cu(2)-N(4)	2.029(15)
P(1)-C(1)	1.77(2)	P(1)-C(7)	1.852(15)
P(1)-C(13)	1.86(2)	P(2)-C(32)	1.83(2)
P(2)-C(43)	1.796(12)	P(2)-C(49)	1.81(2)
N(1)-C(13)	1.37(3)	N(1)-C(17)	1.37(3)
N(2)-C(18)	1.39(3)	N(2)-C(22)	1.27(3)
N(3)-C(23)	1.33(4)	N(3)-C(27)	1.38(4)
N(4)-C(28)	1.33(3)	N(4)-C(32)	1.35(3)
N(5)-C(33)	1.28(4)	N(5)-C(37)	1.37(4)
N(6)-C(38)	1.32(3)	N(6)-C(42)	1.34(3)
C(1)-C(2)	1.395(0)	C(1)-C(6)	1.395(0)
C(2)-C(3)	1.395(0)	C(3)-C(4)	1.395(0)
C(4)-C(5)	1.395(0)	C(5)-C(6)	1.395(0)
C(7)-C(8)	1.395(0)	C(7)-C(12)	1.395(0)
C(8)-C(9)	1.395(0)	C(9)-C(10)	1.395(0)
C(10)-C(11)	1.395(0)	C(11)-C(12)	1.395(0)

Table 3.37. /continued

C(13)-C(14)	1.33(4)	C(14)-C(15)	1.44(5)
C(15)-C(16)	1.28(4)	C(16)-C(17)	1.49(4)
C(17)-C(18)	1.41(3)	C(18)-C(19)	1.40(5)
C(19)-C(20)	1.66(5)	C(20)-C(21)	1.21(5)
C(21)-C(22)	1.45(5)	C(23)-C(24)	1.47(5)
C(24)-C(25)	1.11(5)	C(25)-C(26)	1.53(5)
C(26)-C(27)	1.32(4)	C(27)-C(28)	1.41(3)
C(28)-C(29)	1.37(3)	C(29)-C(30)	1.44(4)
C(30)-C(31)	1.38(4)	C(31)-C(32)	1.39(3)
C(33)-C(34)	1.50(9)	C(34)-C(35)	1.52(12)
C(35)-C(36)	1.66(9)	C(36)-C(37)	1.41(5)
C(37)-C(38)	1.45(4)	C(38)-C(39)	1.43(3)
C(39)-C(40)	1.34(4)	C(40)-C(41)	1.43(4)
C(41)-C(42)	1.39(3)	C(43)-C(44)	1.395(0)
C(43)-C(48)	1.395(0)	C(44)-C(45)	1.395(0)
C(45)-C(46)	1.395(0)	C(46)-C(47)	1.395(0)
C(47)-C(48)	1.395(0)	C(49)-C(50)	1.395(0)
C(49)-C(54)	1.395(0)	C(50)-C(51)	1.395(0)
C(51)-C(52)	1.395(0)	C(52)-C(53)	1.395(0)

Table 3.37. /continued

C(53)-C(54)	1.395(0)	P(3)-F(1)	1.53(3)
P(3)-F(2)	1.62(2)	P(3)-F(3)	1.57(3)
P(3)-F(4)	1.55(2)	P(3)-F(5)	1.53(3)
P(3)-F(6)	1.63(3)	P(4)-F(7)	1.59(2)
P(4)-F(8)	1.54(3)	P(4)-F(9)	1.52(3)
P(5)-F(10)	1.46(5)	P(5)-F(11)	1.43(7)
P(5)-F(12)	1.53(6)	P(5)-F(13)	1.51(5)
P(5)-F(14)	1.57(6)	P(5)-F(15)	1.56(6)

Table 3.38. Interatomic angles (°) for $[Cu_2(\mu\text{-}Ph_2Pbipy)_2(\eta\text{-}bipy)](PF_6)_2$ -

P(1)-Cu(1)-P(2)	121.7(2)	P(1)-Cu(1)-N(5)	i13.0(6)
P(2)-Cu(1)-N(5)	112.3(6)	P(1)-Cu(1)-N(6)	118.3(5)
P(2)-Cu(1)-N(6)	104.5(5)	N(5)-Cu(1)-N(6)	79.3(7)
N(1)-Cu(2)-N(2)	81.9(8)	N(1)-Cu(2)-N(3)	130.5(9)
N(2)-Cu(2)-N(3)	96.8(9)	N(1)-Cu(2)-N(4)	143.8(7)
N(2)-Cu(2)-N(4)	119.0(8)	N(3)-Cu(2)-N(4)	79.2(9)
Cu(1)-P(1)-C(1)	116.3(8)	Cu(1)-P(1)-C(7)	121.7(6)
C(1)-P(1)-C(7)	99.7(10)	Cu(1)-P(1)-C(13)	109.3(7)
C(1)-P(1)-C(13)	102.2(10)	C(7)-P(1)-C(13)	105.6(9)
Cu(1)-P(2)-C(32)	102.4(7)	Cu(1)-P(2)-C(43)	124.9(5)
C(32)-P(2)-C(43)	104.9(8)	Cu(1)-P(2)-C(49)	115.4(6)
C(32)-P(2)-C(49)	105.5(9)	C(43)-P(2)-C(49)	101.9(9)
Cu(2)-N(1)-C(13)	129.8(14)	Cu(2)-N(1)-C(17)	115.4(14)
C(13)-N(1)-C(17)	114.0(2)	Cu(2)-N(2)-C(18)	109.0(2)
Cu(2)-N(2)-C(22)	129.0(2)	C(18)-N(2)-C(22)	123.0(2)
Cu(2)-N(3)-C(23)	130.0(2)	Cu(2)-N(3)-C(27)	111.0(2)
C(23)-N(3)-C(27)	119.0(3)	Cu(2)-N(4)-C(28)	115.1(13)
Cu(2)-N(4)-C(32)	125.8(13)	C(28)-N(4)-C(32)	119.0(2)
Cu(1)-N(5)-C(33)	125.0(2)	Cu(1)-N(5)-C(37)	114.0(2)

Table 3.38. /continued

C(33)-N(5)-C(37)	120.0(3)	Cu(1)-N(6)-C(38)	112.2(13)
Cu(1)-N(6)-C(42)	125.8(13)	C(38)-N(6)-C(42)	122.0(2)
P(1)-C(1)-C(2)	118.3(8)	P(1)-C(1)-C(6)	119.7(8)
C(2)-C(1)-C(6)	120.0(0)	C(1)-C(2)-C(3)	120.0(0)
C(2)-C(3)-C(4)	120.0(0)	C(3)-C(4)-C(5)	120.0(0)
C(4)-C(5)-C(6)	120.0(0)	C(1)-C(6)-C(5)	120.0(0)
P(1)-C(7)-C(8)	120.8(6)	P(1)-C(7)-C(12)	119.2(6)
C(8)-C(7)-C(12)	120.0(0)	C(7)-C(8)-C(9)	120.0(0)
C(8)-C(9)-C(10)	120.0(0)	C(9)-C(10)-C(11)	120.0(0)
C(10)-C(11)-C(12)	120.0(0)	C(7)-C(12)-C(11)	120.0(0)
P(1)-C(13)-N(1)	111.6(13)	P(1)-C(13)-C(14)	121.0(2)
N(1)-C(13)-C(14)	127.0(2)	C(13)-C(14)-C(15)	116.0(3)
C(14)-C(15)-C(16)	122.0(4)	C(15)-C(16)-C(17)	117.0(3)
N(1)-C(17)-C(16)	121.0(2)	N(1)-C(17)-C(18)	115.0(2)
C(16)-C(17)-C(18)	124.0(2)	N(2)-C(18)-C(17)	118.0(2)
N(2)-C(18)-C(19)	124.0(2)	C(17)-C(18)-C(19)	118.0(2)
C(18)-C(19)-C(20)	109.0(3)	C(19)-C(20)-C(21)	121.0(4)
C(20)-C(21)-C(22)	122.0(4)	N(2)-C(22)-C(21)	121.0(3)
N(3)-C(23)-C(24)	121.0(3)	C(23)-C(24)-C(25)	121.0(5)

Table 3.38. /continued

C(24)-C(25)-C(26)	121.0(5)	C(25)-C(26)-C(27)	118.0(3)
N(3)-C(27)-C(26)	118.0(3)	N(3)-C(27)-C(28)	116.0(2)
C(26)-C(27)-C(28)	126.0(3)	N(4)-C(28)-C(27)	118.0(2)
N(4)-C(28)-C(29)	126.0(2)	C(27)-C(28)-C(29)	116.0(2)
C(28)-C(29)-C(30)	113.0(2)	C(29)-C(30)-C(31)	124.0(3)
C(30)-C(31)-C(32)	115.0(2)	P(2)-C(32)-N(4)	115.0(13)
P(2)-C(32)-C(31)	122.0(2)	N(4)-C(32)-C(31)	123.0(2)
N(5)-C(33)-C(34)	123.0(5)	C(33)-C(34)-C(35)	127.0(8)
C(34)-C(35)-C(36)	97(7)	C(35)-C(36)-C(37)	125.0(5)
N(5)-C(37)-C(36)	120.0(3)	N(5)-C(37)-C(38)	116.0(2)
C(36)-C(37)-C(38)	124.0(3)	N(6)-C(38)-C(37)	117.0(2)
N(6)-C(38)-C(39)	122.0(2)	C(37)-C(38)-C(39)	121.0(2)
C(38)-C(39)-C(40)	117.0(2)	C(39)-C(40)-C(41)	122.0(3)
C(40)-C(41)-C(42)	117.0(2)	N(6)-C(42)-C(41)	120.0(2)
P(2)-C(43)-C(44)	119.1(4)	P(2)-C(43)-C(48)	120.8(4)
C(44)-C(43)-C(48)	120.0(0)	C(43)-C(44)-C(45)	120.0(0)
C(44)-C(45)-C(46)	120.0(0)	C(45)-C(46)-C(47)	120.0(0)
C(46)-C(47)-C(48)	120.0(0)	C(43)-C(48)-C(47)	120.0(0)
P(2)-C(49)-C(50)	117.2(6)	P(2)-C(49)-C(54)	122.2(6)

Table 3.38. /continued

C(50)-C(49)-C(54)	120.0(0)	C(49)-C(50)-C(51)	120.0(0)
C(50)-C(51)-C(52)	120.0(0)	C(51)-C(52)-C(53)	120.0(0)
C(52)-C(53)-C(54)	120.0(0)	C(49)-C(54)-C(53)	120.0(0)
F(1)-P(3)-F(2)	88.6(13)	F(1)-P(3)-F(3)	80.5(14)
F(2)-P(3)-F(3)	91.9(13)	F(1)-P(3)-F(4)	86.9(13)
F(2)-P(3)-F(4)	175.4(12)	F(3)-P(3)-F(4)	86.5(13)
F(1)-P(3)-F(5)	103(2)	F(2)-P(3)-F(5)	95.6(13)
F(3)-P(3)-F(5)	172(2)	F(4)-P(3)-F(5)	86.3(12)
F(1)-P(3)-F(6)	169.7(14)	F(2)-P(3)-F(6)	90.9(14)
F(3)-P(3)-F(6)	89.0(2)	F(4)-P(3)-F(6)	93.4(14)
F(5)-P(3)-F(6)	87.0(2)	F(7)-P(4)-F(8)	93.4(12)
F(7)-P(4)-F(9)	92.5(14)	F(8)-P(4)-F(9)	90.0(2)
F(7)-P(4)-F(7)	178.4(13)	F(8)-P(4)-F(8)	85.0(2)
F(9)-P(4)-F(9)	94.0(3)	F(10)-P(5)-F(11)	87.0(4)
F(10)-P(5)-F(12)	91.0(3)	F(11)-P(5)-F(12)	97.0(4)
F(10)-P(5)-F(13)	176.0(3)	F(11)-P(5)-F(13)	96.0(3)
F(12)-P(5)-F(13)	92.0(3)	F(10)-P(5)-F(14)	84.0(3)
F(11)-P(5)-F(14)	92.0(4)	F(12)-P(5)-F(14)	170.0(4)

Table 3.38 ./continued

F(13)-P(5)-F(14)	92.0(3)	F(10)-P(5)-F(15)	82.0(3)
F(11)-P(5)-F(15)	165.0(4)	F(12)-P(5)-F(15)	93.0(3)
F(13)-P(5)-F(15)	95.0(3)	F(14)-P(5)-F(15)	77.0(3)

Table 3.40. Crystal data for [Cu$_2$(μ-Ph$_2$Pbipy)$_2$(μ-I)](PF$_6$)

Formula	Cu$_2$C$_{44}$H$_{34}$N$_4$P$_3$F$_6$I
Molecular mass	1079.69
Crystal system	monoclinic
Space group	C2 / c
a (Å)	11.9460
b (Å)	15.3111
c (Å)	23.5780
β (°)	93
V (Å^3)	4306
Z	4
D_c (g cm^{-3})	1.67
F (000)	2144
μ (cm^{-1})	19
Absorption corrections	Semi Empirical[87]
Measured intensities	3214
Unique intensities	2858
Unique intensities with [$F_o > 3\sigma$ (F_o)]	2643
$\Delta\rho_{max}$ (eÅ^{-3})	0.707
Maximum least squares shift to error ratio	0.005
Weighting scheme parameter g in $w = 1/[\sigma^2(F) + g(F^2)]$	0.010
R = Σ ($F_o - F_c$) / ΣF_o	0.0485
R$_w$ = Σ_w ½ ($F_o - F_c$) / ΣF_w½F_o	0.0627
Scan Mode	ω - 2θ
ω scan angle	0.75 + 0.34tanθ
Horizontal Aperture Width (mm)	2.70 + 0.40tanθ
Scattering Range	3 $\leq \theta \leq$ 23
Number of parameters	273

Table 3.41. Fractional Coordinates (x10^4) and Isotropic Thermal Factors ($\mathring{A}^2$, x10^3) for

[Cu$_2$(μ-Ph$_2$Pbipy)$_2$(μ-I)](PF$_6$)

	x/a	y/b	z/c	$\underline{U}_{eq}$
I	0	-1366(1)	2500	57(1)
Cu	2(1)	105(1)	3088(1)	34(1)
P (1)	-1392(1)	1041(1)	1956(1)	33(1)
N (1)	-1650(3)	595(3)	3038(2)	30(1)
N (2)	-538(3)	-284(3)	3864(2)	36(1)
C (1)	-2530(4)	966(4)	1399(2)	39(1)
C (2)	-3133(5)	1682(4)	1194(3)	47(1)
C (3)	-3971(5)	1577(4)	772(3)	53(1)
C (4)	-4193(5)	787(5)	546(3)	59(2)
C (5)	-3603(5)	54(4)	740(3)	52(2)
C (6)	-2785(4)	143(4)	1168(2)	41(1)
C (7)	-969(4)	2181(4)	1883(2)	42(1)
C (8)	-1413(5)	2883(4)	2160(3)	52(1)
C (9)	-1086(6)	3727(5)	2036(4)	69(2)
C (10)	-335(7)	3874(5)	1645(4)	84(2)
C (11)	146(8)	3171(5)	1352(4)	83(2)
C (12)	-184(6)	2329(4)	1476(3)	61(2)
C (13)	-2168(4)	1015(3)	2611(2)	33(1)

Table 3.40. /continued

	x/a	y/b	z/c	$\underline{U}_{eq}$
C (14)	-3213(5)	1406(4)	2657(3)	48(1)
C (15)	-3694(5)	1364(4)	3166(3)	49(1)
C (16)	-3181(4)	934(4)	3613(2)	42(1)
C (17)	-2160(4)	518(3)	3540(2)	36(1)
C (18)	-1583(4)	-38(3)	3975(2)	35(1)
C (19)	-2090(5)	-319(5)	4444(3)	59(2)
C (20)	-1505(5)	-855(5)	4842(3)	57(2)
C (21)	-457(5)	-1114(4)	4734(3)	54(2)
C (22)	12(5)	-809(4)	4248(3)	51(1)
P (2)	2500	2500	0	42(1)
F (1)	2831(7)	2939(6)	582(3)	151(3)
F (2)	1809(5)	1843(5)	352(3)	132(2)
F (3)	3625(5)	1993(5)	119(3)	137(2)

* isotropic temperature factor

$$\underline{U}_{eq} = \frac{1}{3}\Sigma_i\Sigma_j\underline{U}_{ij}\underline{a}^*_i\underline{a}^*_j(a_i.a_j)$$

Table 3.41. Anisotropic Thermal Factors ($\mathring{A}^2$, x10^3) for [Cu$_2$(μ-Ph$_2$Pbipy)$_2$(μ-I)](PF$_6$)

	U (11)	U (22)	U (33)	U (23)	U (13)	U (12)
I	89(1)	30(1)	55(1)	0	16(1)	0
Cu	29(1)	37(1)	36(1)	2(1)	6(1)	-1(1)
P (1)	30(1)	40(1)	29(1)	5(1)	5(1)	5(1)
N (1)	26(2)	32(2)	32(2)	2(2)	8(2)	0(2)
N (2)	36(2)	37(2)	36(3)	4(2)	6(2)	5(2)
C (1)	36(3)	46(3)	35(3)	12(2)	7(2)	3(2)
C (2)	50(3)	45(3)	45(3)	5(3)	-5(3)	14(3)
C (3)	51(3)	51(4)	56(4)	2(3)	-7(3)	8(3)
C (4)	38(3)	89(5)	49(4)	10(3)	3(2)	-9(3)
C (5)	43(3)	56(4)	56(4)	9(3)	6(3)	-5(3)
C (6)	38(3)	49(3)	37(3)	0(2)	5(2)	-11(2)
C (7)	34(3)	53(3)	40(3)	4(3)	4(3)	6(2)
C (8)	54(3)	39(3)	62(4)	-5(3)	6(3)	-1(3)
C (9)	73(5)	61(5)	75(5)	13(4)	10(4)	-3(3)
C (10)	78(5)	46(4)	130(8)	15(5)	28(5)	-1(3)
C (11)	111(6)	46(4)	94(6)	20(4)	42(5)	2(4)
C (12)	61(4)	49(4)	77(5)	6(3)	26(3)	0(3)
C (13)	27(2)	38(3)	35(3)	4(2)	6(2)	5(2)

Table 3.41./continued

	U (11)	U (22)	U (33)	U (23)	U (13)	U (12)
C (14)	38(3)	59(4)	47(4)	5(3)	11(2)	11(2)
C (15)	35(3)	64(4)	47(4)	4(3)	9(2)	13(2)
C (16)	46(3)	51(4)	31(3)	5(2)	17(2)	13(2)
C (17)	33(3)	43(3)	35(3)	-5(2)	9(2)	0(2)
C (18)	39(3)	38(3)	29(3)	-5(2)	3(2)	0(2)
C (19)	59(4)	81(5)	39(4)	25(3)	22(3)	10(3)
C (20)	65(4)	65(4)	43(4)	18(3)	15(3)	13(3)
C (21)	65(4)	54(4)	43(4)	8(3)	3(3)	5(3)
C (22)	45(3)	60(4)	49(4)	12(3)	6(3)	17(3)
P (2)	37(1)	37(1)	51(1)	2(1)	-9(1)	-7(1)
F (1)	164(6)	180(7)	109(5)	-64(5)	-8(4)	-52(5)
F (2)	95(4)	165(6)	132(5)	73(5)	-31(5)	-56(4)
F (3)	79(3)	134(6)	194(7)	42(5)	-16(4)	30(3)

Table 3.42. Interatomic distances (Å) for $[Cu_2(\mu\text{-}Ph_2Pbipy)_2(\mu\text{-}I)](PF_6)$

I-Cu	2.644(1)	Cu-N(1)	2.109(4)
Cu-N(2)	2.060(4)	Cu-Cu'	2.770(1)
Cu-P(1)	2.200(3)	P(1)-C(1)	1.843(5)
P(1)-C(7)	1.827(6)	P(1)-C(13)	1.844(5)
N(1)-C(13)	1.319(6)	N(1)-C(17)	1.365(7)
N(2)-C(18)	1.343(7)	N(2)-C(22)	1.355(7)
C(1)-C(2)	1.386(8)	C(1)-C(6)	1.399(8)
C(2)-C(3)	1.384(9)	C(3)-C(4)	1.342(10)
C(4)-C(5)	1.390(10)	C(5)-C(6)	1.374(8)
C(7)-C(8)	1.380(8)	C(7)-C(12)	1.394(8)
C(8)-C(9)	1.386(10)	C(9)-C(10)	1.339(11)
C(10)-C(11)	1.417(12)	C(11)-C(12)	1.384(10)
C(13)-C(14)	1.394(7)	C(14)-C(15)	1.359(9)
C(15)-C(16)	1.361(8)	C(16)-C(17)	1.394(7)
C(17)-C(18)	1.476(7)	C(18)-C(19)	1.359(8)
C(19)-C(20)	1.405(9)	C(20)-C(21)	1.350(9)
C(21)-C(22)	1.382(9)	P(2)-F(1)	1.560(6)
P(2)-F(2)	1.566(5)	P(2)-F(3)	1.564(5)

Table 3.43. Interatomic angles (°) for [Cu₂(μ-Ph₂Pbipy)₂(μ-I)](PF₆)

I-Cu-N(1)	107.4(1)	I-Cu-N(2)	103.1(1)
N(1)-Cu-N(2)	79.4(2)	Cu-I-Cu'	63.2(0)
Cu'-P(1)-C(13)	116.1(3)	C(1)-P(1)-C(7)	100.9(2)
C(1)-P(1)-C(13)	102.2(2)	C(7)-P(1)-C(13)	104.8(3)
Cu-N(1)-C(13)	127.9(3)	Cu-N(1)-C(17)	112.4(3)
C(13)-N(1)-C(17)	119.3(4)	Cu-N(2)-C(18)	115.5(3)
Cu-N(2)-C(22)	127.1(4)	C(18)-N(2)-C(22)	117.2(5)
P(1)-C(1)-C(2)	123.3(5)	P(1)-C(1)-C(6)	118.1(4)
C(2)-C(1)-C(6)	118.6(5)	C(1)-C(2)-C(3)	120.1(6)
C(2)-C(3)-C(4)	120.7(6)	C(3)-C(4)-C(5)	120.8(6)
C(4)-C(5)-C(6)	119.3(6)	C(1)-C(6)-C(5)	120.5(5)
P(1)-C(7)-C(8)	125.7(4)	P(1)-C(7)-C(12)	114.9(5)
C(8)-C(7)-C(12)	119.2(6)	C(7)-C(8)-C(9)	120.4(6)
C(8)-C(9)-C(10)	120.6(7)	C(9)-C(10)-C(11)	120.8(7)
C(10)-C(11)-C(12)	118.4(7)	C(7)-C(12)-C(11)	120.5(7)
P(1)-C(13)-N(1)	114.4(3)	P(1)-C(13)-C(14)	123.2(4)
N(1)-C(13)-C(14)	122.4(5)	C(13)-C(14)-C(15)	118.0(5)
C(14)-C(15)-C(16)	120.9(5)	C(15)-C(16)-C(17)	119.0(5)

Table 3.43. /continued

N(1)-C(17)-C(16)	120.2(5)	N(1)-C(17)-C(18)	116.0(4)
C(16)-C(17)-C(18)	123.8(5)	N(2)-C(18)-C(17)	115.5(5)
N(2)-C(18)-C(19)	122.0(5)	C(17)-C(18)-C(19)	122.5(5)
C(18)-C(19)-C(20)	120.1(6)	C(19)-C(20)-C(21)	118.6(6)
C(20)-C(21)-C(22)	118.6(6)	N(2)-C(22)-C(21)	123.5(5)
F(1)-P(2)-F(2)	85.8(4)	F(1)-P(2)-F(3)	83.2(5)
F(2)-P(2)-F(3)	93.4(4)	F(1)-P(2)-F(1)	180.0(0)
F(2)-P(2)-F(2)	180.0(0)	F(3)-P(2)-F(3)	180.0(0)

Table 3.44. Crystal data for [Cu$_2$(μ-Ph$_2$Pbipy)$_2$(μ-Br)](PF$_6$)

Formula	Cu$_2$C$_{44}$H$_{34}$N$_4$P$_3$F$_6$Br
Molecular mass	1032.69
Crystal system	monoclinic
Space group	C2 / c
a (Å)	11.9146
b (Å)	15.1717
c (Å)	23.9278
β (°)	93
V (Å^3)	4318
Z	4
D_c (g cm^{-3})	1.59
F (000)	2072
μ (cm^{-1})	22
Absorption corrections	Semi Empirical[87]
Measured intensities	6413
Unique intensities	3653
Unique intensities with [$F_o > 3\sigma$ (F_o)]	2263
$\Delta\rho_{max}$ (eÅ^{-3})	2.903
Maximum least squares shift to error ratio	0.060
Weighting scheme parameter g in $w = 1/[\sigma^2(F) + g\,(F^2)]$	0.078
$R = \Sigma\,(\,F_o - F_c\,)\,/\,\Sigma\,F_o$	0.1821
$R_w = \Sigma_w\,\frac{1}{2}\,(\,F_o - F_c\,)\,/\,\Sigma\,F_w\frac{1}{2}F_o$	0.1877
Scan Mode	$\omega - 2\theta$
ω scan angle	0.48 + 0.34tanθ
Horizontal Aperture Width (mm)	2.70 + 0.40tanθ
Scattering Range	$3 \leq \theta \leq 23$
Number of parameters	138

Table 3.45. Fractional Coordinates ($x10^4$) and Isotropic Thermal Factors ($Å^2$, $x10^3$) For [$Cu_2(\mu$-$Ph_2Pbipy)_2(\mu$-$Br)$](PF_6)

	x/a	y/b	z/c	$\underline{U}_{eq}$
Br	0	6279(2)	2500	87(1)
Cu	8(2)	4899(2)	1923(1)	7(1)
P (1)	-1389(4)	3958(3)	1949(2)	7(1)
N (1)	1641(11)	4407(9)	1968(6)	0(3)*
N (2)	545(12)	5285(11)	1186(7)	9(3)*
C (1)	-965(17)	2780(13)	1881(9)	14(4)*
C (2)	-1387(18)	2123(16)	2149(10)	23(5)*
C (3)	-1146(26)	1249(21)	1990(14)	51(8)*
C (4)	-297(26)	1139(21)	1603(14)	49(8)*
C (5)	143(24)	1772(19)	1367(13)	41(7)*
C (6)	-186(20)	2655(16)	1473(10)	25(5)*
C (7)	-2504(15)	4029(12)	1407(8)	8(4)*
C (8)	-2782(16)	4851(13)	1169(9)	12(4)*
C (9)	-3616(21)	4999(16)	734(11)	27(6)*
C (10)	-4142(21)	4193(18)	538(11)	31(6)*
C (11)	-3939(18)	3394(16)	758(10)	22(5)*
C (12)	-3045(20)	3265(16)	1168(10)	28(5)*
C (13)	2186(14)	3912(12)	2425(8)	5(4)*

Table 3.45. /continued

	x/a	y/b	z/c	$\underline{U}_{eq}$
C (14)	3175(18)	3561(15)	2352(10)	23(5)*
C (15)	3667(19)	3521(16)	1843(11)	27(5)*
C (16)	3184(17)	4030(14)	1419(9)	18(5)*
C (17)	2198(16)	4453(13)	1490(8)	14(4)*
C (18)	1628(16)	5038(13)	1045(9)	10(4)*
C (19)	2118(20)	5274(17)	560(11)	27(5)*
C (20)	1595(18)	5789(15)	165(9)	21(5)*
C (21)	435(19)	6074(15)	292(10)	22(5)*
C (22)	-44(19)	5793(15)	770(10)	23(5)*
P (2)	2500	2500	0	70(2)
F (1)	3651(19)	3014(16)	118(10)	77(6)*
F (2)	2781(19)	2013(15)	563(9)	75(6)*
F (3)	1762(19)	3195(15)	326(10)	75(6)*

* isotropic temperature factor

$$\underline{U}_{eq} = \tfrac{1}{3}\Sigma_i\Sigma_j\underline{U}_{ij}\underline{a}^*_i\underline{a}^*_j(a_i.a_j)$$

Table 3.46. Anisotropic Thermal Factors ($\mathring{A}2$, x103) for [Cu$_2$(μ-Ph$_2$Pbipy)$_2$(μ-Br)](PF$_6$)

	U (11)	U (22)	U (33)	U (23)	U (13)	U (12)
Br	131(3)	57(2)	73(2)	0	18(2)	0
Cu	4(1)	11(2)	7(2)	1(1)	3(1)	0(1)
P (1)	4(2)	15(3)	3(2)	-4(2)	1(2)	-3(2)
P (2)	65(4)	63(5)	80(5)	-5(4)	-13(4)	-1(4)

Table 3.47. Interatomic distances (Å) for [Cu₂(μ-Ph₂Pbipy)₂(μ-Br)](PF₆)

Cu-Br	2.507(3)	Cu-P(1)'	2.197(5)
Cu-Cu'	2.762(4)	Cu-N(1)	2.082(14)
Cu-N(2)	2.00(2)	P(1)-C(1)	1.87(2)
P(1)-C(7)	1.81(2)	N(1)-C(13)	1.45(2)
N(1)-C(17)	1.36(2)	N(2)-C(18)	1.40(3)
N(2)-C(22)	1.41(3)	C(1)-C(2)	1.30(3)
C(1)-C(6)	1.40(3)	C(2)-C(3)	1.41(4)
C(3)-C(4)	1.42(4)	C(4)-C(5)	1.25(4)
C(5)-C(6)	1.42(3)	C(7)-C(8)	1.40(3)
C(7)-C(12)	1.43(3)	C(8)-C(9)	1.42(3)
C(9)-C(10)	1.44(4)	C(10)-C(11)	1.34(4)
C(11)-C(12)	1.42(3)	C(13)-C(14)	1.31(3)
C(14)-C(15)	1.38(4)	C(15)-C(16)	1.38(3)
C(16)-C(17)	1.36(3)	C(17)-C(18)	1.52(3)
C(18)-C(19)	1.38(3)	C(19)-C(20)	1.35(4)
C(20)-C(21)	1.50(3)	C(21)-C(22)	1.37(3)
P(2)-F(1)	1.59(2)	P(2)-F(2)	1.56(2)
P(2)-F(3)	1.60(2)		

Table 3.48. Interatomic angles (°) for [Cu$_2$(μ-Ph$_2$Pbipy)$_2$(μ-Br)](PF$_6$)

Br-Cu-P(1)'	120.1(2)	Br-Cu-N(1)	107.6(4)
P(1)'-Cu-N(1)	118.2(4)	Br-Cu-N(2)	104.6(5)
P(1)'-Cu-N(2)	119.7(5)	N(1)-Cu-N(2)	78.8(6)
Cu-Br-Cu'	66.8(1)	Cu'-P(1)-C(1)	114.3(6)
Cu'-P(1)-C(7)	117.9(7)	C(1)-P(1)-C(7)	100.7(9)
Cu-N(1)-C(13)	127.1(11)	Cu-N(1)-C(17)	115.9(11)
C(13)-N(1)-C(17)	116.3(14)	Cu-N(2)-C(18)	118.6(13)
Cu-N(2)-C(22)	127.6(13)	C(18)-N(2)-C(22)	114(2)
P(1)-C(1)-C(2)	125(2)	P(1)-C(1)-C(6)	113(2)
C(2)-C(1)-C(6)	122(2)	C(1)-C(2)-C(3)	120(2)
C(2)-C(3)-C(4)	117(2)	C(3)-C(4)-C(5)	123(2)
C(4)-C(5)-C(6)	121(3)	C(1)-C(6)-C(5)	117(2)
P(1)-C(7)-C(8)	119.4(14)	P(1)-C(7)-C(12)	122(2)
C(8)-C(7)-C(12)	118(2)	C(7)-C(8)-C(9)	125(2)
C(8)-C(9)-C(10)	112(2)	C(9)-C(10)-C(11)	125(2)
C(10)-C(11)-C(12)	121(2)	C(7)-C(12)-C(11)	118(2)
N(1)-C(13)-C(14)	119(2)	C(13)-C(14)-C(15)	124(2)
C(14)-C(15)-C(16)	116(2)	C(15)-C(16)-C(17)	120(2)

Table 3.48. /continued

N(1)-C(17)-C(16)	123(2)	N(1)-C(17)-C(18)	114(2)
C(16)-C(17)-C(18)	123(2)	N(2)-C(18)-C(17)	112(2)
N(2)-C(18)-C(19)	125(2)	C(17)-C(18)-C(19)	123(2)
C(18)-C(19)-C(20)	123(2)	C(19)-C(20)-C(21)	115(2)
C(20)-C(21)-C(22)	121(2)	N(2)-C(22)-C(21)	123(2)
F(1)-P(2)-F(2)	86.4(12)	F(1)-P(2)-F(3)	94.7(12)
F(2)-P(2)-F(3)	89.4(12)	F(1)-P(2)-F(1)	180.0(0)
F(2)-P(2)-F(2)	180.0(0)	F(3)-P(2)-F(3)	180.0(0)

Table 3.49. Crystal data for [Cu$_2$(μ-Ph$_2$Pbipy)$_2$(μ-SEt)](PF$_6$)

Formula	Cu$_2$C$_{46}$H$_{39}$N$_4$P$_3$F$_6$S
Molecular mass	1013.91
Crystal system	monoclinic
Space group	P2$_1$ / c
a (Å)	11.7884
b (Å)	15.6727
c (Å)	23.7853
β (°)	94
V (Å^3)	4382
Z	4
D_c (g cm^{-3})	1.54
F (000)	2064
μ (cm^{-1})	12
Absorption corrections	Semi Empirical[87]
Measured intensities	6510
Unique intensities	3958
Unique intensities with [$F_o > 3\sigma$ (F_o)]	1783
$\Delta\rho_{max}$ (eÅ^{-3})	1.100
Maximum least squares shift to error ratio	-0.09
Weighting scheme parameter g in $w = 1/[\sigma^2(F) + g\,(F^2)]$	0.003
R = Σ (F_o - F_c) / Σ F_o	0.1287
R$_w$ = Σ_w ½ (F_o - F_c) / Σ F_w½F_o	0.1207
Scan Mode	ω - 2θ
ω scan angle	1.00 + 0.34tanθ
Horizontal Aperture Width (mm)	2.70 + 0.40tanθ
Scattering Range	3 $\leq$ θ $\leq$ 23
Number of parameters	216

Table 3.50. Fractional Coordinates (x10⁴) and Isotropic Thermal Factors (Å² , x10³) for [Cu₂(μ-Ph₂Pbipy)₂(μ-SEt)](PF₆)

	x/a	y/b	z/c	U$_{eq}$
Cu(1)	2334(3)	7339(3)	2087(2)	24(1)
Cu(2)	2310(3)	7513(3)	3214(2)	29(1)
S	1986(8)	8584(7)	2568(5)	35(3)
P (1)	1071(8)	6305(7)	2121(4)	27(3)
P (2)	3824(8)	6665(7)	3257(4)	27(3)
C (1)	-143(16)	6389(15)	1584(8)	27(10)*
C (2)	-370(16)	7212(15)	1382(8)	28(10)*
C (3)	-1242(16)	7348(15)	962(8)	49(12)*
C (4)	-1885(16)	6661(15)	743(8)	36(11)*
C (5)	-1657(16)	5838(15)	944(8)	26(10)*
C (6)	-786(16)	5702(15)	1365(8)	18(9)*
C (7)	1503(23)	5221(13)	1992(12)	47(13)*
C (8)	2295(23)	5147(13)	1588(12)	62(15)*
C (9)	2649(23)	4342(13)	1422(12)	50(13)*
C (10)	2211(23)	3611(13)	1661(12)	57(14)*
C (11)	1419(23)	3685(13)	2065(12)	61(14)*
C (12)	1065(23)	4490(13)	2231(12)	24(10)*
C (17)	116(18)	6944(12)	3627(8)	39(12)*

Table 3.50. /continued

	x/a	y/b	z/c	$\underline{U}_{eq}$
N (1)	715(18)	6831(12)	3178(8)	14(7)*
C (13)	280(18)	6320(12)	2768(8)	3(7)*
C (14)	-697(18)	5852(12)	2815(8)	35(11)*
C (15)	-1252(18)	5905(12)	3305(8)	29(10)*
C (16)	-789(18)	6425(12)	3733(8)	10(8)*
C (18)	657(19)	7561(15)	4064(10)	39(10)*
N (2)	1679(19)	7860(15)	3957(10)	29(8)*
C (19)	129(19)	7789(15)	4540(10)	51(13)*
C (20)	606(19)	8423(15)	4886(10)	62(15)*
C (21)	1671(19)	8724(15)	4777(10)	60(14)*
C (22)	2223(19)	8357(15)	4347(10)	45(12)*
C (23)	4943(15)	6676(15)	3832(8)	4(8)*
C (24)	5302(15)	7477(15)	4029(8)	33(9)*
C (25)	6177(15)	7543(15)	4455(8)	57(12)*
C (26)	6694(15)	6807(15)	4684(8)	43(12)*
C (27)	6335(15)	6006(15)	4487(8)	69(16)*
C (28)	5460(15)	5940(15)	4060(8)	21(9)*
C (29)	3440(22)	5542(13)	3263(11)	38(12)*

Table 3.50. /continued

	x/a	y/b	z/c	$\underline{U}_{eq}$
C (30)	3953(22)	4909(13)	2957(11)	34(11)*
C (31)	3657(22)	4055(13)	3025(11)	58(14)*
C (32)	2849(22)	3835(13)	3399(11)	42(12)*
C (33)	2337(22)	4468(13)	3706(11)	62(15)*
C (34)	2632(22)	5321(13)	3638(11)	34(11)*
C (39)	4600(18)	6997(15)	1685(7)	41(12)*
N (3)	4075(18)	7020(15)	2165(7)	15(7)*
C (35)	4670(18)	6789(15)	2639(7)	28(10)*
C (36)	5794(18)	6546(15)	2654(7)	37(11)*
C (37)	6352(18)	6576(15)	2163(7)	34(11)*
C (38)	5773(18)	6935(15)	1691(7)	33(11)*
C (40)	3981(17)	7535(16)	1210(9)	36(10)*
N (4)	2881(17)	7664(16)	1285(9)	31(8)*
C (41)	4425(17)	7678(16)	698(9)	50(12)*
C (42)	3779(17)	8117(16)	284(9)	48(13)*
C (43)	2700(17)	8374(16)	400(9)	68(15)*
C (44)	2284(17)	8143(16)	904(9)	32(11)*
C (45)	3337(37)	9173(28)	2526(20)	57(14)*
C (46)	3862(39)	9424(30)	3091(21)	62(15)*

Table 3.50. /continued

	x/a	y/b	z/c	$\underline{U}_{eq}$
P (3)	0	0	10000	46(5)
F (1)	9223(21)	498(19)	373(10)	77(9)
F (2)	9176(27)	190(21)	-527(12)	115(11)
F (3)	10606(37)	798(25)	-86(15)	169(16)
P (4)	5000	0	5000	55(6)
F (4)	5307(28)	619(28)	5465(18)	159(16)
F (5)	5284(71)	705(36)	4642(22)	252(30)
F (6)	3811(28)	258(34)	5011(26)	213(22)

* isotropic temperature factor

$$\underline{U}_{eq} = \tfrac{1}{3}\Sigma_i\Sigma_j\underline{U}_{ij}\underline{a}^*_i\underline{a}^*_j(a_i.a_j)$$

Table 3.51. Anisotropic Thermal Factors ($\AA^2$, x10³) for [Cu₂(μ-Ph₂Pbipy)₂(μ-SEt)](PF₆)

	U (11)	U (22)	U (33)	U (23)	U (13)	U (12)
Cu(1)	16(3)	36(4)	22(3)	-1(3)	10(2)	-7(3)
Cu(2)	30(3)	27(3)	33(3)	7(3)	20(2)	4(3)
S	26(6)	32(7)	50(8)	7(6)	19(6)	8(5)
P (1)	18(6)	53(8)	12(6)	10(6)	11(5)	8(5)
P (2)	11(5)	43(8)	27(7)	3(6)	6(5)	1(5)
P (3)	14(9)	71(15)	53(14)	-19(12)	21(9)	-8(9)
F (1)	67(19)	129(26)	39(17)	-42(18)	27(15)	11(18)
F (2)	135(29)	142(31)	58(22)	-78(23)	-58(21)	76(26)
F (3)	253(48)	149(37)	127(34)	-50(29)	168(35)	-91(36)
P (4)	36(12)	58(15)	72(16)	-15(15)	10(11)	-9(11)
F (4)	91(27)	201(45)	184(45)	-135(40)	6(27)	-1(27)
F (5)	461(108)	150(48)	152(49)	63(41)	80(54)	53(60)
F (6)	61(27)	225(53)	353(71)	-227(55)	13(36)	8(30)

Table 3.52. Interatomic distances (Å) for [Cu₂(μ-Ph₂Pbipy)₂(μ-SEt)](PF₆)

Cu(1)-Cu(2)	2.697(6)	Cu(1)-S	2.314(11)
Cu(1)-P(1)	2.207(12)	Cu(1)-N(3)	2.11(2)
Cu(1)-N(4)	2.12(2)	Cu(2)-S	2.289(12)
Cu(2)-P(2)	2.221(11)	Cu(2)-N(1)	2.16(2)
Cu(2)-N(2)	2.04(2)	S-C(45)	1.85(4)
P(1)-C(1)	1.85(2)	P(1)-C(7)	1.81(2)
P(1)-C(13)	1.86(2)	P(2)-C(23)	1.83(2)
P(2)-C(29)	1.82(2)	P(2)-C(35)	1.85(2)
C(1)-C(2)	1.395(0)	C(1)-C(6)	1.395(0)
C(2)-C(3)	1.395(0)	C(3)-C(4)	1.395(0)
C(4)-C(5)	1.395(0)	C(5)-C(6)	1.395(0)
C(7)-C(8)	1.395(0)	C(7)-C(12)	1.395(0)
C(8)-C(9)	1.395(0)	C(9)-C(10)	1.395(0)
C(10)-C(11)	1.395(0)	C(11)-C(12)	1.395(0)
C(17)-N(1)	1.336(0)	C(17)-C(16)	1.380(0)
C(17)-C(18)	1.52(2)	N(1)-C(13)	1.335(0)
C(13)-C(14)	1.377(0)	C(14)-C(15)	1.382(0)
C(15)-C(16)	1.383(0)	C(18)-N(2)	1.336(0)
C(18)-C(19)	1.378(0)	N(2)-C(22)	1.337(0)

Table 3.52. /continued

C(19)-C(20)	1.383(0)	C(20)-C(21)	1.384(0)
C(21)-C(22)	1.380(0)	C(23)-C(24)	1.395(0)
C(23)-C(28)	1.395(0)	C(24)-C(25)	1.395(0)
C(25)-C(26)	1.395(0)	C(26)-C(27)	1.395(0)
C(27)-C(28)	1.395(0)	C(29)-C(30)	1.395(0)
C(29)-C(34)	1.395(0)	C(30)-C(31)	1.395(0)
C(31)-C(32)	1.395(0)	C(32)-C(33)	1.395(0)
C(33)-C(34)	1.395(0)	C(39)-N(3)	1.338(0)
C(39)-C(38)	1.384(0)	C(39)-C(40)	1.55(2)
N(3)-C(35)	1.334(0)	C(35)-C(36)	1.377(0)
C(36)-C(37)	1.384(0)	C(37)-C(38)	1.388(0)
C(40)-N(4)	1.337(0)	C(40)-C(41)	1.379(0)
N(4)-C(44)	1.336(0)	C(41)-C(42)	1.383(0)
C(42)-C(43)	1.382(0)	C(43)-C(44)	1.377(0)
C(45)-C(46)	1.49(6)	P(3)-F(1)	1.53(2)
P(3)-F(2)	1.56(2)	P(3)-F(3)	1.46(3)
P(4)-F(4)	1.50(4)	P(4)-F(5)	1.45(5)
P(4)-F(6)	1.46(3)		

Table 3.53. Interatomic angles (°) for [Cu$_2$(μ-Ph$_2$Pbipy)$_2$(μ-SEt)](PF$_6$)

Cu(2)-Cu(1)-S	53.7(3)	Cu(2)-Cu(1)-P(1)	88.9(3)
S-Cu(1)-P(1)	117.1(4)	Cu(2)-Cu(1)-N(3)	91.2(5)
S-Cu(1)-N(3)	111.4(7)	P(1)-Cu(1)-N(3)	118.6(7)
Cu(2)-Cu(1)-N(4)	153.6(7)	S-Cu(1)-N(4)	108.6(8)
P(1)-Cu(1)-N(4)	117.5(7)	N(3)-Cu(1)-N(4)	77.0(7)
Cu(1)-Cu(2)-S	54.6(3)	Cu(1)-Cu(2)-P(2)	85.2(3)
S-Cu(2)-P(2)	124.2(4)	Cu(1)-Cu(2)-N(1)	89.1(5)
S-Cu(2)-N(1)	103.6(7)	P(2)-Cu(2)-N(1)	113.6(7)
Cu(1)-Cu(2)-N(2)	156.8(7)	S-Cu(2)-N(2)	109.5(8)
P(2)-Cu(2)-N(2)	117.6(8)	N(1)-Cu(2)-N(2)	78.1(7)
Cu(1)-S-Cu(2)	71.7(3)	Cu(1)-S-C(45)	102.0(14)
Cu(2)-S-C(45)	108(2)	Cu(1)-P(1)-C(1)	114.3(9)
Cu(1)-P(1)-C(7)	119.0(10)	C(1)-P(1)-C(7)	99.4(13)
Cu(1)-P(1)-C(13)	113.8(7)	C(1)-P(1)-C(13)	99.3(10)
C(7)-P(1)-C(13)	108.6(12)	Cu(2)-P(2)-C(23)	124.2(9)
Cu(2)-P(2)-C(29)	112.4(10)	C(23)-P(2)-C(29)	99.7(13)
Cu(2)-P(2)-C(35)	112.4(8)	C(23)-P(2)-C(35)	101.0(10)
C(29)-P(2)-C(35)	104.9(12)	P(1)-C(1)-C(2)	115.0(8)
P(1)-C(1)-C(6)	125.0(8)	C(2)-C(1)-C(6)	120.0(0)

Table 3.53. /continued

C(1)-C(2)-C(3)	120.0(0)	C(2)-C(3)-C(4)	120.0(0)
C(3)-C(4)-C(5)	120.0(0)	C(4)-C(5)-C(6)	120.0(0)
C(1)-C(6)-C(5)	120.0(0)	P(1)-C(7)-C(8)	114.0(9)
P(1)-C(7)-C(12)	125.8(9)	C(8)-C(7)-C(12)	120.0(0)
C(7)-C(8)-C(9)	120.0(0)	C(8)-C(9)-C(10)	120.0(0)
C(9)-C(10)-C(11)	120.0(0)	C(10)-C(11)-C(12)	120.0(0)
C(7)-C(12)-C(11)	120.0(0)	N(1)-C(17)-C(16)	122.0(0)
N(1)-C(17)-C(18)	114.3(12)	C(16)-C(17)-C(18)	122.7(12)
Cu(2)-N(1)-C(17)	114.4(5)	Cu(2)-N(1)-C(13)	127.7(5)
C(17)-N(1)-C(13)	117.9(0)	P(1)-C(13)-N(1)	115.1(6)
P(1)-C(13)-C(14)	122.4(6)	N(1)-C(13)-C(14)	122.5(0)
C(13)-C(14)-C(15)	119.3(0)	C(14)-C(15)-C(16)	118.0(0)
C(17)-C(16)-C(15)	118.8(0)	C(17)-C(18)-N(2)	115.4(12)
C(17)-C(18)-C(19)	122.2(12)	N(2)-C(18)-C(19)	122.3(0)
Cu(2)-N(2)-C(18)	117.7(6)	Cu(2)-N(2)-C(22)	124.6(6)
C(18)-N(2)-C(22)	117.7(0)	C(18)-C(19)-C(20)	119.2(0)
C(19)-C(20)-C(21)	117.8(0)	C(20)-C(21)-C(22)	118.8(0)
N(2)-C(22)-C(21)	121.9(0)	P(2)-C(23)-C(24)	116.3(8)
P(2)-C(23)-C(28)	123.7(8)	C(24)-C(23)-C(28)	120.0(0)

Table 3.53. /continued

C(23)-C(24)-C(25)	120.0(0)	C(24)-C(25)-C(26)	120.0(0)
C(25)-C(26)-C(27)	120.0(0)	C(26)-C(27)-C(28)	120.0(0)
C(23)-C(28)-C(27)	120.0(0)	P(2)-C(29)-C(30)	124.6(9)
P(2)-C(29)-C(34)	115.3(9)	C(30)-C(29)-C(34)	120.0(0)
C(29)-C(30)-C(31)	120.0(0)	C(30)-C(31)-C(32)	120.0(0)
C(31)-C(32)-C(33)	120.0(0)	C(32)-C(33)-C(34)	120.0(0)
C(29)-C(34)-C(33)	120.0(0)	N(3)-C(39)-C(38)	121.3(0)
N(3)-C(39)-C(40)	112.6(12)	C(38)-C(39)-C(40)	117.5(12)
Cu(1)-N(3)-C(39)	116.2(5)	Cu(1)-N(3)-C(35)	125.8(5)
C(39)-N(3)-C(35)	117.8(0)	P(2)-C(35)-N(3)	114.9(6)
P(2)-C(35)-C(36)	121.9(6)	N(3)-C(35)-C(36)	122.6(0)
C(35)-C(36)-C(37)	119.2(0)	C(36)-C(37)-C(38)	117.3(0)
C(39)-C(38)-C(37)	117.9(0)	C(39)-C(40)-N(4)	113.2(11)
C(39)-C(40)-C(41)	122.9(11)	N(4)-C(40)-C(41)	121.9(0)
Cu(1)-N(4)-C(40)	116.5(5)	Cu(1)-N(4)-C(44)	124.4(5)
C(40)-N(4)-C(44)	117.5(0)	C(40)-C(41)-C(42)	119.0(0)
C(41)-C(42)-C(43)	117.9(0)	C(42)-C(43)-C(44)	119.4(0)
N(4)-C(44)-C(43)	122.3(0)	S-C(45)-C(46)	113(3)
F(1)-P(3)-F(2)	90.3(14)	F(1)-P(3)-F(3)	88(2)

Table 3.53. /continued

F(2)-P(3)-F(3)	90(2)	F(1)-P(3)-F(1)	180.0(0)
F(2)-P(3)-F(2)	180.0(0)	F(3)-P(3)-F(3)	180.0(0)
F(4)-P(4)-F(5)	84(3)	F(4)-P(4)-F(6)	89(2)
F(5)-P(4)-F(6)	94(3)	F(4)-P(4)-F(4)	180.0(0)
F(5)-P(4)-F(5)	180.0(0)	F(6)-P(4)-F(6)	180.0(0)

CHAPTER FOUR

THE SYNTHESIS OF RHODIUM, PALLADIUM AND PLATINUM
MONONUCLEAR COMPLEXES CONTAINING PENDANT
PHOSPHORUSBIPYRIDYL LIGANDS:
POTENTIAL PRECURSORS FOR THE SYNTHESIS OF LIGAND
BRIDGED HETERONUCLEAR COMPLEXES

AIM:

The aim of the work described in this chapter was to synthesise mononuclear rhodium, palladium and platinum complexes containing the ligand Ph_2Pbipy, bonded in a pendant co-ordination mode, *i.e.* with only the phosphorus atom bonded to the metal centre. These mononuclear complexes could then be reacted with suitable metal precursors to form ligand bridged heteronuclear complexes.

4.1. INTRODUCTION

Binuclear transition metal complexes have been studied fairly extensively, but to a large extent most of the complexes synthesised have been symmetric species involving two like metals with identical coordination environments. [90] Bridging phosphine ligands, particularly dppm have been used extensively to connect two metal centres, but these ligands generally do not lead to hetero-binuclear complexes. [91-100]

However, it is envisaged that hetero-binuclear complexes may offer advantages over homo-binuclear complexes because the different metal centres could possibly perform separate, unique functions. This would be especially useful in the homogeneous catalysis of the electrochemical reduction of carbon dioxide by a hetero-binuclear complex, since the presence of different metal atoms could result in the carbon dioxide coordinating differently at each

metal atom; this could then result in different types of coupling between the carbon dioxide molecule and therefore the formation of different reduction products.

Balch and co-workers have employed 2-diphenylphosphinopyridyl (Ph_2Ppy) to synthesise a range of mononuclear rhodium, palladium and platinum complexes containing the Ph_2Ppy ligand coordinated in a pendant fashion. (*see Figure 4.1*).[58,101-105]

$[Rh(Ph_2Ppy)_2(CO)Cl]$ $[M(Ph_2Ppy)_2Cl_2]$ (M=Pd,Pt)
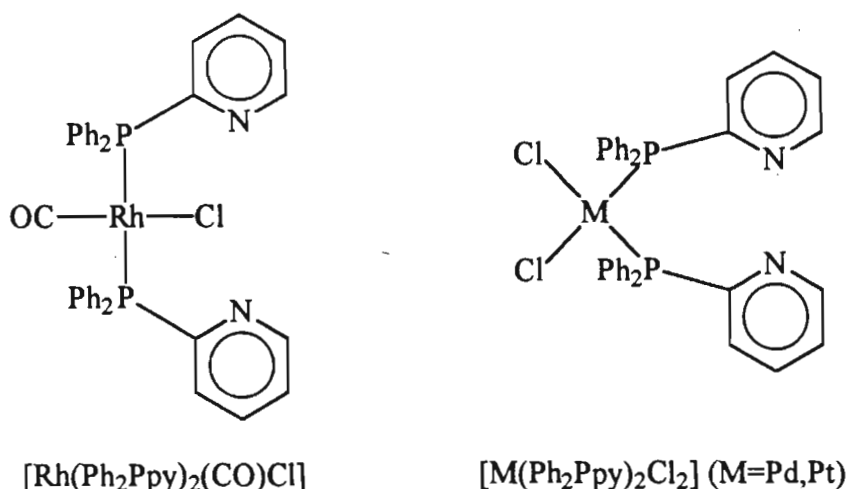
Figure 4.1. Rhodium, palladium and platinum mononuclear complexes of Ph_2Ppy

In these mononuclear complexes, the nitrogen atom is uncoordinated and can therefore bond to a second and different metal atom and in this context the reaction between $[Pd(COD)Cl_2]$ and $[Rh(Ph_2Ppy)_2(CO)Cl]$ results in the formation of $[RhPd(\mu-Ph_2Ppy)_2(CO)Cl_3]$[58,101] (*see scheme 4.1*). Interestingly, the reaction between $[Pt(COD)Cl_2]$ and $[Rh(Ph_2Ppy)_2(CO)Cl]$ does not result in the formation of $[RhPt(\mu-Ph_2Ppy)_2(CO)Cl_3]$ but rather produces $[Pt(Ph_2Ppy)Cl_2]$ and $[Rh_2(\mu-Ph_2Ppy)(\mu-CO)Cl_2]$. The reaction between $[Pt(Ph_2Ppy)_2Cl_2]$ and $[Rh_2(CO)_2Cl_2]_2$ results in the formation of $[Pt(Ph_2Ppy)_2Cl][Rh(CO)_2Cl_2]$.[59]

Scheme 4.1. Synthesis of [RhPd(μ-Ph$_2$Ppy)$_2$(CO)Cl$_3$]
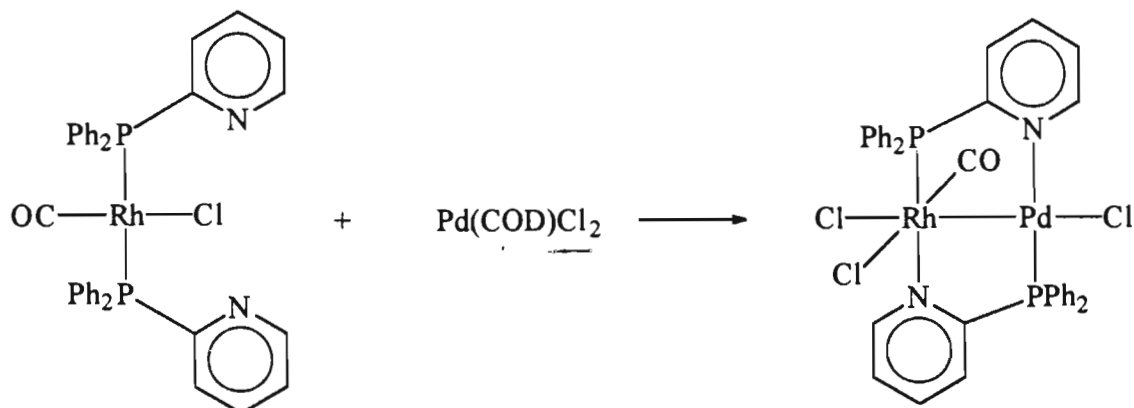
Binuclear Pt(I) and Pd(I) complexes are generally prepared by a conproportionation reaction involving the appropriate compounds of M(II) and M(0) {M=Pt,Pd}. The reaction between [Pt(Ph$_2$Ppy)$_2$Cl$_2$] and [Pd$_2$(dba)$_3$] resulted in the formation of [PdPt(μ-Ph$_2$Ppy)$_2$Cl$_2$] (*see Scheme 4.2*).[103] Balch and co-workers obtained a dinuclear rhodium complex [Rh$_2$(μ-Ph$_2$Ppy)$_2$(μ-CO)Cl$_2$] by reacting the mononuclear rhodium complex, [Rh(Ph$_2$Ppy)$_2$(CO)Cl] with [Rh(CO)$_2$Cl]$_2$ [102] (*see Figure 4.2*).

Scheme 4.2. Formation of [PdPt(μ-Ph₂Ppy)₂Cl₂]

$$\text{Scheme 4.2. Formation of } [PdPt(\mu\text{-}Ph_2Ppy)_2Cl_2]$$

Figure 4.2. Molecular structure diagram of [Rh₂(μ-Ph₂Ppy)₂(μ-CO)Cl₂]
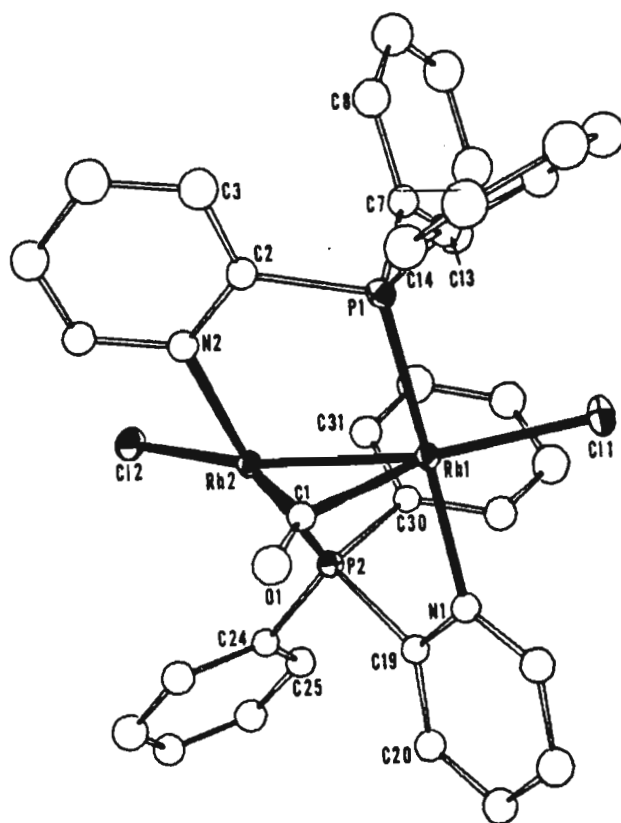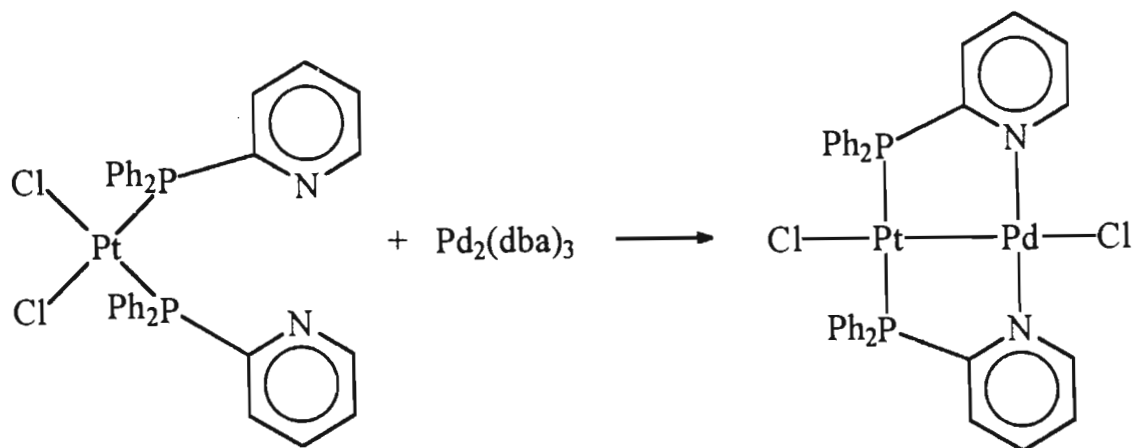
$$\text{Figure 4.2. Molecular structure diagram of } [Rh_2(\mu\text{-}Ph_2Ppy)_2(\mu\text{-}CO)Cl_2]$$

Cotton and Matusz synthesised a dirhodium complex [Rh$_2$(μ-Ph$_2$Ppy)$_2$(μ-OAc)$_2$Cl$_2$], by reacting Ph$_2$Ppy with [Rh$_2$(OAc)$_4$(MeOH)$_2$] in the presence of LiCl (see Figure 4.3). Interestingly, the two Ph$_2$Ppy ligands are cis to each other whereas the two ligands in other reported dinuclear complexes are trans to each other.[106]
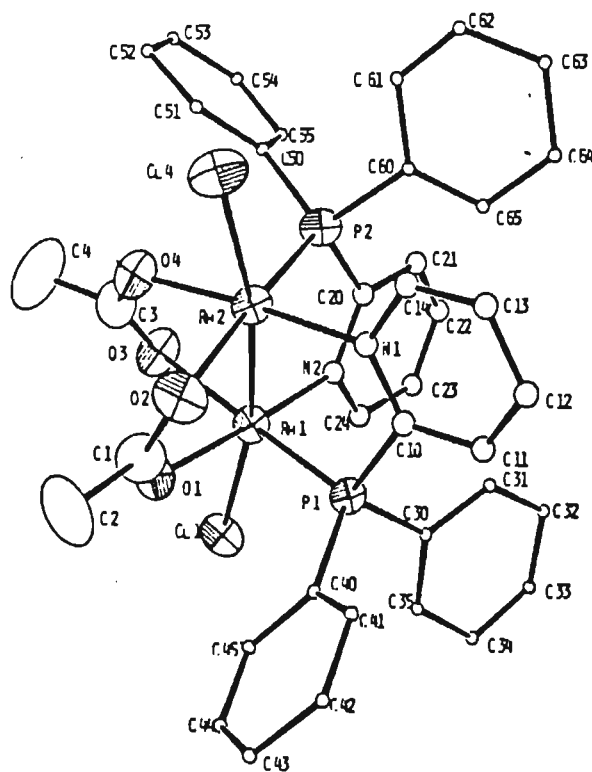
Figure 4.3. Molecular structure diagram of [Rh$_2$(μ-Ph$_2$Ppy)$_2$(μ-OAc)$_2$Cl$_2$]

4.2. RESULTS AND DISCUSSION

4.2.1. Synthesis and characterisation of [Pt(Ph₂Pbipy)₂Cl₂] (36)

Treatment of a dichloromethane solution of Ph_2Pbipy with a dichloromethane solution of
$[Pt(PhCN)_2Cl_2]$ under a nitrogen atmosphere followed by precipitation with diethyl ether
produces an off white air stable solid in fairly low yields (*see scheme 4.3*). Elemental analyses
for carbon, hydrogen and nitrogen indicated the formulation of the product as being
$[Pt(Ph_2Pbipy)_2Cl_2]$.

Scheme 4.3. Synthesis of [Pt(Ph₂Pbipy)₂Cl₂]
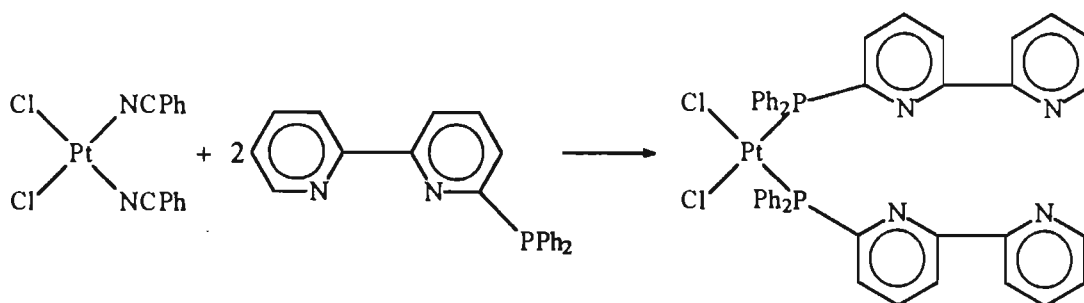
The infrared spectrum indicates the presence of the ligand; this is confirmed by the ^{1}H nmr
spectrum in which the aromatic resonances occur between 7.2 - 8.6ppm. The ^{31}P{^{1}H} nmr
spectrum a sharp peak at 12.94ppm and two ^{195}Pt satellite peaks at 69.87 and -43.98ppm
respectively. The ^1J(Pt-P) coupling constant is 3666Hz which compares well with ^1J(Pt-P)
coupling constants obtained for *cis*-$[Pt(Ph_2Ppy)_2Cl_2]$ (^1J(Pt-P)=3675.6Hz),[59] $[Pt(Ph_2Ppy)_2Br_2]$
(^1J(Pt-P)=3673Hz)[101] and $[Pt(Ph_3P)_2Cl_2]$ (^1J(Pt-P)=3618Hz).[107] The magnitude of the ^1J(Pt-P)
coupling constant is consistent with the presence of Pt(II).[100] In the ^{195}Pt{^{1}H} nmr spectrum

a triplet is observed at -4264.6, -4480.2 and -4695.8ppm (*see Figure 4.5*). The ^1J(Pt-P) coupling constants are 3667 and 3667Hz, these values being close to the value obtained from the ^{1}P{^{1}H} nmr spectrum. The phosphorus and platinum spectra indicate that only one isomer is formed from this reaction and also that the complex is mononuclear.
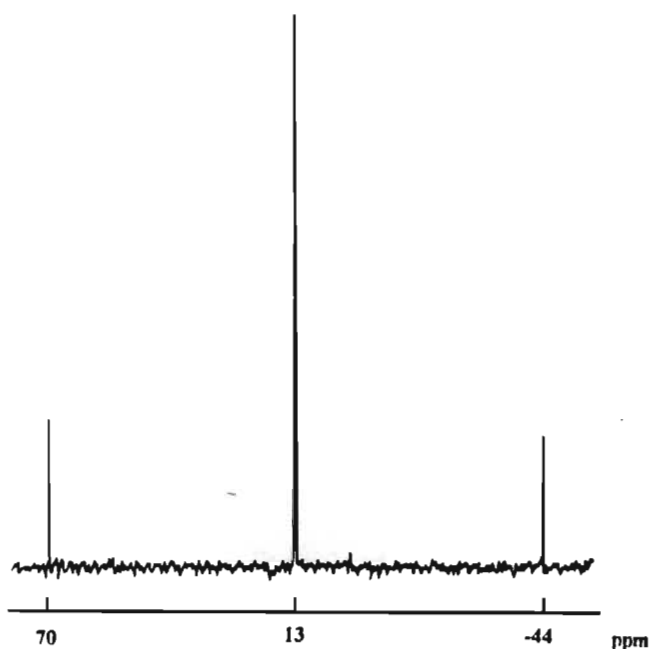
Figure 4.4. ^{31}P{^{1}H} n.m.r spectrum of Pt(Ph$_2$Pbipy)$_2$Cl$_2$
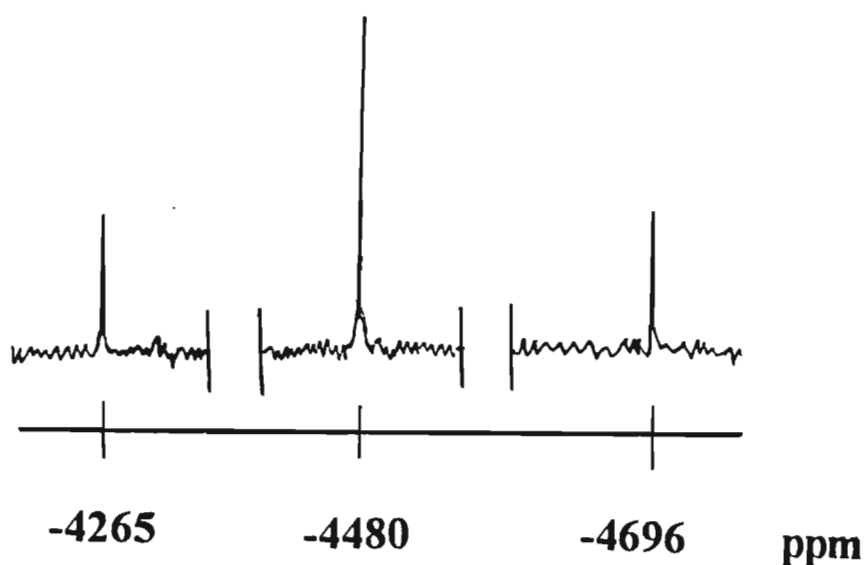
Figure 4.5. ^{195}Pt{^{1}H} n.m.r spectrum of Pt(Ph$_2$Pbipy)$_2$Cl$_2$

4.2.2. Reactions between [Pt(Ph₂Pbipy)₂Cl₂] and other suitable metal precursors

[Pt(Ph₂Pbipy)₂Cl₂] has two pendant Ph₂Pbipy ligands, the nitrogen atoms of the bipyridyl fragment being uncoordinated and should therefore be able to coordinate to another metal atom. Therefore reactions were attempted in an endeavour to synthesise heteronuclear complexes.

4.2.2.1. Reaction with [Cu(MeCN)₄](PF₆)

Treatment of a dichloromethane solution of [Pt(Ph₂Pbipy)₂Cl₂] with a dichloromethane solution of [Cu(MeCN)₄]⁺ under a nitrogen atmosphere resulted in the formation of a red-brown solution. A yellow crystalline solid was precipitated out of solution by the addition of diethyl ether.

The infrared, ¹H nmr and the ³¹P{¹H} nmr spectra of the yellow crystalline material were identical to that obtained for the dicopper species, [Cu₂(Ph₂Pbipy)₂(MeCN)₂](PF₆)₂ (5), described in the preceding chapter. Microanalytical analyses confirmed that the dicopper species had been formed.

The reaction was repeated several times; the order of addition was reversed and the molar ratios of the reactants were varied. However, the dicopper species was formed in all cases. It appears that the Ph₂Pbipy ligand has a high affinity for copper and thus the dicopper complex is formed.

4.2.2.2. Reaction with [Ag(COD)₂](BF₄)

Treatment of a dichloromethane solution of [Pt(Ph₂Pbipy)₂Cl₂] with a dichloromethane solution of [Ag(COD)₂]⁺ under a nitrogen atmosphere resulted in the formation of a light yellow solution. An off white crystalline solid was precipitated out of solution by the addition of diethyl ether.

The infrared, ^{1}H nmr and the ^{31}P{^{1}H} nmr spectra of the yellow crystalline material were identical to that obtained for the disilver species, $[Ag_2(Ph_2Pbipy)_2(MeCN)_2](BF_4)_2$, which has already been synthesised by colleagues in the laboratory.[85] Microanalytical analyses confirmed that the disilver species had been formed.

The reaction was repeated several times; the order of addition was reversed and the molar ratios of the reactants were varied. However, the disilver species formed in all cases indicating that the Ph$_2$Pbipy ligand has a high affinity for silver and thus the disilver complex is formed.

4.2.2.3. Reaction with [Au(tht)Cl]

Treatment of a dichloromethane solution of $[Pt(Ph_2Pbipy)_2Cl_2]$ with a dichloromethane solution of [Au(tht)Cl] under a nitrogen atmosphere resulted in the deposition of a black solid on the bottom of the flask and the formation of a faint gold mirror on the flask surface. The black solid is most probably platinum metal. The order of addition was reversed and the molar ratios of the reactants were varied; however, there was no change in the results obtained.

The infrared, ^{1}H nmr and the ^{31}P{^{1}H} nmr spectra of the mother liquor is similar to those obtained for the Ph$_2$Pbipy ligand (*see section 2.3*). The ^{31}P{^{1}H} nmr also indicated that most of the Ph$_2$Pbipy ligand had been oxidised to Ph$_2$P(O)bipy.

4.2.3. Synthesis and characterisation of [Pd(Ph$_2$Pbipy)$_2$Cl$_2$] (37)

Treatment of a dichloromethane solution of Ph$_2$Pbipy with a dichloromethane solution of [Pd(PhCN)$_2$Cl$_2$] under a nitrogen atmosphere followed by precipitation with diethyl ether produces a yellow air stable solid in good yields (*see scheme 4.4*) . Elemental analyses indicated the formulation of the product as being [Pd(Ph$_2$Pbipy)$_2$Cl$_2$].

The infrared spectrum of [Pd(Ph$_2$Pbipy)$_2$Cl$_2$] has the characteristic peaks due to the Ph$_2$Pbipy ligand. The ^{1}H nmr spectrum indicates that the ligand is present, the aromatic resonances occurring between 7.2 - 8.6ppm. The ^{31}P{^{1}H} nmr spectrum actually has two sharp peaks at 29.05 and 23.14ppm, the ratio of these peaks being 1:2, which indicates that in solution there is a mixture of *cis* and *trans* isomers. Interestingly, Balch and co-workers reported that they obtained a mixture of isomers (ratio of peaks = 1:1.9) when they reacted Ph$_2$Ppy with [Pd(PhCN)$_2$Cl$_2$], evidence for this coming from the ^{31}P{^{1}H} nmr spectrum of the complex [Pd(Ph$_2$Ppy)$_2$Cl$_2$] which has two peaks at 29.70 and 23.39ppm.[103]

Scheme 4.4. Synthesis of [Pd(Ph$_2$Pbipy)$_2$Cl$_2$]
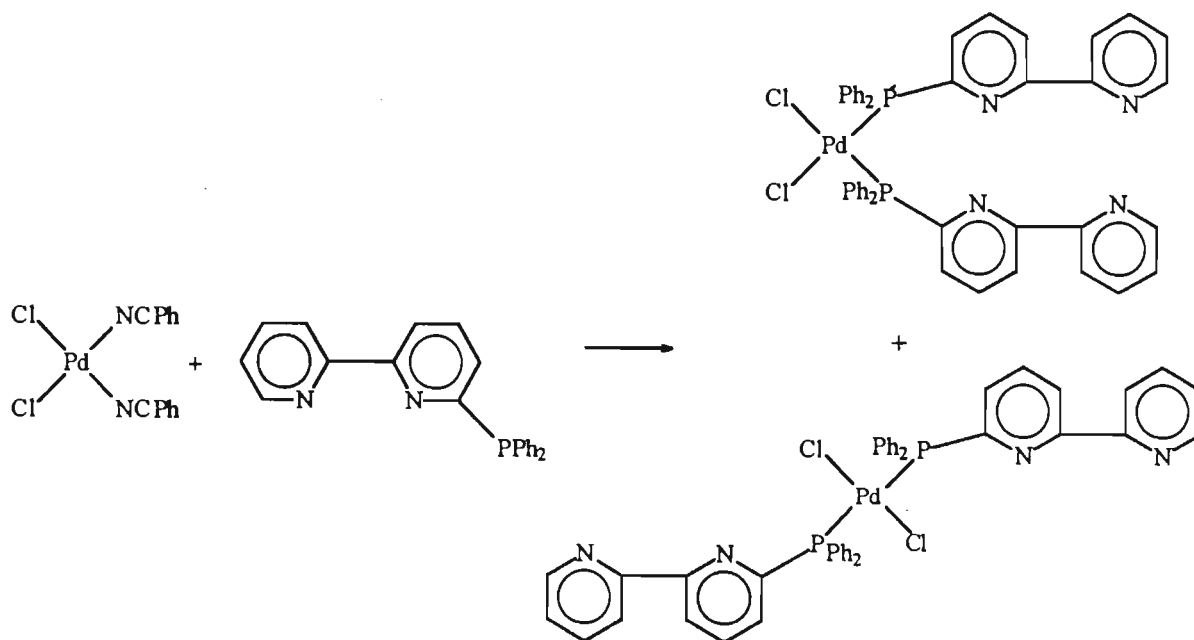
The mononuclear complex [Pd(Ph$_2$Pbipy)$_2$Cl$_2$], has two pendant Ph$_2$Pbipy ligands, the nitrogen atoms of the bipyridyl fragment being uncoordinated and should therefore be able to coordinate to another metal atom. Therefore similar reactions to those attempted between [Pt(Ph$_2$Pbipy)$_2$Cl$_2$] and group 11 metal precursors were attempted with the palladium monomer. Unfortunately, the results obtained for reaction between the palladium monomer and these metal precursors mirrored those obtained for the platinum complex.

4.2.3. Synthesis, characterisation and x-ray crystal structure of [Rh(Ph$_2$Pbipy)$_2$(CO)Cl] (38)

Treatment of a dichloromethane solution of [Rh(CO)$_2$Cl]$_2$ with a dichloromethane solution of four equivalents of 6-diphenylphosphino-2,2'-bipyridine under a nitrogen atmosphere resulted in the formation of as an air stable yellow crystalline solid by the addition of an equal volume of diethyl ether to the dichloromethane solution after the addition was complete (*see scheme 4.5*). Elemental analyses indicated the formulation of the product as being [Rh(Ph$_2$Pbipy)$_2$(CO)Cl].

Scheme 4.5. Synthesis of [Rh(CO)(Cl)(Ph$_2$Pbipy)$_2$]
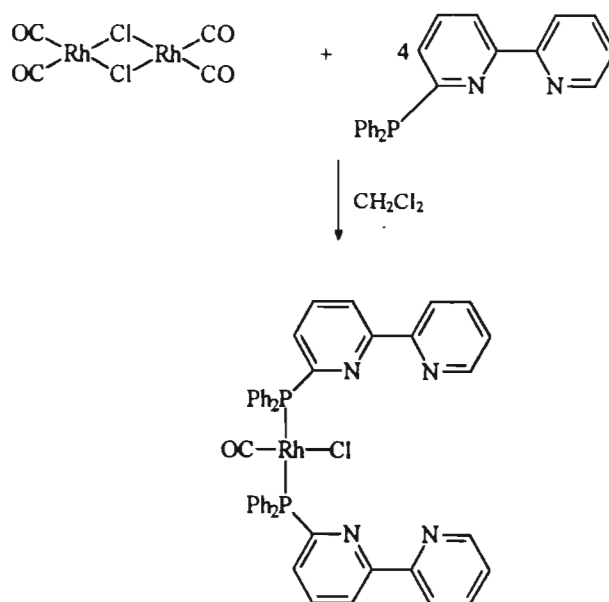
[Rh(Ph$_2$Pbipy)$_2$(CO)Cl] closely resembles [Rh(Ph$_2$Ppy)$_2$(CO)Cl] and [Rh(PPh$_3$)$_2$(CO)Cl] in appearance and physical properties. [58,108-110] The infrared spectrum of [Rh(CO)(Cl)(Ph$_2$Pbipy)$_2$] indicates the presence of the Ph$_2$Pbipy ligand. The peak at 1982cm^{-1} is due to the terminal carbonyl, this compares well with the values obtained for the terminal carbonyls in [Rh(Ph$_2$Ppy)$_2$(CO)Cl] (υ_{CO}= 1962cm^{-1}) and [Rh(PPh$_3$)$_2$(CO)Cl] (υ_{CO} 1982 cm^{-1}).[101]

The ^{1}H nmr and ^{13}C nmr spectra indicate that the ligand is present and coordinated, with the aromatic proton resonances in the ^{1}H nmr occurring between 7.2 and 8.6ppm. The ^{31}P{^{1}H} nmr spectrum of the complex shows a doublet occurring at 24.0ppm; the doublet occurring because there is coupling between the rhodium nucleus of spin = ½ and phosphorus. The ^1J(Rh-P) coupling constant of 126Hz compares well with the coupling constants obtained for [Rh(Ph$_2$Ppy)$_2$(CO)Cl] {^1J(Rh-P) = 127.8Hz} and [Rh(PPh$_3$)$_2$(CO)Cl] {^1J(Rh-P) = 124Hz}[101] (*see Figure 4.6*).

26 22   ppm
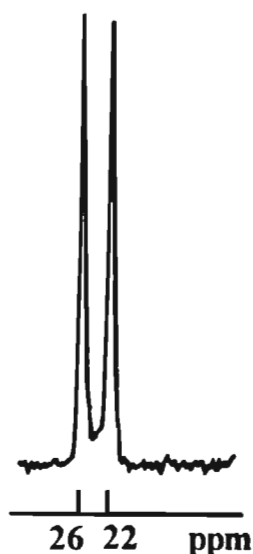
Figure 4.6. ^{31}P{^{1}H} spectrum of [Rh(Ph$_2$Pbipy)$_2$(CO)Cl]

Single crystals suitable for x-ray crystallography were grown by the slow cooling of a dichloromethane-diethyl ether solution of the complex. The molecular structure of [Rh(Ph$_2$bipy)$_2$(CO)Cl] is depicted in *Figure 4.7* together with the atomic numbering scheme. *Tables 4.4 to 4.8* list selected bond lengths and angles.

The molecular structure indicates that the two Ph₂Pbipy ligands are coordinated in a pendant manner through the phosphorus atoms, *i.e.* the nitrogen atoms of the bipyridyl portion of the Ph₂Pbipy ligand are not coordinated. The rhodium atom is bound to the chloride ligand, the two phosphorus atoms of the pendant Ph₂Pbipy ligands and the carbonyl carbon. The coordination geometry is square planar as evidenced by the angles subtended at the rhodium atom. The P(1)-Rh-P(2) angle is 177.2(1)° indicating that the two Ph₂Pbipy ligands are *trans* to each other. The angles subtended by the *cis*-disposed ligands fall in the range 87.5(4)° - 88.6(1)° (*see Table 4.7*). The terminal carbonyl group is almost linear as evidenced by a Rh-C(1)-O bond angle of 176.9(12)°. The Rh-P(1) and the Rh-P(2) distances of 2.324(3)Å and 2.3357(3)Å compare well with Rh-P distances observed in other rhodium complexes.[58] The Rh-Cl distance of 2.347(3)Å and the Rh-C(1) distance of 1.798(14)Å also compare well with Rh-Cl and Rh-C(O) distances observed in other rhodium complexes.[111,112]
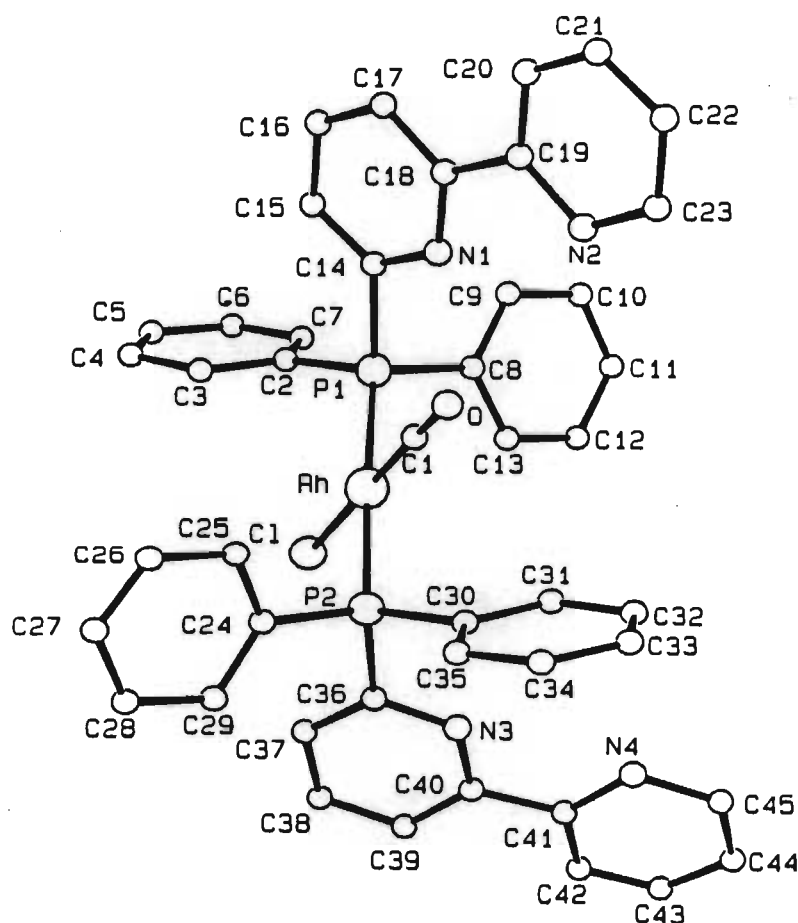
Figure 4.7. Crystal structure diagram of [Rh(Ph₂Pbipy)₂(CO)Cl]

As discussed the nitrogen atoms of the Ph₂Pbipy ligands are uncoordinated and could therefore coordinate to another metal centre. Therefore reactions identical to those attempted with [Pt(Ph₂Pbipy)₂Cl₂] and [Pd(Ph₂Pbipy)₂Cl₂] and group 11 metal precursors were attempted. Unfortunately, the results obtained for these reactions between the rhodium monomer and these metal precursors were identical to those obtained for the platinum and palladium complexes. These experiments demonstrated that it is unlikely that heteronuclear complexes can be synthesised from the reaction between the group 11 metal precursors and the three mononuclear complexes (36), (37) and (38).

4.2.4. *Synthesis and characterisation of [Rh₃(Ph₂Pbipy)₂(CO)₃Cl₃]* (39)

Treatment of a dichloromethane solution of Rh(Ph₂Pbipy)₂(CO)Cl with an equimolar dichloromethane solution of [Rh(CO)₂Cl]₂ under a nitrogen atmosphere followed by precipitation with diethyl ether produces a red-brown solid. This complex is also obtained if the order of addition is reversed. Microanalytical analyses for carbon, hydrogen, nitrogen, chlorine and phosphorus indicated the formulation of the product as being [Rh₃(Ph₂Pbipy)₂(CO)₃Cl₃] (*see Table 4.1*). The complex is soluble in dichloromethane, chloroform and benzene but is moderately soluble in acetonitrile. The complex, either in solution or as a solid decomposes slowly upon prolonged exposure to air.

The ¹H nmr spectrum indicates that the ligand is present and the aromatic proton resonances occur between 7.3 and 8.5ppm. Inspection of the infrared spectrum in the carbonyl region indicates that there are three bands present at 2073(s), 1992(s) and 1780(m)cm⁻¹ (*see Figure 4.8*). The bands at 2073 and 1992cm⁻¹ indicate the presence of terminal carbonyls while the band at 1780 cm⁻¹ indicates that a bridging carbonyl is present. The presence of the bridging carbonyl in the infrared spectrum implies that the complex cannot be mononuclear.

The ³¹P{¹H} nmr spectrum of [Rh₃(Ph₂Pbipy)₂(CO)₃Cl₃] is shown in *Figure 4.9* and one can clearly distinguish a doublet occurring at 52.0, the doublet being due to the coupling between the rhodium and phosphorus atoms, the ¹*J*(Rh-P) coupling constant is 145Hz. A closer

examination of the doublet reveals fine structure. In particular, when the $^{31}P\{^1H\}$ nmr spectrum is expanded it is evident that each member of the doublet is further split into several peaks though the resolution is not sufficient to discern a well defined pattern (*see Figure 4.9*). In view of the further splitting of the doublet peaks, it can be concluded that the complex is unlikely to be mononuclear. If the complex were mononuclear with two different isomers present in solution for example, two distinct sets of resonances of different chemical shift would be expected. Indeed, the fine structure on the doublet peaks is reminiscent of that observed in several dinuclear rhodium complexes which contain chemically equivalent, but magnetically inequivalent phosphorus atoms. [113-120]

2200   2000   1700   cm^{-1}
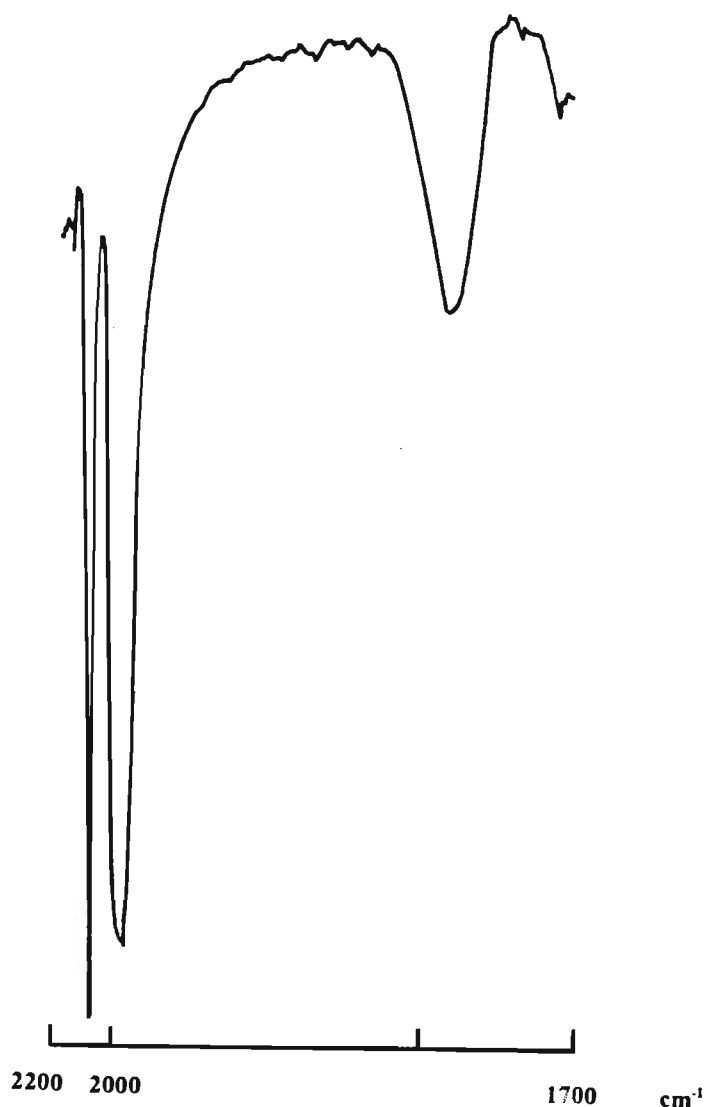
Figure 4.8. Infra red spectrum of [Rh$_3$(Ph$_2$Pbipy)$_2$(CO)$_3$Cl$_3$]

EXPANDED SPECTRUM

54   50 ppm

54 50 ppm
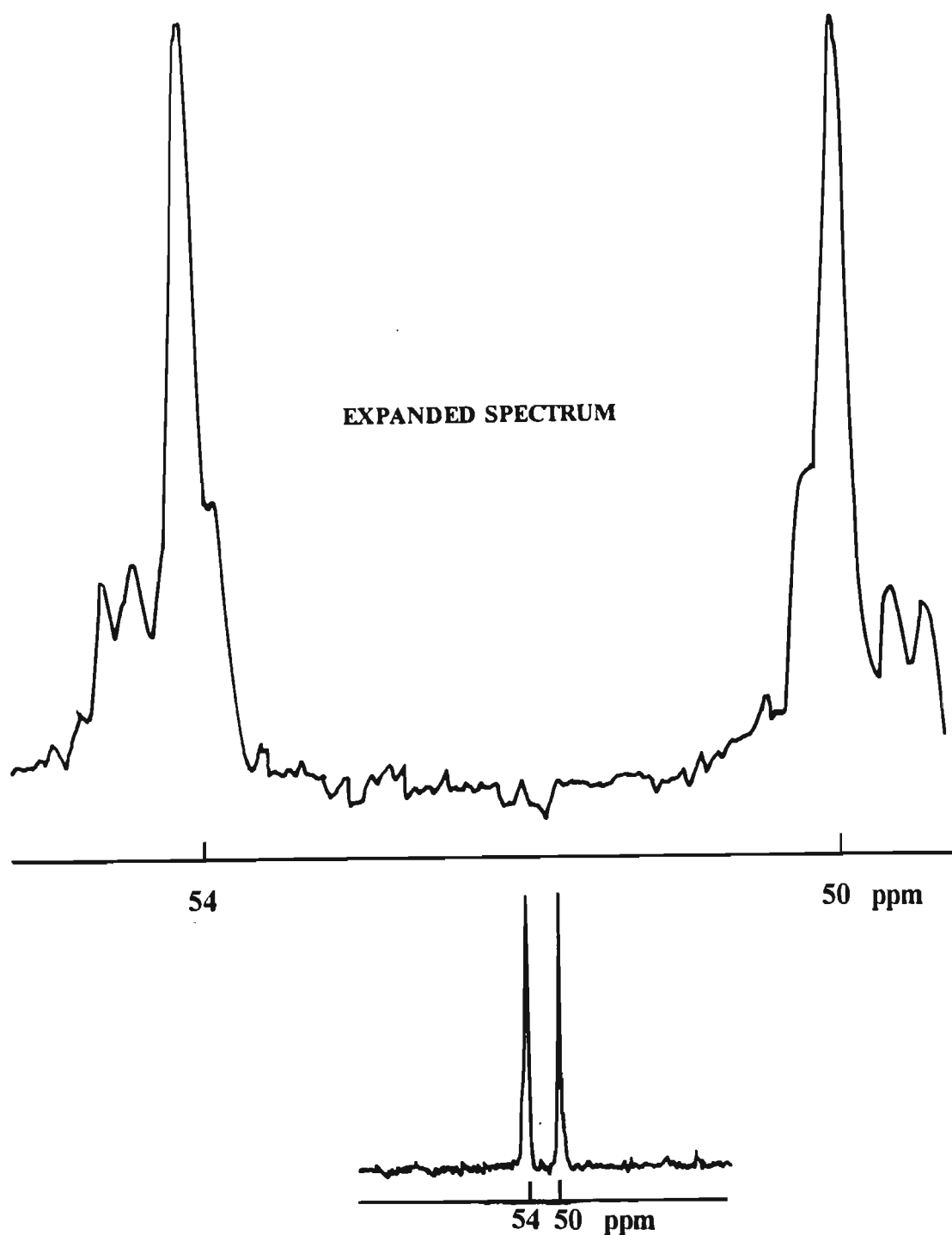
Figure 4.9. $^{31}P\{^1H\}$ nmr spectrum of $[Rh_3(Ph_2Pbipy)_2(CO)_3Cl_3]$

The proposed structure for $[Rh_3(Ph_2Pbipy)_2(CO)_3Cl_3]$ is illustrated in *figure 4.10* and is obtained by combining the spectral evidence and the results from the microanalytical analyses. Both the infrared and $^{31}P\{^1H\}$ nmr spectra indicate that the complex is not mononuclear and

it could be dinuclear. However, this would mean that one would have to somehow have to fit two Ph$_2$Pbipy ligands (which are tridentate), at least three carbonyl ligands (from the infrared spectrum) and at least two chloride ligands (to ensure that the complex is neutral) around two rhodium centres; *i.e.* each rhodium atom would have to be six coordinate. This is extremely unlikely coordination number for rhodium(I) in a dinuclear complex.[58,121] Hence we have proposed that the complex is trinuclear. Equation 4.1 best summarises the probable reaction that occurs;

$$\text{Rh(Ph}_2\text{Pbipy)}_2\text{(CO)Cl} + [\text{Rh(CO)}_2\text{Cl}]_2 \rightarrow [\text{Rh}_3\text{(Ph}_2\text{Pbipy)}_2\text{(CO)}_3\text{Cl}_3] + 2\text{CO}....4.1$$

It is important to note that the electron count at each rhodium obeys the 18 electron rule and it is also evident from *figure 4.10* that the original ligand coordination of the Rh(Ph$_2$Pbipy)$_2$(CO)Cl monomer is discernible around the central rhodium. Indeed, equation 4.1 indicates that Rh(Ph$_2$Pbipy)$_2$(CO)Cl has functioned as a metal containing ligand in its reaction with [Rh(CO)$_2$(Cl)]$_2$. Certainly, the microanalytical data are consist with the formulation [Rh$_3$(Ph$_2$Pbipy)$_2$(CO)$_3$Cl$_3$]. Several attempts were made to grow single crystals; different solvent systems as well as different crystal growing techniques were utilised but the compound always precipitated out as a powder.
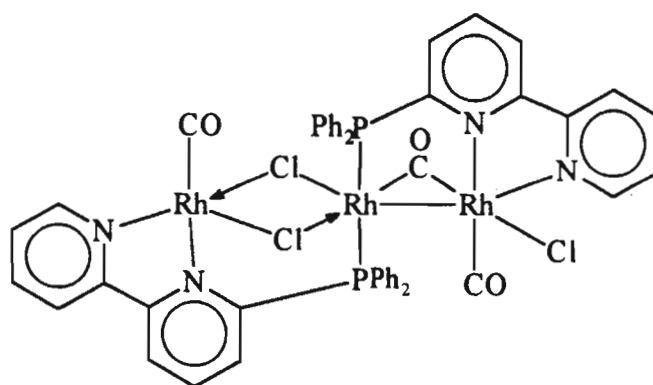
Figure 4.10. Proposed structure of [Rh$_3$(Ph$_2$Pbipy)$_2$(CO)$_3$Cl$_3$]

Due to the limited solubility of (39) in acetonitrile the cyclic voltammetric experiments were carried out in dichloromethane. However, (39) is not reduced within the solvent limits and therefore no other electrochemical studies were undertaken.

4.2.5. Synthesis and characterisation of [Rh₃(Ph₂Pbipy)₂(CO)₅Cl]X₂ {where X = BF₄(40), PF₆(41) or SbF₆(42)}

Treatment of an acetonitrile solution of $[Rh(CO)_2Cl]_2$ with two equivalents of an acetonitrile solution of AgX (X = BF_4, PF_6 or SbF_6) resulted in the precipitation of AgCl and the formation of $[Rh(CO)_2(MeCN)_2]X$ in solution.[122] AgCl was removed by filtration and $[Rh(CO)_2(MeCN)_2]X$ was precipitated out of solution by addition of diethyl ether. ¹H nmr and infrared spectra, as well as satisfactory microanalytical analyses were obtained.

Treatment of an acetonitrile solution of $[Rh(Ph_2Pbipy)_2(CO)Cl]$ with an acetonitrile solution of two mole equivalents $[Rh(CO)_2(MeCN)_2]X$ under a nitrogen atmosphere followed by precipitation with diethyl ether produces a orange-red solid. Elemental analyses for carbon, hydrogen, nitrogen and phosphorus indicated the formulation of the product as being $[Rh_3(Ph_2Pbipy)_2(CO)_5Cl]X_2$ {X = BF_4(40), PF_6(41) and SbF_6(42)} (*see Table 4.1*). The complex is soluble in dichloromethane and acetonitrile but not in benzene. The complex decomposes slowly upon prolonged exposure to air in solution or as a solid.

The ¹H nmr spectrum indicates that the Ph₂Pbipy ligand is present with the aromatic proton resonances occurring between 7.2ppm and 8.6ppm.[*] The infrared spectrum in the carbonyl region indicates the presence of three bands at 2075(m), 2000(m) and 1793(s)cm⁻¹ (*see Figure 4.11*). The bands at 2075 and 2000cm⁻¹ are associated with the presence of terminal carbonyls while the band at 1793cm⁻¹ indicates that at least one bridging carbonyl is present. An interesting difference between the neutral complex (39) and these ionic complexes is that the band due the bridging carbonyl is more intense in the ionic complexes probably implying that

---

[*] All spectral data used in the discussion are for the $[Rh_3(Ph_2Pbipy)_2(CO)_5Cl](SbF_6)_2$ complex. Refer to tables 4.2 and 4.3 after the experimental section for more information.

more than one bridging carbonyl is present. The infrared spectrum, due to the presence of the bridging carbonyl indicates that the complex cannot be mononuclear. The presence of intense peaks in the infrared spectrum at 660cm^{-1} (SbF$_6$), 841cm^{-1} (PF$_6$), and 1061cm^{-1} (BF$_4$) indicates that the complexes are not neutral.

2200 2000   1800 cm^{-1}

Figure 4.11. Infra red spectrum of [Rh$_3$(Ph$_2$Pbipy)$_2$(CO)$_5$Cl]$^{2+}$

The ^{31}P{^{1}H} nmr spectrum of [Rh$_3$(Ph$_2$Pbipy)$_2$(CO)$_5$Cl]$^{2+}$ is similar to that obtained for the neutral complex (**4**) (*see Figure 4.9*). Thus a doublet occurs at 52.2ppm, the doublet arising because there is coupling between the rhodium and phosphorus atoms, the ^1J(Rh-P) coupling constant is 145Hz. A closer examination of the doublet reveals fine structure. In particular, when the ^{31}P{^{1}H} nmr spectrum is expanded it is evident that each member of the doublet is further split into several peaks though the resolution is not sufficient to discern a well defined pattern (*see Figure 4.9*). In view of the further splitting of the doublet it can be concluded that the complex is unlikely to be mononuclear.

The proposed structure is illustrated in *figure 4.12* and is obtained from combining the spectral evidence and the results from the microanalytical analyses. Both the infrared and

^{31}P{^{1}H} nmr spectra indicate that the complex is not mononuclear. We have proposed that the complex is trinuclear. Equation 4.2 best summarises the probable reaction that occurs;
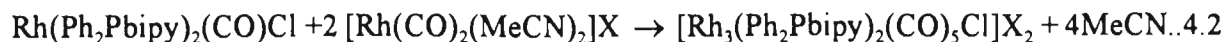
$$Rh(Ph_2Pbipy)_2(CO)Cl + 2\,[Rh(CO)_2(MeCN)_2]X \rightarrow [Rh_3(Ph_2Pbipy)_2(CO)_5Cl]X_2 + 4MeCN..4.2$$

It is important to note that the electron count at each rhodium obeys the 18 electron rule and it is also evident from *figure 4.12* that the original ligand coordination of the [Rh(Ph$_2$Pbipy)$_2$(CO)Cl] monomer is discernible around the central rhodium. Indeed, equation 4.2 indicates that [Rh(Ph$_2$Pbipy)$_2$(CO)Cl] has functioned as a metal containing ligand in its reaction with [Rh(CO)$_2$(MeCN)$_2$]$^+$ *i.e.* the two pendant bipyridyl units have replaced four acetonitriles. Certainly, the microanalytical data is consist with the formulation [Rh$_3$(Ph$_2$Pbipy)$_2$(CO)$_5$Cl]X$_2$. Several attempts were made to grow single crystals, different solvent systems as well as different crystal growing techniques being utilised but the crystals always lost solvent when removed from the mother liquor.
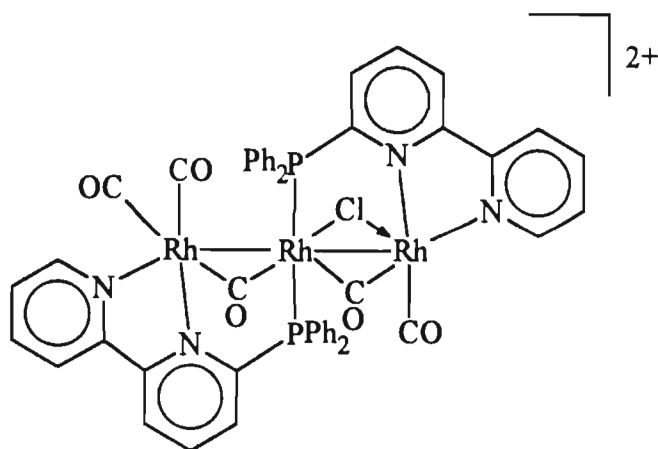
Figure 4.12. Proposed structure of [Rh$_3$(Ph$_2$Pbipy)$_2$(CO)$_5$Cl]$^{2+}$

The [Rh(Ph$_2$Pbipy)$_2$(CO)Cl] monomer was also reacted with the [Rh(COD)(MeCN)$_2$]X (where X = BF$_4$, PF$_6$, or SbF$_6$) precursors under the same conditions as described above. It is interesting to note that [Rh$_3$(Ph$_2$Pbipy)$_2$(CO)$_5$Cl]$^{2+}$ is also formed in these reactions albeit in very low yields (28% for the SbF$_6$ salt). Clearly, the reaction is non-stoichiometric; the source of the additional carbonyls in [Rh$_3$(Ph$_2$Pbipy)$_2$(CO)$_5$Cl]$^{2+}$ probably arising from some decomposition of Rh(Ph$_2$Pbipy)$_2$(CO)Cl.

The cyclic voltammogram of [Rh$_3$(Ph$_2$Pbipy)$_2$(CO)$_5$Cl](SbF$_6$)$_2$ (42) recorded in acetonitrile (0.1M TBAP) at room temperature under an argon atmosphere exhibits three reduction waves at E_{pc} = -1.51V, $E_{1/2}$ = -1.88 and $E_{1/2}$ = -2.18V *vs* Ag/AgCl (*see Figure 4.13*). These waves are associated with the reduction of the dication [Rh$_3$(Ph$_2$Pbipy)$_2$(CO)$_5$Cl]$^{2+}$, the anions not being reduced within the solvent limit. The first reduction has a peak current (i_{pc}) considerably larger than those for the second two reduction waves, suggesting that it involves a two electron reduction process and the second two reductions involve one electron transfers. An i_{pa}/i_{pc} value of 0.60 for the first wave indicates that the first reduction is irreversible, while i_{pa}/i_{pc} ratios of *ca* 1.0 for the second two waves indicate that the later two reductions are reversible. We suggest that the first two electron reduction proceeds *via* an ECE mechanism where the chemical step involves the loss of chloride ions, similar to that observed for the electrochemical reduction of [Cu$_2$(μ-Ph$_2$Pbipy)$_2$(μ-Cl)]$^+$ cation. Should this be the case the species present in solution following the third reduction will be monoanionic. It appears that a total of four electrons can be taken up by the system without disintegration of the basic trinuclear structure, at least on the time scale of the cyclic voltammetric experiment.

Under a carbon dioxide atmosphere at room temperature, the initial reduction wave at $E_{1/2}$ = -1.51 *vs* Ag/AgCl was unchanged, however there was a current enhancement just beyond the second reduction wave (*see Figure 4.13*). This enhancement of the cathodic current indicated that the reduced form of [Rh$_3$(Ph$_2$Pbipy)$_2$(CO)$_5$Cl]$^{2+}$, presumably a neutral and possibly solvento species behaves as an electrocatalyst for the reduction of carbon dioxide. It should be noted that the original features of the cyclic voltammogram are restored by purging the solution with argon for a few minutes. Bulk electrolysis experiments were attempted with

$[Rh_3(Ph_2Pbipy)_2(CO)_5Cl]^{2+}$; but the complex breaks up during the experiment with deposition of rhodium metal.
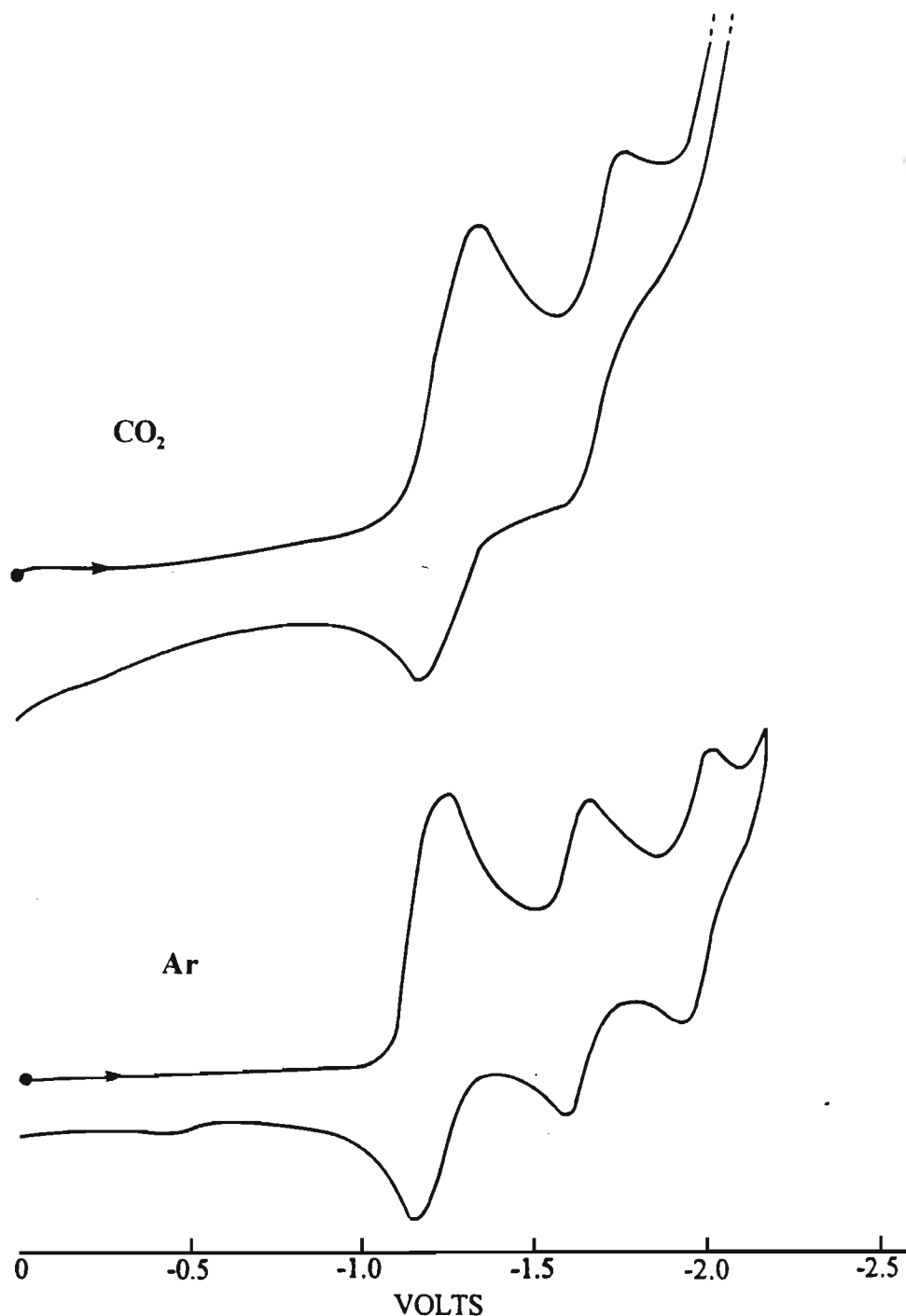
Figure 4.13. Cyclic voltammograms of $[Rh_3(Ph_2Pbipy)_2(CO)_5Cl]^{2+}$ (42) measured in acetonitrile (10^{-3}M solution, 0.1M TBAP) at Pt. Scan rate 200mVs^{-1}; T = 25°C

4.2.6. Synthesis and characterisation of [Rh₃(Ph₂Pbipy)(CO)₅(MeCN)₂]X₃ {where X = BF₄ (43), PF₆ (44) or SbF₆(45)}

4.2.6. Synthesis and characterisation of $[Rh_3(Ph_2Pbipy)(CO)_5(MeCN)_2]X_3$ {where X = BF_4 (43), PF_6 (44) or SbF_6(45)}

Treatment of two equivalents of Ph₂Pbipy with three equivalents of [Rh(CO)₂(MeCN)₂]X in acetonitrile solution followed by precipitation with diethyl ether produces an orange-red salt characterised as [Rh₃(Ph₂Pbipy)₂(CO)₅(MeCN)₂]X₃ {X = BF₄ (43), PF₆ (44) or SbF₆ (45)}. Elemental analyses for carbon, hydrogen, nitrogen and phosphorus indicated the formulation of the product as being [Rh₃(Ph₂Pbipy)₂(CO)₅(MeCN)₂]X₃ *(see Table 4.1)*. The complex is soluble in dichloromethane and acetonitrile but insoluble in benzene. However [Rh₃(Ph₂Pbipy)₂(CO)₅(MeCN)₂]X₃ decomposes slowly in solution or solid upon prolonged exposure to air.

The ¹H nmr spectrum exhibits Ph₂Pbipy ligand peaks between 7.2 and 8.6ppm, the methyl resonance from the coordinated acetonitrile being present at 2.01ppm.[2*] The infrared spectrum in the carbonyl region is similar to that for [Rh₃(Ph₂Pbipy)₂(CO)₅Cl]X₂ and reveals three bands present at 2050(m), 2002(m) and 1803(s) cm⁻¹. The bands at 2050 and 2002cm⁻¹ indicate the presence of terminal carbonyls while the band at 1803cm⁻¹ indicates that at least one bridging carbonyl is present. The presence of a bridging carbonyl peak indicates that the complex cannot be mononuclear. Intense peaks associated with the counter anions in the infrared spectrum at 660cm⁻¹ (SbF₆), 841cm⁻¹ (PF₆), and 1061cm⁻¹ (BF₄) indicates that the complexes are not neutral.

The ³¹P{¹H} nmr spectrum of [Rh₃(Ph₂Pbipy)₂(CO)₅(MeCN)₂]X₃ is shown in *Figure 4.14*, and one can clearly distinguish a doublet occurring at 49.9ppm, the doublet being due to the coupling between the rhodium and phosphorus atoms, with a ¹*J*(Rh-P) coupling constant of 145Hz. A closer examination of the doublet reveals fine structure. In particular, when the ³¹P{¹H} nmr spectrum is expanded it is evident that each member of the doublet is further split into several peaks though the resolution is not sufficient to discern a well defined pattern

---

[2*]   All spectral data used in the discussion are for the [Rh₃(Ph₂Pbipy)₂(CO)₅(MeCN)₂](SbF₆)₃ complex. Refer to tables 4.2 and 4.3 after the experimental section for more information.

(see Figure 4.14). In view of the further splitting of the doublet peaks, it can be concluded that the complex is unlikely to be mononuclear. The symmetric pattern observed in the $^{31}P\{^1H\}$ nmr spectrum probably implies that the phosphorus atoms are equivalent.
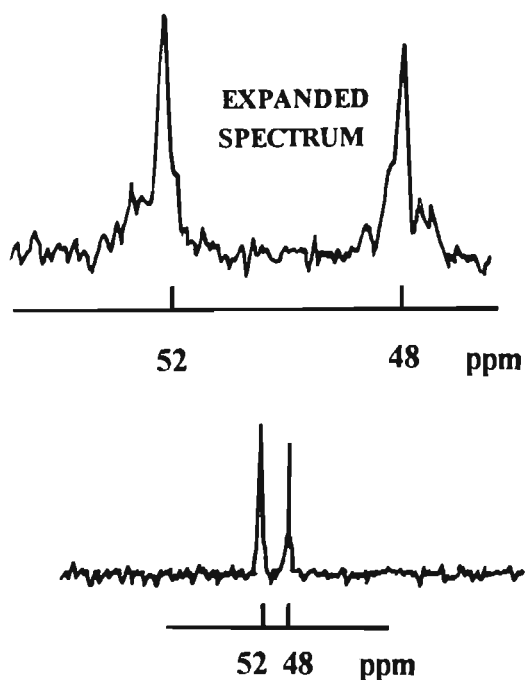
Figure 4.14. $^{31}P\{^1H\}$ nmr spectrum of $[Rh_3(Ph_2Pbipy)_2(CO)_5(MeCN)_2]X_3$
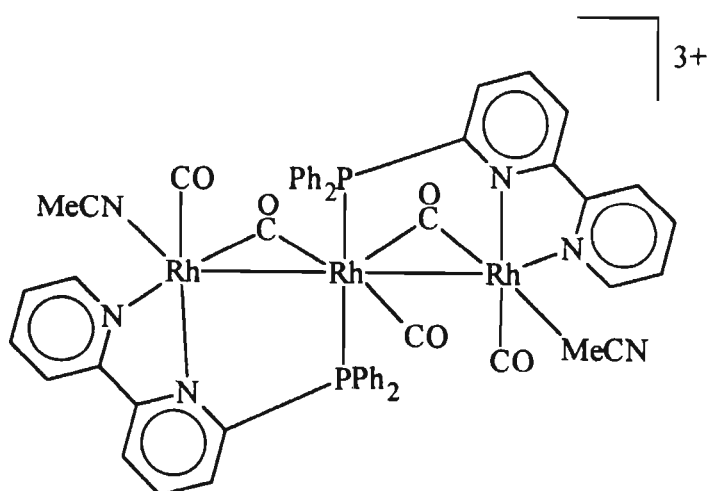
Figure 4.15. Proposed structure of $[Rh_3(Ph_2Pbipy)_2(CO)_5(MeCN)_2]^{3+}$

The structure that we have proposed is illustrated in *Figure 4.15* and it is based on the spectral evidence and the results from the microanalytical analyses. Both the infrared and $^{31}P\{^1H\}$ nmr spectra indicate that the complex is not mononuclear and it could be dinuclear. However, this would mean that one would have to somehow have to fit two Ph$_2$Pbipy ligands (which are potentially tridentate), at least three carbonyl ligands (from the infrared spectrum) and two acetonitrile ligands (from the ^{1}H nmr) around two rhodium centres; this clearly cannot be accomplished. Hence we have proposed that the complex is trinuclear. Equation 4.3 best summarises the probable reaction that occurs;

$$2Ph_2Pbipy + 3[Rh(CO)_2(MeCN)_2]X \rightarrow [Rh_3(Ph_2Pbipy)_2(CO)_5(MeCN)_2]X_3 + 4MeCN....4.3$$
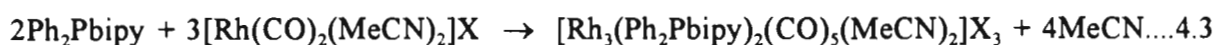
It is important to note that the electron count at each rhodium obeys the 18 electron rule. We could not predict that the product of this reaction would be trinuclear but the spectroscopic properties are very similar to those of the trinuclear rhodium complexes already discussed. Certainly, the microanalytical data is consistent with the formulation [Rh$_3$(Ph$_2$Pbipy)$_2$(CO)$_5$(MeCN)$_2$]$^{3+}$. Several attempts were made to grow single crystals, different solvent systems as well as different crystal growing techniques were utilised. Unfortunately the crystals always lost solvent when removed from the mother liquor.

The cyclic voltammogram of [Rh$_3$(Ph$_2$Pbipy)$_2$(CO)$_4$(MeCN)$_2$](SbF$_6$)$_3$ (45) recorded in acetonitrile (0.1M TBAP) at room temperature under an argon atmosphere exhibits four reduction waves at $E_{1/2}$ = -1.30, $E_{1/2}$ = -1.63, $E_{1/2}$ = -2.00 and $E_{1/2}$ = -2.18V *vs* Ag/AgCl (*see Figure 4.16*). All four reduction waves appear to be reversible with i_{pa}/i_{pc} ratios of *ca* 1.0 and peak-to-peak separations of *ca* 59mV. It appears that a total of four electrons can be taken up by the system without disintegration of the basic trinuclear structure, at least on the time scale of the cyclic voltammetric experiment. No new peaks appear and no peaks disappear during a repetitive scans indicating that the complex remains intact during the cycling process.

Under a carbon dioxide atmosphere at room temperature, the initial reduction waves at $E_{1/2}$ = -1.32 and $E_{1/2}$ = -1.63 *vs* Ag/AgCl are unaffected, however there was a current enhancement

at the onset of the third reduction wave. This enhancement of the cathodic current indicated that the reduced form of $[Rh_3(Ph_2Pbipy)_2(CO)_4(MeCN)_2]^{3+}$, presumably a neutral species behaves as an electrocatalyst for the reduction of carbon dioxide. It should be noted that the original features of the cyclic voltammogram are restored by purging the solution with argon for a few minutes. Bulk electrolysis experiments were attempted with $[Rh_3(Ph_2Pbipy)_2(CO)_4(MeCN)_2]^{3+}$; but the complex breaks up during the experiment with deposition of rhodium metal. It can be concluded that the complex does behave as an electrocatalyst when it is intact and therefore there is current enhancement in the cyclic voltammogram experiment, however on the time scale of the bulk electrolysis experiment the complex breaks down.
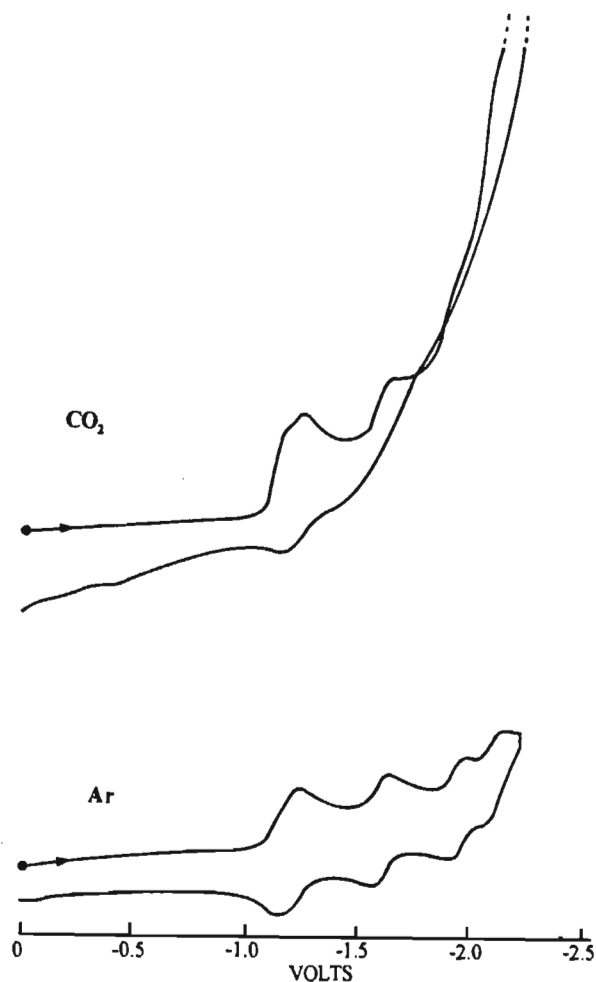
Figure 4.16. Cyclic voltammograms of $[Rh_3(Ph_2Pbipy)_2(CO)_5(MeCN)_2]^{3+}$ (45) measured in acetonitrile (10^{-3}M solution, 0.1M TBAP) at Pt. Scan rate 200mVs^{-1}; T = 25°C

4.3. EXPERIMENTAL

4.3.1. Synthesis of [Pt(Ph₂Pbipy)₂Cl₂] (36)

4.3.1. Synthesis of [Pt(Ph$_2$Pbipy)$_2$Cl$_2$] **(36)**

A solution of [Pt(PhCN)₂Cl₂] (*47.2mg, 0.100mmol*) in dichloromethane (5ml) was added dropwise under a nitrogen atmosphere to a stirred solution of Ph₂Pbipy (*68mg, 0.200mmol*) in dichloromethane (5ml). The resultant light yellow solution was stirred for a further hour and the volume was halved. Diethyl ether was added and the solution was kept at 0°C overnight. The solvent was decanted and the white powder which had separated was washed with diethyl ether and then dried in air.

Yield: 45%

4.3.2. Synthesis of [Pd(Ph$_2$Pbipy)$_2$Cl$_2$] (37)

A solution of [Pd(PhCN)₂Cl₂] (*38.4mg, 0.100mmol*) in dichloromethane (5ml) was added dropwise under a nitrogen atmosphere to a stirred solution of Ph₂Pbipy (*68mg, 0.200mmol*) in dichloromethane (5ml). The resultant light yellow solution was stirred for a further hour and the volume was halved. Diethyl ether was added and the solution was kept at 0°C overnight. The solvent was decanted and the yellow powder which had separated was washed with diethyl ether and then dried in air.

Yield: 89%

4.3.3. Synthesis of [Rh(Ph$_2$Pbipy)$_2$(CO)Cl] (38)

A solution of [Rh(CO)₂Cl]₂ (*39mg, 0.100mmol*) in dichloromethane (5ml) was added dropwise under a nitrogen atmosphere to a stirred solution of Ph₂Pbipy (*136mg, 0.400mmol*) in dichloromethane (5ml). The resultant light yellow solution was stirred for a further hour and the volume was halved. Diethyl ether was added and the solution was kept at 0°C overnight. The solvent was decanted and the yellow crystals which had separated were washed with diethyl ether and then dried in air.

Yield: 95%

4.3.4. Synthesis of [Rh$_3$(Ph$_2$Pbipy)$_2$(CO)$_3$Cl$_3$] **(39)**

A solution of [Rh(CO)$_2$Cl]$_2$ (*39mg, 0.100mmol*) in dichloromethane (10ml) was added dropwise under a nitrogen atmosphere to a stirred solution of [Rh(Ph$_2$Pbipy)$_2$(CO)Cl] (*84.7mg, 0.100mmol*) in dichloromethane (15ml). The resultant orange-red solution was stirred for a further hour and the volume was halved. Diethyl ether was added and the solution was kept at 0°C overnight. The solvent was decanted and the orange-red powder which had separated were washed with diethyl ether and then dried *in vacuo*. The complex was then recrystallised from a dichloromethane-diethyl ether solution.

Yield: 68%

4.3.5. Synthesis of [Rh$_3$(Ph$_2$Pbipy)$_2$(CO)$_5$Cl](X)$_2$ {where X = BF$_4$(**40**), *PF$_6$*(**41**) *or SbF$_6$*(**42**)}

Method 1:

A solution of [Rh(CO)$_2$(MeCN)$_2$](X) (*0.200mmol*) in acetonitrile (10ml) was added dropwise under a nitrogen atmosphere to a stirred solution of [Rh(Ph$_2$Pbipy)$_2$(CO)Cl] (*84.7mg, 0.100mmol*) in acetonitrile (15ml). The resultant red solution was stirred for a further hour and the volume was halved. Diethyl ether was added and the solution was kept at 0°C overnight. The solvent was decanted and the orange-red powder which had separated were washed with diethyl ether and then dried *in vacuo*. The complex was then recrystallised from a dichloromethane-diethyl ether solution.

Yield: (40) = 78%, (41) = 83% and *(42) = 89%*

Method 2

An solution of [Rh(COD)(MeCN)$_2$](X) (*0.200mmol*) in acetonitrile (10ml) was added dropwise under a nitrogen atmosphere to a stirred solution of [Rh(Ph$_2$Pbipy)$_2$(CO)Cl] (*84.7mg, 0.100mmol*) in acetonitrile (10ml). The red solution was stirred for an hour and then the volume was halved. Diethyl ether was added and the solution was cooled at 0°C overnight. The solvent was decanted and the orange-red solid was washed with diethyl ether and dried *in vacuo*. The complex was then recrystallised from an dichloromethane-diethyl ether solution.

Yield: (40) = 13%, (41) = 18% and *(42) = 27%*

4.3.6. Synthesis of [Rh₃(Ph2Pbipy)2(CO)5(MeCN)2](X)3   {where X = BF₄(43), PF₆(44) or SbF₆(45)}

A solution of [Rh(CO)₂(MeCN)₂](X) *(0.300mmol)* in acetonitrile (10ml) was added dropwise under a nitrogen atmosphere to a stirred solution of (Ph₂Pbipy) *(68.2mg, 0.200mmol)* in acetonitrile (15ml). The resultant red solution was stirred for a further hour and the volume was halved. Diethyl ether was added and the solution was kept at 0°C overnight. The solvent was decanted and the orange-red powder which had separated were washed with diethyl ether and then dried *in vacuo*. The complex was then recrystallised from a acetonitrile-diethyl ether solution.

Yield: (43) = 84%, (44) = 86% and *(45) = 90%*

See Section 3.5. for electrochemical procedures

Table 4.1. Microanalytical analyses for platinum, palladium and rhodium complexes

Compound	Calculated (%)				Found (%)			
	C	H	N	P	C	H	N	P
36	55.82	3.62	5.92	-	55.52	3.70	6.01	-
37	61.59	3.99	6.53	-	61.89	4.01	6.67	-
38	63.81	4.05	6.61	-	63.46	3.96	6.21	-
39	47.85	2.90	4.75	5.25	48.08	3.22	5.01	5.55
40	43.97	2.56	4.19	4.60	44.05	2.67	4.31	4.48
41	40.45	2.36	3.85		40.14	2.44	3.99	-
42	35.96	2.09	3.42	3.79	35.58	2.27	3.76	3.98
43	43.25	2.74	5.71	4.21	43.35	2.81	5.66	4.13
44	39.40	2.50	5.20	7.67	39.82	2.69	5.41	7.88
45	33.18	2.10	4.38	3.23	33.57	2.33	4.51	3.31

Table 4.2. Infrared data for platinum, palladium and rhodium complexes

Compound	Carbonyl peaks (cm^{-1})	Anion peaks (cm^{-1})
38	1982(s)	-
39	2074(s), 1992(s), 1780(m)	-
40	2048(m), 1997(m), 1747(s)	1061(s)
41	2060(m), 2001(m), 1782(s)	841(s)
42	2075(m), 2000(m), 1794(s)	660(s)
43	2019(m), 2000(m), 1747(s)	1061(s)
44	2030(m), 2000(m), 1784(s)	841(s)
45	2050(m), 2002(m), 1803(s)	660(s)

Table 4.3. $^{31}P\{^1H\}$ nmr data

Compound	Peaks (ppm)	^1J(M-P) Hz
Pt(Ph$_2$Pbipy)$_2$Cl$_2$	69.9, 12.9, -44.0	3666
Pd(Ph$_2$Pbipy)$_2$Cl$_2$	29.1, 23.1	-
Rh(Ph$_2$Pbipy)$_2$(CO)Cl	25.9, 22.1	126
Rh$_3$(Ph$_2$Pbipy)$_2$(CO)$_3$Cl$_3$	54.2, 49.7	145
[Rh$_3$(Ph$_2$Pbipy)$_2$(CO)$_5$Cl](BF$_4$)$_2$	54.2, 49.8	143
[Rh$_3$(Ph$_2$Pbipy)$_2$(CO)$_5$Cl](PF$_6$)$_2$	54.6, 50.0	147
[Rh$_3$(Ph$_2$Pbipy)$_2$(CO)$_5$Cl](SbF$_6$)$_2$	54.3, 49.8	145
[Rh$_3$(Ph$_2$Pbipy)$_2$(CO)$_5$(MeCN)$_2$](BF$_4$)$_3$	50.9, 46.3	143
[Rh$_3$(Ph$_2$Pbipy)$_2$(CO)$_5$(MeCN)$_2$](PF$_6$)$_3$	51.6, 46.1	145
[Rh$_3$(Ph$_2$Pbipy)$_2$(CO)$_5$(MeCN)$_2$](SbF$_6$)$_3$	52.1, 47.6	145

Table 4.4 Crystal data for [Rh(Ph₂Pbipy)₂(CO)Cl]

Formula	$RhClOC_{45}H_{34}N_4P_2$
Molecular mass	847.10
Crystal system	monoclinic
Space group	$P2_1 / c$
a (Å)	9.3778
b (Å)	20.6772
c (Å)	19.9327
β (°)	95
V (Å³)	3848
Z	4
D_c (g cm⁻³)	0.15
F (000)	1728
μ (cm⁻¹)	0.63
Absorption corrections	Semi Empirical[87]
Measured intensities	5712
Unique intensities	4633
Unique intensities with [$F_o > 3\sigma$ (F_o)]	2812
$\Delta\rho_{max}$ (eÅ⁻³)	0.648
Maximum least squares shift to error ratio	-0.05
Weighting scheme parameter g in $w = 1/[\sigma^2(F) + g(F^2)]$	0.003
$R = \Sigma$ ($F_o - F_c$) / ΣF_o	0.0642
$R_w = \Sigma_w$ ½ ($F_o - F_c$) / ΣF_w½F_o	0.0628
Scan Mode	$\omega - 2\theta$
ω scan angle	$0.40 + 0.34\tan\theta$
Horizontal Aperture Width (mm)	$2.70 + 0.40\tan\theta$
Scattering Range	$3 \leq \theta \leq 23$
Number of parameters	262

Table 4.5. Fractional Coordinates (x10⁴) and Isotropic Thermal Factors (Å² , x10³) For [Rh(Ph₂Pbipy)(CO)Cl]

	x/a	y/b	z/c	$\underline{U}_{eq}$
Rh	1534(1)	1455(1)	3642(1)	32(1)
P (1)	918(3)	2473(2)	4017(2)	32(1)
P (2)	2222(3)	458(2)	3228(2)	35(1)
Cl	-187(3)	1585(2)	2717(2)	51(1)
O	3717(11)	1229(5)	4776(5)	77(3)
N (1)	2573(10)	2567(5)	5188(5)	36(3)
N (2)	5423(15)	2329(7)	5711(7)	97(5)
N (3)	3119(10)	486(4)	1998(5)	43(3)
N (4)	5617(14)	789(6)	1437(7)	85(4)
C (1)	2858(14)	1332(6)	4344(7)	48(4)*
C (2)	-977(12)	2677(6)	3865(6)	39(3)*
C (3)	-1965(13)	2215(6)	4041(6)	41(3)*
C (4)	-3431(14)	2374(7)	3993(7)	54(4)*
C (5)	-3875(14)	2995(7)	3745(7)	57(4)*
C (6)	-2912(15)	3432(7)	3560(7)	62(4)*
C (7)	-1428(14)	3285(6)	3612(7)	52(4)*
C (8)	2179(13)	3705(6)	3970(6)	45(3)*
C (9)	1882(12)	3125(5)	3623(6)	35(3)*

Table 4.5. /continued

	x/a	y/b	z/c	$\underline{U}_{eq}$
C (10)	2896(14)	4206(6)	3654(7)	53(4)*
C (11)	3265(14)	4114(6)	3005(7)	50(4)*
C (12)	2979(14)	3528(7)	2669(7)	60(4)*
C (13)	2280(14)	3027(6)	2991(7)	52(4)*
C (14)	1241(12)	2674(5)	4926(6)	37(3)*
C (15)	135(12)	2909(6)	5296(6)	41(3)*
C (16)	518(13)	3047(6)	5984(6)	46(3)*
C (17)	1909(13)	2941(6)	6266(6)	40(3)*
C (18)	2914(13)	2699(6)	5854(6)	41(3)*
C (19)	4409(13)	2578(6)	6144(6)	43(3)*
C (20)	4710(12)	2720(5)	6792(6)	34(3)*
C (21)	6022(17)	2621(7)	7075(8)	71(5)*
C (22)	7115(16)	2369(8)	6718(8)	71(5)*
C (23)	6824(16)	2217(7)	6031(8)	64(4)*
C (24)	1312(13)	-230(6)	3594(7)	42(3)*
C (25)	1259(15)	-210(7)	4286(8)	65(4)*
C (26)	584(16)	-732(8)	4617(8)	72(5)*
C (27)	-62(16)	-1208(7)	4230(8)	69(5)*

Table 4.5. /continued

	x/a	y/b	z/c	$\underline{U}_{eq}$
C (28)	19(16)	-1253(8)	3544(8)	76(5)*
C (29)	770(14)	-762(7)	3200(7)	54(4)*
C (30)	4148(12)	270(6)	3404(6)	38(3)*
C (31)	5065(14)	782(6)	3273(7)	50(4)*
C (32)	6575(15)	654(7)	3386(7)	64(4)*
C (33)	7080(15)	67(7)	3622(7)	64(4)*
C (34)	6141(15)	-424(7)	3757(7)	65(4)*
C (35)	4640(14)	-321(6)	3636(6)	48(4)*
C (36)	1935(12)	366(5)	2306(6)	37(3)*
C (37)	611(13)	223(6)	1951(7)	47(3)*
C (38)	531(14)	173(7)	1244(7)	55(4)*
C (39)	1775(14)	301(6)	927(7)	50(4)*
C (40)	3037(12)	467(6)	1322(7)	42(3)*
C (41)	4337(14)	654(6)	1000(7)	48(4)*
C (42)	4297(13)	683(6)	343(6)	40(3)*
C (43)	5490(17)	865(7)	67(8)	73(5)*
C (44)	6800(16)	985(7)	433(8)	65(4)*
C (45)	6869(14)	966(6)	1119(7)	52(4)*

* isotropic temperature factor

$$\underline{U}_{eq} = \tfrac{1}{3} \sum_i \sum_j \underline{U}_{ij} \underline{a}^*_i \underline{a}^*_j (a_i . a_j)$$

Table 4.6. Anisotropic Thermal Factors ($Å^2$, x10^3) for [Rh(Ph$_2$Pbipy)$_2$(CO)Cl]

	U (11)	U (22)	U (33)	U (23)	U (13)	U (12)
Rh	31(1)	32(1)	34(1)	-1(1)	4(1)	1(1)
P (1)	30(2)	30(2)	37(2)	0(2)	6(2)	2(2)
P (2)	33(2)	35(2)	39(2)	-3(2)	6(2)	-1(2)
Cl	48(2)	62(2)	42(2)	-7(2)	-7(2)	12(2)
O	89(8)	68(7)	67(7)	-13(6)	-34(6)	33(6)
N (1)	37(6)	40(6)	30(6)	2(5)	1(5)	-1(5)
N (2)	76(10)	118(13)	98(12)	-6(10)	7(9)	11(9)
N (3)	42(6)	35(6)	52(7)	5(5)	11(5)	0(5)
N (4)	92(10)	64(9)	104(11)	8(8)	37(9)	15(8)

Table 4.7. Interatomic distances (Å) for [Rh(Ph₂Pbipy)₂(CO)Cl]

Rh-P(1)	2.324(3)	Rh-P(2)	2.335(3)
Rh-Cl	2.347(3)	Rh-C(1)	1.798(14)
P(1)-C(2)	1.824(12)	P(1)-C(9)	1.840(12)
P(1)-C(14)	1.856(12)	P(2)-C(24)	1.844(12)
P(2)-C(30)	1.848(12)	P(2)-C(36)	1.843(12)
O-C(1)	1.142(14)	N(1)-C(14)	1.326(14)
N(1)-C(18)	1.364(14)	N(2)-C(19)	1.44(2)
N(2)-C(23)	1.42(2)	N(3)-C(36)	1.341(14)
N(3)-C(40)	1.343(15)	N(4)-C(41)	1.44(2)
N(4)-C(45)	1.43(2)	C(2)-C(3)	1.399(15)
C(2)-C(7)	1.40(2)	C(3)-C(4)	1.41(2)
C(4)-C(5)	1.42(2)	C(5)-C(6)	1.35(2)
C(6)-C(7)	1.42(2)	C(8)-C(9)	1.40(2)
C(8)-C(10)	1.41(2)	C(9)-C(13)	1.36(2)
C(10)-C(11)	1.38(2)	C(11)-C(12)	1.40(2)
C(12)-C(13)	1.41(2)	C(14)-C(15)	1.414(15)
C(15)-C(16)	1.41(2)	C(16)-C(17)	1.39(2)
C(17)-C(18)	1.40(2)	C(18)-C(19)	1.49(2)
C(19)-C(20)	1.33(2)	C(20)-C(21)	1.32(2)

Table 4.7. /continued

C(21)-C(22)	1.40(2)	C(22)-C(23)	1.41(2)
C(24)-C(25)	1.39(2)	C(24)-C(29)	1.42(2)
C(25)-C(26)	1.44(2)	C(26)-C(27)	1.36(2)
C(27)-C(28)	1.38(2)	C(28)-C(29)	1.45(2)
C(30)-C(31)	1.40(2)	C(30)-C(35)	1.37(2)
C(31)-C(32)	1.44(2)	C(32)-C(33)	1.37(2)
C(33)-C(34)	1.39(2)	C(34)-C(35)	1.42(2)
C(36)-C(37)	1.40(2)	C(37)-C(38)	1.41(2)
C(38)-C(39)	1.40(2)	C(39)-C(40)	1.40(2)
C(40)-C(41)	1.48(2)	C(41)-C(42)	1.31(2)
C(42)-C(43)	1.35(2)	C(43)-C(44)	1.39(2)
C(44)-C(45)	1.36(2)		

Table 4.8. Interatomic angles (°) for [Rh(Ph₂Pbipy)₂(CO)Cl]

P(1)-Rh-P(2)	177.2(1)	P(1)-Rh-Cl	88.6(1)
P(2)-Rh-Cl	90.9(1)	P(1)-Rh-C(1)	93.0(4)
P(2)-Rh-C(1)	87.5(4)	Cl-Rh-C(1)	178.4(4)
Rh-P(1)-C(2)	115.1(4)	Rh-P(1)-C(9)	112.3(4)
C(2)-P(1)-C(9)	105.6(5)	Rh-P(1)-C(14)	119.6(4)
C(2)-P(1)-C(14)	100.1(5)	C(9)-P(1)-C(14)	102.2(5)
Rh-P(2)-C(24)	112.9(4)	Rh-P(2)-C(30)	114.6(4)
C(24)-P(2)-C(30)	104.1(6)	Rh-P(2)-C(36)	115.1(4)
C(24)-P(2)-C(36)	106.6(6)	C(30)-P(2)-C(36)	102.4(5)
C(14)-N(1)-C(18)	118.3(10)	C(19)-N(2)-C(23)	115.1(13)
C(36)-N(3)-C(40)	118.9(11)	C(41)-N(4)-C(45)	116.8(13)
Rh-C(1)-O	176.9(12)	P(1)-C(2)-C(3)	117.3(9)
P(1)-C(2)-C(7)	121.5(10)	C(3)-C(2)-C(7)	121.1(11)
C(2)-C(3)-C(4)	119.3(12)	C(3)-C(4)-C(5)	119.1(12)
C(4)-C(5)-C(6)	121.0(13)	C(5)-C(6)-C(7)	120.9(13)
C(2)-C(7)-C(6)	118.6(13)	C(9)-C(8)-C(10)	119.3(12)
P(1)-C(9)-C(8)	120.0(9)	P(1)-C(9)-C(13)	118.3(10)
C(8)-C(9)-C(13)	121.6(12)	C(8)-C(10)-C(11)	119.1(12)
C(10)-C(11)-C(12)	120.9(13)	C(11)-C(12)-C(13)	119.6(13)

Table 4.8. /continued

C(9)-C(13)-C(12)	119.4(13)	P(1)-C(14)-N(1)	114.0(9)
C(14)-C(15)-C(16)	116.3(11)	C(15)-C(16)-C(17)	120.2(12)
C(16)-C(17)-C(18)	118.6(12)	N(1)-C(18)-C(17)	122.3(11)
N(1)-C(18)-C(19)	118.1(11)	C(17)-C(18)-C(19)	119.6(12)
N(2)-C(19)-C(18)	118.6(12)	N(2)-C(19)-C(20)	124.8(13)
C(18)-C(19)-C(20)	116.6(12)	C(19)-C(20)-C(21)	119.1(13)
C(20)-C(21)-C(22)	122 (2)	C(21)-C(22)-C(23)	120(2)
N(2)-C(23)-C(22)	119.0(14)	P(2)-C(24)-C(25)	115.6(10)
P(2)-C(24)-C(29)	122.4(10)	C(25)-C(24)-C(29)	121.9(13)
C(24)-C(25)-C(26)	119.5(14)	C(25)-C(26)-C(27)	118(2)
C(26)-C(27)-C(28)	123(2)	C(27)-C(28)-C(29)	120(2)
C(24)-C(29)-C(28)	116.6(13)	P(2)-C(30)-C(31)	114.3(9)
P(2)-C(30)-C(35)	122.9(10)	C(31)-C(30)-C(35)	122.8(12)
C(30)-C(31)-C(32)	116.3(12)	C(31)-C(32)-C(33)	121.4(14)
C(32)-C(33)-C(34)	120.7(14)	C(33)-C(34)-C(35)	119.6(14)
C(30)-C(35)-C(34)	119.2(13)	P(2)-C(36)-N(3)	112.9(9)
P(2)-C(36)-C(37)	124.3(9)	N(3)-C(36)-C(37)	122.7(12)
C(36)-C(37)-C(38)	118.8(12)	C(37)-C(38)-C(39)	118.0(13)
C(38)-C(39)-C(40)	119.2(13)	N(3)-C(40)-C(39)	122.4(11)

Table 4.8. /continued

N(3)-C(40)-C(41)	117.2(11)	C(30)-C(40)-C(41)	120.4(12)
N(4)-C(41)-C(40)	117.4(12)	N(4)-C(41)-C(42)	122.7(13)
C(40)-C(41)-C(42)	120.0(13)	C(41)-C(42)-C(43)	118.4(14)
C(42)-C(43)-C(44)	124(2)	C(43)-C(44)-C(45)	118.5(14)
N(4)-C(45)-C(44)	119.2(14)		

APPENDIX 1

GENERAL EXPERIMENTAL DETAILS

1. INSTRUMENTATION

Carbon, hydrogen and nitrogen analyses were performed by the Microanalytical Laboratory, University of Natal, Pietermaritzburg. Carbon, hydrogen, nitrogen, phosphorus and chlorine analyses were performed by Analytische Laboratorien, Gummersbach, Germany and by Galbraith Laboratories, Knoxville, Tennessee, U.S.A.

Infrared spectra (solid state and solution) were recorded on a Shimadzu FT-1400 infrared spectrometer.

UV/vis spectra were recorded on a Shimadzu UV-201PC UV/vis spectrophotometer.

$^{31}P\{^{1}H\}$ n.m.r spectra were recorded on a Varian FT-80A spectrometer running at 32.086MHz.
The $^{195}Pt\{^{1}H\}$ n.m.r spectrum was recorded on a Varian FT-80A spectrometer.
^{1}H and ^{13}C n.m.r spectra were recorded on a Gemini 200 spectrometer.
Deuterated solvents were used in all cases.

Mass spectra were recorded on a Hewlett-Packard HP5988A gas chromatographic mass spectrometer.

Gas chromatographic analyses were performed on a Varian Vista 4600.

Electrochemical measurements were performed using a PAR 175 universal programmer, a PAR 173 potentiostat, fitted with a PAR 176 current follower and connected to a HP 7045A X-Y recorder, and a locally made coulometer (Electronics Workshop, University of Natal).

APPENDIX 2

1. THEORY OF CYCLIC VOLTAMMETRY AND ROTATING DISC ELECTRODE (RDE) VOLTAMMETRY

The theory and interpretation of cyclic voltammetry has been described in a number of books, papers and reviews.[125-129] The theory and application of rotating disc electrode (RDE) voltammetry has been well documented in references 130 and 131. There are, however, a few relationships which are relevant to the discussion that follows and these will be briefly described here.

1.2. THEORY OF CYCLIC VOLTAMMETRY

Cyclic voltammetry is used for characterising redox properties of electroactive species and to study the mechanism of redox reactions. The magnitudes of the anodic peak current (i_{pa}), cathodic peak current (i_{pc}), anodic peak potential (E_{pa}) and cathodic peak potential (E_{pc}) are the important parameters of a wave in a cyclic voltammogram. For an electrochemically reversible redox couple the following relationships hold:

$$E_{\frac{1}{2}} = (E_{pa} + E_{pc}) / 2 \qquad (5.1)$$

$$\Delta E_p = E_{pa} - E_{pc} \approx 0.059/n \qquad (5.2)$$

$$i_p = (2.69 \times 10^5) A c n^{3/2} D^{1/2} v^{1/2} \qquad (5.3)$$

where i_p = peak current   [A]

(NOTE: Net peak currents after correction for background/charging currents)

         A = electroactive surface area of electrode   [cm^2]

         c = concentration of electroactive species   [$mol.cm^{-3}$]

         n = number of electrons transferred in redox process

D = diffusion coefficient of electroactive species $[cm^2.s^{-1}]$

v = scan rate $[V.s^{-1}]$

If the redox couple is also chemically reversible, the values of i_{pa} and i_{pc} should be identical, *i.e.*; $i_{pa}/i_{pc} = 1$. However, the ratio of peak currents can be significantly influenced by a chemical reaction coupled to the electrode process; in these cases i_{pa} and i_{pc} are no longer equal and the wave is said to be irreversible.

The half wave potential $(E_{½})$ is a measure of the ease of which the electron transfer occurs. ΔE_p is the characteristic of the reversibility of the system, if $\Delta E_p = 0.059/n$ then the system is said to be reversible.

1.2. THEORY OF ROTATING DISC ELECTRODE VOLTAMMETRY

In rotating electrode voltammetry the applied potential is varied linearly with time. Rotating disc electrode voltammetry is generally used to study the mechanism and kinetics of the electrode reactions that occur. Levich[132] and Riddiford[133] have derived the equation for the diffusion controlled limiting current (i_l);

$$i_l = 0.62nFA\upsilon^{-1/6}\omega^{1/2}D^{2/3}c \qquad (5.4)$$

where
F = Faraday $[C]$

υ = kinematic viscosity of the solution $[cm^2\ s^{-1}]$

ω = angular frequency $[s^{-1}]$

$\omega = 2\pi f$, f = rotations per second

and the other parameters as defined in section 5.2.1.

For a reversible electron transfer, apart from at very low overpotentials, the current is limited purely by mass transport and the Levich equation (5.4) is relevant. Thus, if we measure the current at any potential as a function of rotation rate (ω) we get $i \propto \omega^{½}$ and so $1/i \propto 1/\omega^{½}$.

Thus plotting $1/i$ *vs* $1/\omega^{\frac{1}{2}}$ at different potentials will give a series of lines all passing through the origin.

For an irreversible electron transfer, in the limiting current region (*i.e.* on the plateau), the current again depends on the rate of mass transport and not the kinetics of electron transfer. However on the slope of the wave there is mixed control, the current depends on the rates of both mass transport and electron transfer. Therefore, only on the plateau is the levich equation (5.4) valid. On the slope of the wave (where we have to take into account the combination of mass transport and electron transfer kinetics) the relationship between current and rotation rate is given by:[130]

$$1/i = 1/nFAkc + (1/0.62FAcD^{2/3}v^{-1/6})(1/\omega^{\frac{1}{2}})*1 \qquad (5.5)$$

A plot of $1/i$ *vs* $1/\omega^{\frac{1}{2}}$ should give a series of parallel straight lines, the intercepts on the y axis can be used to calculate k, the potential dependent rate constant. A plot of log k *vs* E should be linear and can be extrapolated to E_o (the equilibrium potential for the electron transfer process) to find k (the standard rate constant).

In the quasi-reversible case, both the forward and backward electron transfer processes must be considered and on the slope of the wave $1/i$ *vs* $1/\omega^{\frac{1}{2}}$ is given by:

$$1/i = 1/nFAc(k_R - k_o) + (\{k_f+k_b\}/0.62nFAc(k_R-k_o)D^{2/3}v^{-1/6})(1/\omega^{\frac{1}{2}}) \qquad (5.6)$$

k_R = rate constant for reduced species
k_O = rate constant for oxidised species
k_f = rate constant for forward reaction
k_b = rate constant for reverse reaction

---

*1 The second term in the equation(5.5) can be seen to take into account the mass transfer, compare to levich equation(5.4). The first term takes into account electron transfer kinetics.

However, if the reduced form is not initially present, then equation 5.6 becomes;

$$1/i = 1/nFAC\,k_O + (\{k_f+k_b\}/0.62nFACk_OD^{2/3}v^{-1/6})(1/\omega^{1/2})$$
(5.7)

A plot of $1/i$ vs $1/\omega^{1/2}$ gives a series of straight lines except this time the slopes are dependent on the potential because k is included in the terms defining the slope.

APPENDIX 3

CRYSTAL STRUCTURE DETERMINATIONS

1. DATA COLLECTION

The intensities of the reflections were measured at 22°C with an Enraf-Nonius CAD-4 diffractometer using graphite monochromated Mo-Kα radiation.

Cell constants were obtained by fitting the setting angles of three reflections of 25 high order reflections. During data collection, the orientation matrix was redetermined if any of the setting angles of three reflections, measured every 200 hundred reflections, deviated by more than 0.1° from the theoretical value. Three standard reflections were measured every hour to check on any possible decomposition of the crystal. An ω-2θ scan with a variable speed up to a maximum of 5.49° min^{-1} was used. The ω angle changed as $a_{\omega} + b_{\omega}\tan\theta$ (°), the horizontal aperture as $a_h + b_h\tan\theta$ (mm), but was limited to the range 1,3-5,9mm. The vertical slit was fixed at 4mm. Optimal values of a_{ω}, b_{ω}, a_h and b_h were determined for each crystal by a critical evaluation of peak shape for several reflections with different values of θ using the program OTPLOT (Omega-Thetha plot; Enraf-Nonius diffractometer control program, 1988). Where applicable, a linear decay correction was applied using the mean value of linear curves fitted through three intensity control reflections, measured at regular time intervals. Data were corrected for Lorentz and polarization effects, and where possible for absorption by psi-scan (empirical) method.[87]

2. STRUCTURE SOLUTION AND REFINEMENT

Direct methods or the Patterson function were used to solve the phase problem. Once a suitable phasing model was found, successive applications of Fourier and difference Fourier techniques allowed the location of the remaining non hydrogen atoms. In general, hydrogen

atoms were not located but, where the location of a hydrogen atom was particularly important, a difference Fourier, calculated with low angle reflections weighted relative to the high angle reflections, was employed. Weighted full matrix least squares methods were always used to refine the structure; the weighting scheme was chosen so as to give the smallest variation of the mean value of $\omega(Fo\text{-}Fc)$[134] as a function of the magnitude *Fo*. Scattering factor data were taken from reference ref. For all these calculations, the programs; SHELX-76[135] and SHELX-86[136] were employed. Plotting of the structures was performed using the program ORTEP[137] while the tabulation of fractional coordinates, thermal parameters, interatomic distances and angles was achieved using the program TABLES.[138]

REFERENCES

1. M.Aresta; *Carbon dioxide as a source of carbon*; p. 1-22; M. Aresta and G. Forti; Eds; Reidel Publ.; 1987.

2. M. Aresta; E. Quaranta and I. Tommasi; *Utilization of Carbon Dioxide: A Strategy for the Control of its Level in the Atmosphere*; p. 517-550;

3. C. Amatore; J. -M. Saveant; *J. Am. Chem. Soc.*, 1981, **103**, 5021.

4. C. Amatore; L. Nadjo; J.-M. Saveant; *J. Electroanal. Chem., Interfacial Electrochem.*, 1977, **78**, 403.

5. S.Ikedo; K. Ito; T. Murata; *Nagoya Kogyo Daigaku Gakuho*, 1975, **27**, 209.

6. S. Chao; C. J. Stalder; M. S. Wrighton; *J. Am. Chem. Soc.*, 1984, **106**, 3673.

7. N. S. Lewis; C. Lieber; *J. Am. Chem. Soc.*, 1984, **106**, 5033.

8. R. Eisenberg; B. Fisher; *J. Am. Chem. Soc.*, 1980, **102**, 7363.

9. J. Y. Becker; R. Eger; L. Kaufman; B. Vainas; *J. Chem. Soc., Chem. Commun.*, 1985, 1471.

10. Y. Matsumoto; M. Tezuka; A. Tsuchiya; Y. Uchida; T. Yajima; *J. Am. Chem. Soc.*, 1982, **104**, 6834.

11. J. Hawecker; M. M. Lehn; R. Ziessel; *J. Chem. Soc., Chem. Commun.*, 1984, 328.

12. C. M. Bolinger; D. Conrad; J. A. Gilbert; T. J. Meyer; N. Story; B. P. Sullivan; *J. Chem. Soc., Chem. Commun.*, 1985, 796.

13. S. Slater; J. H. Wagenknecht; *J. Am. Chem. Soc.*, 1984, **106**, 5367.

14. J. L. Roberts; D. T. Sawyer; *J. Electroanal. Chem.*, 1965, **9**, 1.

15. N. Novac; P. G. Russel; S. Srinivasan; M. Steinberg; *J. Electrochem. Soc.*, 1977, **124**, 1329.

16. E. Heitz; V. Kaiser; *Ber. Bunsen. Gesell.*, 1973, **77**, 818.

17. J. C. Gressin; D. Michelet; L. Nadjo; J. -M. Saveant; *Nouv. J. Chim.*, 1979, **3**, 545.

18. C. M. Bolinger; M. R. M. Bruce; E. Megehee; T. J. Meyer; T. R. O'Toole; B. P. Sullivan; H. Thorp; *Catalytic Activation of Carbon Dioxide*, p. 52-90, W. M. Ayers Ed., American Chemical Society, Washington, DC., 1988.

19. C. Amatore; J. -M. Saveant; *J. Electroanal. Chem.*, 1981, **125**, 22.

20. D. J. Pearce; D. Pletcher; *J. Electranal. Chem.*, 1986, **201**, 317.

21. M. Hammouche; D. Lexa; M. Momentaeu; J. -M. Saveant; *J. Am. Chem. Soc.*, 1991, **113**, 8455.

22. D. L. DuBois; A. Miedaner; *J. Am. Chem. Soc.*, 1987, **109**, 113.

23. P. Lemoine; *Coord. Chem. Rev.*, 1982, **47**, 55.

24. J. W. Lauher; *J. Am. Chem. Soc.*, 1978, **100**, 5305.

25. J. P. Collman; R. J. Finke; E. J. Moore; F. R. Munch; R. K. Rothrock; *Inorg.Chem.*, 1982, **21**, 146.

26. P. Lemoine; *Coord. Chem. Rev.*, 1988, **83**, 169.

27. M. Absi-Halibi; . Beurich; C. U. Pittman; M. G. Richmond; F. Richter; H. Vahrenkamp; *Angew. Chem., Int. Ed. Engl.*, 1982, **21**, 786.

28. M. Tezuka; A. Tsuchiya; T. Yajima; *J. Am. Chem. Soc.*, 1982, **104**, 6834.

29. B. -H. Chang; *J. Organomet. Chem.*, 1985, **291**, C31.

30. R. E. Lentz; C. P. Kubiak; K. S. Ratcliff; *Organometallics*, 1992, **11**, 1986.

31. H. Ishida; K. Tanaka; T. Tanaka; *Chem. Lett.*, 1985, 405.

32. H. Ishida; K. Tanaka; T. Tanaka; *Organometallics*, 1987, **6**, 181.

33. H. Nagao; S. -H. Peng; K. Tanaka; T. Tanaka; *Organometallics*, 1992, **11**, 1450.

34. H. Nagao; S. -H. Peng; K. Tanaka; T. Tanaka; B. -C. Tzeng; *Organometallics*, 1992, **11**, 3171.

35. K. Fujiki; H. Ishida; T. Ohba; K. Ohkubo; K. Tanaka; T.Tanaka; T. Terada; *J. Chem. Soc., Dalton Trans.*, 1990, 2155.

36. J. Hawecker; J.-M. Lehn: R. Ziessel; *J. Chem. Soc.,Chem. Commun.*, 1983, 536.

37. J. Hawecker; J.-M. Lehn: R. Ziessel; *Helv. Chim. Acta*, 1986, **69**, 1990.

38. J. Hawecker; J.-M. Lehn: R. Ziessel; *J. Chem. Soc.,Chem. Commun.*, 1984, 328.

39. R. C. Angelici; J. R. Graham; *J. Am. Chem. Soc.*; 1965, **87**, 5586.

40. A. J. Lees; M. J. Schadt; *Inorg. Chem.*; 1986, **25**, 675.

41. C. M. Bolinger, D. Conrad, T. J. Meyer, B. P.Sullivan, W. J. Vinnig; *J. Chem. Soc., Chem. Commun.*,1985, 1414.

42. G. Ferrandi; D. Geiger; C. Kutal; M. A. Webber; *Organometallics*; 1985, **4**, 2161.

43. P. Christensen; A. Hamnett; A. V. G. Muir; J. A. Timney; *J. Chem. Soc., Dalton Trans.*, 1992, 1455.

44. C. M. Bolinger, D. Conrad, J. A. Gilbert, T. J. Meyer, N. Story, B. P. Sullivan, *J. Chem. Soc.,Chem. Commun.*,1985, 796.

45. C. M. Bolinger, T. J. Meyer, N. Story, B. P. Sullivan, *Inorg. Chem.*, 1988, **27**, 4582.

46. K. J. Brewer, H. Place, S. C. Rasmussen, M. M. Richter, E. Yi, *Inorg. Chem.*, 1990, **29**, 3926.

47. M. R. Bruce, A. Downward, E. Megehee, T. J. Meyer, B. P. Sullivan, H. Thorp, *Oganometallics*, 1988, 7, 238.

48. M. R. Bruce, A. Downward, E. Megehee, T. J. Meyer, J. R. Pugh, B. P. Sullivan, H. Thorp, T. R. O'Toole, *Inorg. Chem.*, 1992, **31**, 4864

49. M. R. M. Bruce, T. J. Meyer, J. R. Pugh, B. P. Sullivan, *Inorg. Chem.*, 1991, **30**, 86.

50. T. Augutsson, V. Ramanathan, *J. Atmos. Sci.*, 1977, **34**, 448

51. O. T. Benfey, F. H. Westheimer, *J. Am. Chem. Soc.*, 1956, **78**, 5309.

52. F. Case, *J. Org. Chem.*, 1966, **31**, 2398.

53. D. Hager, G. R. Newkome, *J. Org. Chem.*, 1978, **43**, 947.

54. J. S. Field, R. J. Haines, C. J. Parry, S. H. Sookraj, *S. Afr. J. Chem.*, 1993, **46**, 70.

55. E.Constable, *Adv. Inorg. Chem. Radiochem.*, 1986, **30**, 69

56. E.Constable, *Adv. Inorg. Chem. Radiochem.*, 1989, **33**, 1

57. G. Bruno, F. Faraone, E. Rotondo, S. L. Schiavo, *Organometallics*, 1991, **10**, 1613.

58. A. L. Balch, J. P. Farr, M. M. Olmstead, *Inorg. Chem.*, 1983, **22**, 1229.

59. A. L. Balch, J. P. Farr, M. M. Olmstead, F. Wood, *J. Am. Chem. Soc.*, 1983, **105**, 792.

60. R. Bohra, V. Jain, V. Jakkal, *J. Organomet. Chem.*, 1990, **319**, 417.

61. G. Wilkinson, Ed., *Comprehensive Coordination Chemistry*, 1987, 5, chapter 53, p533, Pergamon Press

62. K. D. Karlin, J. Zubietta, *Copper Coordination Chemistry : Biochemical Perspectives*, 1983, Adenine Press, Guiderland, New York.

63. K. D. Karlin, J. Zubietta, *Copper Coordination Chemistry : Biochemical Perspectives*, 1989, Adenine Press, Guiderland, New York.

64. T. N. Sorrell, *Tetrahedron*, 1989, **45**, 3.

65. Y. Gultneh, K. D. Karlin, *Prog. Inorg. Chem.*, 1987, **35**, 219.

66. J. K. Kochi, R. A. Sheldon, *Metal Catalysed Oxidations of Organic Compounds*, Academic Press, New York, 1981.

67. R. J. Puddephatt, *Chem. Soc. Rev.*, 1983, **12**, 99.

68. M. Marsich, G. Nardin, L. Randaccio, *J. Am. Chem. Soc.*, 1973, **95**, 4053.

69. M. Marsich, G. Nardin, L. Randaccio, *Acta Crystallog., Sect. B.*, 1974, **30**, 1377.

70. N. Bresconi, M. Marsich, G. Nardin, L. Randaccio, *Inorg. Chim. Acta*, 1974, **10**, 15.

71. A. Camus, G. Nardin, L. Randaccio, *Inorg. Chim. Acta*, 1975, **12**, 23.

72. G. Nardin, L. Randaccio, E. Zanqrando, *J. Chem. Soc., Dalton Trans.*, 1975, 2566.

73. R. Bau, D. M. Ho, *Inorg. Chem.*, 1983, **22**, 4079.

74. A. Camus, N. Marsich, A. M. Lanfredi, A. Tiripicchio, *J. Chem. Soc., Chem. Commun.*, 1983, 1126.

75. A. Camus, R. Capelletti, A. M. Lanfredi, N. Marsich, F. Ugozzoli, *Inorg. Chim. Acta*, 1993, **206**, 173.

76. A. Camus, N. Marsich, G. Pellizer, *J. Organomet. Chem.*, 1983, **259**, 367.

77. A. Camus, N. Marsich, G. Nardin, *J. Organomet. Chem.*, 1982, **239**, 429.

78. J. Diez, M. P. Gamasa, J. Gimeno, A. Tiripicchio, M. T. Camellini, *J. Chem. Soc., Dalton Trans.*, 1987, 1275.

79. J. Diez, M. P. Gamasa, J. Gimeno, M. Lanfranchi, A. Tiripicchio, *J. Chem.Soc., Dalton Trans.*, 1990, 1027.

80. M. P. Gamasa, J. Gimeno, M. Lanfranchi, E. Lastra, A. Tiripicchio, *J. Chem. Soc., Dalton Trans.*, 1989, 1499.

81. W. Schauerte, D. Wood, unpublished results

82. B. Warwick, unpublished results

83. P. Pregosin, ^{31}P and ^{13}C NMR of Transition Metal Phosphine Complexes, 1979, Springler-Verlag, New York.

84. D. F. Shriver, Ed. *Inorganic Synthesis*, 1979, **19**, 90, Wiley Interscience, N. Y.

85. C. J. Parry, *Ph.D. Thesis*, University of Natal, 1994.

86. M. F. Huff, D. L. Reger, *Organometallics*, 1992, **11**, 69.

87.   F. Mathews, A. North, D. Philips, *Acta. Crystallogr., Sect. A.*, 1968, **24**

88.   R. J. Haines, C. P. Kubiak, R. E. Wittrig, *Inorg. Chem.*, 1994, **33**, 4723.

89.   K. W. Frese, Jr., *Electrochemical and Electrocatalytic Reactions of Carbon Dioxide*, pp 145-216, H. E. Guard, K. Krist, B. P. Sullivan, Editors.

90.   M. H. Chisholm, *ACS Symp.Ser.*, 1981, **55**.

91.   A. L. Balch, *ACS. Symp. Ser.*, 1981, No. 155, 167.

92.   R. J. Puddephatt, *ACS. Symp. Ser.*, 1981, No. 155, 187.

93.   A. L. Balch, *Adv. Chem. Ser.*, 1982, **196**, 243.

94.   J. T. Mague, S. H. de Vries, *Inorg. Chem.*, 1980, **19**, 3743.

95.   A. R. Sanger, *J. Chem. Soc., Dalton Trans.*, 1981, 228.

96.   R. Eisenberg, C. P. Kubaiak, *J. Am. Chem. Soc.*, 1980, **102**, 3637.

97.   R. S. Dickson, J. Cowie, *Inorg. Chem.*, 1981, **20**, 2682.

98.   F. A. Cotton, J. M. Tromp, *J. Am. Chem. Soc.*, 1974, **96**, 4422.

99.   R. Colton, M. J. McCormick, C. D. Pannan, *J. Chem. Soc., Chem. Commun.*, 1977, 823.

100. D. M. Hoffman, R. Hofmann, *Inorg. Chem.*, 1981, **20**, 3543.

101. A. L. Balch, J. P. Farr, M. M. Olmstead, *J. Am. Chem. Soc*, 1980, **102**, 6655.

102. A. L. Balch, J. P. Farr, C. H. Hunt, M. M. Olmstead, *Inorg. Chem.*, 1981, **20**, 1182.

103. A. L. Balch, J. P. Farr, A. Maissonat, *Inorg. Chim. Acta.*, 1981, **53**, L217.

104. A. L. Balch, J. P. Farr, F. E. Wood, *Inorg. Chem.*, 1983, **22**, 3387.

105. A. L. Balch, J. P. Farr, M. M. Olmstead, N. M. Rutherford, F. E. Wood, *Organometallics*, 1983, **2**, 1758.

106. F. A. Cotton, M. Matusz, *Inorg. Chim. Acta.*, 1988, **143**, 45.

107. W. J. Geary, *Coord. Chem. Rev.*, 1971, **7**, 81.

108. F. G. Mann, J. Watson, *J. Org. Chem.*, 1948, **13**, 502.

109. A. L. Balch, Y. S. Sohn, *J. Am. Chem. Soc.*, 1974, **96**, 1144.

110. J. P. Jesson, D. L. Linder, P. Z. Meakin, C. A. Tolman, *J. Am. Chem. Soc.*, 1974, **96**, 2762.

111. A. L. Balch, B. Tulyathan, *Inorg. Chem.*, 1977, **16**, 2840.

112. M. C. Bennet, P. B. Donaldson, *Inorg. Chem.*, 1977, **16**, 655.

113.   J. A. Ibers, R. M. Kirchner, D. W. Meek, *J. Am. Chem. Soc.*, 1974, **96**, 2762.

114.   C. Jones, M. J. Maah, J. F. Nixon, S. I. Al-Resayes, *J. Organomet. Chem.*, 1994, **468**, 107.

115.   R. W. Kunz, P. S. Pregosin, *NMR: Basic Princ. Prog.*, 1979, **16**, 101.

116.   R. J. Lawson, J. R. Shapely, *Inorg. Chem.*, 1978, **17**, 2963.

117.   M. A. Bennet, R. N. Johnson, T. W. Turney, *Inorg. Chem.*, 1976, **15**, 2938.

118.   R. Mathieu, J. F. Nixon, *J. Chem. Soc., Chem. Commun.*, 1974, 147.

119.   J. Evans, B. F. G. Johnson, J. Lewis, J. R. Norton, *J. Chem. Soc., Chem. Commun.*, 1973, 79.

120.   J. T. Mague, A. R. Sanger, *Inorg. Chem.*, 1979, **18**, 2060.

121.   F. A. Cotton, G. Wilkinson, *Advanced Inorganic Chemistry, 4th edition*, Wiley-Interscience, New York, 1980.

122.   C. Brown, B. T. Heaton, L. Longhetti, W. T. Pavey, D. O. Smith, *J. Organomet. Chem.*, 1980, **192**, 93.

123.   W. L. F. Armarego, D. D. Perrin, D. R. Perrin, *Purification of Laboratory Chemicals*, 2nd edn., Permgamon Press, New York, 1980.

124.   C. Mann, *Electroanal. Chem.*, 1969, **3**, 57.

125.   R. S. Nicholson, I. Shain, *Anal. Chem.*, 1964, **36**, 706.

126.   R. S. Nicholson, I. Shain, *Anal. Chem.*, 1965, **37**, 178.

127.   J. Heinz, *Angew. Chem. Int. Ed. Engl.*, 1984, **23**, 831.

128.   G. A. Mabbot, *J. Chem. Ed.*, 1983, **60**, 697.

129.   W. R. Heineman, P. T. Kissinger, *J. Chem. Ed.*, 1983, **60**, 702.

130.   R. Greef, R. Peat, L. M. Peter, D. Pletcher, J. Robinson, *Instrumental Methods in Electrochemistry*, Ellis Horwood Limited, Chichester, 1985

131.   J. A. Bard, L. R. Faulkner, *Eletrochemical Methods, Fundamentals and Applications*, John Wiley and Sons, New York, 1980.

132.   V. G. Levich, *Physicochemical Hydrodynamics*, Prentice Hall, Englewood Cliffs, New Jersey, 1962.

133.   A. C. Riddiford, *Adv. Electrochem. Eng.*, 1966, **4**, 47.

134. *"International Tables for X-ray Crystallography"*, 1974, **4**, pp 99, 149, Birmingham Kynoch Press.

135. G. M. Sheldrick, SHELX-76, Program for Crystal Structure Determination, University of Cambridge, 1976.

136. G. M. Sheldrick, SHELX-86, Program for Crystal Structure Determination, University of Gottingen, 1986.

137. C. K. Johnson, ORTEP-II, A Fortran Thermal-Ellipsoid Plot Program for Crystal Structure Illustrations, Oak Ridge National Laboratory, 1976.

138. D. C. Liles, Program for Tabulation of Crystallographic Data, Council for Scientific and Industrial Research (Pretoria), 1988.